

Medical University of South Carolina

MEDICA

MUSC Theses and Dissertations

2017

Development of Class I and Sub-Class I Selective Inhibitors of Lysine Deacylases: Implications for Inflammation and Hematologic Malignancies

Jesse Jordan McClure
Medical University of South Carolina

Follow this and additional works at: <https://medica-musc.researchcommons.org/theses>

Recommended Citation

McClure, Jesse Jordan, "Development of Class I and Sub-Class I Selective Inhibitors of Lysine Deacylases: Implications for Inflammation and Hematologic Malignancies" (2017). *MUSC Theses and Dissertations*. 370.

<https://medica-musc.researchcommons.org/theses/370>

This Dissertation is brought to you for free and open access by MEDICA. It has been accepted for inclusion in MUSC Theses and Dissertations by an authorized administrator of MEDICA. For more information, please contact medica@muscd.edu.

Development of Class I and sub-Class I selective inhibitors of Lysine

Deacylases: implications for inflammation and hematologic

malignancies

by

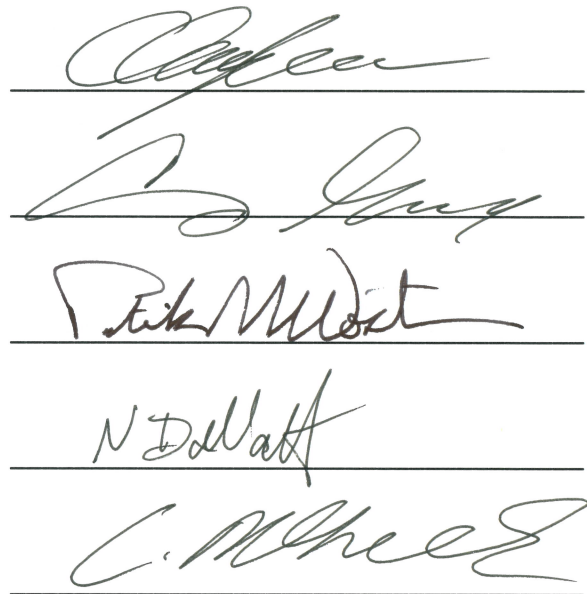
Jesse Jordan McClure

A dissertation submitted to the faculty of the Medical University of South Carolina in partial fulfillment of the requirements for the degree of Doctor of Philosophy in the College of Graduate Studies.

Department of Drug Discovery and Biomedical Sciences, 2017

Approved by:

Chairman, Advisory Committee



The image shows five handwritten signatures, each written on a horizontal line. From top to bottom, the signatures are: 1. A cursive signature that appears to be 'C. M. ...'. 2. A cursive signature that appears to be 'B. ...'. 3. A cursive signature that appears to be 'R. ...'. 4. A cursive signature that appears to be 'N. ...'. 5. A cursive signature that appears to be 'C. ...'.

TABLE OF CONTENTS

ACKNOWLEDGMENTS	3
ABSTRACT	4
LIST OF FIGURES AND TABLES	6
CHAPTERS	
1 INTRODUCTION	8
1.1. Histone Deacetylases: a brief history and background	8
1.2. Role of HDACs in the NF- κ B inflammatory cascade	12
1.3. Role of HDACs in human cancers	15
1.4. Development of inhibitors for Zn ²⁺ -dependent HDACs	20
1.5. Aims of this study	30
2 MATERIALS AND METHODS	32
2.1. Materials	32
2.2. Methods	41
3 RESULTS AND DISCUSSION	51
3.1. Role of Histone Deacetylases as Lysine Deacylases: Impact in Medicinal Chemistry and Inflammatory Diseases.	51
3.2. Development of Allosteric Hydrazide-Containing Class I Histone Deacetylase Inhibitors for Use in Acute Myeloid Leukemia.	74
3.3. In vivo testing and mechanistic determination of Hydrazide-Containing Class I Histone Deacetylase Inhibitors.	100
4 SUMMARY	107
5 CONCLUSIONS AND PERSPECTIVES	108
6 APPENDICES	117
6.1. Detailed Synthetic Procedures	117
6.2. Analytical NMR for lead compounds	146
REFERENCES	177

ACKNOWLEDGMENTS

I dedicate this body of work to Tim McClure. The worst scientist anyone's ever met, but the best dad I could have received. There's not a day that goes by that I don't think about you.

I'd like to thank James for his constant boot to throat tactic of teaching. I may have raised your blood pressure a few (40) mmHg, but you taught me how to be the shrewdest scientist that is sure to make paper submission for others a living hell. I can't thank you enough for your teachings and patience.

To Elizabeth, I don't think enough can be said about your work in the Chou lab. I hate to say you're the lab mom, but, the lab would fall apart very quickly without your touch. Thank you for being a great teacher and a sounding board.

I'd like to acknowledge the members of my committee, many of whom saw me rise from pharmacy student to now Ph.D. Without your guidance I would have never gotten to where I am now, nor the trajectory I aim to achieve.

I'd like to thank Dr. Stu Parnham for his help with my seemingly random problems with the NMR core. I will likely never understand 95% of what you do, but thanks for trying to teach me anyway.

To Dr. Yuri Peterson, thank you for always jumping in head first into my rabbit holes of computational and thought experiments. I wish we could have worked together more.

To Dr. Himes, thanks for appreciating my eclectic pop culture references and me occasionally making fun of you.

I'd like to thank the rest of my family for their care packages and kind words and nodding their head enthusiastically while being secretly bewildered when I discussed my research. Love you.

ABSTRACT

The acetylation status of lysine residues on histone proteins has long been attributed to a balance struck between the catalytic activity of Histone Acetyl Transferases and Histone Deacetylases (HDAC). HDACs were identified as the sole removers of acetyl post-translational modifications (PTM) of histone lysine residues. Studies into the biological role of HDACs have also elucidated their role as removers of acetyl PTMs from lysine residues of non-histone proteins. These findings, coupled with high-resolution mass spectrometry studies that revealed the presence of acyl-group PTMs on lysine residues of non-histone proteins, brought forth the possibility of HDACs acting as removers of both acyl- and acetyl-based PTMs. We posited that HDACs fulfill this dual role, and sought to investigate their specificity. Utilizing a fluorescence-based assay and biologically relevant acyl-substrates, the selectivity of zinc-dependent HDACs toward these acyl-based PTMs were identified. These findings were further validated using cellular models and molecular biology techniques. As a proof of principal, an HDAC3 selective inhibitor was designed using HDAC3's substrate preference. This resulting inhibitor demonstrates nanomolar activity and >30 fold selectivity toward HDAC3 compared to the other class I HDACs. This inhibitor is capable of increasing p65 acetylation, attenuating NF- κ B activation and thereby preventing downstream nitric oxide signaling. Additionally, this selective HDAC3 inhibition allows for control of HMGB-1 secretion from activated macrophages without altering the acetylation status of histones or tubulin.

In addition to this substrate-driven design of a novel HDAC3 selective inhibitor, we sought to tackle one of the biggest hurdles yet to be overcome for the continued improvement of HDAC inhibitors. First generation HDAC inhibitors frequently utilize a metal binding hydroxamic acid

moiety. The N-hydroxyl group of this motif is highly subject to sulfation/glucuronidation-based inactivation in humans; compounds containing this motif require much higher dosing in clinic to achieve therapeutic concentrations. With the goal of developing a second generation of HDAC inhibitors, lacking this hydroxamate, we designed a series of potent and selective class I HDAC inhibitors using a hydrazide motif. These inhibitors are impervious to glucuronidation and demonstrate allosteric inhibition. In vitro and ex vivo characterization of our lead analogs' efficacy, selectivity, and toxicity profiles demonstrate they possess low nanomolar activity against models of Acute Myeloid Leukemia (AML) and are at least 100-fold more selective for AML than solid immortalized cells such as Hek293 or human peripheral blood mononuclear cells. Further, these compounds seem to kill through a non-caspase-mediated mechanism with possible involvement of p53. Lead analogs demonstrate favorable half lives in vivo (>3 hours) and are possess promising bioavailability profiles. Lastly, these compounds are non-inferior to current FDA approved HDAC inhibitors, vorinostat and panobinostat, in causation of mutagenesis.

LIST OF FIGURES AND TABLES

Chapter 1:

Figure 1.1. Microscopic and Mechanistic Overview of HDAC- and HAT-Based Chromatin Remodeling.	10
Figure 1.2. Zn-Containing HDAC Classification.	12
Figure 1.3. Depiction of NF- κ B signaling and activation cascade.	14
Figure 1.4. FDA Approved HDAC Inhibitors and Approved Uses.	22
Figure 1.5. Sequence Alignment of Human class I HDACs.	26
Figure 1.6. Depiction of all known class I HDAC complexes.	28
Figure 1.7. Crystal structure of HDAC3 (PDB:4A69) with Ins(1,4,5,6)P ₄ bound and Corepressor.	29

Chapter 3:

Figure 3.1. Acyl-substrate synthesis and en bloc profiling.	53
Figure 3.2. Acyl-substrate profiling.	56
Figure 3.3. HDAC3 purity test.	57
Figure 3.4. Role of HDACs 3+6 in cellular deacetylation.	60
Figure 3.5. Role of HDAC3 in cellular deacetylation.	62
Figure 3.6. Roles of HDACs 3 and 6 on global cellular acetylation and deacetylation.	64
Figure 3.7. Antibody cross reactivity comparison with acetylated Bovine Serum Albumin.	66
Figure 3.8. Substrate-specificity driven development of HDAC3 selective inhibitor.	68
Figure 3.9. Time dependent Kinetics of HDACs 1-3 vs 2a .	71
Figure 3.10. Effects of HDAC inhibition on NF- κ B p65 acetylation and inflammatory responses.	72
Figure 3.11. Western blot analysis of RAW264.7 cells.	73
Figure 3.12. ESI-LCMS glucuronidation assay.	85
Figure 3.13. ESI-LCMS glucuronidation assay of 11l and 13b .	87
Figure 3.14. Lineweaver-Burke plots of 12d , 13b , and vorinostat vs. recombinant HDACs 1 and 3.	89
Figure 3.15. Vmax plots of 12d , 13b , and vorinostat vs. recombinant HDACs 1 and 3.	90
Figure 3.16. Molecular modeling and binding study of HDAC3.	91
Figure 3.17. Molecular modeling of 12d , 13b , and vorinostat against HDAC3.	92
Figure 3.18. Ex vivo analysis of lead compounds as single agents against AML.	95

Figure 3.19. Extrapolated analysis and correlation between assay screens and potency of lead compounds.	97
Figure 3.20. Selectivity and toxicity profiling of lead inhibitors.	99
Figure 3.21. Ames test of lead hydrazide and FDA approved HDAC inhibitors.	100
Figure 3.22. Pk/Pd profiling of 13b and 14a .	103
Figure 3.33. Western Blot Analysis of MV4-11 at 12 hours with various HDAC inhibitors.	105
Table 3.1. Key isozyme profiling values.	58
Table 3.2. SAR of substrate-driven HDAC3 specific inhibitors.	69
Table 3.3. In vitro inhibition of Hek293 lysates and recombinant HDAC3 for series 11 inhibitors.	77
Table 3.4. Class I HDAC and Hek293 lysate IC ₅₀ values for 11I .	78
Table 3.5. In vitro inhibition of Hek293 lysates and recombinant HDAC3 for series 12 inhibitors.	80
Table 3.6. Class I HDAC and Hek293 lysate IC ₅₀ values for series 12 inhibitors.	81
Table 3.7. In vitro inhibition of recombinant HDACs 1, 2, and 3 and Hek293 lysate for series 13 inhibitors.	84
Table 3.8. Leukemia and myeloma cell line data for 13b .	94
Scheme 3.1. Butylhydrazide derivatives synthesis.	75
Scheme 3.2. N-(4-(hydrazide)benzyl)benzamide derivatives synthesis.	79
Scheme 3.3. N-(4-(hydrazide)benzyl)cinnamamide derivatives synthesis.	83
Chapter 5:	
Figure 5.1. Crystal structure overlay of key pocket residues in HDACs 1-3.	111
Figure 5.2. Proposed Hydrazide Derivative with transcinnamic acid and tyrosine mimetic.	116

Chapter 1: INTRODUCTION

1.1. Histone Deacetylases: a brief history and background

In the early 1970s, researchers interrogated the effects of an enzyme isolated from calf thymus. The enzyme in question was shown to produce free acetyl groups in the presence of acetylated histones. Due to its early discovered function, this enzyme was aptly named Histone Deacetylase (HDAC).¹ Before the discovery of HDAC, and even before the discovery there was more than one HDAC, it was known that the reverse process, the acetylation of histones and other proteins, involved an enzyme family known as Histone Acetyl Transferases (HAT).² In addition to this enzymatic-based ligation, acetyl groups have also been shown to be ligated onto the ϵ -nitrogen termini of lysine residues via a forward favored reaction involving the charged primary amines of lysine and CoA bound acetyl groups.³⁻⁵ So why does your body consume all of this energy to put on and remove these acetyl groups from histones? They, after all, must be somewhat important due to their homologous presence in eukaryotes as basic as yeast.⁶ More specifically, what is the difference between acetylated and non-acetylated histones?

Well, one thing our bodies are known for is their incredibly efficient usage of space. The function of acetylated and non-acetylated histones fills a very valued space saving purpose. Unwound DNA is far too large to be stored in the nucleus of cells without further compaction and compression. As such, the human body utilizes a protein known as a histone to condense the DNA further, allowing for efficient storage, but also fulfilling another function. If your DNA was always unwound, you'd have very limited control over transcription of the very accessible DNA. So our bodies use histones to wrap the DNA around, akin to a thread around a spool, or a garden

hose around its rack, to allow for very compact storage while simultaneously regulating transcription.

Looking more into the mechanics of the DNA:Histone interaction, we know that there are eight subtypes of histones that form an octameric structure.⁷ How tightly the DNA coils around the histones depends on the post-translational modification status of the histone bound lysine residues. With the vast majority of ϵ -nitrogens on non-modified lysines residues carrying a positive charge at physiological pH, they are naturally ionically attracted to the negatively-charged phosphate groups found in DNA. As such, when no acetyl group, or other post-translational modification, is present on these lysine residues, they are able to form tight ionic interactions with negatively charged phosphate groups of DNA. If the histone bound lysine residues are extensively modified, and thus lacked their usual positive charge, the DNA will be relatively weakly bound to the histone. This state, referred to as euchromatin, allows access to the DNA for transcription. However, if largely unmodified, the positively-charged lysine residues allow for extensive interaction with DNA resulting in very tightly packed heterochromatin. This heterochromatin allows for very little transcription of DNA (**Figure 1.1**).

Indeed the post-translational modification state of histones is akin to a tug-of-war between HDACs and HATs. The resulting balance between the two has produced much interest in the field of medicine and molecular biology with the most well-known role these enzymes play seen in cancer. Extensive research has been performed on the roles of HDACs in cancers. Nearly universally, HDACs are seen upregulated in a wide variety of cancers ranging from breast to lung to hematologic malignancies.⁸⁻¹¹

Furthering the complexity into research surrounding the role of HDACs in cancer biology, 18 HDAC isozymes have been identified in the past 50 years.¹² These enzymes can be broken down

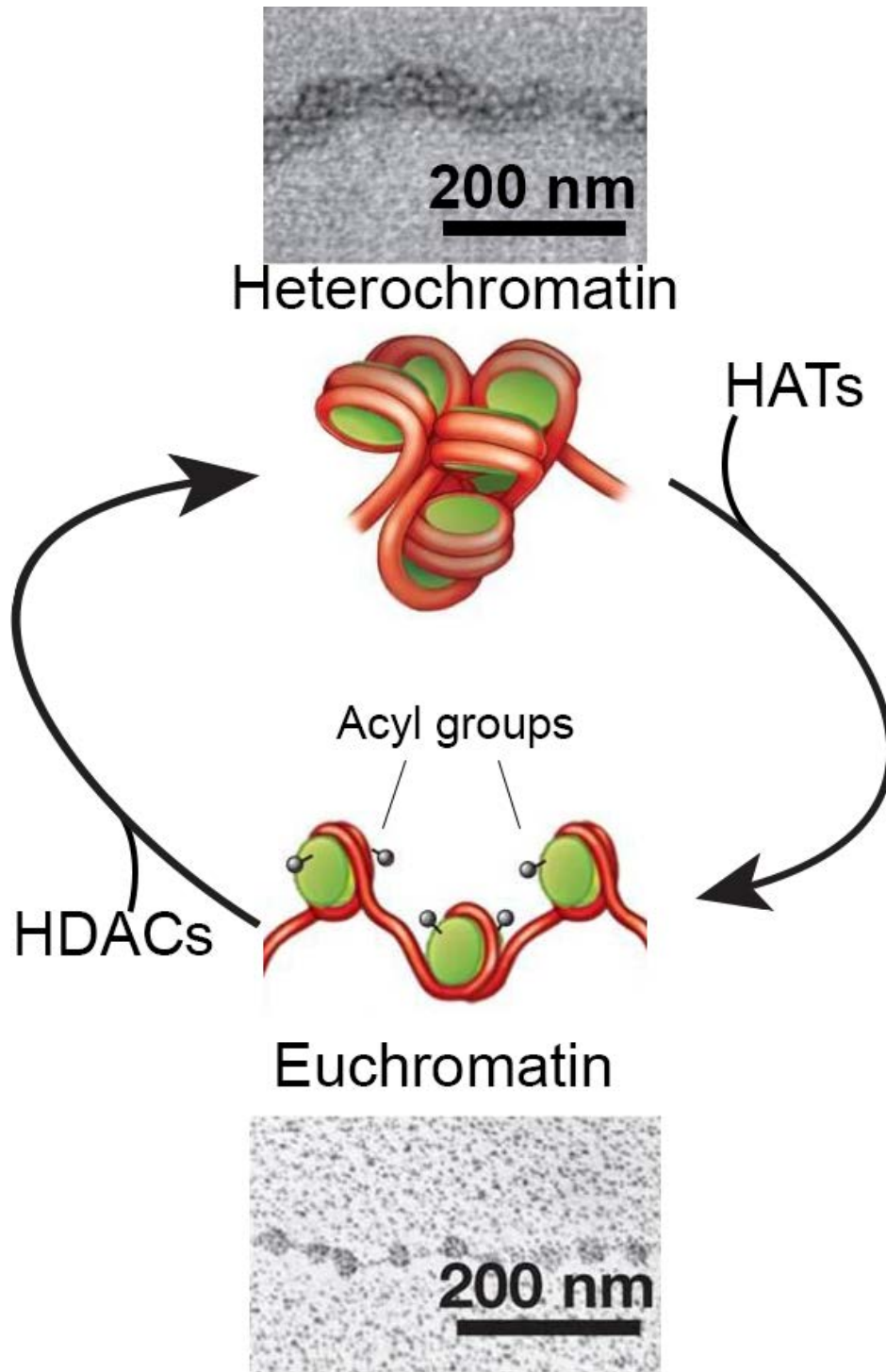


Figure 1.1 Microscopic and Mechanistic Overview of HDAC- and HAT-Based Chromatin Remodeling. Figure adapted from McGraw Hill.

phylogenetically into four classes. Class I contains HDACs 1-3 and HDAC8. Class II is comprised of HDACs 4-7 and HDACs 9 and 10. Class III is commonly referred to as the Sirtuin enzymes. Whereas class I, II, and IV HDACs contain an active Zn^{2+} metal, which is used for coordination of the post-translationally modified lysine with the catalytic histidines in the active site, class III Sirtuins are NAD^+ dependent and are generally unaffected by traditional HDAC inhibitors. Class IV contains only HDAC11 (**Figure 1.2**). Much debate and research has led to a mixed answer about the importance, roles, and functions of HDACs 4, 5, 7-11. These isozymes are capable of binding traditional acetylated substrates, yet seem to have no deacetylase activity toward them.¹³⁻¹⁵ As such, it has been posited that they serve as readers of lysine residue post translational status.¹⁶ However, it is evident that HDACs 1-3, and 6 have defined, well studied roles in a multitude of diseases.¹⁷⁻²⁹ Additionally, as they are the primary erasers of lysine residue modifications, HDACs 1-3 and 6 are often given the most attention as targets for medicinal chemistry.

One last broad topic worth mentioning in this section is the presence of an allosteric site on certain HDAC isozymes.³⁰ This site, generally occupied by inositol phosphates leads to significant increases in deacetylase activity, but also complex formation and recruitment.³¹⁻³² This is particularly interesting because it seems to be related to the complexes that the individual isozymes can take part in and form; that is to say that without Inositol Phosphate, certain HDAC-containing complexes are unable to form. Even more detailed analysis has found that only certain forms of Inositol Phosphate are capable of fully “engaging” this activity. Particularly Inositol (1, 4, 5, 6) Phosphate forces a different conformation in the allosteric pocket than does Inositol (6) Phosphate.³¹ This, along with the HDAC isozyme specific complex formation, becomes relevant

for the development of HDAC inhibitors and will be discussed more in depth later in the introduction.

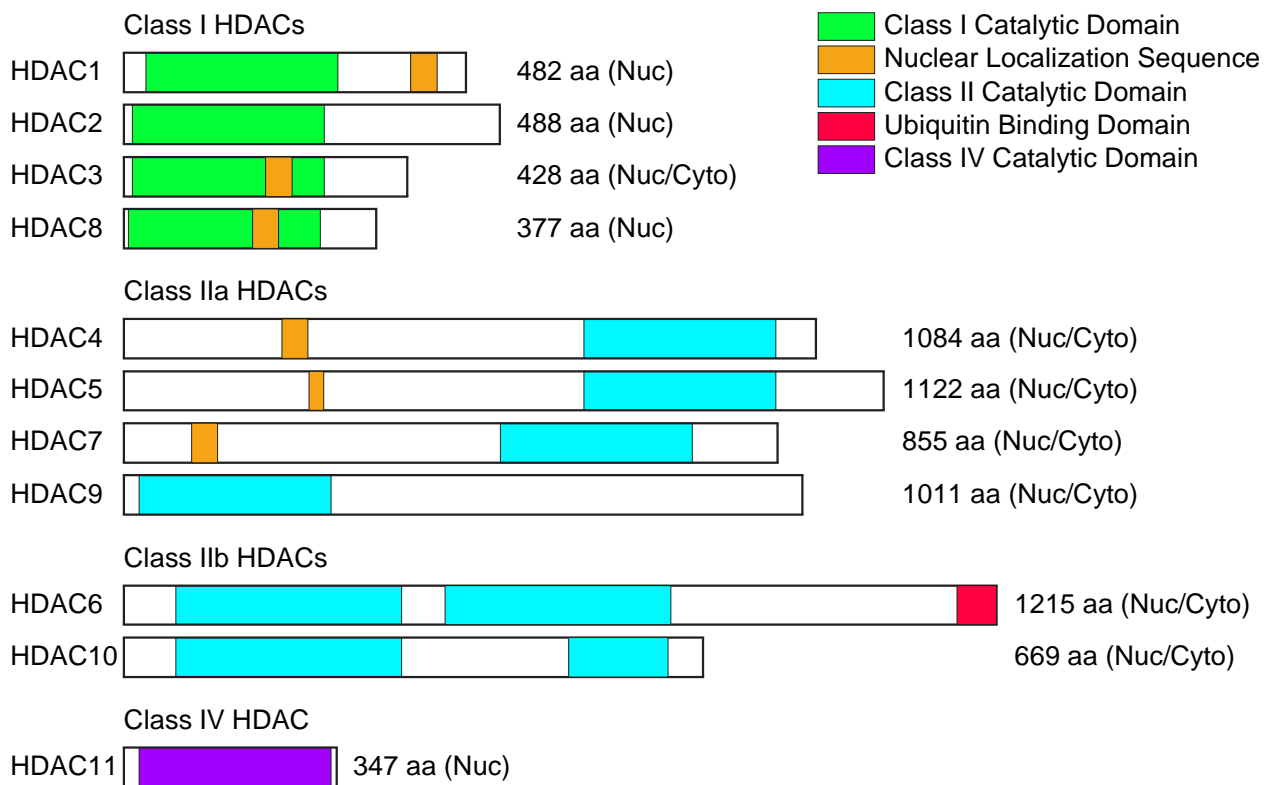


Figure 1.2 Zn-Containing HDAC Classification

1.2. Role of HDACs in the NF- κ B inflammatory cascade

Thus far, a good amount of time has been spent generally speaking about HDACs, but not much time has been spent on why they are worth targeting in the field of medicinal chemistry. As previously eluded, there are a multitude of disease states and pathways that are becoming recognized as being controlled wholly, or at least in part, by the actions of HDACs. Once such pathway is the NF- κ B p65 inflammation cascade. The NF- κ B family of proteins contains five transcription factors. These proteins generally form heterodimers that, based on composition, perform different and sometimes even contradicting roles. The five proteins are p65/RelA,

p50/NF- κ B1, p52/NF- κ B2, RelB, and c-Rel. Both p50 and p52 are cleaved from p105 and p100 respectively to form their “active” forms.³³ A wide variety of proinflammatory cytokines, such as TNF α , serve to activate NF- κ B.³⁴ This process involves activation of the I κ B-kinase complex. Signaling from a myriad of signaling factors leads to phosphorylation of I κ B α by IKK. Once phosphorylated, I κ B α is flagged for proteasomal degradation by subsequent ubiquitinylation. Once degraded, the NF- κ B complex is free from I κ B α and considered activated. This activated complex then forms a larger complex with the NF- κ B heterodimer to allow for nuclear translocation (**Figure 1.3**).³⁴ Once in the nucleus, NF- κ B binds exposed DNA and activates transcription of proinflammatory chemo and cytokines as well as proteins that are antiapoptotic in nature.

In more recent literature, it has been shown that specific acetylation sites on p50 and p65 subunits of NF- κ B dictate nuclear translocation, DNA transcription, and to some extent, what proteins are transcribed after entering the nucleus.³⁵⁻⁴¹ Following these studies, it was shown that HDACs 1, 2, and 3 are largely responsible for the deacetylation of these subunits, and even more specifically, the individual HDACs have preferred lysine residues that they will deacetylate. Taken together, this finding pointed toward selective HDAC inhibition leading toward selective control over the NF- κ B inflammation cascade at a transcriptional level. Indeed, preliminary data holds this to be true. HDAC3 alone controls the acetylation status of K122 and K123 of p65. Acetylation on these lysine residues is associated with decreased DNA binding time.⁴² As such it should be considered that an uninhibited HDAC3 promotes NF- κ B:DNA binding through ways of removing acetyl groups on these lysine residues. It has been postulated, and previously shown,

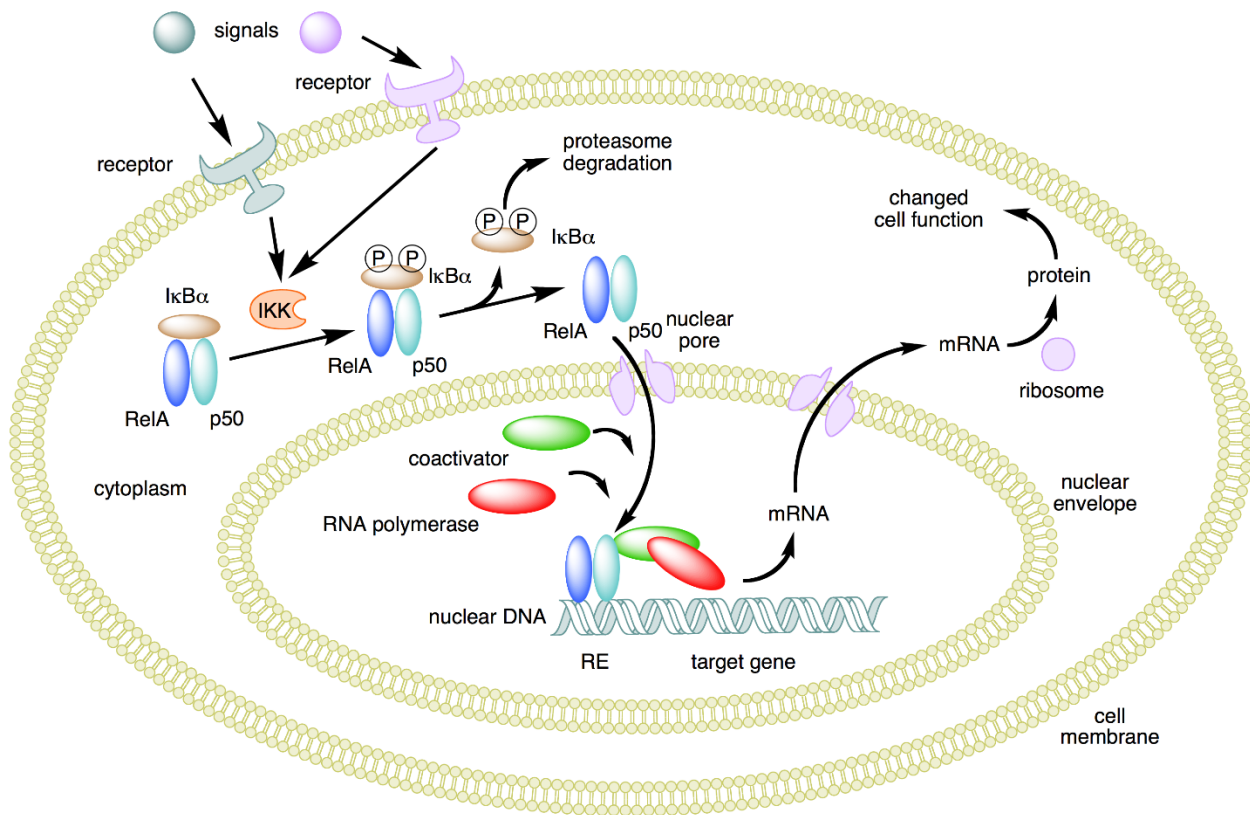


Figure 1.3 Depiction of NF-κB signaling and activation cascade

that selective HDAC3 inhibition can reduce NF-κB:DNA binding.⁴³ Uninhibited HDACs 1 and 2 were deemed to be anti-inflammatory in nature as they control acetylation status of K218 and K221 of p65.

When acetylated, these lysine residues diminish binding of NF-κB to IκBα and thus increase nuclear binding time. As such, when inhibited, the cells enter a largely inflamed state.³⁸ Combining these findings, we can see that if achievable, selective HDAC3 inhibition that does not affect the deacetylation function of HDACs 1 or 2 would lead to an ideal, anti-inflammatory state. This selective inhibition would be defined by hyperacetylation of K122 and K123 leading to

decreased nuclear binding of NF- κ B as well as normal acetylation of K218 and K221. The latter leading to increased NF- κ B:I κ B α interaction, and thus diminished NF- κ B:nuclear binding.

Unfortunately, designing an HDAC3 selective inhibitor that is >100 fold selective compared to HDACs 1 or 2 has largely been unachieved. The primary method of attempting to achieve selectivity was performed based on small alterations in protein pockets gleaned from crystal structures. This venture has been largely unfruitful with only one established and well documented inhibitor possessing more than 30 fold selectivity.⁴⁴ This, in turn, has complicated the design of an HDAC3 selective inhibitor for use in inflammatory diseases. One of the aims of this paper, which will be more formally written later on in this chapter, is the design of an HDAC3 selective inhibitor using a substrate-driven medicinal chemistry approach rather than a crystal structure one.

1.3. Role of HDACs in Human Cancers

Naturally when one thinks of cancer biology they probably associate it with the word complex. Indeed, the role of HDACs in cancers further adds to this complexity. It's been shown that nearly every type of cancer has some form of aberrant HDAC biology, be it a significant overexpression, hyperactivity, or even mutants that lack activity.⁴⁵⁻⁴⁸ That's not to say that HDAC status is the only thing that feeds into the pathogenesis of cancers, but it's certainly too common of a theme to be dismissed easily. Further muddying the waters regarding their role is the realization that HDACs don't control only the acetylation status of histones as their name would imply, but rather the acetylation status of many different lysine residues associated with many proteins.⁴⁹ Even more complicated still is the idea that on top of all of these different ways HDACs

can affect cancer growth, one could have normally active, normally concentrated HDACs that are aberrantly recruited to target genes. This is indeed the case in Acute Myeloid Leukemia with HDACs 1, 2, and 3 and the oncogenic proteins AML1-ETO and PML-RAR.^{46, 50} To demonstrate the effect this has on defining potential targets for the treatment of hematologic malignancies, the combination of HDAC inhibitors with retinoids has been met with some success. The inhibition of HDACs allowing for the normal expression of Trans Retinoic Acid Receptor and concomitant activation of these receptors with their natural retinoid ligands allows for the cell to undergo a “detransformation” back to a non-cancerous state.⁵¹⁻⁵²

In addition to the role that class I HDACs play in hematologic malignancies, they’ve also been shown to be overexpressed in many solid tumor cells. This, however, should be interpreted carefully as little clinical efficacy has been shown thus far, only in vitro and lower phyla have shown promising and/or consistent results. This is in contrast to the rather surprising clinical successes of HDAC inhibitors in hematologic malignancies/non-solid tumors. HDACs 1 and 2 are seen to be overexpressed individually in prostate, gastric, colon, breast, colorectal, and cervical cancers among others.⁵³⁻⁵⁸

So what exactly differentiates solid from non-solid tumors? Further, why have HDAC inhibitors struck such resounding success with one, but not so much the other? Before discussion of biological differences between the cancer types, it is relevant to discuss the methods by which HDAC inhibitors can kill cells, and indeed there are several. One such way, and in no particular order of importance, is their role in autophagy.⁵⁹ Autophagy can be a two-edged sword when it comes to treating cancer.⁶⁰ Forcing a cell to upregulate autophagy may cause it to surveil its damaged or aberrant organelles and neatly succumb to apoptosis. On the other hand it may allow

the cell to evade treatments or conditions that induce metabolic stresses that would normally kill the cell. Indeed it has been proposed that upregulated autophagy is the explanation for resistance and refraction to treatment in clinic for a variety of cancers.⁶¹⁻⁶² HDAC6 in particular has a unique role in this pathway due to its ability to sense and bind free ubiquitin. As such, it serves as a link between the cell's proteasomal degradation pathway and autophagic clearance.⁶³ If HDAC6 senses increased concentrations of free ubiquitin, indicative of low amounts of ubiquitinated proteins and therefore low metabolic stress, it may downplay or inactivate autophagic pathways. However, in the absence of these free ubiquitins, it may serve to upregulate or activate autophagic pathways to aid in the clearance of misfolded proteins through a non-proteasomal mechanism.⁶⁴ While a fascinating and complex target for neurodegenerative diseases and resistant/refractory multiple myeloma, HDAC6's role in autophagy exceeds the scope of this work. More relevant to this work, however, is the role of HDACs 1 and 2 in autophagy. Knockdown/inhibition of HDACs 1 and 2 concomitantly blocks autophagic flux in skeletal muscle.⁶⁵ Additionally, inhibition of HDAC1 can promote autophagy by accumulation of the autophagosomal marker LC3.⁶⁶ These data prove as promising pathways to further interrogate as more about the roles of HDACs as individual enzymes and as an aggregate becomes increasingly recognized and established in the biological underpinnings of cancer, both the growth and sustenance thereof.

Another, and perhaps more familiar, pathway that HDACs utilize to affect cancer growth is through the cell cycle. Inhibition of HDACs has been shown to induce G₁ cell cycle arrest via cyclin-dependent kinase induction.⁶⁷ HDACs 1 and 2 are known to directly bind promoters of p21, 27, and 57 and negatively affect their expression.⁶⁸⁻⁶⁹ Inhibition of these isozymes is conversely

associated with increased expression of p21, 27, and 57.⁷⁰ In addition to this prevention of S-phase transition is the impaired mitotic cell growth that ultimately can also halt the cell between the G₂/M phases. The pan-HDAC inhibitor panobinostat is capable of doing just this, with its mechanism being attributed to the degradation of Aurora A and Aurora B kinases via inhibition of HDACs 3 and 6.⁷¹⁻⁷²

Lastly, but certainly not an exhaustion of the pathways HDACs affect, it's been well demonstrated that HDACs regulate apoptosis through the change of expression of pro- and anti-apoptotic proteins.⁷³ This includes both increased susceptibility to apoptosis as well as directly engaging the extrinsic and intrinsic pathways of apoptosis.⁷⁴⁻⁷⁵ For the extrinsic pathway activation, this has been shown in mice, transcending the possibility it was an in vitro phenomenon.⁷⁶ Further giving weight to the findings, and demonstrating the effect of medicinal chemistry efforts towards HDACs, inhibition of HDACs 1-3 is necessary for both caspase-8 activation as well as expression of an apoptotic protein known as FLICE-like inhibitory protein.⁷⁷⁻⁷⁸ Perhaps the best known, most studied, and therefore least understood proapoptotic protein, p53, also has been shown to be controlled by HDACs.⁷⁹⁻⁸¹ Acetylation of p53 has been shown to stabilize the protein, as well as allow for its nuclear translocation and thus transcriptional activation.⁸²⁻⁸³ p53 is crucial in regulating damaged cells and preventing the continued growth of an otherwise abnormal or oncogenic cell.⁸⁴⁻⁸⁵ As this is a crucial role in ensuring the host doesn't succumb to the chronic mutations that would otherwise lead to a cancerous growth, p53 is very tightly regulated. In a healthy, normally functioning cell, p53 is kept at low concentrations. When the cell is exposed to a wide variety of stresses, p53 is activated, its cellular concentration

increases, and as such, the cell is more likely to undergo neat, programmed cell death, apoptosis.⁸⁵

You may have previously gathered that HDAC inhibitors have a seeming selectivity for hematologic malignancies and other “soft” cancers compared to solid tumor. This, after all, is very apparent just by looking at the very narrow window of diseases that all FDA-approved HDAC inhibitors fall within. So what is the primary difference that separates the two? Why are HDAC inhibitors seemingly less effective against solid tumor cells when compared to hematologic cancers? To answer this at a 10,000 foot view, one of the broadest answers may be the pathogenesis of the two types. Solid tumors, unlike hematologic malignancies, do not stem from a stem cell type progenitor. As such, this transformation process, in some cases several steps, is thus a perfect area to look towards for answers. Further, and more importantly to the rationale behind this body of evidence is if HDACs affect the transformation process?

Indeed this question has been recently looked at in acute promyelocytic leukemia (APL). The researchers demonstrated that HDAC3 selectively controls the initiation step of APLs progression. This comes as a very novel finding, as until this publication, there was no previous evidence that HDACs can directly control oncogenesis, they were previously thought to be controllers of maintenance. Furthering their claim, selective HDAC3 inhibition was found to abrogate completely oncogenesis in vivo.²⁰

In addition to this rather novel finding, the p53 acetylation status and activity have also been heavily studied in acute myeloid leukemia (AML). In this cancer, p53 is found to be mutated in only 5-8% of patients.⁸⁶⁻⁸⁸ Upwards of a log fold lower than all cancers as an aggregate.⁸⁹ Furthering this connection, there has been a fair amount of research into the role p53 plays in

the initiation, development, and maintenance of AML. p53 expression is well associated with outcomes in clinic, with a strong correlation between increased expression and shorter survival times.⁹⁰ Research into how HDAC inhibitors affect AML growth has thus far been largely clinic to bench side driven. That is, much of what we learn is whether or not these agents work rather than how they work.⁹¹ Essentially all typical methods of inducing cell death, apoptosis, lethal autophagy, stabilization of p53, etc. been attributed to HDAC inhibitors effect on leukemia cells in vitro, but an exact mechanism remains to be elucidated.

1.4. Development of inhibitors for Zn²⁺-dependent HDACs

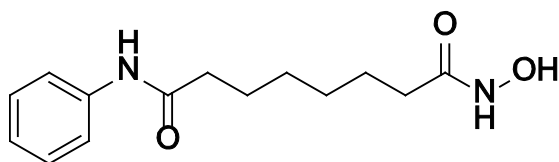
Now that we're more familiar with some general ideas and in some cases more exacts of diseases that HDACs can play a role in, and to what degree, we can begin to see the rationalization of their inhibitor design. The design of HDAC inhibitors started with a very humble and common compound. Certainly anyone reading this has worked with the very first, very non-potent HDAC inhibitor, Dimethyl Sulfoxide (DMSO). Charlotte Friend discovered DMSO's ability to differentiate erythroleukemia cells into normal cells in 1971.⁹² It would be another 25 years before the mechanism of hyperacetylation of the histones with DMSO treatment was discovered. While an interesting finding, the effective dose of DMSO was ~0.25M. However this curious discovery unknowingly sparked the initial efforts into HDAC drug discovery. The first improvement from DMSO was N-methylacetamide. This compound was able to achieve effective differentiation at 30 mM, an approximate log decrease compared to DMSO. Further efforts were then focused on building off of this rather small molecule. Addition of a hexyl chain and capping each end with acetamides led to HMBA. Already we can start to see the long alkyl chain that is present in

vorinostat (SAHA). It was after more rounds of medicinal chemistry efforts that SAHA was born. Replacing one acetamide with a benzamide and the other with a hydroxamate, researchers were able to obtain a 2 μ M inhibitor, roughly 2500 times more potent than HMBA.⁹³

SAHA wasn't instantly known to be an HDAC inhibitor. Indeed, based on the structure and activity it was nearly instantaneously ruled out as a DNA intercalating agent, however what target it bound to was anyone's guess. The hydroxamic acid was thought to be binding to a metal ion, and was deemed the "active" end of the molecule, with the opposite benzamide serving as an anchor and the connecting alkyl chain serving as an area of highly flexible linkage.

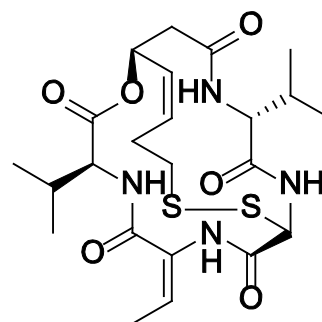
Since SAHA's FDA approval for Cutaneous T-cell Lymphoma, three additional HDAC inhibitors for two different hematologic malignancies have entered the market. Thereby marking HDACs and their inhibitors as demonstrably relevant targets and efficacious inhibitors for cancers affecting the blood in particular (**Figure 1.4**). However, all approvals thus far have been for pan-HDAC inhibitors. This non-specific inhibition naturally has led to several problems with off-target toxicities and unfavorable side effect manifestations for patients. More recent ventures into selective HDAC inhibitor design, as demonstrated by the interest in specificity with pipeline drugs, has focused on developing inhibitors selective for HDACs 1, 2, 3, and 6, as these have been shown to be the major targets of acylation-level control.

Despite being a class I HDAC, HDAC8 is largely overlooked due to its markedly decreased ability to deacylate biologically relevant substrate compared to the other isozymes in its class.⁹⁴ Throughout this writing, any reference to class I HDACs or specific inhibitors of class I HDACs will not include HDAC8 unless otherwise mentioned.



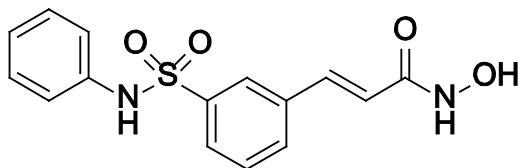
vorinostat

Cutaneous T-cell Lymphoma



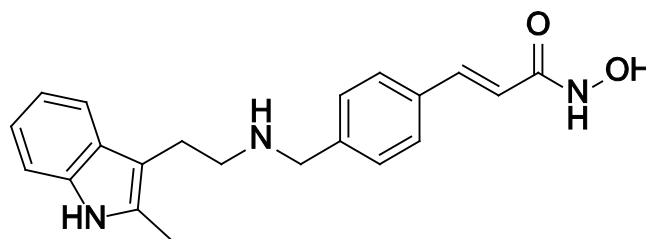
romidepsin

Cutaneous T-cell Lymphoma



belinostat

Peripheral T-cell Lymphoma



panobinostat

Resistant/refractory Multiple Myeloma

Figure 1.4 FDA Approved HDAC Inhibitors and Approved Uses.

The development of HDAC6 specific inhibitors has proven to be fairly achievable. By far the most commonly used example is Tubastatin A. By utilizing a three fused ring system, this inhibitor selectively inhibits HDAC6 through a steric bulk mechanism. Its three-ring structure prevents its hydroxamate moiety to reach the Zn^{2+} atom in the longer tunnels of HDACs 1-3. However, it is freely available to reach the Zn^{2+} atom in the shorter tunnel of HDAC6's catalytic pocket.⁹⁵ The necessity of HDAC6 specific inhibitors has become increasingly important as a key mechanism of Multiple Myeloma drug resistance is realized. As it currently stands, standard of care for Multiple Myeloma utilizes a Proteasome Inhibitor such as bortezomib. This agent demonstrates very high increases in disease free progression time frames for patients. However, nearly 100% of patients become resistant and refractory to its treatment. The mechanism underlying this has not been

fully delineated, but is thought to be secondary to upregulated autophagic clearance of misfolded proteins.⁹⁶ Bortezomib, by preventing a major source of misfolded protein clearance, essentially works by clogging up the cell with “junk” misfolded proteins. Cancerous cells avoid the apoptosis this build up would normally induce by upregulation of an alternative pathway that can relieve the cell’s stress. This autophagic clearance is largely due to HDAC6’s unique ability, via its ubiquitin binding domain, to coordinate the transport of these misfolded proteins to lysosomal structures to be cleared by autophagosomes.⁶³ As such, it was hypothesized that HDAC6 inhibition may be useful in combatting bortezomib-resistant/refractory forms of Multiple Myeloma. Indeed, there was some truth to this hypothesis with the FDA approval of panobinostat for resistant/refractory Multiple Myeloma. Panobinostat, however, is a pan-HDAC inhibitor. Pipeline therapies as well as agents in Phase I-III clinical trials that are truly HDAC6 selective have showed mixed results or were used at doses that negated their HDAC6 selectivity.⁹⁷

The design of class I specific inhibitors, and sub-class I specific inhibitors has proved to be much more challenging than HDAC6, and will receive an overwhelming majority of the focus of this body of evidence. To begin, HDACs 1-3 have an extremely high level of homology (**Figure 1.5**). This homology has been largely the driving force preventing adequate discovery of selective inhibitors of these isozymes. Not only do the isozymes display this high level of homology, but their catalytic pockets are identical with respect to amino acid residues. This, and the inability to discern key differences between the pockets of HDACs 1-3 derived from their respective crystal structures, has led to very little success from a medicinal chemistry standpoint.

Further complicating these attempts are the abilities of class I HDACs to form complexes *in vivo*. HDACs 1 and 2 are even able to be interchangeably used in the NuRD, CoREST, MiDAC, and

SIN3 complexes, meaning if one was to achieve truly selective inhibition of HDAC 1 or 2, the body could utilize the other in these complexes, abrogating the effects of the inhibitor. Taken together, selective inhibition of these isozymes may not necessarily equate to selective effects in vivo.⁹⁸⁻¹⁰³ Inhibition of a class I HDAC isozyme in one complex may have a desired effect but be completely offset by a negative aspect of its inability to act in another complex that performs a different role. One unifying theme between all class I HDACs is their recruitment to these complexes comes through the ELM2-SANT domain that, while diverse, is present in these isozymes. Interestingly, HDAC3 is uniquely able to enter the SMRT/NCOR complex due to the inter isozyme variability in this region. As such, much more effort has been placed into designing HDAC3 selective inhibitors compared to inhibitors of HDACs 1 or 2 (**Figure 1.6**). That being said, it is important to discuss the functions these complexes have to better understand the complementary or often times clashing roles they play in the cell.

The NuRD complex is known to participate in replication and repair of DNA.¹⁰⁴⁻¹⁰⁵ In addition to this function, KO and transgenic mouse models lacking key components of the NuRD complex show its function in tumorigenesis and the embryonic development.¹⁰⁶ In particular, it seems to be a tight regulator of hematopoietic differentiation, especially in the differentiation of myeloid lineage cells.¹⁰⁷ Closely related to this are the findings that this complex also greatly impacts the transformation process into B and T cells alike.¹⁰⁸⁻¹¹⁰

The CoREST complex tends to interact with the chromatin more than the NuRD complex. Further, its role seems to be more neuronally centered. It has been shown to regulate both gene expression and stem cell fate of neurons.¹¹¹ Further, unlike the dimerized single active enzyme NuRD complex, CoREST maintains a monomer conformation while having two active enzymes,

HDAC1/2 and LSD1. As such, it maintains a much more chromatin focused role, with the SANT2 domain of CoREST interacting directly with the DNA.¹¹²⁻¹¹³

The MiDAC complex is tightly associated with cyclin A. As such, it demonstrates much more of a role in cell cycle control.¹¹⁴ Further, with its presence seemingly only in mitotic cells, this is strongly correlated to the findings that HDAC affects the cell-cycle, particularly the G₁/S and G₂/M phases.¹¹⁵

The last HDAC1/HDAC2 complex SIN3 is essential to T cell development in addition to embryo development.¹¹⁶ Other roles include the growth regulation of tumors. Unique to this complex is the lack of ELM2-SANT domain,¹¹⁷ thereby suggesting recruitment and formation of this complex is mediated through an atypical mechanism compared to other known complexes.

Finally, the SMRT/NCoR complex is unique in the sense that the only class I HDAC that is recruited to it is HDAC3. Furthering itself in uniqueness from the other complexes, is its ability to recruit class IIa HDACs, the “readers.” Although, to date, this purpose has not been fully elucidated.¹¹⁸ This complex, like the NuRD and MiDAC complexes, is activated by Inositol Phosphates.^{30, 103} This activation is done through an allosteric site that is found on both HDACs 1 and 3 (**Figure 1.7**) shown in bright green. Interestingly, however, different Inositol Phosphates activate these two isozymes individually. HDAC1 is activated by InsP₆ whereas HDAC3 is activated by Ins(1,4,5,6)P₄.³¹ Furthering this vexing matter is the effect of mutating a key Arginine residue (Arg270) for HDAC1 and (Arg265) for HDAC3. Mutation of this amino acid for HDAC3 results in a functioning enzyme that is able to form complexes, however, mutating the homologous amino acid in HDAC1 results in an inactive complex.³¹ These rather novel findings may lead to the design of inhibitors that are complex specific while abusing these subtle, but important, differences.

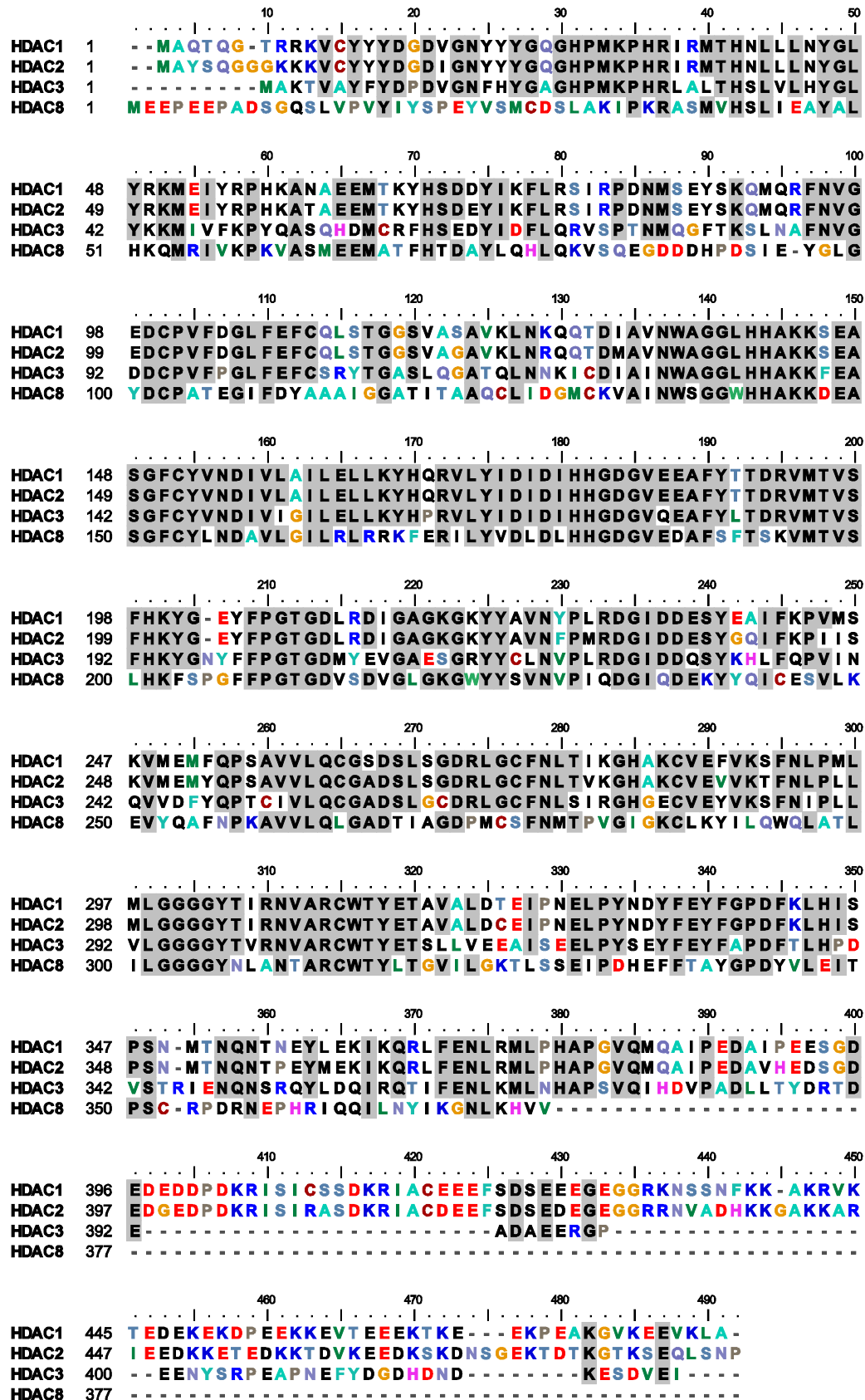


Figure 1.5 Sequence Alignment of Human class I HDACs.

One last issue plaguing drug discovery efforts with class I HDACs is the continued use of archaic metal-chelating groups such as the hydroxamate (hydroxamic acid) or *ortho*-aminoanilide (benzamides). These motifs are commonly used for developing inhibitors of HDACs as they chelate dicationic metals and “neutralize” the ability of the active site Zn^{2+} to successfully coordinate with modified lysines, thereby preventing deacylation. The hydroxamate group, until the FDA approval of vorinostat, was considered to be an undesirable motif in medicinal chemistry.¹¹⁹ The non-selective metal chelating properties of the hydroxamate are what allow it to bind the catalytic Zn^{2+} metal that HDACs rely on, but also cause compounds containing these groups to be associated with many undesirable effects secondary to non-targeted active site metal chelation.¹²⁰⁻¹³⁵ While all FDA approved inhibitors demonstrate very strong efficacy in the sub-micromolar range, the doses given in clinic are relatively much higher. The reason for this increased required dose, and the subsequent side effects due to off-target effects, could be in part to a metabolic inactivation of some of these compounds. The hydroxamic acid that is present on three of the four FDA approved HDAC inhibitors, vorinostat, panobinostat, and belinostat, is known to be sulfated or glucuronidated extensively, specifically by UDP glucuronosyltransferase 1A1.¹³⁶⁻¹³⁸ In the case of vorinostat, the process of glucuronidation has been demonstrated to abrogate its HDAC inhibition activity, and is further evidenced with its issues concerning achieving therapeutic concentrations in clinic. As belinostat and panobinostat also share this hydroxamic acid motif, and have subsequently been shown to be glucuronidated in vivo, a safe assumption can be made that this metabolism causes inactivation for these compounds as well.

Attempts to generate novel, non-hydroxamic acid metal-chelating motifs have resulted in the use of *ortho*-aminoanilide-based HDAC inhibitors, most notably MS-275 (entinostat). However,

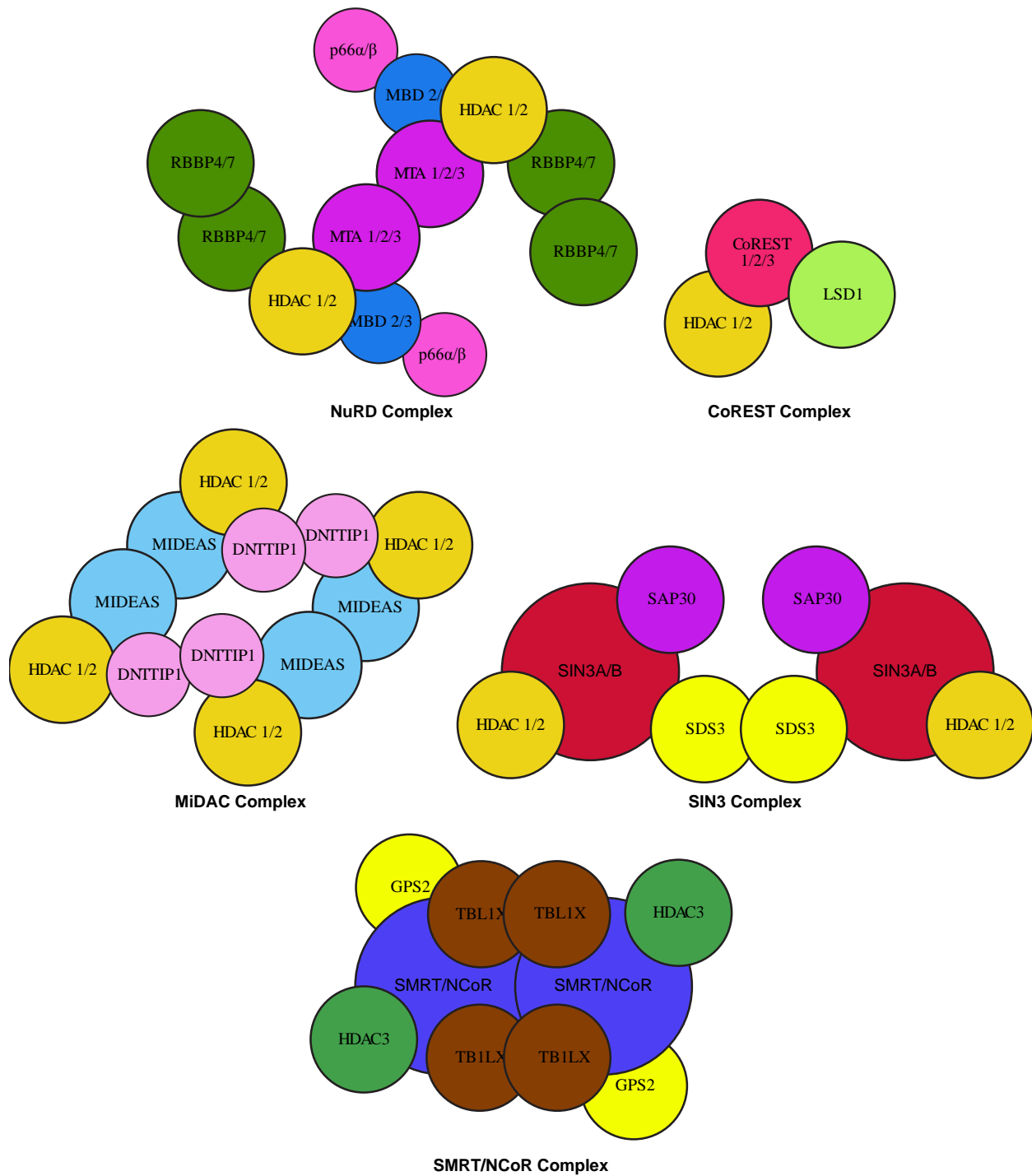


Figure 1.6 Depiction of all known class I HDAC complexes.

the benzylic primary amine of this motif is also subject to glucuronidation-based inactivation.¹³⁹

Further, this inhibitor was shown to be hepatotoxic in mice.¹⁴⁰ In a more recent attempt to

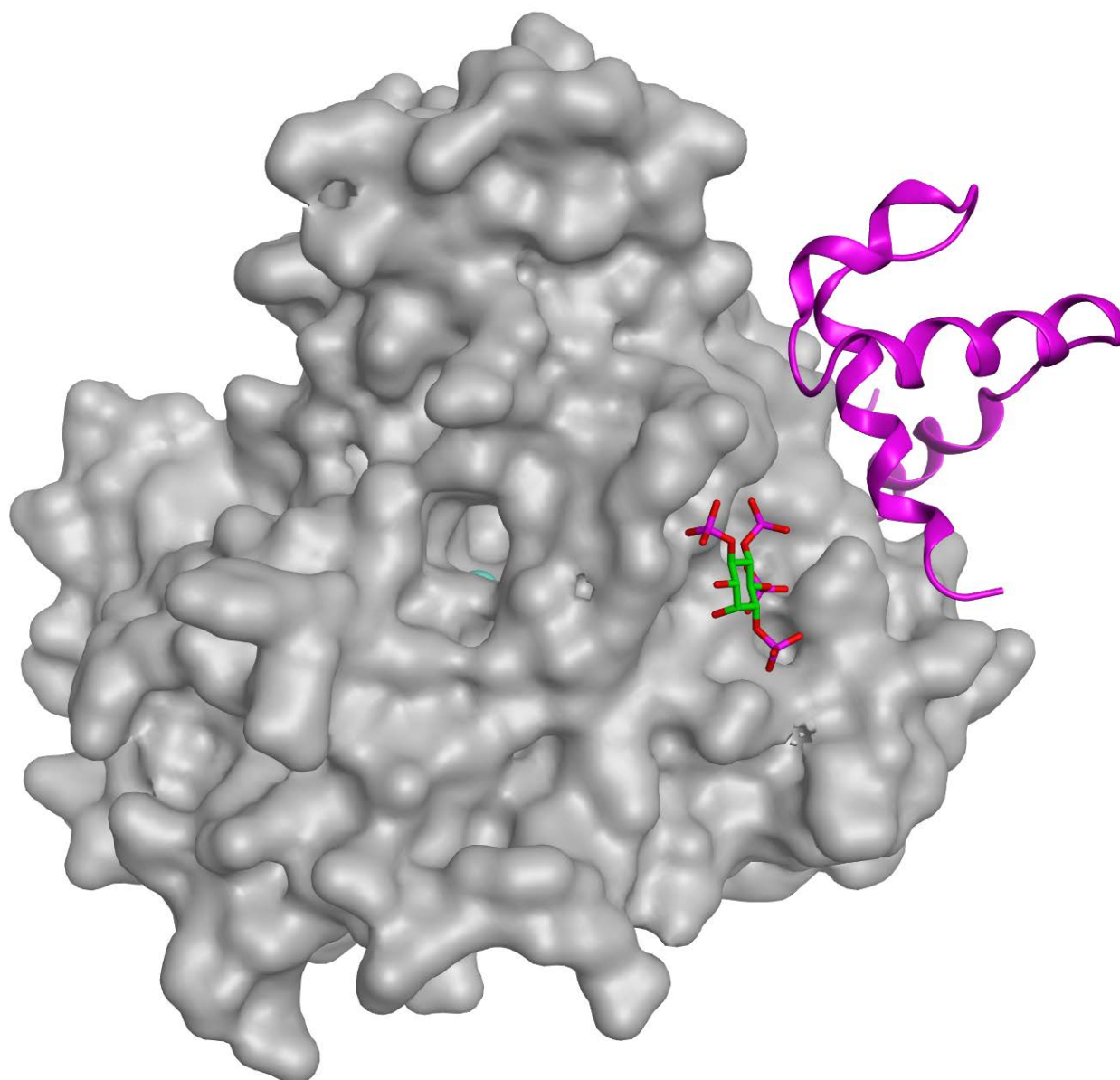


Figure 1.7 Crystal structure of HDAC3 (PDB:4A69) with Ins(1,4,5,6)P₄ bound and Corepressor

generate non-hydroxamic acid metal-chelating motifs, Wang and colleagues demonstrated a novel, potent, class I HDAC-specific inhibitor series based around a hydrazide motif.¹⁴¹ Their synthetically refined, lead analog from their initial publication possessed 60 nM HDAC3 inhibition, 500 nM and 100 nM for HDACs 1 and 2 respectively, and at least 20 fold selectivity for class I HDACs compared to HDAC6. Further, their lead compound possessed higher potency than

the similarly selective *ortho*-aminoanilide-based inhibitor entinostat, and contained a novel moiety that would not likely be subject to glucuronidation/sulfation, making it an attractive starting point for the development of second generation HDAC inhibitors.

Additional efforts have focused on the role of HDACs in complexes and the role of various forms of Inositol Phosphate with HDAC function and complexation.

These previous findings and gaps in knowledge led to two different hypotheses to approach a similar problem: developing novel HDAC inhibitors that broke the mold from the traditional method of designing inhibitors around very slight changes in crystal structure active sites to achieve selectivity. The first hypothesis to arise was that, if indeed HDACs were capable of more than just deacetylation and participated in deacylation, do they have some level of specificity towards one or more substrates *in vitro* and *ex vivo*? If so, could this selectivity be used to develop substrate-driven inhibitors rather than crystal-structure driven inhibitors? The second hypothesis stemmed from the novel hydrazide moiety. Is the hydrazide motif discovered by Wang et al. actually chelating Zn^{2+} or is it the first instance of an allosteric HDAC inhibitor?

1.5. Aims of this study

The aims of this study are largely related to the study of class I HDACs as well as designing inhibitors selective for this class, as well as selective for individual isozymes of class I. The current state of literature and knowledge regarding the ability of zinc-dependent HDACs to function as deacylases is nearly completely absent. Further, with the relatively recent focus on class I HDACs in both inflammation and leukemias, developing novel inhibitors for class I HDACs/HDAC3 could prove to be very relevant in clinic. Lastly, the continued use of metal-chelation based HDAC

inhibitors has become too detrimental to continue. The nonspecific binding, drug:drug interactions, poor bioavailability in clinic, and general intolerability of these agents demonstrates the many flaws with which HDAC inhibitors currently hold. As such, my Aims are as follows:

Aim 1: Determine if zinc-dependent Histone Deacetylases have deacylase activity outside of acetyl-, trifluoroacetyl-, and crotonyl-based modifications.

Aim 1.1: If so, determine if there are groups that are selectively removed by a class or sub-class of isozymes.

Aim 2: Develop an HDAC3 selective inhibitor utilizing a substrate-based design approach.

Aim 3: Further enhance the hydrazide-based HDAC inhibitors beyond their current ~150 nM potency and determine if they are impervious to glucuronidation.

Aim 3.1: If a novel compound utilizing this structure can be obtained, determined its efficacy in a multitude of hematologic malignancies.

2 MATERIALS AND METHODS

2.1 Materials

Flasks and Plates

96 well “U” bottom black plates were purchased from Greiner (Ref: 650209)

96 well “U” bottom clear plates were purchased from Falcon (Ref: 353910)

Sterile, 6 well clear flat bottom plates were purchased from Greiner (Ref: 657 160)

Sterile, 24 well clear flat bottom plates were purchased from Greiner (Ref: 662 160)

75 cm² sterile cell culture flasks were purchased from Greiner (Ref: 658 175)

Buffers

Tris-HDAC buffer was made from: 50 mM Tris-Base purchased from Fisher Scientific (Ref: BP152-1), 137 mM NaCl purchased from Fisher Scientific (Ref: S671-3), 2.7 mM KCl purchased from Sigma (Ref: P-4504), 1mM MgCl₂ purchased from VWR (Ref: 0288-100G), in sterile filtered RNA-ase free water purchased from Gibco (Ref: 15230-162).

RIPA buffer is made from: 50 mM Tris-Base, 150 mM NaCl, 5 mM EDTA purchased from Gibco (Ref: 15575), 0.1% (w/v) SDS purchased from Sigma (Ref: L3490-100G), 0.5% (w/v) Sodium Deoxycholate purchased from Sigma (Ref: D6750-100G), 1% (v/v) Triton X-100 purchased from Sigma (Ref: T-8532) in sterile filtered RNA-ase free water, 1% (v/v) Protease/Phosphatase inhibitor purchased from Thermo (Ref: 1861280) is added.

Cell Lines and Media

MV4-11 cells were purchased from ATCC (Ref: CRL-9591)

RAW 264.7 cells were purchased from ATCC (Ref: TIB-71)

Hek293 cells were purchased from ATCC (Ref: CRL-1573)

HeLa cells were purchased from ATCC (Ref: CRM-CCL-2)

RPMI-8226 cells were purchased from ATCC (Ref: CCL-155)

RS4;11 cells were purchased from ATCC (Ref: CRL-1873)

K-562 cells were purchased from ATCC (Ref: CCL-243)

HL-60 cells were purchased from ATCC (Ref: CCL-240)

MOLM-14 cells were purchased from DSMZ (Ref: ACC 777)

Fetal Bovine Serum was purchased from HyClone (Ref: SH30396.03)

Antibiotic-Antimycotic solution was purchased from Gibco (Ref: 15240-062)

MV4-11 media was made from 10% (v/v) Fetal Bovine Serum, 1% (v/v) Anti-Anti in Iscove's

Modified Dulbecco's Medium purchased from Gibco (Ref: 12440-053)

Hek293 media was made from 10% (v/v) Fetal Bovine Serum, 1% (v/v) Anti-Anti in Dulbecco's

Modified Eagle Medium purchased from Gibco (Ref: 11995-065)

HeLa media was made from 10% (v/v) Fetal Bovine Serum, 1% (v/v) Anti-Anti in Dulbecco's

Modified Eagle Medium purchased from Gibco (Ref: 11995-065)

RAW 264.7 media was made from 10% (v/v) Fetal Bovine Serum, 1% (v/v) Anti-Anti in RPMI +

GlutaMAX (RPMI 1640 Medium) purchased from Gibco (Ref: 61870-036)

HL-60 media was made from 20% (v/v) Fetal Bovine Serum, 1% (v/v) Anti-Anti in Iscove's Modified

Dulbecco's Medium purchased from Gibco (Ref: 12440-053)

RS4-11 media was made from 10% (v/v) Fetal Bovine Serum, 1% (v/v) Anti-Anti in RPMI +

GlutaMAX (RPMI 1640 Medium) purchased from Gibco (Ref: 61870-036)

MOLM14 media was made from 20% (v/v) Fetal Bovine Serum, 1% (v/v) Anti-Anti in RPMI + GlutaMAX (RPMI 1640 Medium) purchased from Gibco (Ref: 61870-036)

RPMI-8226 media was made from 10% (v/v) Fetal Bovine Serum, 1% (v/v) Anti-Anti in RPMI + GlutaMAX (RPMI 1640 Medium) purchased from Gibco (Ref: 61870-036)

Peripheral Blood Mononuclear Cells were a generous gift from the laboratory of Dr. Nathan Dolloff (MUSC, Charleston SC)

Hanks' Balanced Salt Solution without Ca²⁺ or Mg²⁺ was purchased from Corning (Ref: 21-022-CV)

Materials for Chemical Synthesis

Ethanol was purchased from Decon labs (Ref: 2701)

Methanol was purchased from Fisher Scientific (Ref: A452-4)

Acetonitrile was purchased from Fisher Scientific (Ref: A996-4)

Methylene Chloride was purchased from Acros (Ref: 61005-0040)

Dimethylformamide was purchased from Acros (Ref: 34843-0010)

Ethyl Ether was purchased from Fisher Scientific (Ref: E138-4)

Ethyl Acetate was purchased from Fisher Scientific (Ref: E196-4)

Tetrahydrofuran was purchased from Acros (Ref: 61045-0010)

4 Angstrom Molecular sieves were purchased from Sigma (Ref: 208604-1kg)

Butyraldehyde was purchased from Acros (Ref: 108090010)

Sodium cyanoborohydride was purchased from Oakwood (Ref: 044871)

4-methoxybenzohydrazide was purchased from Oakwood (Ref: 018771)

Benzofuran-2-carboxylic acid was purchased from Sigma (Ref: 307270)

Oxalyl chloride was purchased from Acros (Ref: 129611000)

Hydrazine monohydrate was purchased from TCI (Ref: H0172)

4-phenoxybenzohydrazide was purchased from Sigma (Ref: PH011385)

Nicotinoyl chloride was purchased from Sigma (Ref: 213381-256)

Triethylamine was purchased from Fisher Scientific (Ref: 04885-1)

methyl [1,1']-biphenyl-4-carboxylate was purchased from Sigma (Ref: P5501)

Thiophene-2-carbonyl chloride was purchased from Sigma (Ref: 288985-256)

2-Furoyl chloride was purchased from Sigma (Ref: 149861)

Hydrocinnamoyl chloride was purchased from Acros (Ref: 134380250)

trans-Cinnamic acid was purchased from Sigma (Ref: 133760-1006)

1-hydroxybenzotriazole was purchased from Oakwood (Ref: M02875)

N, N' -dicyclohexylcarbodiimide was purchased from Acros (Ref: 113901000)

1-naphthoic acid was purchased from Acros (Ref: 128180250)

2-naphthohydrazide was purchased from Sigma (Ref: PH009906)

Methyl 4-(aminoethyl)benzoate was purchased from Sigma (Ref: 479993-5g)

Benzoyl chloride was purchased from Alfa Aesar (A14107)

4-(aminomethyl)benzoic acid was purchased from Sigma (Ref: 283746)

Crotonaldehyde was purchased from Acros (Ref: 427181000)

Isobutyraldehyde was purchased from Sigma (Ref: 240788)

Propanal was purchased from Acros (Ref: 220511000)

Pentanal was purchased from Acros (Ref: 149561000)

3,3,3-trifluoropropanal was purchased from Sigma (Ref: TMT00492)

Cyclopropanecarboxaldehyde was purchased from Sigma (Ref: 272213)

Heptanal was purchased from Acros (Ref: 120320500)

Octanal was purchased from Acros (Ref: 129481000)

Hexanal was purchased from Alfa Aesar (Ref: A16265)

Decanal was purchased from Alfa Aesar (Ref: AAA11656AE)

Acetaldehyde was purchased from Acros (Ref: AC149512500)

Cyclobutanecarboxaldehyde was purchased from Sigma (Ref: CDS017876)

Methyl 4-(aminomethyl)benzoate HCl was purchased from Ark Pharm (Ref: AK691510G)

2,2,2-trifluoroethyl formate was purchased from Oakwood (Ref: 037821)

Propionyl chloride was purchased from Sigma (Ref: P51559-25G)

Butyryl chloride was purchased from Sigma (Ref: 236349)

Crotonyl anhydride was purchased from MP Biomed (Ref: 211133)

Valeryl chloride was purchased from Acros (Ref: 169121000)

Hexanoyl chloride was purchased from Acros (Ref: 169040050)

Heptanoyl chloride was purchased from Alfa Aesar (Ref: AAL0331518)

Octanoyl chloride was purchased from Acros (Ref: 129430050)

Trifluoroacetic anhydride was purchased from Acros (Ref: 14781-1000)

Glutaric anhydride was purchased from Acros (Ref: 119970050)

Adipic acid was purchased from Flukar (Ref: 02130-50G)

N α -(tert-Butoxycarbonyl)-L-Lysine-7-amido-4-methylcoumarin was purchased from Shanghai Scientific (Ref: 28726)

o-Phenylenediamine was purchased from Acros (Ref: 130552500)

(E)-2-pentenoic acid was purchased from Alfa Aesar (Ref: A12689)

Thiophene-2-carboxylic acid was purchased from Sigma (Ref: T32603)

1H-pyrrole-2-carboxylic acid was purchased from Sigma (Ref: P73609)

Oxazole-5-carboxylic acid was purchased from Alfa Aesar (Ref: H3017906)

Isoxazole-5-carboxylic acid was purchased from Alfa Aesar (Ref: 1373903)

Benzofuran-2-carboxylic acid was purchased from Ark Pharm (Ref: AK293015G)

4-fluorobenzene-1,2-diamine was purchased from Matrix (Ref: 004671)

4,5-difluorobenzene-1,2-diamine was purchased from Acros (Ref: 449810010)

3,4-difluorobenzene-1,2-diamine was purchased from Matrix (Ref: 004667)

3,5-difluorobenzene-1,2-diamine was purchased from Matrix (Ref: 007008)

Methyl orange was purchased from Sigma (Ref: 11,451-0)

Sodium hydroxide was purchased from Lancaster (Ref: 13094)

Lithium hydroxide was purchased from Sigma (Ref: 40297-4)

Hydrochloric acid was purchased from Fisher Scientific (Ref: A144SI-212)

Magnesium Sulfate was purchased from Sigma (Ref: 208094-12kg)

Potassium carbonate was purchased from Acros (Ref: 19804-0010)

Formic acid was purchased from Fisher Scientific (Ref: A117-50)

12g RediSepRf High Performance gold Silica prepacked columns were purchased from Teledyne Isco (Ref: 69-2203-345)

5.5g RediSepRf Gold C18 Silica prepacked columns were purchased from Teledyne Isco (Ref: 69-2203-328)

5.5g RediSepRf Gold C18Aq Silica prepacked columns were purchased from Teledyne Isco (Ref: 69-2203-570)

TLC silica gels bound on aluminum were purchased from Merck (Ref: 1.05554.0001)

Thermo Fisher LCQ Fleet HPLC-MS using an Accucore RP-MS HPLC Column, 2.6 μ M particle size, 30x4.6 mm was used for mass spectrometry.

Bruker 400 Mhz was used for ^1H , ^{13}C , and ^{19}F NMR collection.

Teledyne Isco Combiflash Rf200 was used for all purification sequences.

DMSO-d6 was purchased from Acros (Ref: 321290100)

Biological Assay Materials

All recombinant human HDAC isozymes were purchased from BPS biosciences. Lot numbers for HDACs 1-11 respectively: 140113, 110922G, 120524, 130115, 100414, 140110-G20mM, 90402, 110913, 91020-D, 101011, 141104.

2-Mercaptoethanol was purchased from Sigma (Ref: 63689-100ML-F)

LDS Sample Buffer was purchased from Novex (Ref: NP0008)

Pierce BCA Protein Assay Reagent A was purchased from Thermo (Ref: 23228)

Pierce BCA Protein Assay Reagent B was purchased from Thermo (Ref: 1859078)

MES/SDS Running buffer was purchased from Bioland Scientific (Ref: MES01-03)

Transfer buffer for Bis-Tris gels was purchased from Bioland Scientific (Ref: TB01-03)

Tween 20 was purchased from Acros (Ref: 23336-0010)

Bovine Serum Albumin Fraction V was purchased from Fisher (Ref: BP1605-100)

Clarity Western ECL Substrate peroxide solution was purchased from BioRad (Ref: 102030801)

Clarity Western ECL Substrate luminol/enhancer solution was purchased from BioRad (Ref: 102030799)

Mixed gender human liver microsomes were purchased from Xenotech (Ref: H0160)

Alamethacin was purchased from Cayman (Ref: 11425)

Uridine 5'-diphosphoglucuronic acid trisodium salt was purchased from Sigma (Ref: U6751)

Amicon Ultra-2 mL Centrifugal Filters were purchased from Millipore (Ref: UFC201024)

Nitric Oxide detection kit was purchased from Promega (Ref: G2930)

HDAC1 siKO was purchased from IDT (Ref: 121666180)

HDAC3 siKO was purchased from IDT (Ref: 122029888)

HDAC6 siKO was purchased from IDT (Ref: 121666183)

HDAC1 OE plasmid was purchased from AddGene (Ref: 13820)

HDAC3 OE plasmid was purchased from AddGene (Ref: 13819)

HDAC6 OE plasmid was purchased from AddGene (Ref: 13823)

Tecan M200 Pro Spectrophotometer

Resazurin sodium salt was purchased from Sigma (Ref: R7017)

Balb/c mice were purchased through Jackson Laboratories

Antibodies

Acetylated tubulin antibody was purchased from Santa Cruz (Ref: sc-23950)

Actin antibody was purchased from Santa Cruz (Ref: sc-8432)

Acetylated Histone H3 antibody was purchased from Santa Cruz (Ref: sc-56616)

Acetylated Histone H4 antibody was purchased from Santa Cruz (Ref: sc-515319)

Histone H3 antibody was purchased from Santa Cruz (Ref: sc-8654)

p53 antibody was purchased from Santa Cruz (Ref: sc-126)

Hsp90 antibody was purchased from Santa Cruz (Ref: sc-13119)

HDAC6 antibody was purchased from Santa Cruz (Ref: sc-28386)

HDAC1 antibody was purchased from Santa Cruz (Ref: sc-81598)

HDAC3 antibody was purchased from Santa Cruz (Ref: sc-130319)

Acetylated-p65 K122/123 antibody was purchased from Santa LSBio (Ref: LS-C387648)

Acetylated-p53 K382 antibody was purchased from Cell Signaling (Ref: 2525)

p65 antibody was purchased from Santa Cruz (Ref: sc-8009)

conjugated Formyl antibody was purchased from Advanced Targeting (Ref: AB-T100)

conjugated Valeryl antibody was purchased from Advanced Targeting (Ref: AB-T089)

HMGB-1 antibody was purchased from Abcam (Ref: ab18256)

Premade Inhibitors

Tubastatin A was purchased from Biovision (Ref: 1724-1,5)

TrichostatinA was purchased from Cayman (Ref: 89730)

SAHA was purchased from Cayman (Ref: 10009929)

PD-106 was purchased from Cayman (Ref: 13212)

Panobinostat was purchased from Selleck Chem (Ref: S1030)

Entinostat was purchased from Selleck Chem (Ref: S1053)

2.2 Methods

En bloc recombinant HDAC acyl substrate screening

10 μL (2 ng) of recombinant human HDAC isozyme was added to 96 well black plate and briefly centrifuged. 10 μL of acyl-substrate solution (200 μM) was added to their respective wells. The plate was briefly centrifuged and incubated at 30°C for 2 hours. 5 μL of 30 mg/mL trypsin with 6 μM Trichostatin A was added to the solution and briefly centrifuged. After 1 hour, the plate was read via Tecan M200 Pro spectrophotometer at 360 nm (ex.)/460 nm (em.)

V_{max} analysis of recombinant human HDAC isozymes

100 μL (1 ng) of recombinant human HDAC isozyme solution was added to each well of a 96 well black plate. After centrifugation, 100 μL of serially diluted inhibitor at 2.5x desired concentration or 100 μL of 2x desired concentration serially diluted substrate added and incubated for 2 hours at 30°C for 2 hours. If substrate not yet added, 50 μL of serially diluted substrate at 5x concentration added and allowed to incubate at 30°C for an additional 2 hours. If substrate was already present for 2 hours, 50 μL of 30 mg/mL of trypsin and 6 μM TrichostatinA added and allowed to incubate at room temperature for 1 hour. The plate was read via Tecan M200 Pro spectrophotometer at 360 nm (ex.)/460 nm (em.). V_{max} and K_m values were calculated by GraphPad Prism's Michaelis-menten function.

Western blot analyses

Cells were cultured according to ATCC guidelines. Cells were plated at 500k cells/mL x 3 mL in clear, flat bottom 6 well plates. Cells were pre-incubated for 24 hours before addition of inhibitor

at various concentrations. The cells were allowed to incubate for 24 additional hours before being harvested, pelleted, and stored at -80°C . Cell pellets were lysed with $120\ \mu\text{L}$ of RIPA buffer. After lysing, the suspension is ultra-sonicated and centrifuged at $15000\ \text{RPM}$ for 15 minute at 4°C . $80\ \mu\text{L}$ of supernatant was mixed with $40\ \mu\text{L}$ of 15:85 (v/v) β -mercaptoethanol:LDS solution. The mixture was heated at 90°C for 15 minutes and stored for loading at -20°C . Prior to loading, the solution was flash thawed at 90°C . Lysates were based on BCA standard curves. Lysates were run on Invitrogen NuPAGE 4-12% Bis-Tris 15 well gels at 170V for approximately 60 minutes in MES buffer. Gels were transferred to methylcellulose and ran in transfer buffer at 30V for 180 minutes. Primary antibodies were added in 5% (w/v) Bovine Serum Albumin Fraction V. The respective antibody was incubated with the cellulose overnight at 4°C before addition of secondary antibody in 5% (w/v) Bovine Serum Albumin. Blots were incubated with 1:1 mixture of Peroxide/Luminol solution. Images were acquired using a GE ImageQuant LAS 4000. Global lighting adjustments of resulting images were made using Adobe Photoshop CC. Quantification was performed using Image Studio Lite 4.0.

Hek293 lysate deacylase activity

$100\ \mu\text{L}$ (1 ng protein) of Hek293 lysates were added to 96 well black plates. After brief centrifuge, $100\ \mu\text{L}$ buffer solution or 2.5x concentrated inhibitor solution added to respective wells. The plate was briefly centrifuged and incubated at 30°C for 2 hours. $50\ \mu\text{L}$ of $250\ \mu\text{M}$ fluorogenic acyl substrate was added and the plate briefly centrifuged before 2 hour additional incubation at 30°C . $50\ \mu\text{L}$ of $30\ \text{mg/mL}$ of trypsin and $6\ \mu\text{M}$ TrichostatinA added and allowed to incubate at

room temperature for 1 hour. The plate was read via Tecan M200 Pro spectrophotometer at 360 nm (ex.)/460 nm (em.).

Hek293 HDAC 1, 3, and 6, siRNA knockdown

Hek293 cells were cultured in ATCC recommended conditions. siRNAs selective for their respective HDACs were transfected and the cells were harvested 24 hours afterwards. Knockdown was confirmed with Western Blot analysis methodology.

Hek293 overexpression of HDACs 1, 3, 6, and NCoR2

Hek293 cells were cultured in ATCC recommended conditions in antibiotic free media. At 70% confluence in a 75 cm² culture flask the overexpression plasmids were transfected with lipofectamine LTX with plus reagent according to manufacturer's protocol over a 48 hour period. Overexpression was verified with Western Blot analysis methodology.

Acylation of Fatty Acid Free Bovine Serum

10 mg of Fatty Acid Free Bovine Serum Albumin was reacted with 1 mL of Valeryl Chloride (Sigma) or Acetic Anhydride (Acros) overnight at room temperature. These solutions were spun at 4°C at 15,000G for 15 minutes. The supernatant aspirated and the pelleted BSA resuspended in 1 mL of methanol. These washing and centrifugation steps were repeated 4 additional times. Residual volatiles were removed via lyophilization and the resulting dried pellet was resuspended in 1 mL of deionized water.

33.3 mg of Fatty Acid Free Bovine Serum was suspended in 5 mL of 99% Formic Acid (Sigma). The solution was raised to 65°C. 1.2 mL of Acetic Anhydride (Acros) was slowly dropped in via injection over 30 minutes. The solution was allowed to stir for 5 additional minutes before quenching with 1.5 mL of distilled ice water. Volatiles were removed under reduced pressure at room temperature. Residual solution was removed via lyophilization. The resulting pellet was resuspended in 3.3 mL of distilled water. This methodology was adapted from du Vigneaud, Dorfmann, and Loring (1932).

Cross Sensitivity Verification of Formyl-, Acetyl-, and Valeryl-Lysine Antibodies

0.5 μ L of each solution (10 mg/mL) was dotted onto nitrocellulose using a 0.25 μ L – 2 μ L pipette fitted with 10 μ L pipette tip. After the cellulose was dried, it was transferred into a 5% (w/v) solution of Bovine Serum Albumin. 1:1000 (v/v) of respective primary antibody was added and allowed to rock overnight at room temperature. The cellulose was washed several times and appropriate secondary antibody was added (1:1000 (v/v)). This solution was rocked for 1 hour at room temperature before washing and imaging. The nitrocellulose was incubated with a 1:1 solution of peroxide/luminol enhancer. Imaging was performed on GE ImageQuant LAS 4000.

IC₅₀ determination of potential HDAC inhibitors with recombinant human HDACs

50 μ L of enzyme solution (1 ng of enzyme) added to desired wells of 96 well black plate. 50 μ L of serially diluted inhibitor solution added and the plate briefly centrifuged before 5-120 minute incubation at 30°C. 25 μ L of 250 μ M fluorogenic acyl substrate added, the plate briefly centrifuged, and allowed to incubate for an additional 2 hours at 30°C. 50 μ L of 30 mg/mL of

trypsin and 6 μM TrichostatinA added and allowed to incubate at room temperature for 1 hour. The plate was read via Tecan M200 Pro spectrophotometer at 360 nm (ex.)/460 nm (em.).

Nitric Oxide production assay

RAW246.7 cells were cultured at 500,000 cells/mL for 24 hours according to ATCC guidelines. The culture media was refreshed and treatments were added three hours before the LPS (200 ng/mL) challenge. 50 μL of media was collected from each treatment and the media NO concentrations were determined using Griess reagents and Tecan M200 Pro spectrophotometer at 550 nm (em.). Concentrations were calculated based on a standard curve.

HMGB-1 detection

RAW246.7 cells were cultured at 500,000 cells/mL for 24 hours according to ATCC guidelines. The culture media was refreshed and treatments were added three hours before the LPS (200 ng/mL) challenge. Cell media was collected and concentrated using Amicon Ultra-4 spin column. The concentrated lysates were then mixed with 4x LDS loading buffer and run on a 4-12% polyacrylamide gel. The HMGB-1 levels were determined using HMGB-1 monoclonal antibody.

ESI-LCMS Glucuronidation Assays

A buffer solution containing 100 mM Tris HCl buffered to a pH of 7.5 at 37°C was used to dilute HLMs to a concentration of 250 $\mu\text{g}/\text{mL}$. To this solution was added 1 $\mu\text{g}/\text{mL}$ (final) of alamethicin and 5 mM MgCl_2 (final). This solution was rocked gently at 4°C for 15 minutes to allow pore formation. 180 μL of this solution was added to 10 μL of 5 mM inhibitor + 10 μL of 50 mM UDPGA

in H₂O or just 10 µL H₂O. This solution was gently rocked at 37°C for 12 hours before being quenched with a 47:50:3 (v/v/v) solution of water, acetonitrile and formic acid. After a 15 minute centrifugation at 15000g in 37°C conditions, 20 µL of supernatant was directly injected into Thermo LTQ Fleet LCMS.

ESI-LCMS Protocol

Water and methanol with 0.1% (v/v) formic acid were used as mobile phase. A gradient of 10% methanol 90% water was run isocratically for 2 minutes at 500 µL/min. The gradient then increased to 100% methanol over 15 minutes before returning to 10% methanol 90% water over the next three minutes. Capillary temperature was 350°C, with a spray voltage of 5 kV.

Molecular Docking against HDAC3

Modeling and simulations were performed using MOE 2014.09 (Chemical Computing Group, Inc) using structural PDB: 4A69, HDAC3 bound to human NCOR2 corepressor. Before analysis, proteins were protonated at pH 7.4 and structures energy minimized with heavy atoms constrained using the Amber12:ETH forcefield. Initial surface probe simulations focused on using **13b** as a probe for potential interaction sites, docking to the heterodimers using the entire surface as a target. The surface probe simulations left the protein dimer rigid and flexed the ligand. Initial placement calculated 200 poses using triangle matching with London dG scoring; the top 100 poses were then refined using forcefield and Affinity dG scoring. The consensus docking site was determined using Protein Ligand Interaction Fingerprint (PLIF) analysis. The HDAC3 bound to corepressor structure described above was used to estimate the propensity for

ligand binding (PLB) for the entire surface. Settings for MOE SiteFinder were: Probe Radius1: 1.5, probe radius 2: 1.8, isolated donor/acceptor: 3, connection distance: 2.5, minimum site size: 3, radius: 3. The consensus site between the surface probe and PLB analysis was used to create docking dummies for site focused docking simulations with an additional 4.5 angstrom radii. The focused dock used induced fit for the protein, allowing protein and ligand flexing. Initial placement calculated 200 poses using triangle matching with London dG scoring, the top 100 poses were then refined using forcefield and Affinity dG scoring.

MV4-11 EC₅₀ Analysis

The cells were grown according to ATCC protocol. Cells were plated at 20k cells/well in 96-well clear U-bottom plates and pre-incubated for 24 hours. Addition of serially diluted inhibitor (in medium) was performed followed by 48 hours of additional incubation. Addition of CellTiter-Blue occurred to a final concentration of 0.125 mg/mL. The mixture was allowed to incubate until sufficient color change occurred. Cell viability was measured as a function of resorufin intensity using a Tecan M200 Pro spectrophotometer, 560 nm (ex.)/590 nm (em.). Data were normalized to control wells and background was removed. EC₅₀ values were determined using GraphPad Prism's "log(inhibitor) vs. normalized response – Variable slope" function.

Human Peripheral Blood Mononuclear Cell Analysis

Cells were flash thawed from liquid nitrogen using RPMI-1640 media + Glutamax and 15% Fetal Bovine Serum and allowed to incubate overnight at 37°C, 5% CO₂. Cells were centrifuged at 1000 RPM for 5 minutes. Pelleted, healthy cells were reseeded at 50k cells/well and treated

immediately with serially diluted inhibitors (diluted in medium). Cells were allowed to incubate with inhibitor or vehicle for 24 hours before addition of 0.125 mg/mL (final) CellTiter-Blue. The mixture was allowed to incubate until sufficient color change occurred. Cell viability was measured as a function of resorufin intensity using a Tecan M200 Pro spectrophotometer, 560 nm (ex.)/590 nm (em.). Data were normalized to control wells and background was subtracted.

in-vivo MTD studies of **12d**, **13b**, and **14a**

Mice were injected once daily with 100-200 μ L of solution suspended in 95% sterile PBS/5% DMSO or 95% Neobee M5/5% DMSO with compounds of interest at either 10 or 20 mg/kg for 14 days. Mice were continually monitored for signs of moribund. Mice were humanely sacrificed if body mass decreased by more than 20% of baseline. Mice were sacrificed by CO₂ asphyxiation followed by cervical dislocation.

in vivo PK/PD studies of **13b** and **14a**

Animals (rat or mouse) are fed a standard laboratory rodent diet and housed in individual cages on a 12-hour light and 12-hour dark cycle with room temperature maintained at 22 \pm 30C and relative humidity at 50 \pm 20%. Animals are typically fasted overnight before dosing, with food returned after the 6 hour blood samples are obtained. Water is provided *ad libitum* throughout the study. The dosing solution of each test compound is prepared in a desired formulation. Three animals were dosed via intraperitoneal injection at 20 mg/kg. All blood samples (100-300 μ L per sample) are taken via appropriate vein (saphenous, jugular, or submandibular vein) at 5, 15, and 30 min and 1, 2, 4, 6, 8, and 24 h after dosing. Fluid replacement (1.5 mL of 0.9% sodium chloride injection, USP) will be administered subcutaneously once after the 2 hr blood sampling. Blood

samples are collected in BD Microtainer tubes coated with anticoagulant, placed on ice, and within 30 minutes, centrifuged at 15,000g for 5 min to obtain plasma samples. All plasma samples are stored at -70°C until analysis. Bioanalysis of PK/PD Samples Plasma samples are prepared as follows. Two or three volumes of acetonitrile containing internal standard is added to one volume of plasma to precipitate proteins. Samples are centrifuged (3000 g for 10 min) and supernatant removed for analysis by LC-MS/MS. Calibration standards and quality controls are made by preparation of a 1 mg/mL stock solution and subsequently a series of working solutions in methanol : water (1/:1, v/v) which are spiked into blank plasma to yield a series of calibration standard samples in the range of 1 ng/mL to 10 $\mu\text{g}/\text{mL}$ and quality control samples at three concentration levels (low, middle and high). All incurred PK/PD plasma samples are treated identically to the calibration standards and quality control samples. LC-MS-MS analysis is performed utilizing multiple reaction monitoring for detection of characteristic ions for each drug candidate, additional related analytes and internal standard. Pharmacokinetic Data Analysis Plasma concentrations are measured as described above to determine a concentration vs. time profile. The area under the plasma concentration vs time curve (AUC) is calculated using the linear trapezoidal method. Fitting of the data to obtain pharmacokinetic parameters is generally carried out using non-compartmental analysis. Key PK parameters reported following intravenous administration are as follows: terminal half-life $t_{1/2}$, initial plasma concentration C_0 , area under the plasma concentration vs. time curve AUC, volume of distribution at steady-state V_{ss} , total plasma clearance CL_p , and mean residence time MRT. Key PK parameters reported following extravascular administration are as follows: terminal half-life $t_{1/2}$, maximum plasma concentration C_{max} , time to reach maximum plasma concentration t_{max} , area under the plasma

concentration vs. time curve AUC, mean residence time MRT, and bioavailability F. All parameters are expressed for individual animals as well as mean, standard deviation, and coefficient of variation.

3 RESULTS AND DISCUSSION

3.1. Role of Histone Deacetylases as Lysine Deacylases: impact in medicinal chemistry and inflammatory diseases.

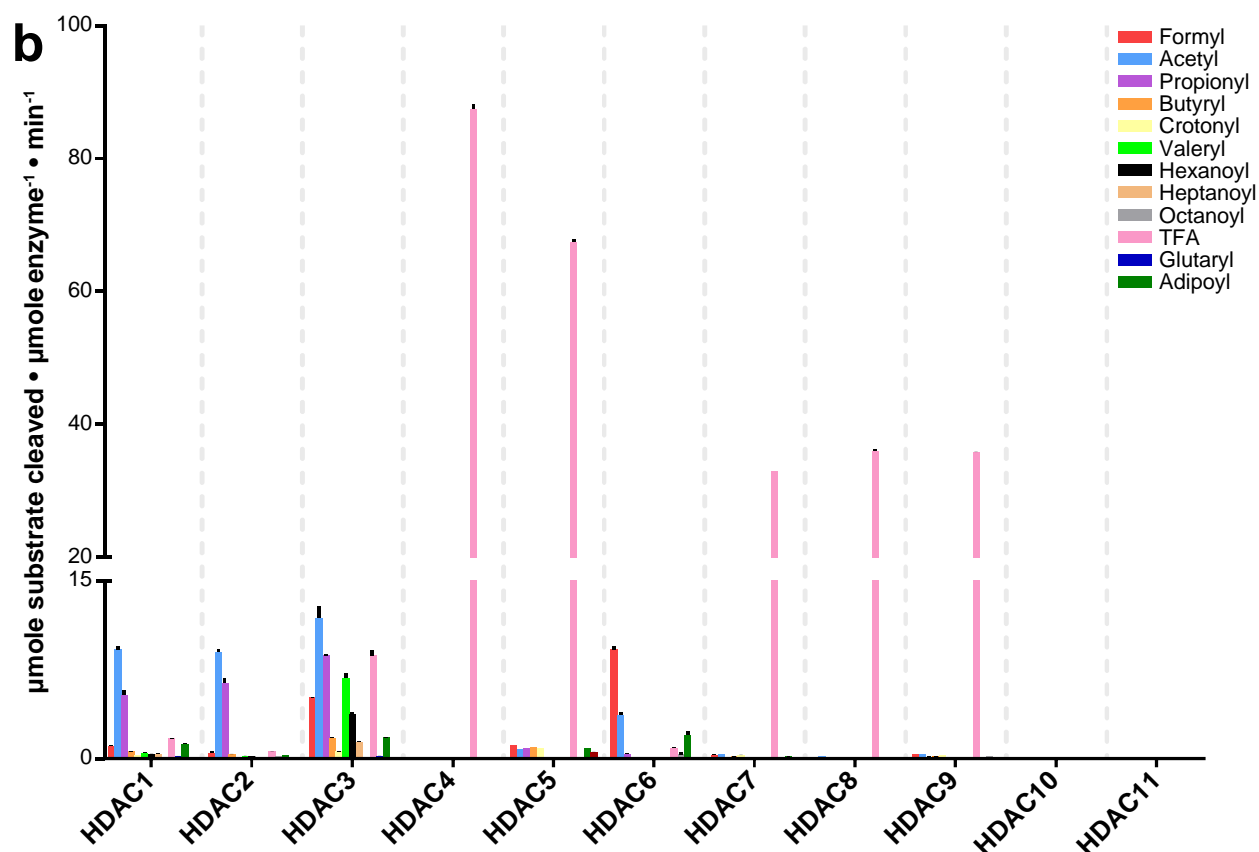
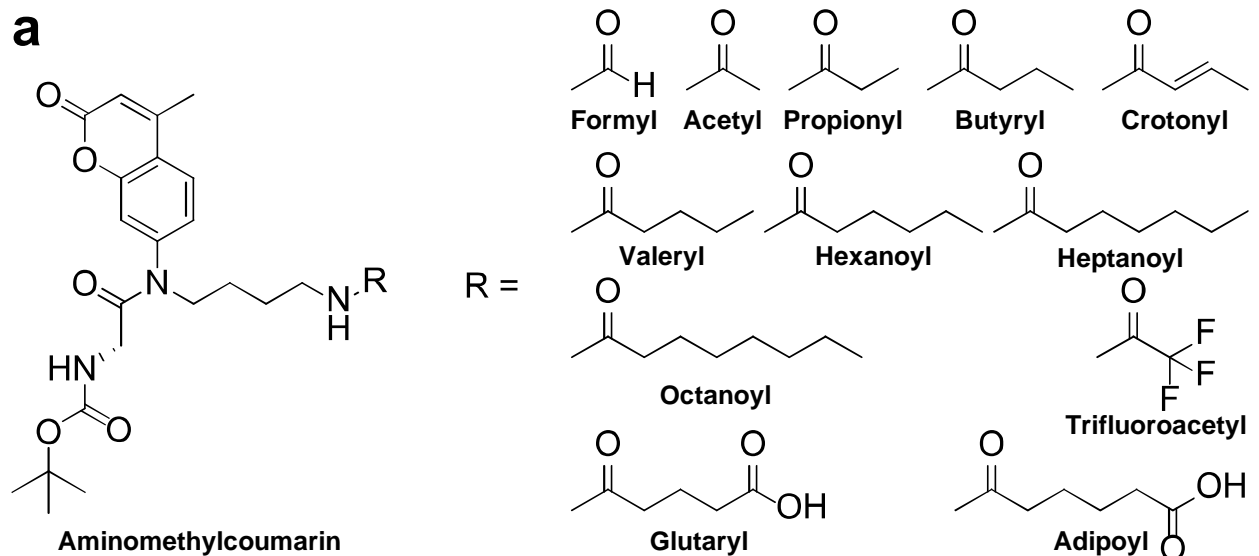
Rationale. Increasing evidence suggests that lysine post-translational modifications (PTMs) play multiple and extensive roles in cell signaling, akin to the well-studied phosphorylation, methylation, or ubiquitinylation PTMs.¹⁴² Initial proteomic studies using high-resolution mass spectrometry have identified at least 3,600 lysine acetylation sites on over 1,750 proteins.¹²⁹ In addition to lysine acetylation, a wider array of lysine acylations have gradually become recognized as important PTMs that control key cellular processes.¹⁴³ These modifications include lysine-formylation, acetylation, propionylation, butyrylation, crotonylation, glutarylation, malonyl/succinylation, and myristoyl/palmitoylation.^{136, 144-151} A common feature of these lysine acylations is most of them originate from coenzyme A (CoA) metabolites. The even numbered acyl groups such as acetyl and butyryl are likely derived from β -oxidation pathways, and the more complex succinyl modification likely stems from succinyl-CoA, most commonly used in regulation of cellular energy homeostasis. This crosstalk between metabolism and PTM status suggest a role for these lysine modifications to regulate enzymes in metabolic pathways.⁵⁰ Further, the identification of the diverse acyl-based PTMs has sparked studies focusing on the conditions under which they are attached and removed, leading to the demonstration that acylation of lysines is a non-specific process performed either through promiscuous Histone Acetyl Transferases or simply by non-catalytic chemical ligation.¹⁵² Unlike the promiscuous and even equilibrium-based ligation of acyl groups to lysines, the removal of these groups seems to be

more carefully controlled.¹⁵² One enzyme family shown to be able to remove glutaryl, malonyl/succinyl, and myristoyl/palmitoyl groups is the Sirtuins.^{136, 151, 153} As class III members of the Histone deacetylase (HDAC) family of enzymes, Sirtuins are NAD⁺-dependent deacylases. Contrarily, class I, II, and IV HDACs are metal-containing deacetylases. It has been suggested that class I, II, and IV HDACs possess the ability to also deacylate lysines rather than an isolated ability to deacetylate them. With this knowledge, we asked if these relatively novel acyl groups were substrates for any Zn²⁺-dependent HDAC, and if so, questioned whether there was any level of specificity these isozymes displayed toward certain acyl substrates.

HDAC isozyme deacylase kinetic profiling. Our study began by developing 12 different aminomethylcoumarin-based fluorogenic substrates that would mimic biologically relevant acyl-group PTMs (**Figure 3.1a**). These substrates were developed based on either known acids/acetyl-CoA bound esters that have been found in the blood stream in high concentrations and are likely to be ligated to the ε-N terminus of lysine or known PTMs shown to exist via mass spectrometry *ex vivo*. The non-biologically relevant Trifluoroacetyl (TFA) substrate was utilized as a positive control for class IIa HDACs and HDAC8 as it is the best-known substrate to be efficiently removed by these HDAC isozymes.¹⁵⁴ Utilizing these substrates and recombinant human HDACs, all zinc-dependent HDAC isozymes were tested *en bloc* for their ability to deacylate each substrate, with particular interest for substrate cleaved over time with constant enzyme and substrate concentrations (**Figure 3.1b**).

As previously reported, HDACs 1, 2, 3, and 6 demonstrated the most robust deacetylase activity compared to all other HDAC isozymes.⁹⁴ Also in line with external findings, class IIa HDACs and HDAC8 only displayed the ability to deacylate the TFA-based substrate.¹⁵ No appreciable

Figure 3.1. Acyl-substrate synthesis and en bloc profiling.



a) Chemical structures of 12 acyl-based substrates synthesized for kinetic profiling purposes. **b)** All synthesized acyl-substrate data against Zinc-dependent HDAC enzymes. $n = 3$; error bars are S.E.M.

deacylase activity was seen for HDACs 10 and 11 which falls in line with a similarly performed

study.⁹⁴ In addition to this, we saw no appreciable activity of any isozyme toward our heptanoyl-, octanoyl-, glutaryl-, or adipoyl-based substrates (**Figure 3.1b**). As such, the results of this experiment directed our focus toward more rigorous interrogation of the deacylase capacity of HDACs 1, 2, 3, and 6.

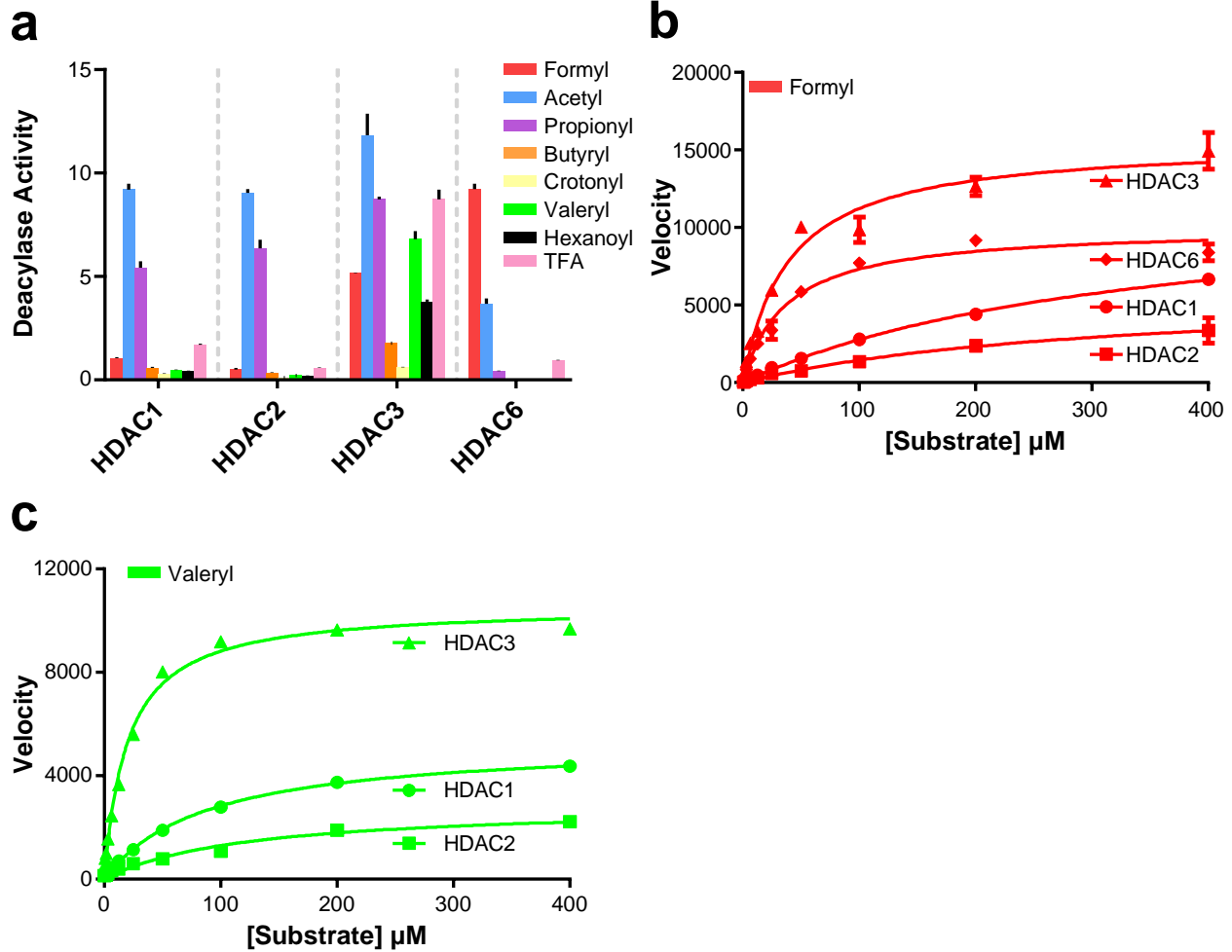
HDACs 3 and 6 demonstrated appreciable deacylase activity with HDAC6 demonstrating higher catalytic activity as a deacylase than as a deacetylase with the concentrations of enzyme and substrate used; HDAC3 possessed by far the most diverse ability to deacylate a variety of substrates, including the TFA-based substrate, with a particular preference for deacylating the butyryl-, crotonyl- and valeryl-based substrates compared to HDACs 1 and 2; and lastly, HDACs 1-3 were able to depropionylate with high catalytic efficiency (**Figure 3.1b** and **Figure 3.2a**). While there have been previous reports of HDAC3 possessing the ability to deacylate the TFA-based substrate⁹⁴, we sought to determine if this finding was due to an impurity of one or more class IIa HDACs in our HDAC3 solution. Briefly, HDAC3 was coincubated with TFA-substrate and vorinostat or diphenyl acetic hydroxamic acid (dPAHA). It has been previously shown that vorinostat possesses no appreciable inhibitory activity for class IIa HDACs⁹⁴ while dPAHA only possesses the ability to inhibit class IIa HDACs.¹⁵⁵ As expected, and in line with previous publications¹⁵⁶, vorinostat, but not dPAHA, was capable of altering HDAC3's ability to deacylate TFA substrate (**Figure 3.3**). Therefore, we are confident in associating this deacylase ability with HDAC3.

To further investigate the key findings from our initial screen, we performed V_{max} kinetic analyses on HDACs 1, 2, 3, and 6 versus substrates that were deacylated by one or more of these isozymes. We determined values of K_m , V_{max} , k_{cat} , and k_{cat}/K_m , the latter being the most well

accepted measurement of catalytic efficiency (**Table 3.1**). Interestingly, the K_m values of our formyl-based substrate vs HDACs 3 and 6 is nearly a log lower than the corresponding values for HDACs 1 and 2. The V_{max} value for HDAC1, despite being higher than the value for HDAC6 is not likely to be achieved in vivo, as the concentration required to achieve this would be in the millimolar range. (**Figure 3.2b and Table 3.1**). HDAC6 is the most catalytically efficient deformylase, however, it is still a more efficient deacetylase. Surprisingly, HDACs 1-3 displayed remarkable catalytic efficiency as depropionylases. Despite this, there appears to be very little difference in selectivity or efficiency between the three isozymes. The last intriguing finding from this kinetic study was the deacylation ability of HDAC3 toward butyryl-, crotonyl-, and valeryl-based substrates. It has been previously reported that HDAC3 was capable of deacylating crotonyl-substrates.¹⁵⁷ Unlike the depropionylase ability of HDACs 1-3, the deacylase activity toward these substrates was very specific to HDAC3. This seems to stem from HDAC3's ability to both bind these substrates more efficiently (lower K_m values) as well as efficiently cleave these substrates (higher k_{cat}/K_m values) from the ϵ -N of lysine than HDACs 1 or 2 (**Figure 3.2c and Table 3.1**). Most interestingly, the crotonyl-substrate binds to HDAC3 with very high affinity, however, there is little substrate turnover (k_{cat}) compared to the canonical acetyl-substrate (**Table 3.1**).

Interrogation of HDACs 3 and 6 as deformylases. Utilizing Hek293 cell lysates and various HDAC inhibitors, we sought to determine if this newly discovered deformylase activity both translated into a more robust cellular-based model and if it was affected by traditional small molecule inhibitors. Vorinostat, a class I and HDAC6 inhibitor⁹⁴; Tubastatin A (tubA), an HDAC6 specific

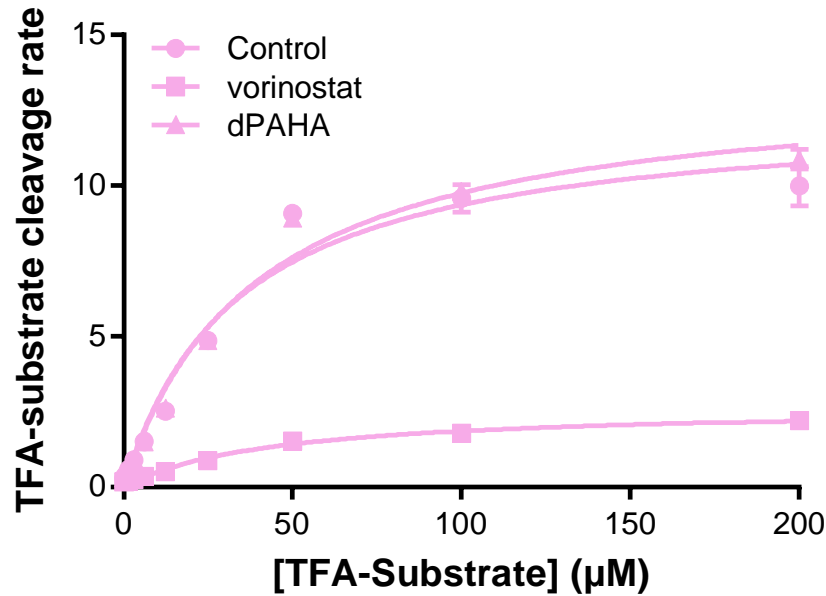
Figure 3.2. Acyl-substrate profiling.



a) Results of en bloc acyl-substrate profiling screen against HDACs 1, 2, 3, and 6. Y-axis units in $\mu\text{mole substrate cleaved} \cdot \mu\text{mole enzyme}^{-1} \cdot \text{min}^{-1}$. **b)** Vmax study of formyl-substrate vs HDACs 1, 2, 3, and 6. Y-axis units in $\text{pmole substrate cleaved} \cdot \text{s}^{-1} \cdot \text{mg enzyme}$. **c)** Vmax study of valeryl-substrate vs HDACs 1, 2, 3, and 6. Y-axis units in $\text{pmole substrate cleaved} \cdot \text{s}^{-1} \cdot \text{mg enzyme}$. $n = 3$; error bars are S.E.M.

inhibitor⁹⁵; and PD106, an HDACs 1-3 inhibitor¹⁵⁸ were all used to interrogate the individual and combined inhibitory effects of these small molecules against HDAC isozymes' cellular deacetylase activity (**Figure 3.4a**). The pan-inhibition of vorinostat at 1 μM demonstrated the ability to inhibit both deacetylation and deacetylation, in line with our kinetics study. The selective HDAC6 inhibitor Tubastatin A at 0.5 μM , well above its IC_{50} of <50 nM, did not affect overall deacetylation activity, but did lower deacetylation activity (**Figure 3.4b**). This is due to

Figure 3.3. HDAC3 purity test.



V_{max} comparison of HDAC3 with TFA-substrate. Y-axis units: $nM \cdot min^{-1}$. 1 μM for vorinostat and dPAHA. 2 hour incubation with inhibitors, 2 hour incubation with substrate. Dunnett's multiple comparisons test yields p-value of 0.6208 comparing dPAHA to control. p-value of 0.0002 comparing vorinostat to control. $n = 3$; error bars are S.E.M.

the ability of HDACs 1-3 to fulfill the deacetylase role in the cell even with an inhibited HDAC6.¹⁵⁹

The HDACs 1-3 inhibitor PD106 at 1 μM also showed a deacetylase inhibition profile akin to Tubastatin A, once again showing that selective inhibition of HDAC3 or HDAC6 is not enough to affect global deacetylation, but can affect deacetylation. Lastly, when Tubastatin A and PD106 were combined, additional lowering in deacetylation activity was seen while leaving deacetylation activity nearly unaffected (**Figure 3.4b**). Despite inhibiting HDACs 1, 2, 3, and 6, the combined treatment only affected deacetylation. This, unlike vorinostat's effect on deacetylation, can be explained through the concentrations used to achieve this result. At 1 μM , PD106 is below its IC_{50} value for HDACs 1 and 2 in Hek293 cells. As such, it is not likely to be inhibiting these enzymes strongly enough to induce a physiologic effect that would be seen with less discriminate class I HDAC inhibition at higher doses.

With the results of small molecule inhibition matching the data from our initial screening, we next interrogated the roles of HDACs 3 and 6 as deacetylases utilizing siRNA knockdown and

Table 3.1. Key isozyme profiling values

HDAC1	K_m (μM)	V_{max} (pmole \cdot s ⁻¹ \cdot mg protein)	k_{cat} (min ⁻¹)	k_{cat}/K_m (M ⁻¹ \cdot s ⁻¹)
Formyl	342	12300	8.24	402
Acetyl	36.6	24800	16.6	7580
Propionyl	13.1	9850	6.62	8410
Butyryl	49.1	1910	1.28	435
Crotonyl	2.40	802	0.380	2670
Valeryl	102	5330	3.56	582

HDAC2	K_m (μM)	V_{max} (pmole \cdot s ⁻¹ \cdot mg protein)	k_{cat} (min ⁻¹)	k_{cat}/K_m (M ⁻¹ \cdot s ⁻¹)
Formyl	313	5980	4.01	214
Acetyl	36.6	4.00x10 ³	2.69	1230
Propionyl	8.53	4.90x10 ³	3.29	6440
Butyryl	21.9	804	0.540	412
Crotonyl	3.20	1010	0.485	2520
Valeryl	122	2880	1.93	264

HDAC3	K_m (μM)	V_{max} (pmole \cdot s ⁻¹ \cdot mg protein)	k_{cat} (min ⁻¹)	k_{cat}/K_m (M ⁻¹ \cdot s ⁻¹)
Formyl	39.1	15600	9.30	3970
Acetyl	17.3	26900	16.0	15400
Propionyl	8.06	13900	8.31	17200
Butyryl	1.03	2560	1.53	24700
Crotonyl	0.114	758	0.362	53700
Valeryl	9.99	11100	6.63	11100

HDAC6	K_m (μM)	V_{max} (pmole \cdot s ⁻¹ \cdot mg protein)	k_{cat} (min ⁻¹)	k_{cat}/K_m (M ⁻¹ \cdot s ⁻¹)
Formyl	37.2	1.00x10 ⁴	19.1	8580
Acetyl	1.93	2130	4.04	34800
Propionyl	161	9.00x10 ²	1.72	178
Butyryl	N.D.	N.D.	N.D.	N.D.
Crotonyl	N.D.	N.D.	N.D.	N.D.
Valeryl	N.D.	N.D.	N.D.	N.D.

lipofectamine-induced transfection for overexpression in Hek293 cells (**Figure 3.4c-f**). Utilizing

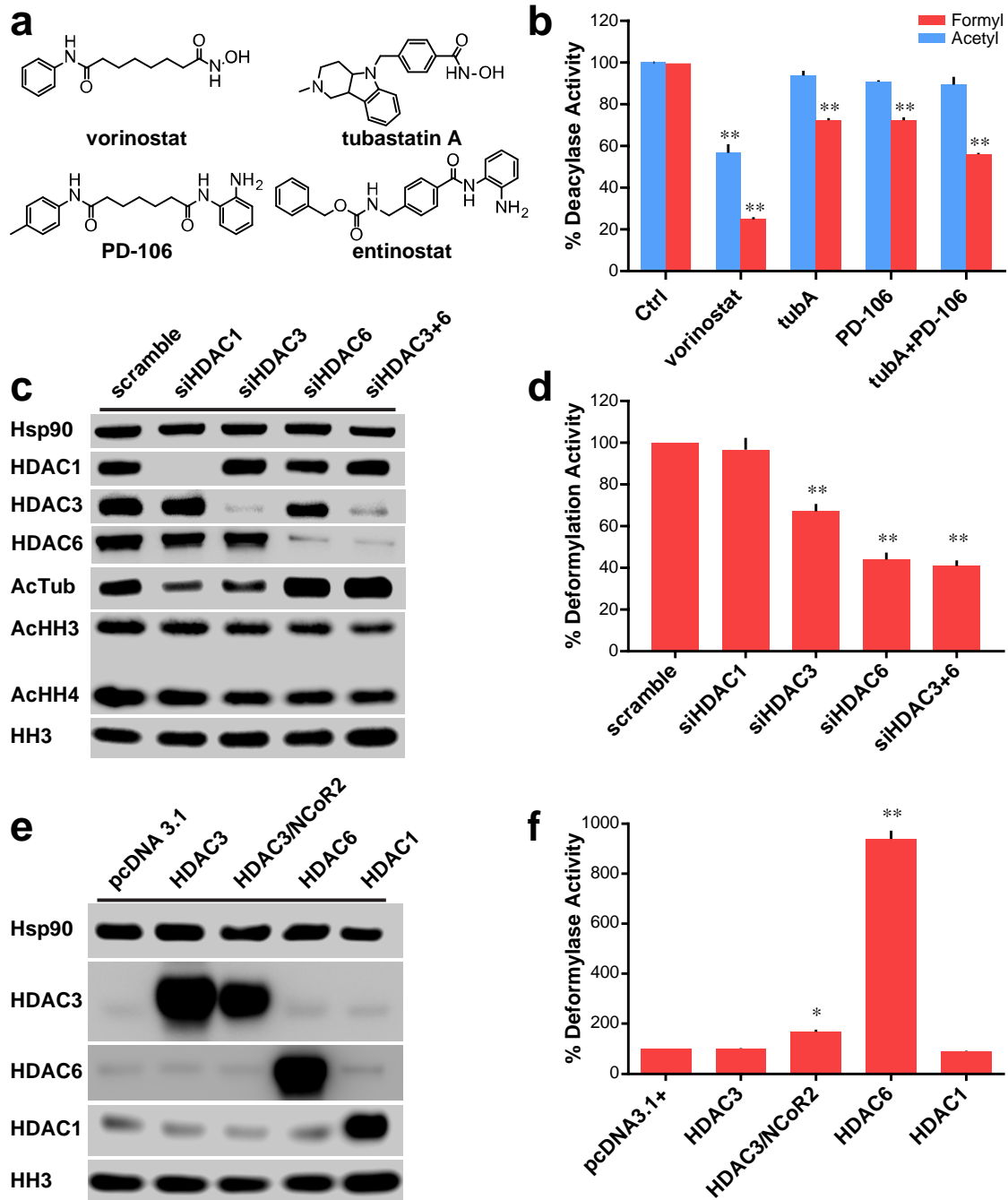
HDAC1 as a negative control, we see its knockdown bears no impact on deacetylation activity.

Knockdown of HDAC3, however, led to an approximate 35% decrease in deacetylation activity

of the cell lysate; knockdown of HDAC6 led to a more robust 55% decrease in deacetylation, and the concomitant knockdown of both isoforms led to a similar effect (**Figure 3.4d**). These data support the previous findings that HDACs 3 and 6 are majority or possibly even sole controllers of deacetylation in the cell with their suppression leading to extensive loss of activity. Following up these studies, we performed overexpression of HDACs 1, 3, and 6 (**Figure 3.4e**). Again, using HDAC1 as a negative control we see its overexpression bears no effect on deacetylase activity. Initial overexpression of HDAC3 without its required co-enzyme NCoR2 led to no appreciable increase in deacetylase activity. However, simultaneous overexpression of both enzymes led to an approximate doubling in activity. Overexpression of HDAC6 in similar fashion displayed a much more robust increase in deacetylation activity, leading to a near 10-fold increase in activity. These increases were not seen in the control pcDNA3.1 plasmid (**Figure 3.4f**). Taken together, these data suggest that HDACs 3 and 6 are both controllers of deacetylation, however, HDAC6 seems to be a more active deacetylase in vitro.

Interrogation of HDAC3's role as a selective deacetylase. We next chose to probe HDAC3's seemingly selective ability to remove short chain fatty acids four to five carbons in length. As carbon chain length for our synthesized substrates exceeded three, deacetylation activity decreased for all isoforms but HDAC3 (**Figure 3.1b** and **Table 3.1**). In particular, we were interested in the potential deacetylase activity of this isoform. Traditionally, short chain fatty acids created in vivo contain an even number of carbons. Valeryl groups, confirmed to exist in human serum as its fatty acid form in the high micromolar range¹⁶⁰, are the result of bacterial-based metabolism of sloughed intestinal cells from gut dwelling flora.¹⁶¹ Combining these data

Figure 3.4. Role of HDACs 3+6 in cellular deformylation



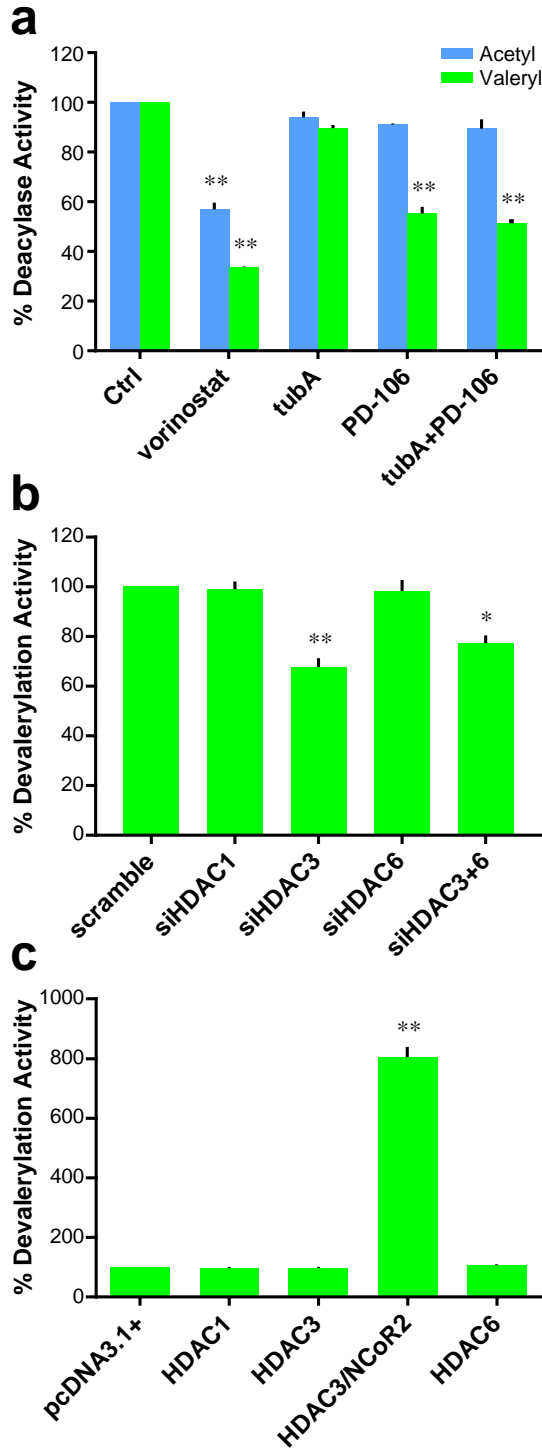
a) Chemical structures of small molecule inhibitors of HDACs 1, 2, 3, and 6. **b)** Comparison of effect on deacetylase and deacetylase activities of HeK293 lysates with various inhibitors for 24 hours; data normalized to control deacetylase activity; vorinostat and PD-106 used at 1 μ M, tubA used at 0.5 μ M. **c)** Western blot analysis of HeK293 cells with various siRNA transfections demonstrating selective and specific knockdown of targeted HDACs. **d)** Deformylase activity of siRNA treated HeK293 lysates; data normalized to scramble deacetylase activity. **e)** Western blot analysis of HeK293 cells transfected with various vectors to overexpress targeted HDACs. **f)** Deformylase activity of transfected HeK293 cells; data normalized to pcDNA3.1+ vector transfected cells. **b, d, and f** are $n = 3$; error bars are S.E.M. **c** and **e** are representative of $n \geq 2$ experiments. * = p -value < 0.01. ** = p -value < 0.0001. All statistical analyses were Dunnett's multiple comparisons of means to the means of their respective controls.

with our findings that HDAC3 may serve as a devalerylase, we discovered a potentially clinically relevant finding and chose to interrogate this observation further.

We proceeded to study the effect of HDAC isozyme inhibition with small molecule inhibitors on HDAC3's potential devalerylase activity using Hek293 lysates. Similar to the prior experiment, the pan-HDAC inhibition of vorinostat led to a lowering in both deacetylation as well as devalerylation (**Figure 3.5a**). The HDAC6 selective inhibitor Tubastatin A displays no effect on deacetylation and devalerylation, in line with our previous experiments that suggest HDAC3 is the only HDAC isozyme capable of devalerylation (**Figure 3.2a**). The utilization of the HDACs 1-3 inhibitor PD-106 demonstrates selective inhibition of devalerylation. The addition of Tubastatin A to this dosage leads to seemingly no difference in overall effect. Taken together, these data give further validity to our initial discovery that HDAC3 possesses devalerylase activity. To further test this finding, we again utilized our Hek293 lysates with HDAC isozymes knocked down (**Figure 3.4c**). With the selective knockdown of HDAC3, but not HDACs 1 or 6, we see an approximately 40% decrease in global deacetylation activity (**Figure 3.5b**). Using the Hek293 lysates with overexpressed HDAC1, HDAC3, HDAC3/NCoR2, and HDAC6 (**Figure 3.4e**), we indeed see that increased cellular concentrations of HDAC3 and its co-enzyme NCoR2 led to substantial increases in the devalerylation activity of our Hek293 lysates while overexpression with other plasmids did not (**Figure 3.4c**).

Interrogation of HDAC inhibitors on global protein formylation and valerylation. A potential pitfall for all previous experiments was that it relied on artificially synthesized fluorogenic substrates. To assuage this possible confounding factor, we utilized antibodies specific toward

Figure 3.5. Role of HDAC3 in cellular devalerylation.



a) Comparison of effect on devalerylase and deacetylase activities of Hek293 lysates with various inhibitors; data normalized to control deacetylase activity; vorinostat and PD-106 used at 1 μ M, tubA used at 0.5 μ M. **b)** Devalerylase activity of siRNA treated Hek293 lysates; data normalized to scramble deacetylase activity. **c)** Devalerylase activity of transfected Hek293 cells; data normalized to pcDNA3.1+ vector transfected cells. Data collected after 24 hours of treatment. n = 3; error bars are S.E.M. * = p-value < 0.01. ** = p-value < 0.0001. All statistical analyses were Dunnett's multiple comparisons of means to the means of their respective controls.

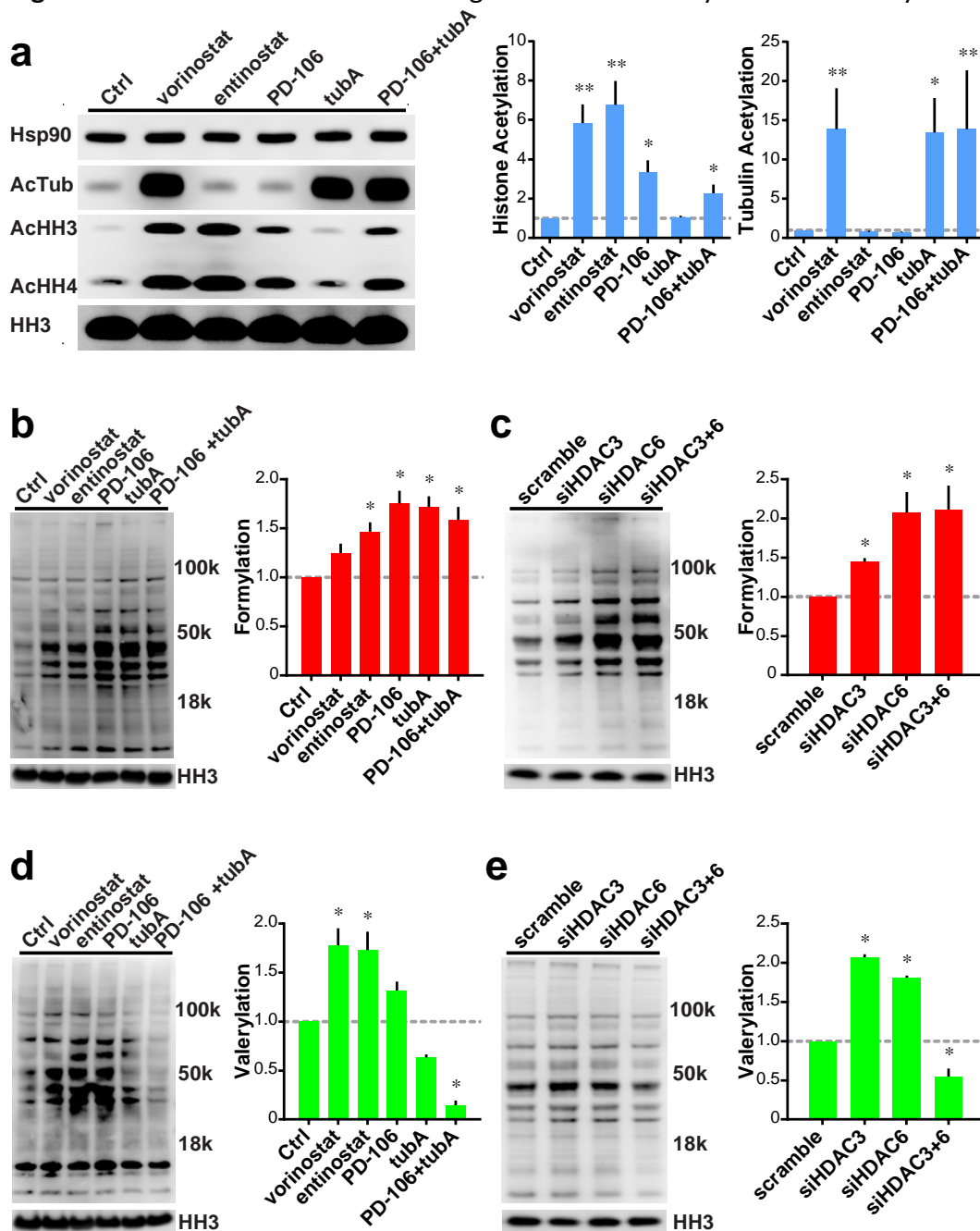
acetyl-, formyl-, and valeryl-lysine PTMs and measured the effect of small molecule inhibition and siRNA knockdown of individual HDAC isozymes on these levels. In agreement with previous results, the pan-HDAC inhibitor vorinostat induced hyper-acetylation of tubulin and histones H3 and H4. Also in line with published research, we see that entinostat¹⁶² and PD106 induced hyper-acetylation of histones without affecting tubulin acetylation levels. The HDAC6 specific inhibitor Tubastatin A, conversely, only affected acetylated tubulin levels (**Figure 3.6a**).

Translating from our previous findings, we see that the pan-HDAC inhibitor vorinostat causes global protein hyper-formylation due to its concomitant inhibition of HDACs 3 and 6, however its increase was not statistically significant with a p-value of 0.072. Entinostat and PD-106 are also capable of this effect, although their mechanism is likely to be through HDAC3 inhibition, without inhibition of HDAC6 at the concentrations used. Lastly, the HDAC6-specific inhibitor Tubastatin A also induced global protein hyper-formylation through its inhibition of HDAC6 (**Figure 3.6b**). The combination of PD-106 and Tubastatin A led to a non-significant decrease compared to either agent alone.

Following these experiments, we utilized siRNA knockdowns of HDACs 3 and 6 to determine the effect of each isozyme more specifically. Knockdown of HDAC3 alone led to a significant rise in global protein formylation levels. Compared to HDAC3, knockdown of HDAC6 led to an even greater, arguably significant, increase in global formylation with a p-value of 0.049. The concomitant knockdown of HDACs 3 and 6 together had no significant effect compared to HDAC6 alone, further suggesting HDAC6's dominant role as a deacylase (**Figure 3.6c**).

Moving our attention toward global protein valerylation, we repeated these experiments using antibodies specific for valerylated lysine. Inhibition of HDAC3 with vorinostat, entinostat,

Figure 3.6. Roles of HDACs 3 and 6 on global cellular formylation and valerylation.



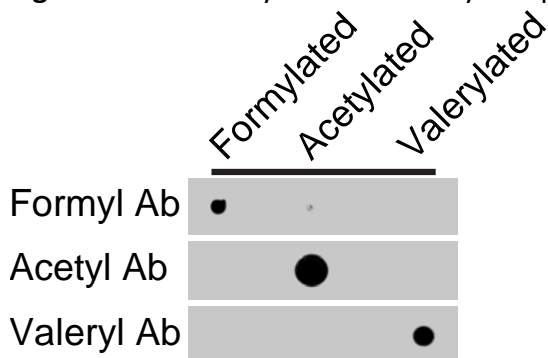
a) left: Western blot analysis of Hek293 cells treated with small molecule HDAC inhibitors. **right:** Quantification of histone and tubulin acetylation normalized to HH3 levels. **b) left:** Global formylation levels of Hek293 cells treated with HDAC inhibitors. **right:** Quantification of global formylation normalized to HH3 levels. **c) left:** Global formylation levels of Hek293 cells treated with siRNA. **right:** Quantification of global formylation normalized to HH3 levels. **d) left:** Global valerylation levels of Hek293 cells treated with HDAC inhibitors. **right:** Quantification of global valerylation normalized to HH3 levels. **e) left:** Global valerylation levels of Hek293 cells treated with siRNA. **right:** Quantification of global valerylation normalized to HH3 levels. All inhibitors used at 1 μ M, except tubA at 0.5 μ M. Data recorded after 24 hours of treatment, representative western blots of $n \geq 3$ experiments; error bars are S.E.M. * = p-value < 0.01. ** = p-value < 0.0001. All statistical analyses were Dunnett's multiple comparisons of means to the means of their respective controls.

or PD-106 led to global protein hyper-valerylation, however the increase for PD-106 was non-significant with a p-value of 0.120. We also see that selective inhibition of HDAC6 with Tubastatin A leads to a non-significant hypo-valerylation (p-value 0.073). Further, combined HDAC3 and HDAC6 inhibition with PD-106+Tubastatin A leads to an even more pronounced, significant hypo-valerylation effect (**Figure 3.6d**). One explanation for this discrepancy was off-target effects of either Tubastatin A or PD-106. We used siRNA to study this, hypothesizing that specific knockdown of either isozyme would more readily determine each isozyme's effect on valerylation levels. Knockdown of HDAC3 led to the expected result of hyper-valerylation, however, knockdown of HDAC6 alone led to a hyper-valerylation as well. Even more interesting still is the hypo-valerylation that occurs when both HDACs 3 and 6 are knocked down together (**Figure 3.6e**). One possible explanation for this discrepancy could lie with the translatability of our valeryl-based substrate in vitro and in cellular lysate models versus the natural substrate. Another explanation is that knockdown of HDAC6 may lead to a dissolution of a key complex required for maintenance of lysine acylation levels.¹⁶³ Lastly, another possibility may be a non-selective antibody. To assuage this possibility we performed dot blot analyses with each antibody against formylated-, acetylated-, or valerylated-bovine serum albumin. The results demonstrate, and in findings with the manufacturer's ELISA specifications, that each antibody is highly selective for its appropriate acyl-group (**Figure 3.7**).

Substrate driven development of HDAC3 specific inhibitor. We realized that the crotonyl-substrate possessed very unique properties with HDAC3, but not HDACs 1, 2, or 6. Its nanomolar Km value led to HDAC3 binding very tightly to the substrate, however, very little substrate

turnover (kcat) was seen. Further, the crotonyl-substrate's binding affinity was over 20-fold selective for HDAC3 compared to HDACs 1 or 2 (**Table 3.1**). Taken together, we hypothesized that the crotonyl-substrate could act as a competitive inhibitor against the canonical acetyl substrate. Further, we wondered if this specificity in K_m translated to specificity in inhibition. Our data show

Figure 3.7. Antibody cross reactivity comparison with acylated Bovine Serum Albumin.



Solutions (10 mg/mL) of acylated BSA were dotted onto nitrocellulose (0.5 μ L) and incubated with various antibodies. There is little appreciable cross-reactivity between all used antibodies indicating a high level of specificity toward advertised target. Representative blot, n = 2.

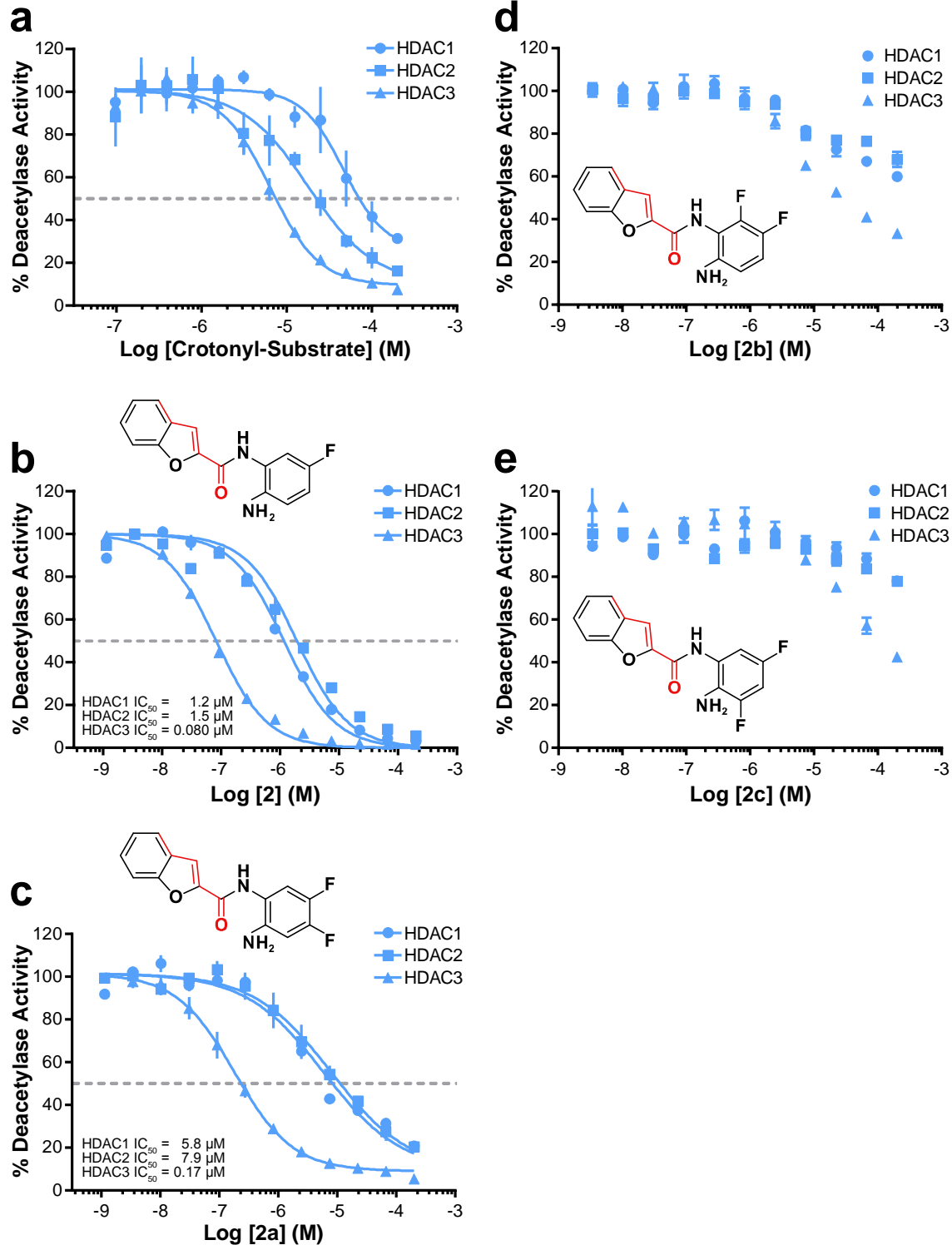
that indeed the crotonyl-substrate is a notably selective HDAC3 inhibitor (**Figure 3.8a**). Encouraged with this result, and recognizing the potential of developing a novel, selective chemical tool to study the HDAC3 isozyme selectively^{10, 164}, we performed a rudimentary SAR analysis based around the trans-geometry of the crotonyl acyl-group, the length of the HDAC3 selective valeryl acyl-group, and the HDAC 1, 2, 3 selective benzamide metal-chelation moiety (**Table 3.2**).

We began simplistically with a benzamide structure with an attachment to mimic the crotonyl- and valeryl-modifications simultaneously, compound **1**. We gained potency by utilizing a trans-cyclopentadiene ring which further forced proper conformation. Between all heterocycles tried, the oxygen containing furan ring of **1a** seemed most promising from its potency and mild selectivity toward HDAC3. Building off of **1a**, addition of a fused benzene ring

led to compound **1f** which demonstrated nanomolar HDAC1 and HDAC3 IC₅₀ values with its benzofuran group. While **1f** was our best lead from the first round of SAR, it lacked the selectivity we believed possible for HDAC3, only demonstrating a 2 fold preference for HDAC3 over HDAC1. Looking back at our initial acyl-substrate screen, we also noted HDAC3's ability to deacylate the TFA-substrate which HDACs 1 and 2 lacked. Additionally, a recent publication also reported on fluorination based HDAC3 selectivity.¹⁶⁵ As such, we utilized these findings by incorporation of a fluorine to **1f** which resulted in compound **2**. This inhibitor possessed 15 fold selectivity for HDAC3 compared to HDAC1 (**Figure 3.8b**) while also increasing its inhibitory potency further toward HDAC3. We added a second fluorine to **2** to generate **2a** which resulted in a slightly weaker HDAC3 inhibitor, but established even greater selectivity of the molecule for HDAC3 (**Figure 3.8c**). Curious to test the effect of fluorination in other positions around the benzene ring, we also developed and interrogated **2b** and **2c**. These inhibitors, possessing different fluorine positioning than **2a** show very little efficacy in vitro (**Figures 3.8d** and **3.8e**). Concluding our substrate driven SAR, compound **2a** possessed an IC₅₀ for HDAC3 of 170 nM and was over 30 fold selective for HDAC3 compared to other class I HDACs. Further testing of **2a** revealed it possessed interestingly selective slow-binding toward HDAC3 but not HDACs 1 or 2 (**Figure 3.9**).

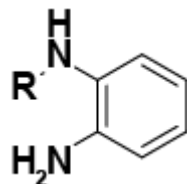
Effects of 2a on NF-κB acetylation, NO signaling, and HMGB-1 secretion. A previous study has shown that cytosolic localization of HDAC3 depends on its interaction with IκBα within an intact NF-κB complex, thereby suggesting that it plays a potential role in the NF-κB signaling.¹⁶⁶ Using **2a**, **2b**, **2c** and other known HDAC inhibitors with different HDAC isozyme selectivity, we examined these HDAC inhibitors' relative effects on acetylation of NF-κB p65, p53, histones H3

Figure 3.8. Substrate-specificity driven development of HDAC3 selective inhibitor.



a) IC_{50} of HDACs 1-3. The crotonyl-substrate serves as a fairly potent and selective HDAC3 inhibitor. IC_{50} values for HDACs 1-3 respectively: 46.5 μ M, 18.1 μ M, 6.42 μ M. **b)** IC_{50} of HDACs 1-3 vs **2**. **c)** IC_{50} of HDACs 1-3 vs **2a**. **d)** IC_{50} of HDACs 1-3 vs **2b**. **e)** IC_{50} of HDACs 1-3 vs **2c**. All data normalized to vehicle (DMSO) control. Graphs **a-c** fit via GraphPad Prism log(inhibitor) vs. normalized response – variable slope parameters. $n \geq 3$; error bars are S.E.M.

Table 3.2. SAR of substrate-driven HDAC3 specific inhibitors.



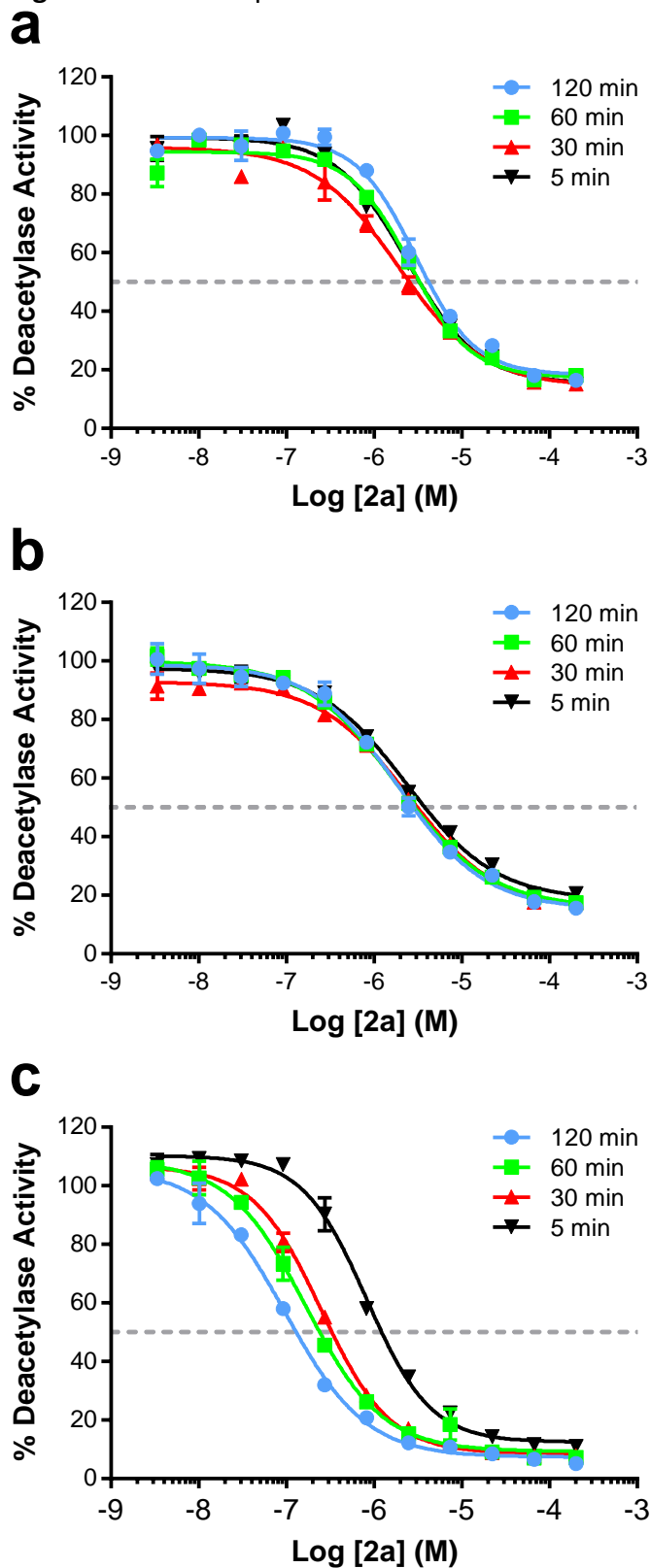
Name	R-Group	HDAC1 IC ₅₀	HDAC3 IC ₅₀
1		16.7 μM	4.00 μM
1a		3.20 μM	0.721 μM
1b		5.31 μM	1.43 μM
1c		6.92 μM	1.80 μM
1d		2.12 μM	0.418 μM
1e		4.11 μM	1.37 μM
1f		0.357 μM	0.209 μM

and H4, and tubulin. The selective HDAC3 inhibitor **2a** induced NF-κB p65 Lys122 and p53 Lys382 acetylation without the induction of histone H3/H4 or tubulin acetylation (**Figure 3.10a**). This

result is consistent with previous studies that demonstrated that deacetylation of Lys122/123 of NF-κB p65 is controlled by HDAC3, and that inhibition of HDACs 1 or 2 has little effect on their acetylation status.⁴² However, our finding that selective HDAC3 inhibition with a small molecule is capable of inducing hyperacetylation of p53 Lys382 is novel. Ryu et al. recently demonstrated that HDAC6 is also capable of controlling the acetylation status of Lys382 of p53.²⁸ Unfortunately, they did not have an HDAC inhibitor capable of targeting HDAC3 without HDAC6 to delineate out the impact of HDAC3 inhibition vs HDAC6 inhibition on this residues acetylation status. Further, they demonstrated the use of tubA at 2 μM for 24 hours was able to induce hyperacetylation of Lys382 in their tested HCT116 and HT29 cells. Our findings do not demonstrate this increase (Figure 6a), but could be a result of a cell-line specific effect or our use of a lower dose comparatively. Further, and against the findings by Ryu et al., the class I selective inhibitor, romidepsin, was shown to induce hyperacetylation of Lys373 and Lys382 at reasonable concentrations in the A549 cell line.¹⁶⁷

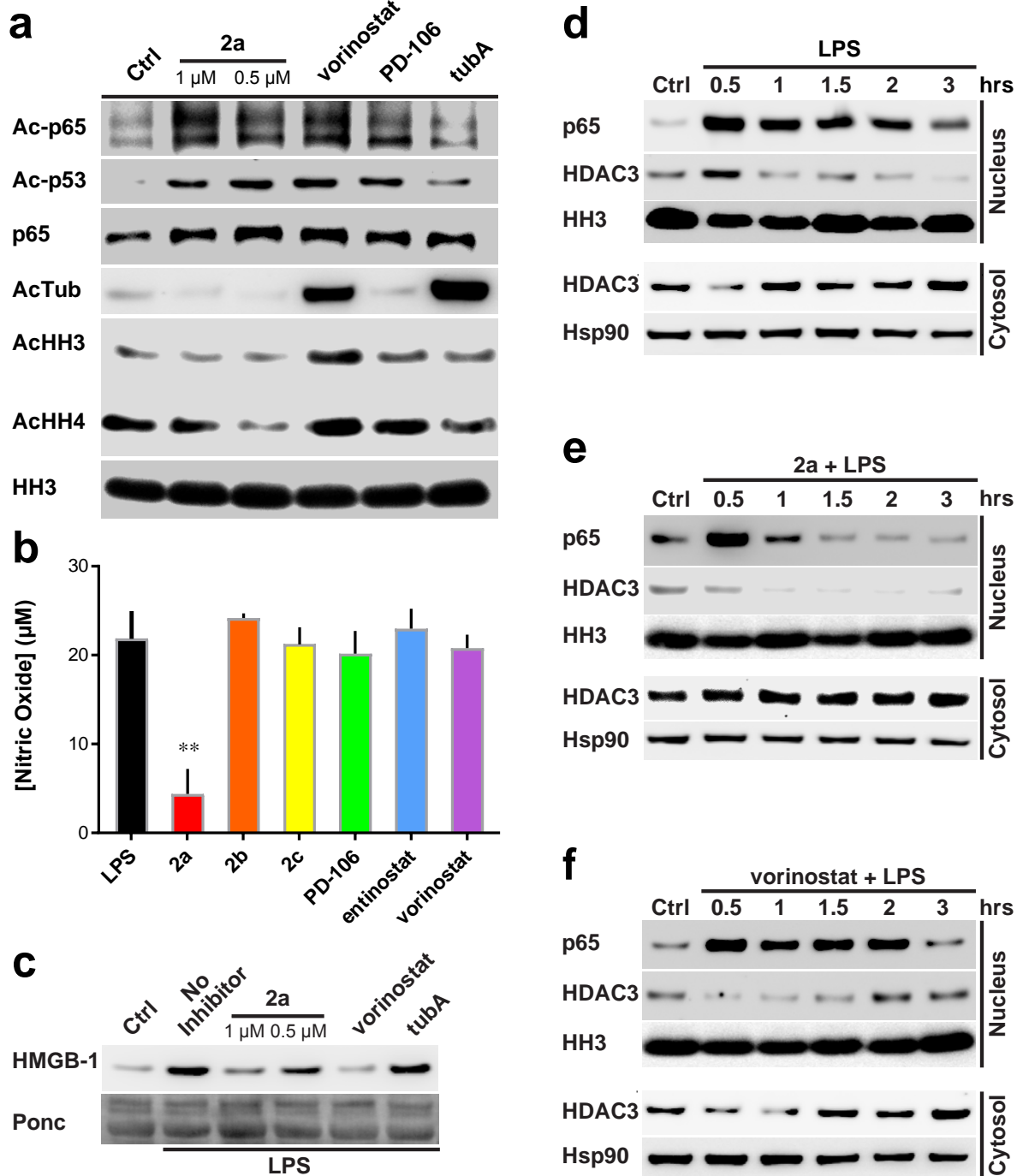
We furthered our investigation on the significance of HDAC3 inhibition and its effects on NF-κB activation, nitric oxide (NO) production, and HMGB-1 secretion in RAW264.7 macrophages challenged with bacterial lipopolysaccharide (LPS). 2a decreases NO production after LPS induction in RAW264.7 while all other inhibitors, including 2b and 2c, failed to affect NO production (Figure 3.10b). It should be noted that PD-106, vorinostat, and entinostat, being HDAC3 inhibitors, did lower Nitric Oxide release. However, when cell viability was taken into account, as these inhibitors proved to be more lethal than 2a-c, it was found this decrease was completely offset when we normalized the data to cell count/viability. LPS also induces HMGB-1

Figure 3.9. Time dependent Kinetics of HDACs 1-3 vs **2a**.



1 a) HDAC1 b) HDAC2 c) HDAC3. **2a** shows time-dependent inhibition toward HDAC3 but not HDACs 1 or 2 at 30°C. n = 2; error bars are S.E.M.

Figure 3.10. Effects of HDAC inhibition on NF- κ B p65 acetylation and inflammatory responses.

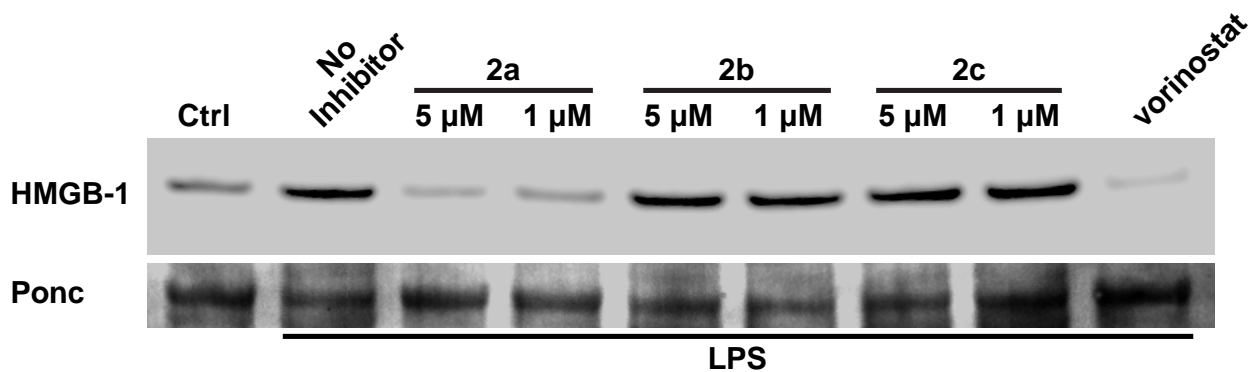


a) Western blot analysis of RAW264.7 cells treated with various HDAC inhibitors; vorinostat and PD-106 used at 1 μ M, tubA at 0.5 μ M. **b)** NO concentration secreted from RAW264.7 treated cells; normalized to control treated viable cell concentration. 1 μ M used for all inhibitors. $n \geq 3$. **c)** Western blot analysis of RAW264.7 cells. HMGB-1 secretion monitoring with ponceau stain as loading control. Cells were treated for six hours. 1 μ M vorinostat and 0.5 μ M tubA used. **d-f)** Western blot analysis of LPS-treated RAW264.7 cells. Nuclear and cytosolic fractions split. **2a** and vorinostat used to assess regulation of HDACs on Ac-p65 subcellular localization. Representative westerns of $n \geq 2$ experiments; error bars are S.E.M. ** = p -value < 0.0001.

secretion, a late mediator of lethality in sepsis, in RAW264.7 cells.¹⁶⁸⁻¹⁶⁹ Previous studies have shown that the HMGB-1 protein contains multiple acetylation and formylation modifications, which control its cellular localization and secretion.^{145, 170} **2a**, but not **2b** or **2c**, also blocked HMGB-1 secretion from the activated macrophage cells (**Figure 3.10c** and **Figure 3.11**). These data suggest that HDAC3 activity is required for proper inflammatory activation and response.

As HDAC3 activity is linked to I κ B α and NF- κ B activation, we further investigated the effect of **2a** on NF- κ B p65 and HDAC3 after LPS induction. As previously reported, LPS induced the nuclear localization of p65 and HDAC3.¹⁶⁶ Cells treated with **2a** had significantly shorter p65 nuclear retention times as well as diminished nuclear localization of HDAC3 (**Figure 3.10d**). Interestingly, in the **2a**-treated cells, the nuclear localization of HDAC3 decreased slowly with time after LPS treatment (**Figure 3.10e**). This effect was not as pronounced in the vorinostat treated cells (**Figure 3.10f**). This suggests that HDAC3 activity is likely involved in multiple regulatory functions, such as its own cellular localization, in addition to p65 acetylation status and gene transcription regulation. Further, selective inhibition of HDAC3, but not pan HDAC inhibition as seen with vorinostat, may be key to controlling HDAC3 and p65 subcellular localization.

Figure 3.11. Western blot analysis of RAW264.7 cells.



HMGB-1 secretion monitoring with ponceau stain as loading control. Cells were treated for six hours. 1 μ M vorinostat used. Representative blot of n = 2 experiments.

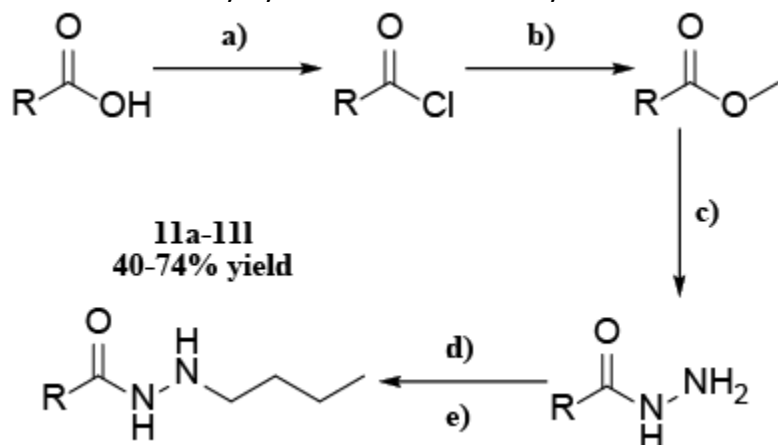
3.2. Development of Allosteric Hydrazide-Containing Class I Histone Deacetylase Inhibitors for Use in Acute Myeloid Leukemia.

The goal of our structure-activity relationship studies for the hydrazide-based compounds was to develop a potent and selective inhibitor of class I HDACs, with particular emphasis on HDAC3 inhibition. HDAC3 has shown increasing promise as a novel target to combat leukemia as its inhibition controls hematopoiesis. As such, lead analogs from these studies were tested in pre-clinical leukemia models to determine efficacy and tested against solid tumor models and PBMCs to demonstrate selectivity.

Chemistry of butylhydrazide analogs. We began our structure-activity relationship studies by attempting to identify an ideal substituent for the carbonyl of the hydrazide motif. As shown in **Scheme 3.1**, we began with either an aromatic carboxylic acid, acyl chloride, or ester. Using commercially available starting materials, we generated the corresponding hydrazide molecule through reactions a, b, and c, depending on the composition of the starting molecule. Target hydrazide compounds were reacted with butylaldehyde to generate the compound of interest. Carboxylic acids were reacted with oxalyl chloride in methylene chloride with catalytic amounts of dimethylformamide (**Scheme 3.1**, reaction a). The resulting acyl chloride, or commercially purchased acyl chlorides were stirred in methanol to give the corresponding methyl ester (**Scheme 3.1**, reaction b). The generated or commercially purchased methyl esters were refluxed in methanol with a hydrazine water salt to generate a hydrazide of interest (**Scheme 3.1**, reaction c). The resulting compounds were then refluxed in ethanol in the presence of magnesium sulfate and butylaldehyde followed by a reduction with sodium cyanoborohydride in acidified methanol

to give the desired products **11a-11l** (**Scheme 3.1**, reactions d and e). A notable exception to this scheme was the synthesis of **11d**, which was unable to be esterified from the commercially available corresponding acyl chloride until the addition of two equivalents of triethylamine. Additionally, compound **11i** spontaneously formed the corresponding pyrazolidinone when reacted with the hydrazine salt due to the presence of an unsaturated bond alpha to the ester carbonyl. Instead, the carboxylic acid starting material was reacted with HOBt and DCC in acetonitrile. The resulting intermediate was reacted with the hydrazine water salt in acetonitrile to yield the corresponding hydrazide. Lastly, compound **11l** was the result of reacting methyl 4-(aminomethyl)benzoate with benzoyl chloride to generate the methyl ester corresponding to **11l**. From here, the reaction carried on as shown in **Scheme 3.1**, reactions d and e.

Scheme 3.1. Butylhydrazide Derivatives Synthesis



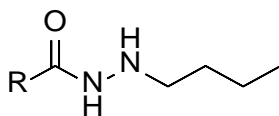
Reagents and conditions: (a) methylene chloride, rt, oxalyl chloride, cat. DMF; (b) MeOH, rt; (c) MeOH, reflux, $\text{NH}_2\text{NH}_2 \cdot \text{H}_2\text{O}$; (d) EtOH, reflux, butaldehyde, MgSO_4 ; (e) MeOH, rt, NaBH_3CN , conc. HCl

HDAC inhibition of series 11 inhibitors. With the primary goal of designing a potent and ideally selective series inhibitor of class I HDAC inhibitors, we screened compounds **11a-11l** against HEK293 cell lysates using a fluorogenic acetylated lysine substrate. All compounds were tested thrice against HEK293 lysate and recombinant HDAC3. If the compound was found to possess an

IC₅₀ less than 100 nM against HDAC3 and less than 1000 nM against HEK293 lysate, it was tested thrice against recombinant HDACs 1 and 2 to determine selectivity for class I. The summation of the corresponding findings are summarized in **Table 3.3**, with data for HDACs 1 and 2 in **Table 3.4**.

The relatively inefficacious compounds **11b**, **11d**, **11f**, and **11g** demonstrated that heterocyclic substitution was not favored compared to phenyl groups. Further, a para position oxygen provided mild benefit as seen in compounds **101** and **11c**. However, a carbon, whether aliphatic or aromatic, was superior in this position, as seen in **11e** and **11l**. Interestingly, the creation of an unsaturated bond at the alpha position to the carbonyl, as seen in compound **11i**, provided ~6-fold increased HDAC3 inhibition when compared to its saturated counterpart **11h**. This can be explained as it creates an acrylamide-like structure which is likely capable of forming covalent bonds with cysteine residues on the HDAC enzyme; allowing for enhanced inhibition ability. While neither compound was particularly potent, it was interesting to see the sharp difference in activity between **11j** and **11k**. This possibly demonstrates that the binding pocket near this position is relatively narrow and the wider surface area of the 1-naphthyl group of **11j** is unable to bind adequately, whereas the 2-naphthyl group of **11k** is able to fit more reasonably or is less sterically hindered. The compound **11l** possessed the most potent carbonyl attachment, with an IC₅₀ of less than 10 nM and K_i of less than 2 nM for HDAC3 and 8- to 10-fold selectivity for HDAC3 compared to HDACs 1 and 2. Using this finding, we next pursued structure activity relationships on substitutions of the β-nitrogen relative to the hydrazide.

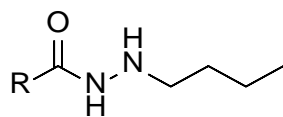
Table 3.3. In vitro inhibition of Hek293 lysates and recombinant HDAC3 for series 11 inhibitors.



Name	R Group	IC ₅₀ ^a (nM)		Name	R Group	IC ₅₀ ^a (nM)	
		HDAC3	Hek293			HDAC3	Hek293
11a		156.7 ± 28.55	727.3 ± 10.75	11g		5001 ± 372.5	>10000
11b		1362 ± 197.3	1688 ± 38.05	11h		1892 ± 227.3	>10000
11c		311.7 ± 42.82	1691 ± 298.3	11i		294.5 ± 32.64	1440 ± 86.09
11d		1547 ± 429.8	4676 ± 909.0	11j		>10000	>10000
11e		68.85 ± 9.39	1307 ± 210.0	11k		892.0 ± 72.47	2844 ± 948.0
11f		903.9 ± 154.3	3461 ± 669.0	11l		8.56 ± 2.06	292.6 ± 8.68

IC₅₀ values (bold) are the mean of at least three experiments. Values after are the Standard Error of the Mean.

Table 3-4. Class I HDAC and Hek293 lysate IC₅₀ values for **11l**.



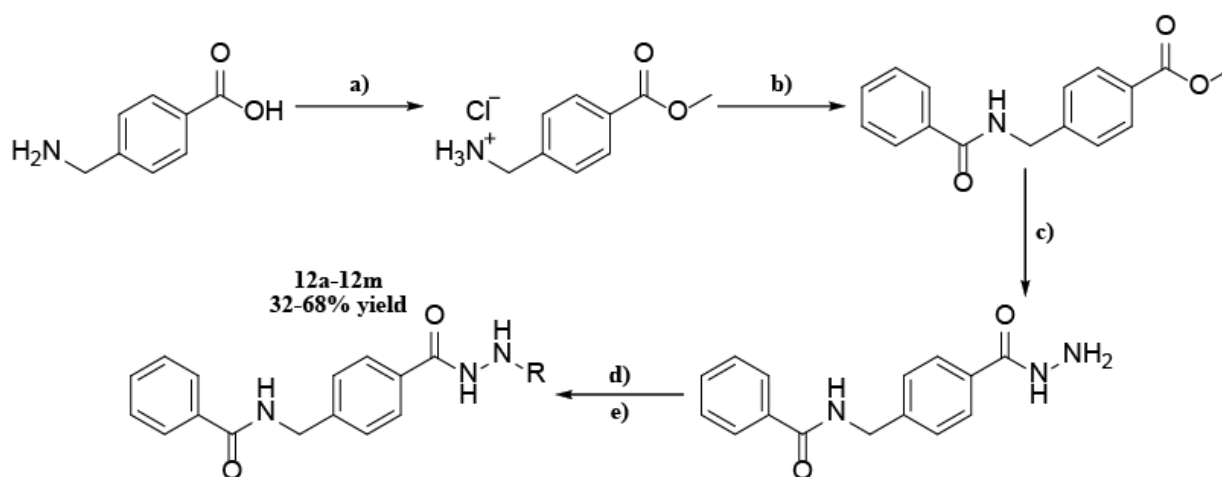
Name	R Group	IC ₅₀ ^a (nM)			
		HDAC1	HDAC2	HDAC3	Hek293
11l		18.87 ± 2.74	65.19 ± 10.41	8.56 ± 2.06	260.6 ± 8.68

IC₅₀ values (bold) are the mean of at least three experiments. Values after are the Standard Error of the Mean.

Chemistry of N-(4-(hydrazide)benzyl)benzamide analogs. We began our second refinement synthetic scheme by generating the N-(4-(hydrazinecarbonyl)benzyl)benzamide which would be used in all subsequent reactions for this group. This was achieved as shown in **Scheme 3.2**, reactions a-c. Briefly, the starting material, 4-(aminomethyl)benzoic acid, was refluxed in methanol and concentrated acid to generate the much more soluble corresponding methyl ester hydrochloride salt (**Scheme 3.2**, reaction a). This intermediate was reacted with benzoyl chloride in ethyl acetate and water in the presence of potassium carbonate to form an amide bond and afford 4-(benzamidomethyl)benzoate (**Scheme 3.2**, reaction b). This was in turn refluxed with the hydrazine water salt in methanol to generate the desired intermediate (**Scheme 3.2**, reaction c). Lastly, this intermediate was N-methylated using various aldehydes in ethanol and magnesium sulfate followed by reduction using sodium cyanoborohydride in acidified methanol to yield the desired products, **12a-12m** (**Scheme 3.2**, reactions d and e).

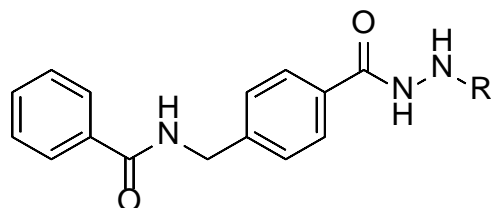
HDAC inhibition of series 12 inhibitors. We screened compounds **12a-12m** thrice against Hek293 lysates and recombinant human HDAC3; the resulting data is summarized in **Table 3.5**. Compounds demonstrating an IC_{50} less than 100 nM against HDAC3 and less than 1000 nM against Hek293 lysates were then tested thrice against recombinant HDACs 1 and 2 to determine selectivity profiles. Data from HDACs 1 and 2 can be found in **Table 3.6**. Generally, branched alkyl substitution, as seen in **12b**, provided inferior inhibition compared to non-branched analogs such as **12d**. There was an overall decrease in inhibition as the chain length increased past six carbons seen with compounds **12h**, **12i**, and **12k**. Cyclic additions at the end of alkyl chains, such as those seen in **12g** and **12m**, provided negligible effects. Lastly, the addition of a trifluoro group for compound **12f** provided worse HDAC3 inhibition compared to the non-fluorinated **12d**. Overall, very little potency was gained from this refinement series, seeing the slight benefit of an N-substituted propyl chain of **12d** compared to the corresponding butyl chain of **11i** which dropped the IC_{50} to less than 5 nM and lowered the K_i to the sub-nanomolar range for HDAC3.

Scheme 3-2. N-(4-(hydrazide)benzyl)benzamide Derivatives Synthesis



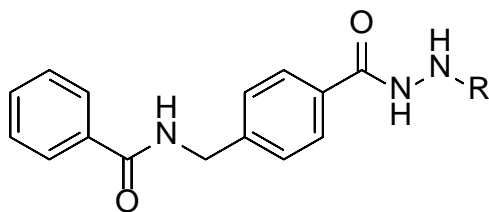
Reagents and conditions: (a) MeOH, reflux, conc. HCl; (b) AcOEt:H₂O (1:1), rt, K₂CO₃; (c) MeOH, reflux, NH₂NH₂·H₂O; (d) EtOH, rt, aldehyde of interest, MgSO₄; (e) MeOH, NaBH₃CN, conc. HCl

Table 3.5. In vitro inhibition of Hek293 lysates and recombinant HDAC3 for series 12 inhibitors.



Name	R Group	IC ₅₀ ^a (nM)		Name	R Group	IC ₅₀ ^a (nM)	
		HDAC3	HEK293			HDAC3	HEK293
12a		1533 ± 227.5	>10,000	12h		568.7 ± 84.9	2161 ± 895.5
12b		>10,000	>10,000	12i		1093 ± 334.4	>10,000
12c		>10,000	>10,000	12j		184.1 ± 74.54	550.2 ± 133.9
12d		3.47 ± 0.48	155.3 ± 27.64	12k		>10,000	>10,000
12e		18.74 ± 4.3	263.6 ± 28.52	12l		187.3 ± 0.6	427.1 ± 110.5
12f		69.10 ± 0.52	1229 ± 136.5	12m		84.44 ± 7.22	1883 ± 212.4
12g		39.93 ± 0.25	1621 ± 196				

IC₅₀ values (bold) are the mean of at least three experiments ± the Standard Error of the Mean.

Table 3.6. Class I HDAC and Hek293 lysate IC₅₀s for series 12 inhibitors

Name	R Group	IC ₅₀ ^a (nM)			
		HDAC1	HDAC2	HDAC3	Hek293
12d		13.16 ±	77.59 ±	3.47 ±	155.3 ±
		2.01	9.52	0.48	27.64
12e		20.20 ±	43.65 ±	18.74 ±	263.6 ±
		5.04	33.16	4.3	28.52

IC₅₀ values (bold) are the mean of at least three experiments ± the Standard Error of the Mean.

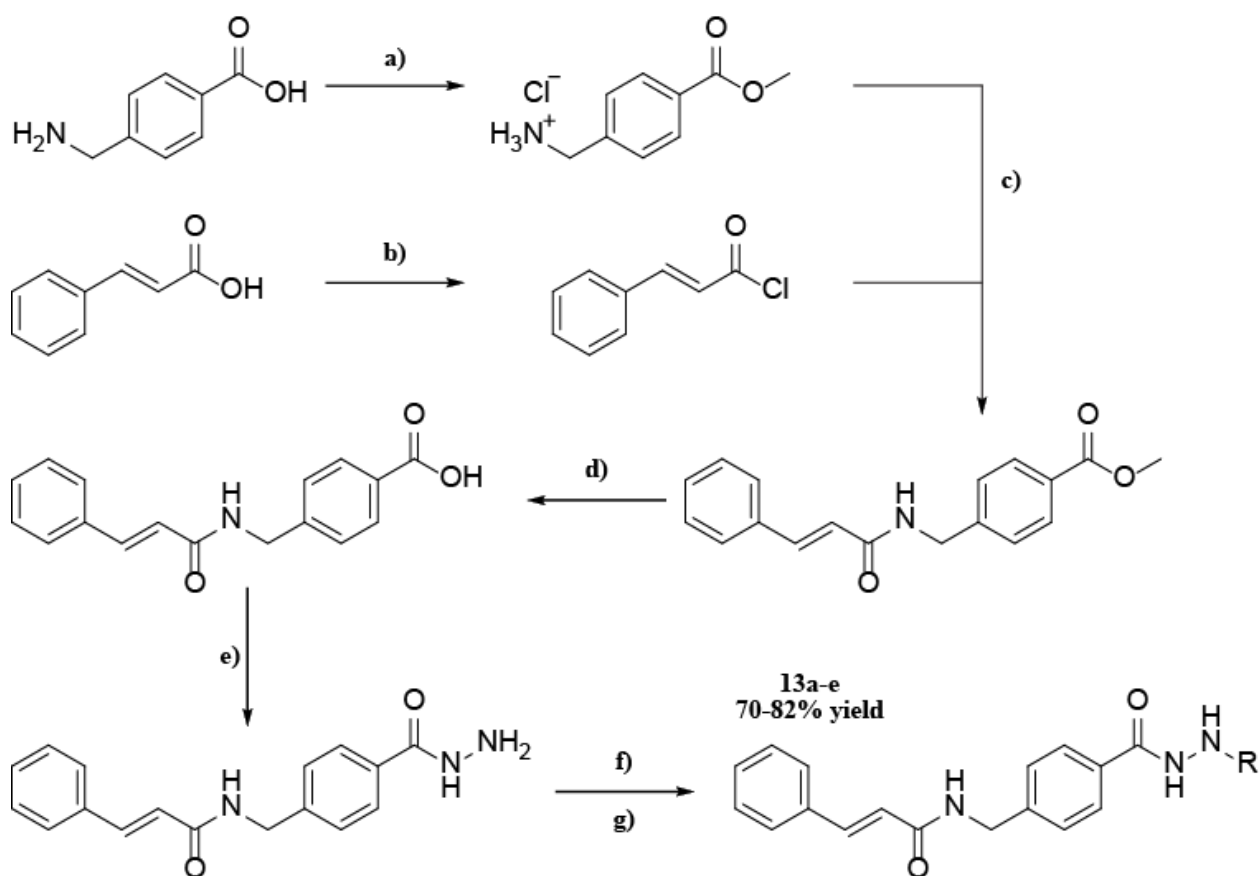
Chemistry N-(4-(hydrazide)benzyl)cinnamamide analogs. With the information from our second structure-activity relationship study providing insight that a non-branched propyl chain substitution on the β-nitrogen of the hydrazide seemingly is ideal, we moved forward by further modifying the carbonyl substituent. We noticed an increase in the use of N-hydroxylated acrylamide groups for HDAC inhibitors, present even in panobinostat and belinostat, as well as a multitude of pre-clinical inhibitors. This motif is a known Michael acceptor and likely forms covalent bonds with the sulfhydryl group of cysteines on proteins in vivo. Curious to see the effect on efficacy of incorporating an α, β unsaturated ketone, a similar Michael acceptor, we developed a cinnamamide derivative to build off of. This was achieved by again refluxing 4-(aminomethyl)benzoic acid in acidified methanol (**Scheme 3.3**, reaction a). Cinnamoyl chloride was formed using cinnamic acid and performing an acyl chlorination using oxalyl chloride in methylene chloride with catalytic amounts of dimethylformamide (**Scheme 3.3**, reaction b). The

product of this reaction was mixed with the benzoate from reaction a in a 1:1 (v/v) mixture of ethyl acetate and water with potassium carbonate to form the corresponding amide bond (**Scheme 3.3**, reaction c). Here, we reacted this compound with lithium hydroxide in a solution of methanol, water, and tetrahydrofuran (2:1:2 v/v) to generate the corresponding carboxylic acid (**Scheme 3.3**, reaction d). While it was never attempted, reactions c and d may theoretically be combined using lithium hydroxide in place of potassium carbonate in reaction c to cleave the methyl ester while also simultaneously forming the amide bond. With the carboxylic acid generated, we performed an amine coupling with HOBt and DCC in dimethylformamide (**Scheme 3.3**, reaction e). This intermediate was then reacted with a hydrazine water salt at 0°C. Finally, the hydrazide was reacted with the aldehyde of interest in ethanol with addition of magnesium sulfate and subsequently reduced using sodium cyanoborohydride in acidified methanol to yield compounds **13a-13e** (**Scheme 3.3**, reactions f and g).

HDAC inhibition of series 13 inhibitors. We ended our in vitro screening by interrogating the IC₅₀ values of **13a-13e** against Hek293 lysates and recombinant human HDACs 1, 2, and 3. The results from these studies are listed in **Table 3.7**. The most striking change when comparing this cinnamamide derivative to the benzamide derivatives are their potencies. All compounds tested display less than 40 nM IC₅₀ values against HDAC3 with the exception of the hexyl chain containing **13e**. The lead candidate from this study was the propyl chain containing **13b**, possessing a sub-nanomolar IC₅₀ and K_i against HDAC3 with 10- and 100-fold selectivity toward HDACs 1 and 2, respectively. The butyl chain derivative, **13c**, that mimicked the substituent of the very potent **11i** provided single-digit nanomolar potency against HDAC3, yet was

approximately 3-5 fold weaker when compared to **13b**. These findings suggest that a β -nitrogen alkyl substituent chain length of 3-4 carbons provides ideal conditions, with the ethyl, pentyl, and hexyl groups of **13a**, **13d**, and **13e**, respectively, having diminished inhibitory prowess when compared to **13b** or **13c**.

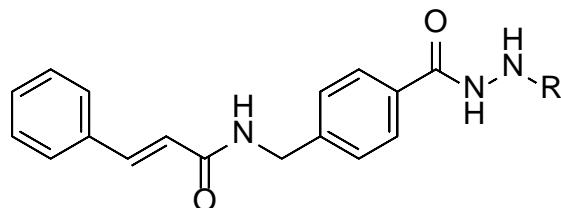
Scheme 3-3. N-(4-(hydrazide)benzyl)cinnamamide Derivatives Synthesis



Reagents and conditions: (a) MeOH, reflux, conc. HCl; (b) DCM, rt, Oxalyl Chloride, cat. DMF; (c) EtOAc:H₂O (1:1), rt, K₂CO₃; (d) MeOH:H₂O:THF (2:1:2), rt, LiOH; (e) DMF, rt, HOBt, DCC; (f) DMF, 0°C, NH₂NH₂·H₂O; (g) EtOH, rt, aldehyde of interest, MgSO₄; (h) MeOH, rt, NaBH₃CN, conc. HCl

Mass spectrometric analysis of select hydrazide-based inhibitors in glucuronidating environments. To demonstrate that these compounds were indeed highly unlikely to be

Table 3.7. In vitro inhibition of recombinant HDACs 1, 2, and 3 and HEK293 Lysate for series 13 inhibitors

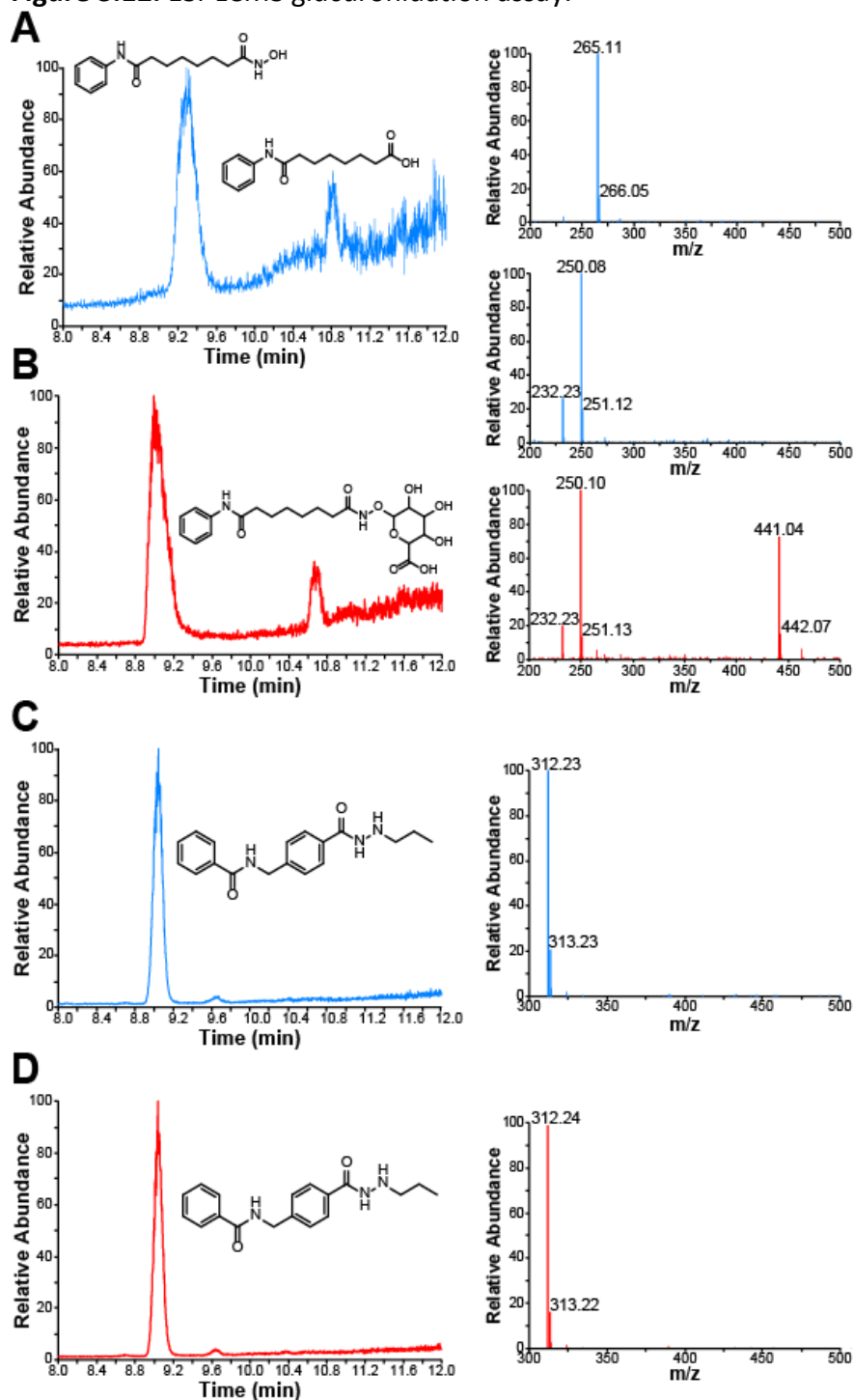


Name	R Group	IC ₅₀ ^a (nM)			
		HDAC1	HDAC2	HDAC3	HEK293
13a		29.49 ± 10.71	76.57 ± 9.74	19.71 ± 1.41	171.1 ± 34.23
13b		11.81 ± 4.16	95.45 ± 34.15	0.95 ± 0.19	124.4 ± 14.02
13c		60.17 ± 20.97	70.03 ± 26.38	3.67 ± 2.86	494.3 ± 209.6
13d		47.36 ± 16.79	99.56 ± 17.44	32.55 ± 1.15	690.7 ± 54.67
13e		81.36 ± 11.96	139.2 ± 29.9	149.8 ± 81.63	1718 ± 139.1

IC₅₀ values (bold) are the mean of at least three experiments ± the Standard Error of the Mean.

glucuronidated in vivo, we adapted and performed an ex vivo assay using a protocol derived from Walsky and colleagues.¹⁷¹ Briefly, vorinostat, **11l**, **12d**, and **13b** were incubated with human liver microsomes, UDP Glucuronic acid, and alamethicin (a pore-forming antibiotic) for 12 hours at 37°C. The reaction was quenched with a 47:50:3 (v/v/v) mixture of water:acetonitrile:formic acid. The vessel was subjected to centrifugation and the supernatant filtered and examined via electrospray ionization liquid chromatography mass spectrometry. A parallel study that lacked UDP Glucuronic acid was performed with each inhibitor as a negative control. Comparing **Figure**

Figure 3.12. ESI-LCMS glucuronidation assay.

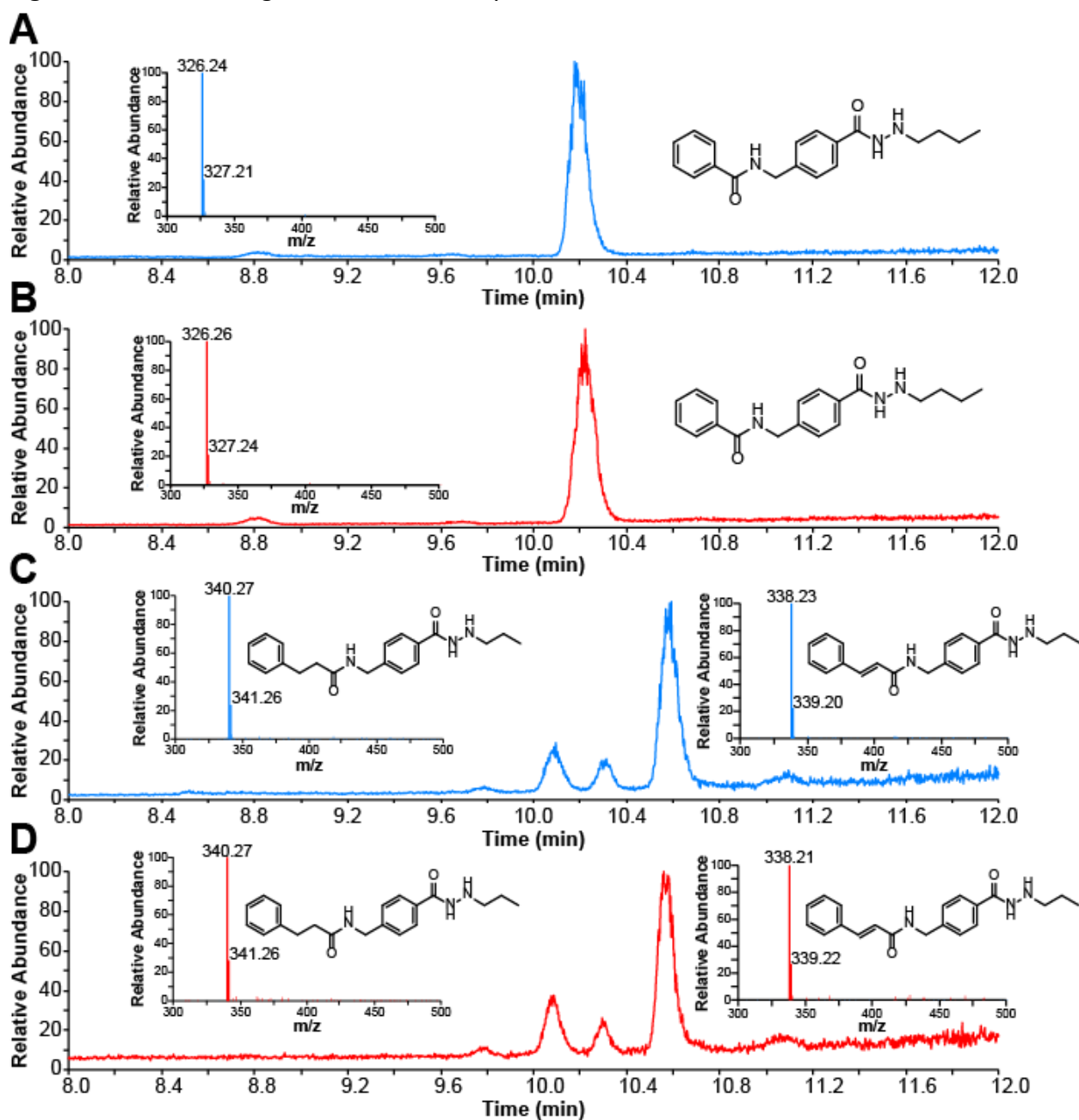


ESI-LCMS TIC spectra of vorinostat incubated with human liver microsomes without UDPGA (blue, **A**) and with UDPGA (red, **B**). Both spectra contain parent compound ($m/z = 265$), a hydrolyzed metabolite ($m/z = 250$), only the UDPGA addition vessel contained the glucuronidated metabolite ($m/z = 441$). ESI-LCMS TIC spectra of **12d** human liver microsomes without UDPGA (blue, **C**) and with UDPGA (red, **D**). Neither vessel contained any detectable metabolites other than parent compound. Representative spectra and mass analyses of $n \geq 3$ repeats.

3.12A (blue) and **Figure 3.12B** (red) demonstrates the presence of the *o*-glucuronidated metabolite of vorinostat with a $(m+H^+)/z$ of 441.04 (**Figure 3.12B**, bottom right), in line with previous findings.¹⁷² This mass shift was not present in the corresponding negative control lacking UDP Glucuronic acid (**Figure 3.12B**, middle right). There are no differences between masses or ionization patterns in any of the hydrazide-containing compounds (**Figures 3.12 C-D**, **Figure 3.13**), suggesting these compounds are not readily glucuronidated in environments where vorinostat is extensively glucuronidated. It was also noted that **13b**, possessing an unsaturated bond, was reduced in this model, despite no NADPH being added to the reaction vessel (**Figures 3.13 C-D**). This may demonstrate a potential metabolite of this compound.

Interrogation of in vitro binding kinetics of hydrazide-containing HDAC inhibitors. Generally speaking, the very reason why groups like *ortho*-aminoanilide or hydroxamates are able to chelate zinc and other dicationic metals is the same reason why they are prime glucuronidation targets. Their possession of primary alcohols and primary amines not only allow them to ionically complex with the positively charged zinc, but also allows them to be extensively inactivated via glucuronidation. After demonstrating that the hydrazide motif was not glucuronidated in ex vivo environments, we questioned whether it was inhibiting HDACs through a direct active zinc chelation. We hypothesized that the compound should demonstrate typical Michaelis-Menten competitive inhibition, similar to vorinostat, if it was truly chelating zinc in the active site of HDACs. Thus, we performed in vitro V_{max} studies using recombinant HDACs 1 and 3 and compounds **12d** and **13b**. Applying a double reciprocal conversion of the data yielded Lineweaver-Burke plots. Surprisingly, and contrary to previous data, our hydrazide-containing

Figure 3-13. ESI-LCMS glucuronidation assay of 11l and 13b



A and B) TIC of inhibitor 11l without (blue) and with (red) addition of UDPGA. One peak at 10.2 minutes with mass analysis demonstrating $m/z = 326$, indicative of parent compound. No additional metabolites found. **C and D**) TIC of inhibitor 13b without (blue) and with (red) addition of UDPGA, several peaks spanning 10.1-10.5 minutes. The first peak is the reduced metabolite, lacking the double bond the parent compound possesses, $m/z = 340$. The second, more prominent peak is the parent compound, $m/z = 338$. Figures are representative of $n \geq 3$ experiments.

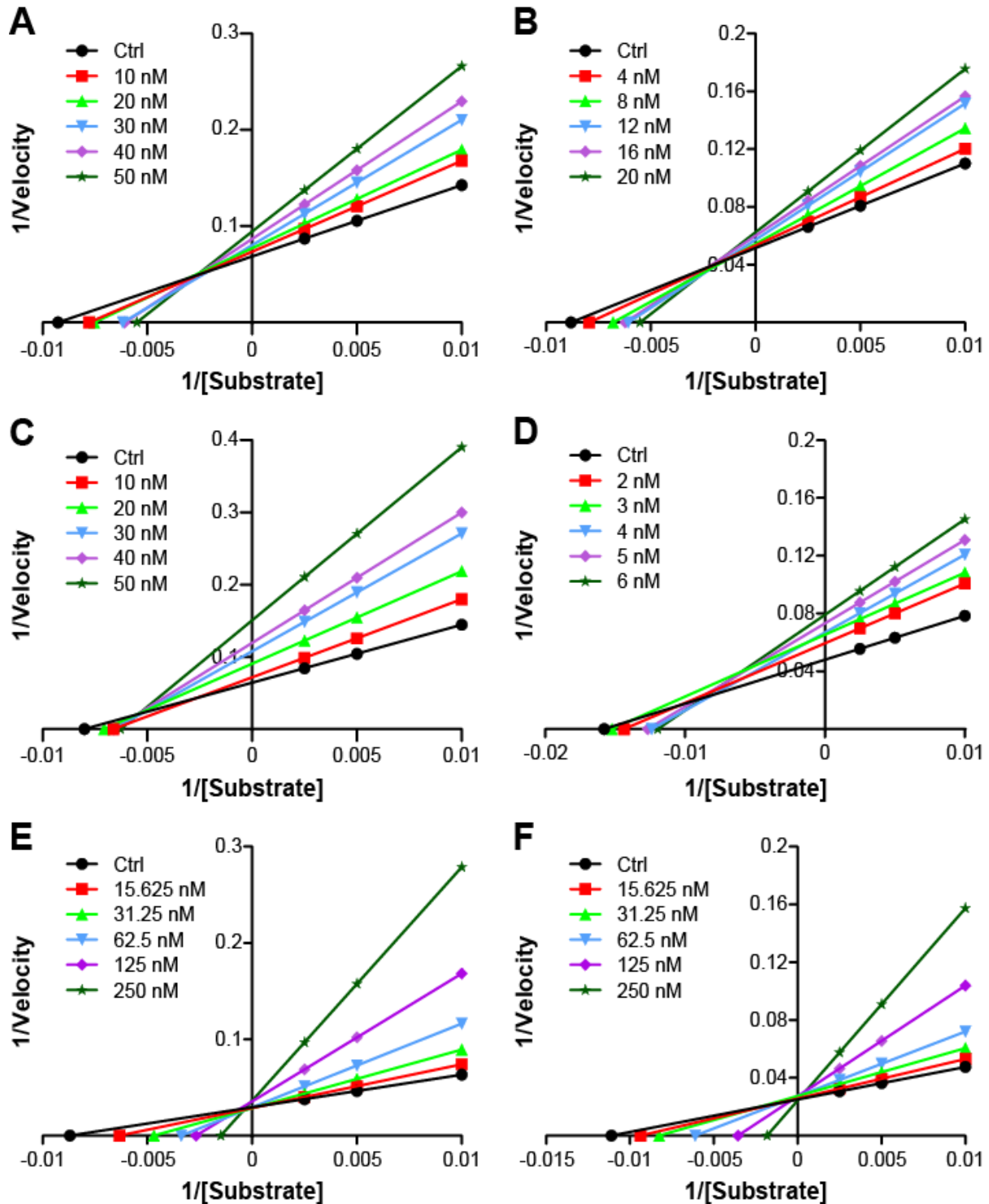
compounds clearly demonstrate a convergence in the 2nd quadrant, indicative of mixed inhibition

(Figures 3.14 A-B) and non-competitive inhibition (Figures 3.14 C-D). This is in direct contrast to

the initial findings published by Wang and colleagues.¹⁴¹ Their published data seem to match a canonical competitive inhibitor, with their corresponding Lineweaver-Burke plots demonstrating all doses and control intersecting directly on the y-axis, representative of $1/V_{\max}$. However, the corresponding V_{\max} plots from which these graphs were derived display changes in V_{\max} . This would mean the y-intercepts on the double reciprocal Lineweaver-Burke plots should be different as well. To further ensure our findings were valid, we used vorinostat as a positive control, a known competitive inhibitor with extensive kinetic analyses published independently.¹⁷³ Matching established data, our results demonstrated complete convergence directly on the y-axis, indicative of competitive inhibition (**Figures 3.14 E-F**), which is in direct agreement with the very similar V_{\max} values seen at each dose. This finding, coupled with the lack of glucuronidation ex vivo, points to an allosteric binding site on class I HDACs that is strongly inhibited by our hydrazide-containing inhibitors, and has little to do with catalytic site zinc chelation. The V_{\max} plots from which these Lineweaver-Burke plots were derived may be seen in **Figures 3.15 A-F**.

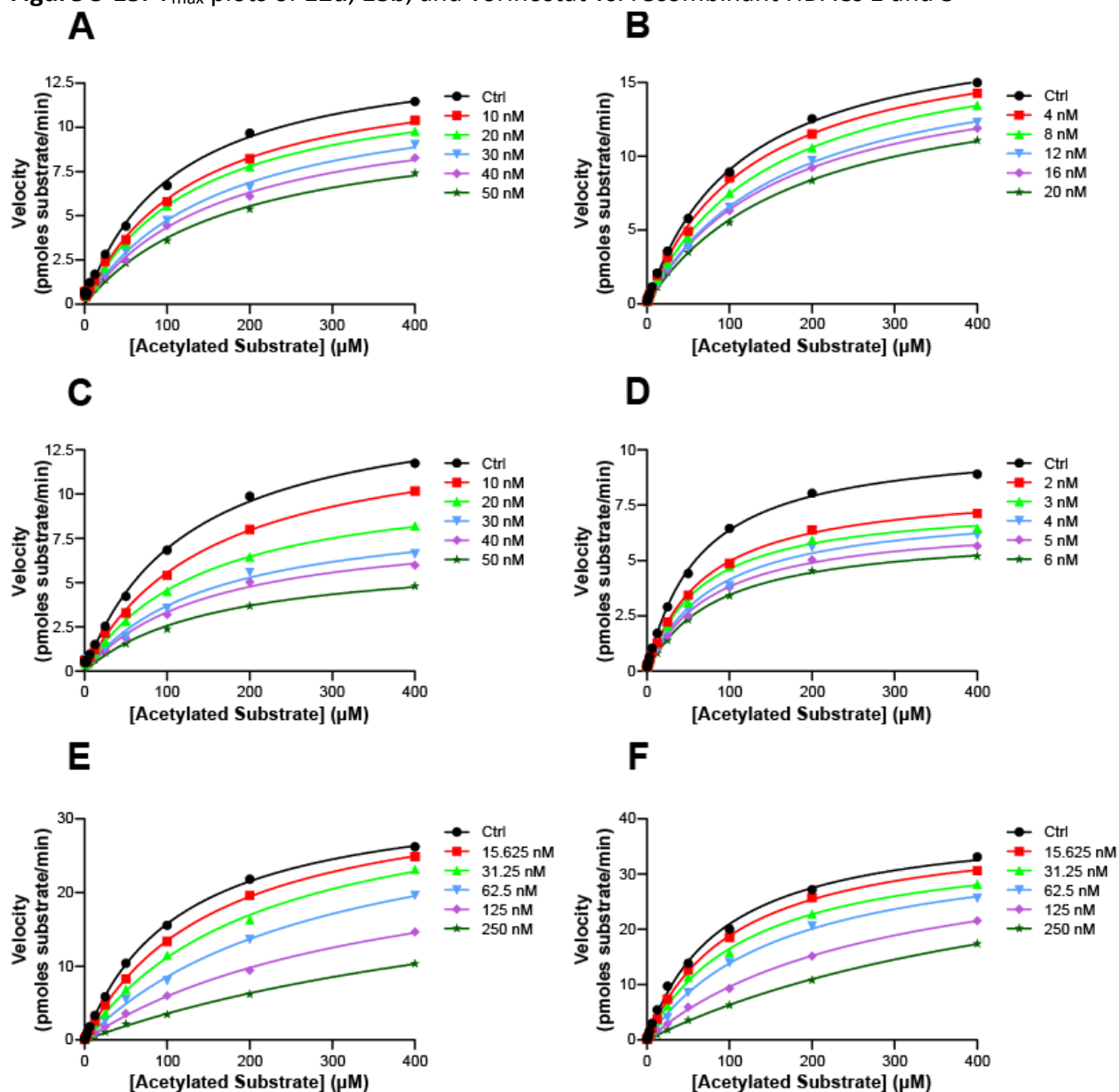
HDAC3 molecular docking study of HDAC inhibitors. With the results thus far suggesting an allosteric binding site, we were curious if we could identify a potential site at which our inhibitors were binding. Using the solution structure of HDAC3 bound to Ncor2, pdb: 4A69, we probed the HDAC3 surface with **13b** resulting in a heavy concentration of poses near the interface with the Ncor2 coenzyme (**Figure 3.16**). We then calculated the propensity for ligand interaction which revealed a very positive binding region directly overlapping with the high density **13b** binding area (**Figure 3.16**). Using this pocket, we performed a flexible induced fit binding of **12d**, **13b**, and vorinostat and calculated binding scores from the top 20 (lowest energy) poses from each set.

Figure 3.14. Lineweaver-Burke plots of **12d**, **13b**, and vorinostat vs. recombinant HDACs 1 and 3



Y-axes units (pmoles acetylated substrate cleaved/min)⁻¹. X-axes units (μmoles)⁻¹. **A and B)** **12d** and HDACs 1 and 3 respectively. Intersection in 2nd quadrant indicative of mixed inhibition. **C and D)** **13b** and HDACs 1 and 3 respectively. Intersection on x-axis and in 2nd quadrant indicative of mixed and non-competitive inhibition. **E and F)** vorinostat and HDACs 1 and 3. Intersection directly on y-axis indicative of competitive inhibition. Representative plots of n ≥ 3 experiments.

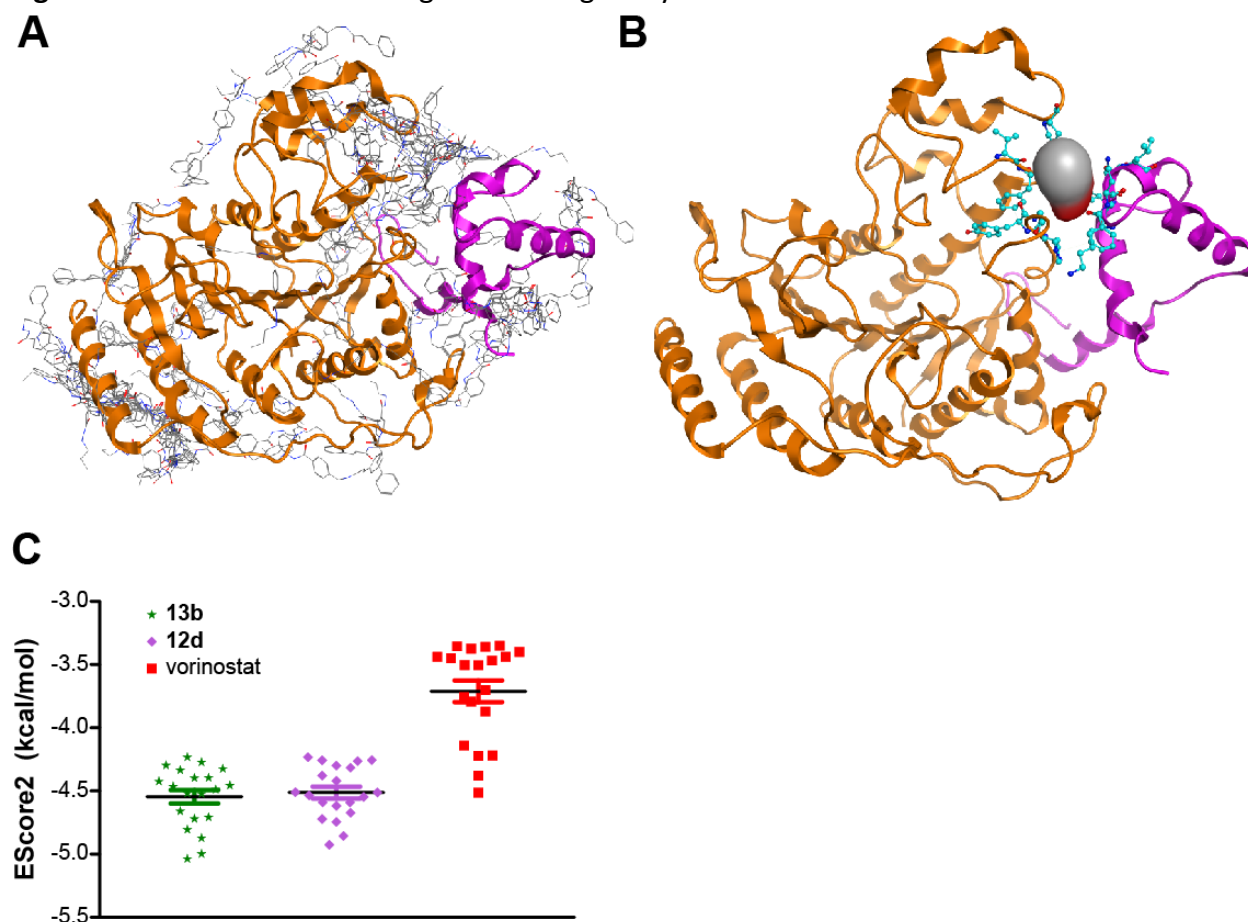
Figure 3-15. V_{max} plots of **12d**, **13b**, and vorinostat vs. recombinant HDACs 1 and 3



A and B) V_{max} plots of **12d** vs HDACs 1 and 3 respectively. A notable decrease in K_m and V_{max} is seen as the concentration of inhibitor increases. **C and D)** V_{max} plots of **13b** vs HDACs 1 and 3 respectively. A more noticeable drop in V_{max} can be seen, as well as a negligible shift in K_m . This is indicative of the more non-competitive binding seen with **13b** compared to **12d**. **E and F)** V_{max} plots of vorinostat vs HDACs 1 and 3. No differences in V_{max} are perceived, all plots reach the same V_{max} , however, a notable shift in K_m occurs, indicative of class competitive inhibition. Representative figures of $n \geq 3$ experiments.

Our lead inhibitors **12d** and **13b** display nearly identical binding scores, which is line with their near identical in vitro activity and electrospatial occupancies. The canonical binder vorinostat bound less tightly to this pocket, as evidenced by its higher energy posing scores (**Figure 3.16**).

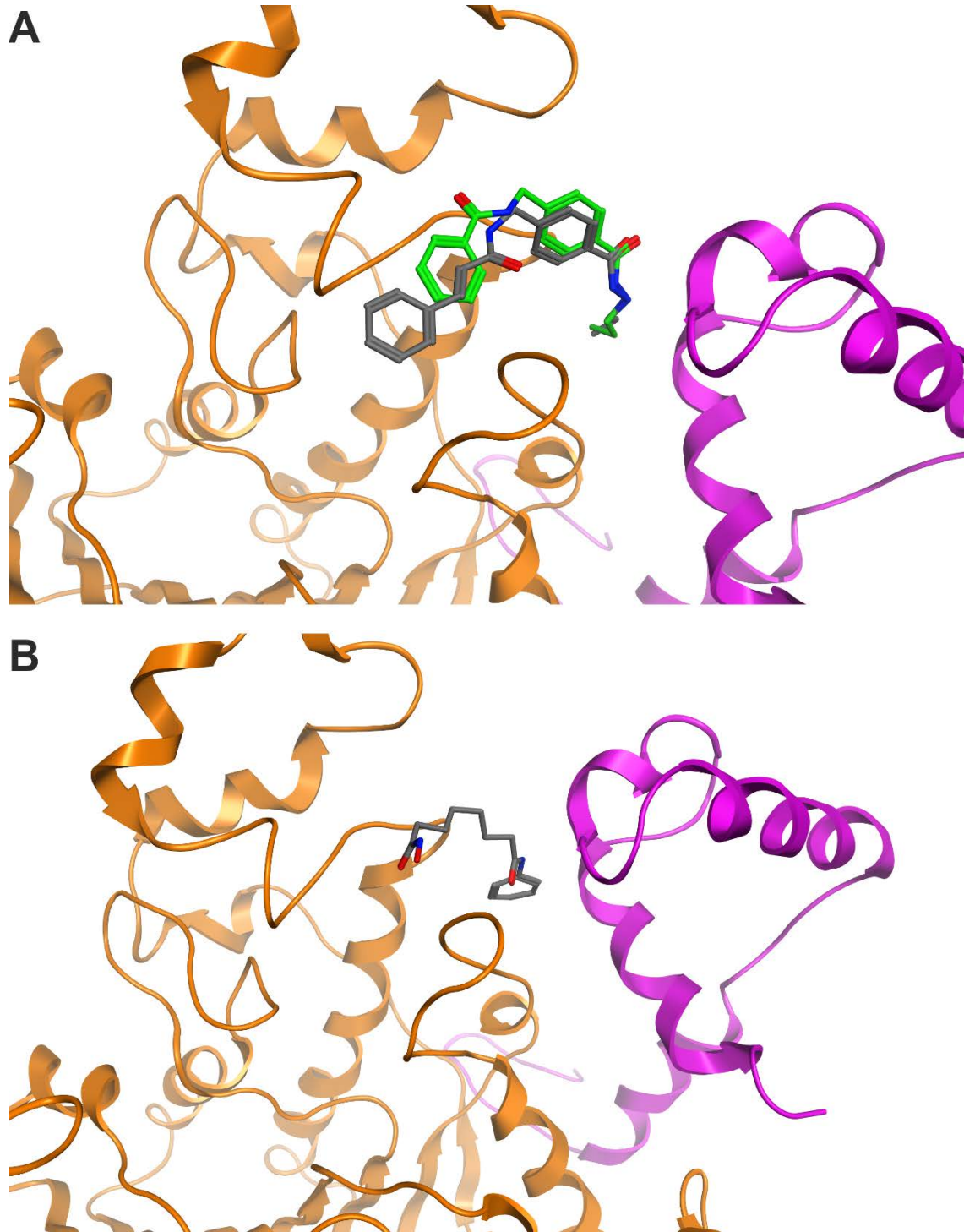
Figure 3.16. Molecular modeling and binding study of HDAC3



A) Rigid target probe of **13b** against HDAC3. PDB file 4A69 used. HDAC3 shown in orange, Ncor2 coenzyme shown in purple. Poses of **13b** shown in carbon grey. An area of high pose density was seen near the 1 o'clock position of this image. **B)** Propensity for ligand interaction function (PLIF). The light grey and red alpha spheres represent three dimensional occupancy of the pocket found. Amino acids in cyan blue represent key interacting residues. Both the **13b** site find study and the PLIF study overlap here, with significant interaction with M78. **C)** Binding scores for top 20 poses of **13b**, **12d**, and vorinostat (lower is better). **13b** and **12d** both demonstrate very similar, superior scores compared to vorinostat, representing a lower binding energy.

Lastly, when we posed the lowest energy poses for 2d and 3b, we see significant overlap in electrospatial occupancy, indicative of homologous modes of binding (**Figure 3.17A**), whereas the lowest pose for vorinostat results in a completely different orientation, with the hydroxamic acid exposed to solvent and its phenyl group serving as the main area of interaction (**Figure 3.17B**). Additionally, a narrow tunnel can be seen where the propyl hydrazide of both **12d** and **13b** fit nicely. This matches the in vitro and ex vivo data demonstrating that adding branching

Figure 3.17. Molecular modeling of **12d**, **13b**, and vorinostat against HDAC3



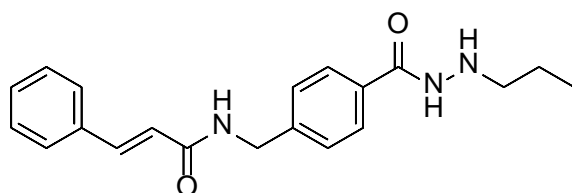
A) HDAC3 molecular docking. PDB: 4A69 used. HDAC3 is seen in orange, Ncor2 seen in purple. Lowest binding energy poses for **12d** (green) and **13b** (carbon grey). Significant electrospatial overlap between these two poses indicative of a key pose the propyl hydrazide group is capable of conforming to. **B)** Lowest binding energy pose for vorinostat (carbon grey). Conformation has its hydroxamic acid interacting with solvent, away from a pocket, with its phenyl group interacting with hydrophobic amino acids. This pose, and all other poses seen, possess much weaker binding interaction than lead analogs **12d** and **13b**.

alkyl chains, or extending the alkyl chains past a length of four carbons leads to markedly diminished inhibition activity. Taken together, these findings illustrate the potential for a novel, allosteric binding site that the propyl hydrazide motif is particularly astute at fitting into. Further, the inhibitors in this dock are nearly 20 angstroms away from the opening of the zinc-containing binding pocket, as such it be expected that these inhibitors are not directly impacting the ability of substrate to enter nor be cleaved by the HDAC isozyme.

Efficacy of lead analog in ex vivo cell models. Satisfied with results of our three structure activity studies and the potential for allosteric inhibitors that are impervious to glucuronidation, we transitioned from recombinant enzyme pre-screening to cellular treatment. Given that HDAC inhibitors are most successful in hematologic malignancies such as lymphomas and myelomas, as shown by their FDA approvals, we screened our most potent inhibitor, **13b**, against an array of leukemia and Multiple Myeloma cell lines. Briefly, MOLM-14, an acute monocytic leukemia cell line¹⁷⁴; HL-60, an acute promyelocytic cell line¹⁷⁵; RS4-11, an acute lymphoblastic leukemia¹⁷⁶; K562, a chronic myelogenous leukemia¹⁷⁷; MV4-11, an acute myeloid leukemia¹⁷⁸; and RPMI-8226, a Multiple Myeloma cell line¹⁷⁹, were all used to determine the efficacy of **13b** against a multitude of different hematologic cancers. Cells were treated for 48 hours before viability was assessed with CellTiter-Blue Cell Viability Assay. The active fluorescent reagent in this assay is resazurin. This molecule is converted by the functional mitochondria in the viable cells to resorufin. Resorufin intensity is therefore directly related to cell viability. The resulting EC₅₀ values from each cell line is summarized in **Table 3.8**.

13b demonstrates the highest level of potency against the AML cell line MV4-11, possessing an EC₅₀ for the cells at less than 50 nM. Taken together with the efficacy toward Molm14 and RS4-11, both acute myeloid leukemia subsets, we can see that **13b** is particularly selective for acute types of leukemia when compared to its lack of efficacy toward the chronic leukemia cell

Table 3.8. Leukemia and myeloma cell line data for **13b**



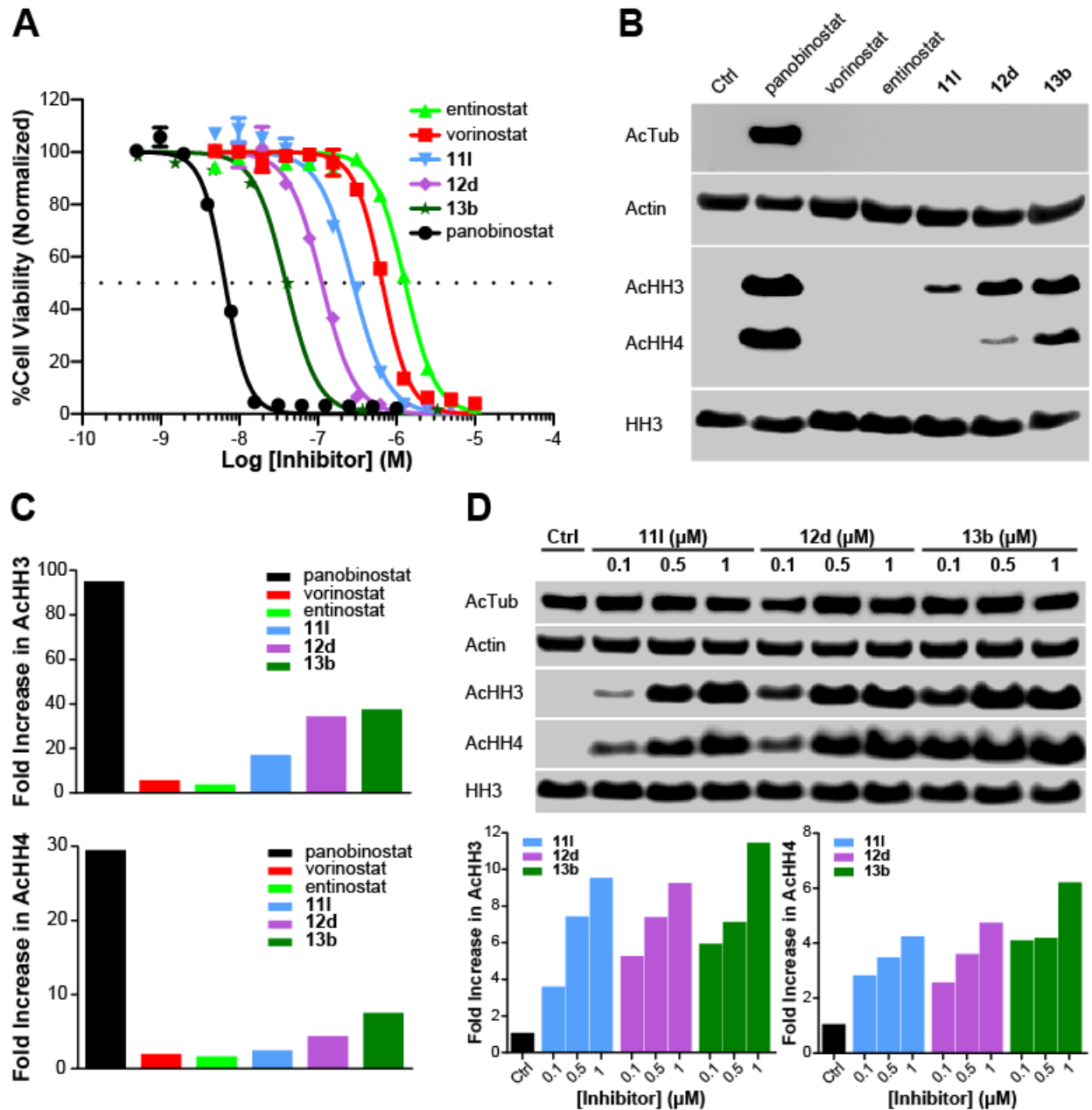
EC₅₀ (nM)

MV4-11	Molm14	RS4-11	K562	HL-60	RPMI-8226
36.37 ± 8.83	76.64 ± 18.37	151.7 ± 44.29	2160 ± 128.3	>10,000	>10,000

EC₅₀ values (bold) are the mean of at least two experiments ± the Standard Error of the Mean.

line, K562 or the chromosomal translocation containing HL-60 cell line. Further, when tested against the classical Multiple Myeloma cell line, RPMI-8226, **13b** demonstrated incomplete kill curves even at mM concentrations. Following the potency findings of **13b** in MV4-11 cells, we assessed the efficacy of **11l**, **12d**, and **13b** in these cells as single agents. Panobinostat, vorinostat, entinostat, **11l**, **12d**, and **13b** were tested against MV4-11 for 48 hours of treatment. Cells were treated with CellTiter-Blue to determine viability which was measured using a spectrophotometer as a function of resorufin intensity. Results from these experiments are shown as an EC₅₀ cell viability curve in **Figure 3.18A**. As a negative control, we also performed this experiment using **12c**, a compound whose structure very closely matches **12d**, differing only by a non-reduced nitrogen-carbon bond, while possessing no appreciable inhibition against recombinant HDAC3. Matching its weak prowess as an HDAC inhibitor from our recombinant

Figure 3.18. Ex vivo analysis of lead compounds as single agents against AML



A) EC₅₀ of HDAC inhibitors against MV4-11 cells after 48 hour treatment. **11l**, **12d**, and **13b** all display lower EC₅₀ values than vorinostat and entinostat, from 38-287 nM. **B)** Western blot analysis of HDAC inhibitors against MV4-11 cells at 100 nM after 24 hours. **11l**, **12d**, and **13b** cause higher upregulation of Acetylated Histones H3 and H4 (AcH3/AcH4) than vorinostat and entinostat. Panobinostat is the only inhibitor to raise Acetylated Tubulin (AcTub) levels at this concentration. **C)** Quantifications of AcH3 and AcH4 from Western blot **B**. Values normalized to actin levels. **D) (Top)** Western blot analysis of **11l**, **12d**, and **13b** at varied doses after 6 hours. All display a dose-dependent increase in AcH3 and AcH4. **(Bottom)** Quantification of Western blot **D**. Values normalized to actin levels. Representative plots and blots of n ≥ 2 experiments. As single agents, these compounds possess less than 300 nM EC₅₀ values against MV4-11 with complete kill curves.

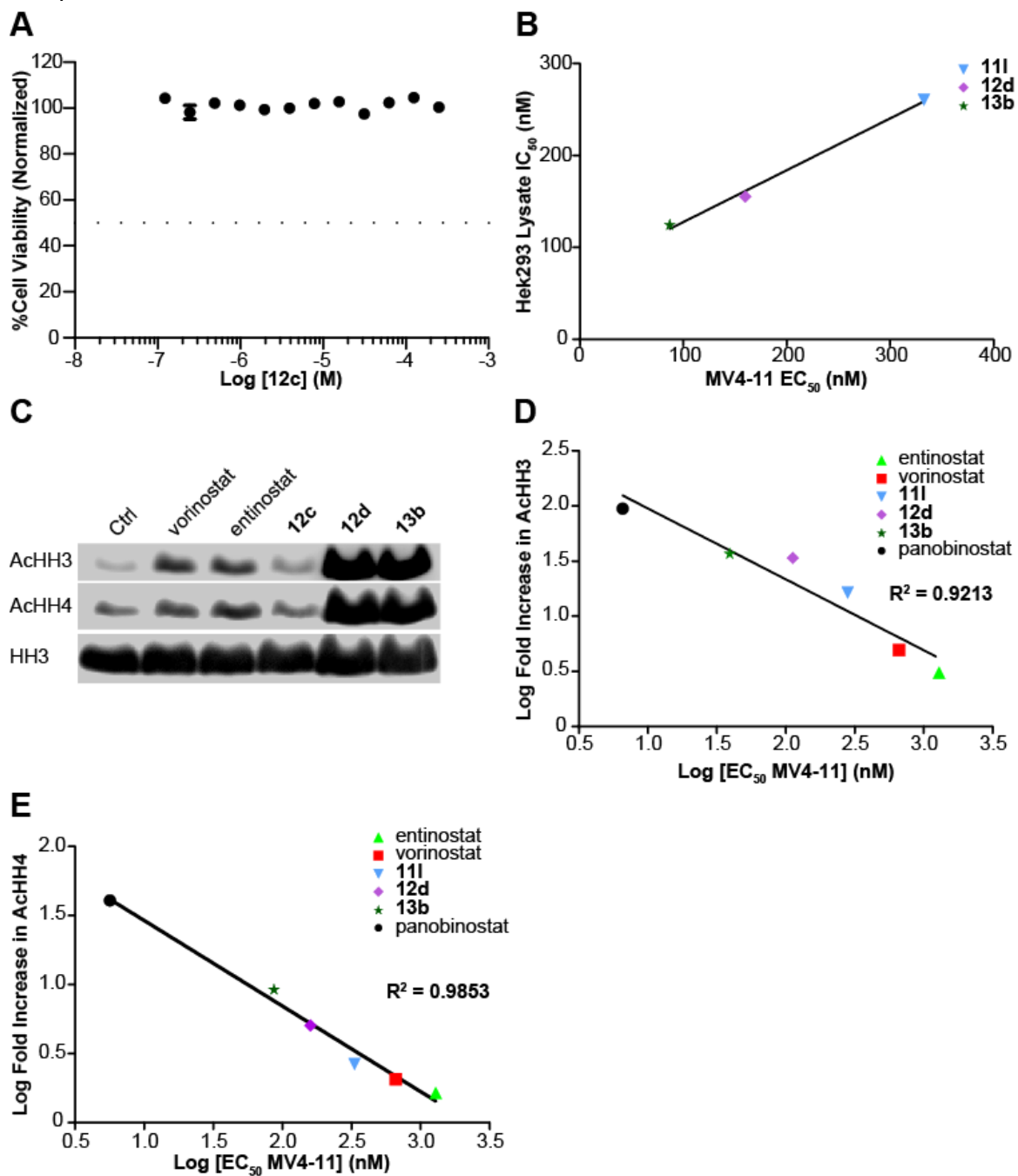
HDAC assay, this compound demonstrated no appreciable activity against MV4-11 cells even at

doses as high as 250 μM (**Figure 3.19A**).

To demonstrate that our initial HDAC activity pre-screening assay was correlative with efficacy against MV4-11 cells, we plotted the compounds' respective potency toward HEK293 lysates as a function of their IC_{50} with their respective EC_{50} values against MV4-11 cells (**Figure 3.19B**). The results demonstrate a linear relationship with considerable correlation, demonstrating the ability of our HDAC activity pre-screen assay to translate to ex vivo potency in AML cells.

To further demonstrate the correlation between MV4-11 cell death with hyperacetylation of histones H3 and H4, we performed Western blot analysis of MV4-11 cell lysates after 24 hour treatment with 100 nM of inhibitor (**Figure 3.19B**). The data demonstrate that our lead inhibitors, **11i**, **12d**, and **13b** are more potent at increasing the concentrations of acetylated histones H3 and H4, markers of HDACs 1, 2, and 3 inhibition, than the FDA approved vorinostat or the *ortho*-aminoanilide-based entinostat (**Figure 3.19 B-C**). Additionally, this upregulation is dose-dependent, with increasing levels of hyperacetylation seen with increasing concentrations of inhibitor (**Figure 3.18D**). As a negative control, we once again used **12c** to further ensure the validity of our pre-cellular screening. At a concentration of 100 nM, **12c** was also used in MV4-11 cells for western blot analysis and demonstrated no appreciable ability to increase acetylation of histones H3 and H4 (**Figure 3.19C**). Further, upregulation of histones H3 and H4 is selective, as our hydrazide based inhibitors do not demonstrate any effect on levels of acetylated tubulin, a marker of HDAC6 inhibition (**Figures 3.18 B and D**). This is an important characteristic, as upregulation of acetylated histones H3 and H4 is inversely and logarithmically correlated with EC_{50} against AML, that is, an increase in acetylated histones H3 and H4 leads to an exponential

Figure 3.19. Extrapolated analysis and correlation between assay screens and potency of lead compounds

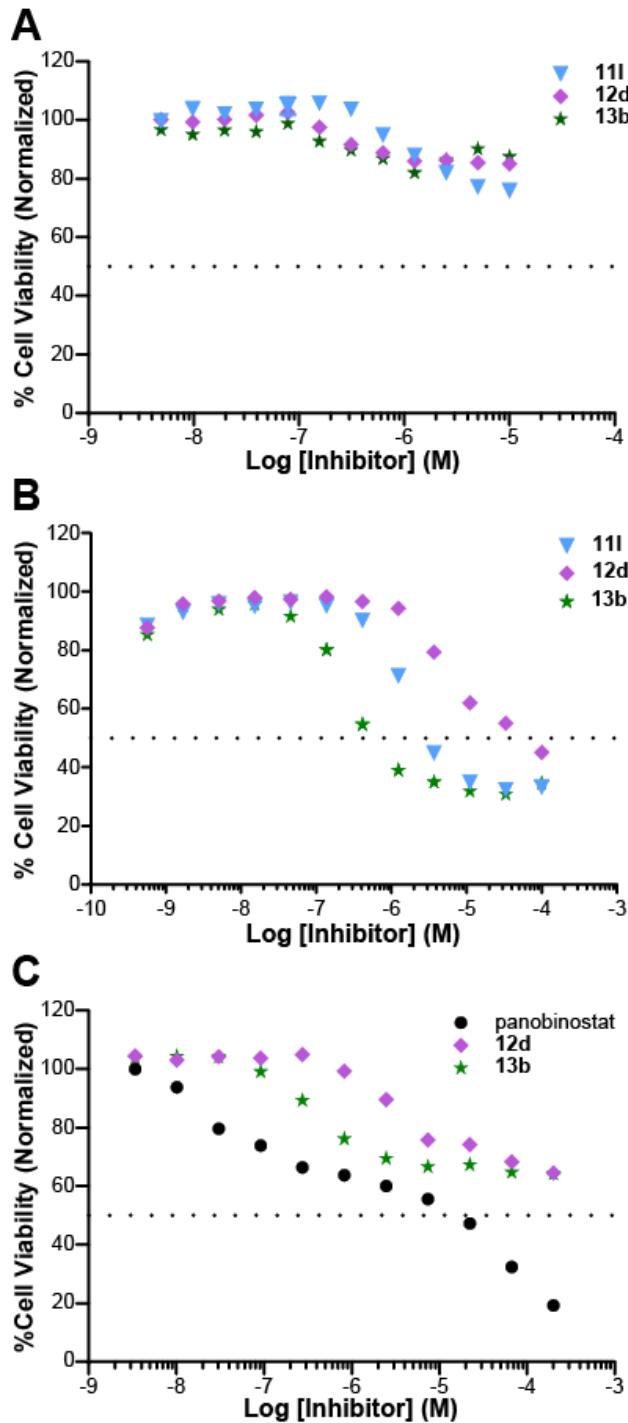


A) MV4-11 EC₅₀. 48 hour treatment, **12c** shows no killing activity. **B)** Correlation between Hek293 lysate screening and MV4-11 EC₅₀. Direct, linear relationship between the two. **C)** Western blot analysis of 100 nM inhibitors in MV4-11 cells for 24 hours, **12c** doesn't increase acetylated histone H3 (AcHH3) or H4 (AcHH4) levels. **D)** Correlation between fold increase in levels of AcHH3 and the EC₅₀ in MV4-11 cells. A direct, inverse relationship is seen in a logarithmic fashion. A logarithmic increase in acetylation of Histone H3 leads to a logarithmic decrease in concentration required to kill 50% of MV4-11 cells. **E)** Correlation between fold increase in AcHH4 and EC₅₀ in MV4-11 cells. A direct, inverse relationship is seen in a logarithmic fashion. A logarithmic increase in acetylation of Histone H3 leads to a logarithmic decrease in concentration required to kill 50% of MV4-11 cells. **A** and **C** are representative figures from n = 2 experiments. **B**, **D**, and **E** were plotted from corresponding representative figures in **Figure 3.15**.

decrease in EC_{50} against these cells (**Figures 3.19 D-E**). This is in sharp contrast to acetylated tubulin, where increasing levels of acetylation are not as directly correlative with EC_{50} against MV4-11 cells (**Figure 3.15B**).

Selectivity and toxicity profiling of lead analogs. Concluding our experiments, we sought to determine if the hydrazide based inhibition of HDACs was a non-selective cell death mechanism, or if it was selective toward non-solid tumor cells, particularly various forms of leukemia. We examined the ex vivo effect of **11l**, **12d**, and **13b** in Hek293 and HeLa cells, well-studied solid tumor cell lines. Briefly, cells were pre-incubated for 24 hours prior to treatment. After treatment, cells were incubated for an additional 48 hours before measurement of cell viability as a function of resorufin intensity was determined. The corresponding EC_{50} values demonstrate at least 100 fold higher selectivity toward the MV4-11 cell line (compare **Figures 3.18A** and **3.20 A-B**). Further, we wanted to examine our lead compounds' toxicity profile against healthy human peripheral blood mononuclear cells (PBMCs). PBMCs were treated with titrating doses of panobinostat, **12d**, or **13b** for 24 hours followed by treatment with CellTiter-Blue. Cell viability was determined as a function of resorufin intensity via spectrophotometer, normalized to control treatment. The data demonstrate **12d** and **13b**'s superiority over panobinostat from a toxicity standpoint. Further, the lack of a Michael acceptor group on **12d** seems to reduce its toxicity toward PBMC's 10 fold compared to **13b** (**Figure 3.20B**). This functional group (present as an acrylamide) may also explain panobinostat's much greater toxicity compared to **12d** and **13b**.

Figure 3.20. Selectivity and toxicity profiling of lead inhibitors

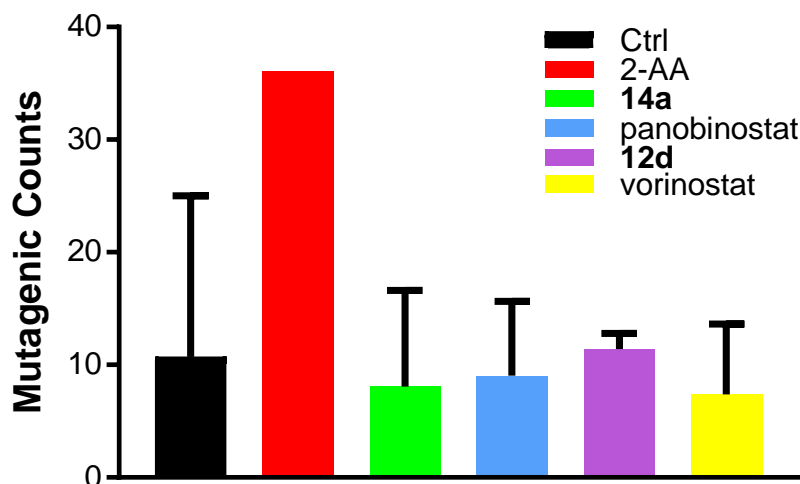


A) EC₅₀ of HEK293. Neither **11i**, **12d**, nor **13b** display effective killing of this solid tumor cell line after 48 hours of treatment. **B)** EC₅₀ of HeLa. Neither **11i**, **12d**, nor **13b** display effective killing of this solid tumor cell line after 48 hours of treatment. **C)** Human PBMC profiling with panobinostat, **12d**, and **13b**. **12d** and **13b** both demonstrate superior toxicity (less PBMC killing) than panobinostat. **12d** shows ~10 fold less toxicity than **13b** until the high micromolar range, well beyond the respective EC₅₀ values of these compounds. Panobinostat displays immediate toxicity as early as 10 nM. Values normalized to vehicle treatment (DMSO). Figures are representative of n ≥ 2 experiments.

3.3. In vivo testing and mechanistic determination of Hydrazide-Containing Class I Histone Deacetylase Inhibitors

With the pre-clinical novelty and successes for inhibitors **12d** and **13b**, our focus turned toward optimization for in vivo experimentations. We first sought to test our lead inhibitors for propensity to cause mutagenesis. We performed a mini-Ames to first ensure that these novel compounds were not inducing genetic mutations. Our compounds, **12d**, and a previously unpublished compound, **14a**, did not induce significant increases in positive mutagenic responses. This was similar to FDA approved vorinostat and panobinostat. Further, our positive control, 2-aminoanthracene induced genetic mutations in nearly 100% of the wells, giving validity to our assay (**Figure 3.21**)

Figure 3.21. Ames test of lead hydrazide and FDA approved HDAC inhibitors.



Error bars are presented as 95% confidence intervals. No data except the positive control, 2-AA, are significant. 12d and 14a are non-inferior to panobinostat or vorinostat. n = 4.

Satisfied with these results, we next performed stability tests in various environments that mimicked the stomach, small intestine, and blood. Briefly, the stomach environment was mimicked with hydrochloric acid and pepsin. The intestinal environment was buffered to a

neutral pH with pancreatin, and human serum was used to mimic a blood environment. **12d**, **13b**, and **14a** were incubated in these environments and samples taken at various time points. Samples were examined compared to baseline via mass spectrometry to determine their half-lives in these environments. Comparing the Area Under the Curve for Total Ion Concentration and UV intensity at 254 nm demonstrated that these compounds were stable for >12 hours, >24 hours, and >24 hours in the stomach, intestine, and blood environment respectively. Satisfied that our lead inhibitors are both non-mutagenic and seemingly stable in vivo, we transitioned to animal studies to determine their respective maximal tolerated doses. It has been previously reported that similar compounds, panobinostat and entinostat, had maximum tolerated doses of 15 and 20 mg/kg/day for 14 days in Balb/c mice. We performed a maximum tolerated dose study using 15 female Balb/c mice in groups of 3. This set up, referred to as a modified Fibonacci sequence, or 3+3 sequence, allows for the fastest and safest determination of maximum tolerated dose.

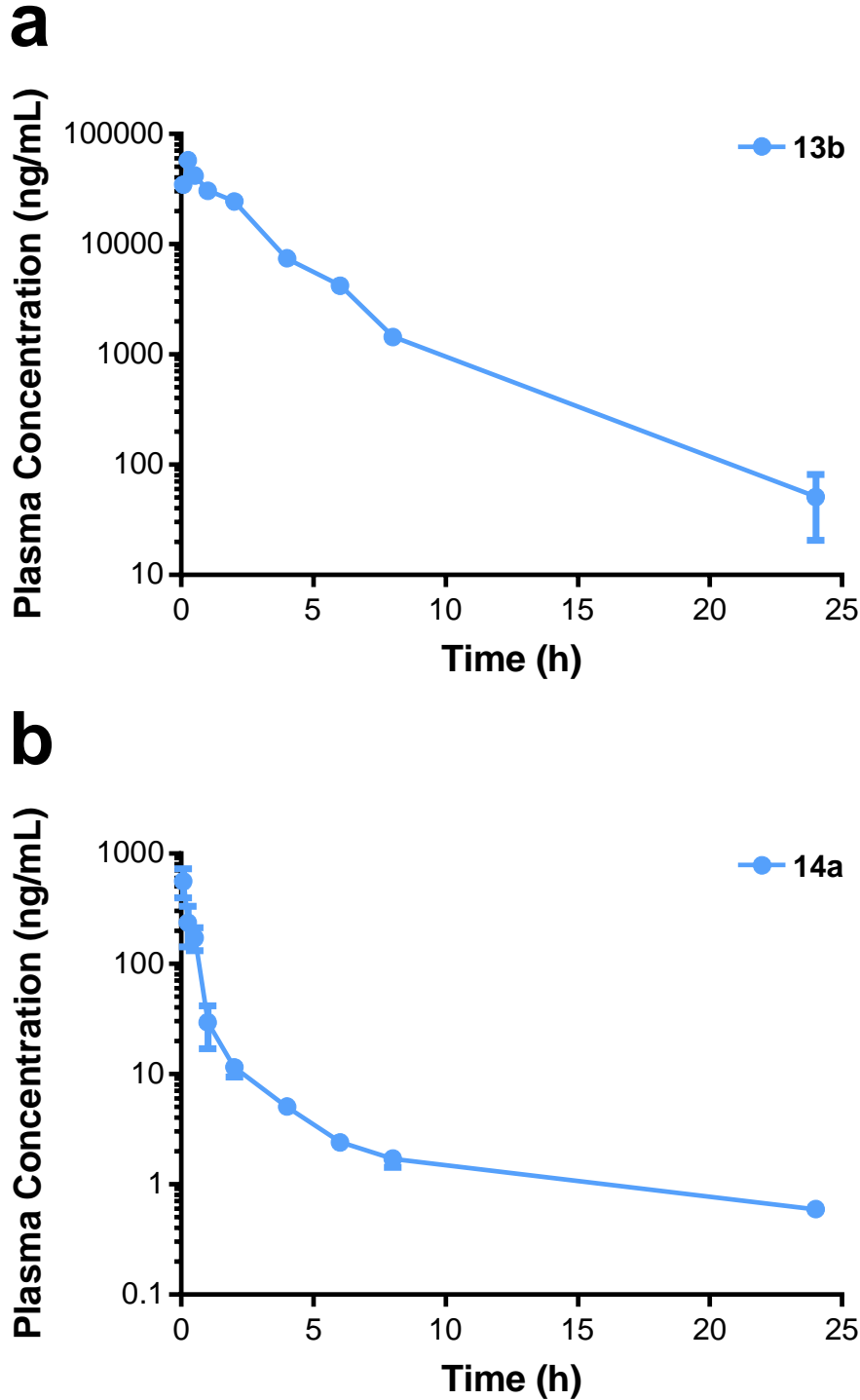
Compound **12d** at 20 mg/kg/day via alternating site IP injection resulted in sacrificed mice at day 6, at 10 mg/kg/day the mice were sacrificed at day 13 of the study. All reasons of sacrifice was for signs of moribund/suffering. Mice were nearly immobile, had unkempt fur, were hunched over, had lost 20% or more of their baseline body mass and were breathing rapidly. The mice were humanely sacrificed via CO₂ asphyxiation followed by cervical dislocation. Blood samples taken before death were run for basic chemistry as well as liver function tests. All results were within normal limits with the exception of elevated potassium. This, however, was likely attributable to 2+ hemolysis of the samples. Autopsy for two of the mice showed a blue, hypoxic looking stomach/intestinal tract, however reasons for this were not apparent.

Compound **13b** at 20 mg/kg/day via alternating site IP injections resulted in sacrificed mice on day 2. Two mice died overnight between injections, and the third was found to be moribund the second morning. Like compound **12d**, the blood chemistry panel and liver function test came back within normal limits. Autopsy revealed no acutely abnormal organ appearance.

Compound **14a**, however, was well tolerated at both 10 and 20 mg/kg/day via alternating site IP injections. All six mice finished the entire treatment with no signs of moribundity or suffering. All six mice were humanely sacrificed and their brains, livers, kidneys, and spleens stored in formalin for future study if necessary.

Puzzled by this difference in toxicities, despite very little difference in structure, we sent out samples for an independent Pk/Pd test for both compounds **13** and **14a**. The experiment was performed in 6 female Balb/c mice, 3 per compound, at 20 mg/kg via one time IP injection. Blood samples were taken at 0.083, 0.25, 0.5, 1, 2, 4, 6, 8, and 24 hours after IP injection. Concentrations were determined via mass spectrometry. Data from all time points and all mice were used to determine the C_{max} , Area Under the Curve, and half-life for both compounds. The resulting data (**Figures 3.22a** and **b**) demonstrate that **13b** possesses a half-life of ~3.2 hours with a C_{max} of 58,600 ng/mL (174 μ M). **14a** showed second-order clearance kinetics, with a half-life of ~8 hours. Its C_{max} , however, was much lower at 559 ng/mL (1.43 μ M). This extremely high C_{max} for **13b** is very likely the reason for the very acute toxicities seen with **12d** and **13b**. To put the C_{max} in perspective, panobinostat's C_{max} determined via a one-time IV injection was only 1.86 μ M at the same 20 mg/kg dose given for **13b**. This ~100 fold difference means our animals were getting 100 times the effective dose as panobinostat.

Figure 3.22. Pk/Pd profiling of **13b** and **14a**.



Data are presented as means of 3 individual mice. Error bars are S.E.M. **13b** shows first-order clearance kinetics. **14a** shows second-order clearance kinetics. Note semi-log plots.

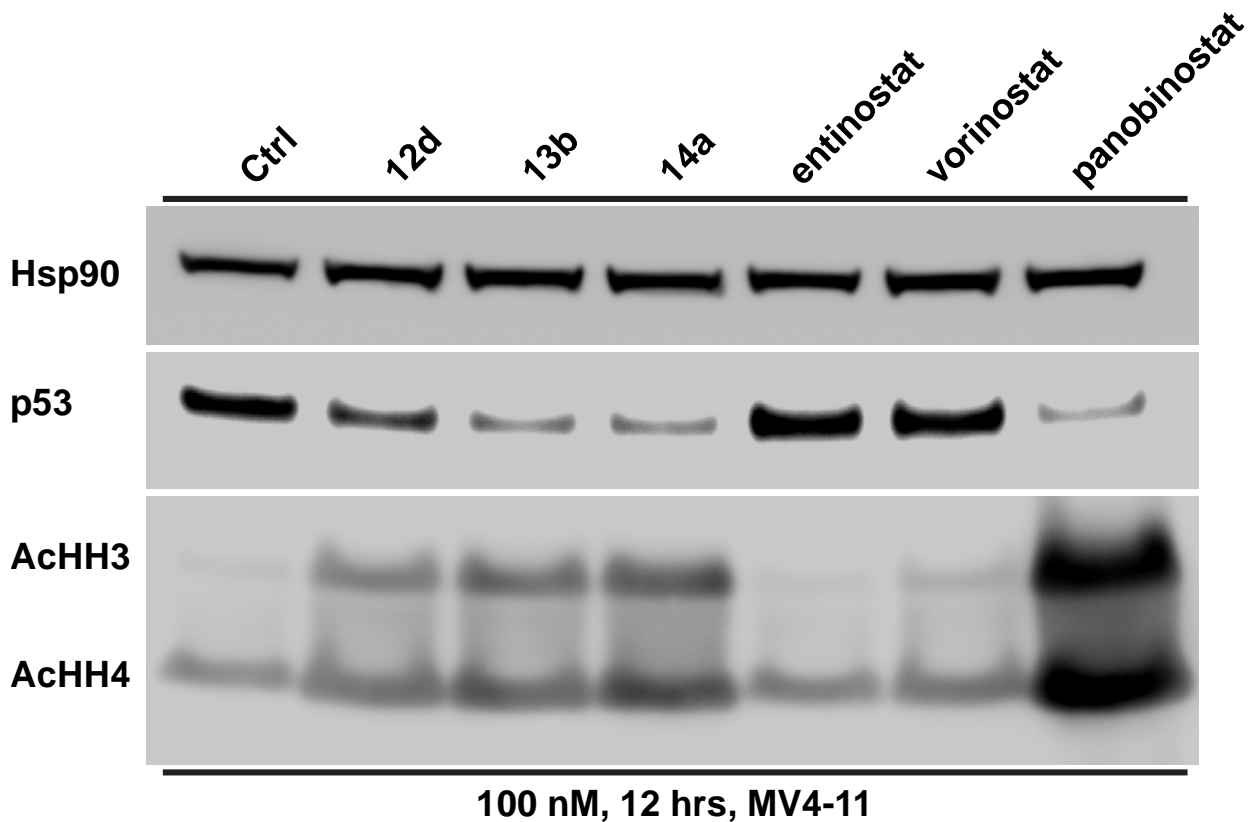
As such, we moved forward with efficacy studies in-vivo using **14a**. Using NOD-scid gamma mice which are devoid of mature B and T cells, Natural Killer Cells, and complement, have defective macrophages and dendritic cells, and low irradiation tolerance, we injected 5 million luciferase-tagged MV4-11 cells via tail vein after 2 Gy irradiation exposure. Mice have received IP injection of 150 mg/kg luciferin doses weekly and imaged to determine rate and extent of engraftment. Upon engraftment in spine, femur, or cranial area, we will begin daily IP injections of **14a** at the previously tested 20 mg/kg dose.

We have attempted to determine in broad strokes what the mechanism behind these hydrazide-based inhibitors is for their apparent selective killing of AML cells. Our first efforts were to determine if these inhibitors either killed AML cells via activation of caspase or if they were killing the cells via an autophagic pathway. MV4-11 cells were incubated with 20 μ M ZVAD-FMK, a polypeptidic pan-inhibitor of caspases, with or without **12d**, **13b**, or **14a** at various doses for 12, 24, and 48 hours. Cell viability was determined via resazurin and the IC₅₀ values of each inhibitor was compared to the values with ZVAD-FMK. There was no apparent nor statistically significant (independent two-sided t-test) difference between the inhibitors alone vs the inhibitor with 20 μ M for any of the three time points tested. Inquiries into the autophagic pathway yielded similarly frustrating results. Similarly performed experiments utilizing 10 and 50 μ M of chloroquine yielded no differences in IC₅₀ values either.

Puzzled by these results, we looked back at our previous data (**Table 3.8**) and saw an interesting trend. The three cell lines which compound **13b** was most efficacious, MV4-11, RS4-11, and Molm14 all have non-mutated and present p53. Further, the three cell lines which showed very little efficacy: K-562, HL-60, and RPMI-8226, all possess either mutated or absent

p53. Curious to follow-up on this interesting finding, we blotted MV4-11 cells treated with **12d**, **13b**, or **14a** as well as panobinostat, vorinostat, and entinostat (**Figure 3.23**). Interestingly, at 12 hours we see a marked decrease in p53 that is correlative with the increase in histone H3 and H4 acetylation.

Figure 3.23. Western Blot Analysis of MV4-11 at 12 hours with various HDAC inhibitors.



That is to say, as HDACs 1-3 are inhibited with more and more potency, p53 levels decrease in a similar fashion. Further, this effect seen seems to be irrespective of cell killing, as Hsp90 levels are approximately equal in all samples. To further test the hypothesis that MV4-11 cells may be being killed through a p53 mediated mechanism, we have sent out our lead inhibitors to the NIH for screening in their 60 cell panel. We will cross-reference the efficacy of our compounds in these cells against the normal, mutated, or absent p53 status. Depending on the results, a sub

analysis may be performed on the data to determine if certain p53 mutations have no impact on their efficacy.

4 SUMMARY

The findings of this body of work are as follows:

Determined the individual isozyme activity for all known zinc-dependent HDACs against a myriad of known lysine-residue based substrates with acyl modifications. Specifically demonstrating the role of HDACs 3 and 6 as deacylases, HDAC1-3 as depropionylases, and HDAC3 as a devalerylase. From this finding we generated a fairly selective HDAC3 inhibitor using a substrate-based medicinal chemistry approach. This inhibitor was used as a tool to confirm that selective HDAC3 inhibition demonstrates anti-inflammatory effects in vitro. These findings met Aims 1, 1.1, and 2.

Additionally, this work covered the further enhancement of hydrazide-based HDAC inhibitors, achieving 0.95 nM inhibitors in vitro. These inhibitors were later shown to be impervious to glucuronidation using ex vivo human liver homogenates. Lead analogues from our synthetic efforts were found to be highly potent and selectively toxic toward acute myeloid leukemia cells. These findings covered Aims 3 and 3.1.

Lastly, we demonstrated the preliminary PK/PD profiles of lead analogues to be favorable for further development. The lead hydrazide-based analogues were sufficiently bioavailable and with appreciable half-lives in vivo. We reported on preliminary and very non-conclusive regarding possible mechanisms by which these inhibitors are selectively killing leukemia cells.

5 CONCLUSIONS AND PERSPECTIVES

5.1. Conclusions and Perspectives: Role of Histone Deacetylases as Lysine Deacylases: Impact in medicinal chemistry and inflammatory diseases.

In this chapter, we investigated HDAC isozyme-specific deacylase activity and demonstrated a biological relevancy of these findings. We have shown that HDACs 3 and 6 possess deacylation activity, confirmed previous findings that HDAC3 has deacetylase activity, presented preliminary evidence that HDACs 1-3 can remove propionyl groups, and demonstrated that HDAC3 has specific activity toward butyryl-, and valeryl-substrates (**Figure 3.2a**). We developed a selective HDAC3 inhibitor **2a** based on the results from our initial deacylase profiling. This inhibitor induced NF- κ B p65 Lys122/Lys123 and p53 Lys382 acetylation without affecting histone or tubulin acetylation. Additionally, **2a** shortened NF- κ B p65 nuclear localization duration and attenuated NO production and HMGB-1 secretion in activated macrophages (**Figure 3.10**).

The presented data suggest that lysine deacylation is likely to be co-regulated by HDACs 3 and 6, with HDAC6 driving more deacylation activity in vitro than HDAC3 (**Figure 3.2b** and **Figure 3.4**). This process is likely to occur in the cytosol as HDAC6 shows high subcellular localization fidelity to this compartment.¹⁸⁰ This result explains why a previous study utilizing mass spectrometry indicates that HDAC activity does not affect nuclear and histone acetylation and is refractory to HDAC inhibitor treatments.¹⁸¹ Additionally, upon treatment with HDAC inhibitors, total protein acetylation levels increased in a manner dependent on the selectivity of the inhibitor (**Figure 3.6b**).

The presented data also suggest HDAC3 has the ability to remove butyryl-, crotonyl-, and valeryl-based PTMs (**Figure 3.1b** and **Figure 3.2a**). Only HDAC inhibitors targeting HDAC3 were capable of inducing an increase in protein valerylation, which is consistent with our in vitro activity profiling (**Figures 3.2a** and **3.5a**). Interestingly, the highly selective HDAC6 inhibitor Tubastatin A blocked induction of valerylated protein by other HDAC inhibitors. Global levels of valerylated cellular proteins also decreased when both HDACs 3 and 6 were concomitantly silenced, similar to the HDAC inhibitor results. Silencing of either HDAC3 or HDAC6 resulted in an increase in valerylated protein levels; suggesting that the elimination of HDAC6 likely affects HDAC3 devalerylase activity (**Figure 3.6d**). This may be explained through the known complexes in which HDACs 3 and 6 both have been shown to reside.^{163, 182} Another possible explanation involves acetyl groups and valeryl groups competing for the same lysine residues. If HDAC6 is inhibited and acetyl groups are either more ubiquitous or are more favorably ligated to free lysine residues than valeryl groups, we would expect the lysine residues to be stabilized with more acetyl groups rather than valeryl. This is due to the cross coverage that a multitude of HDACs perform in the remove of acetyl groups whereas only HDAC3 seems to be able to remove valeryl modifications. This would in turn lead to an overall decrease in valerylated lysine residues compared to acetylated. With respect to the knockdown data demonstrating hypervalerylation, this may be in part to a compensatory mechanism of the cell that behaves differently than reversible small molecule inhibition.

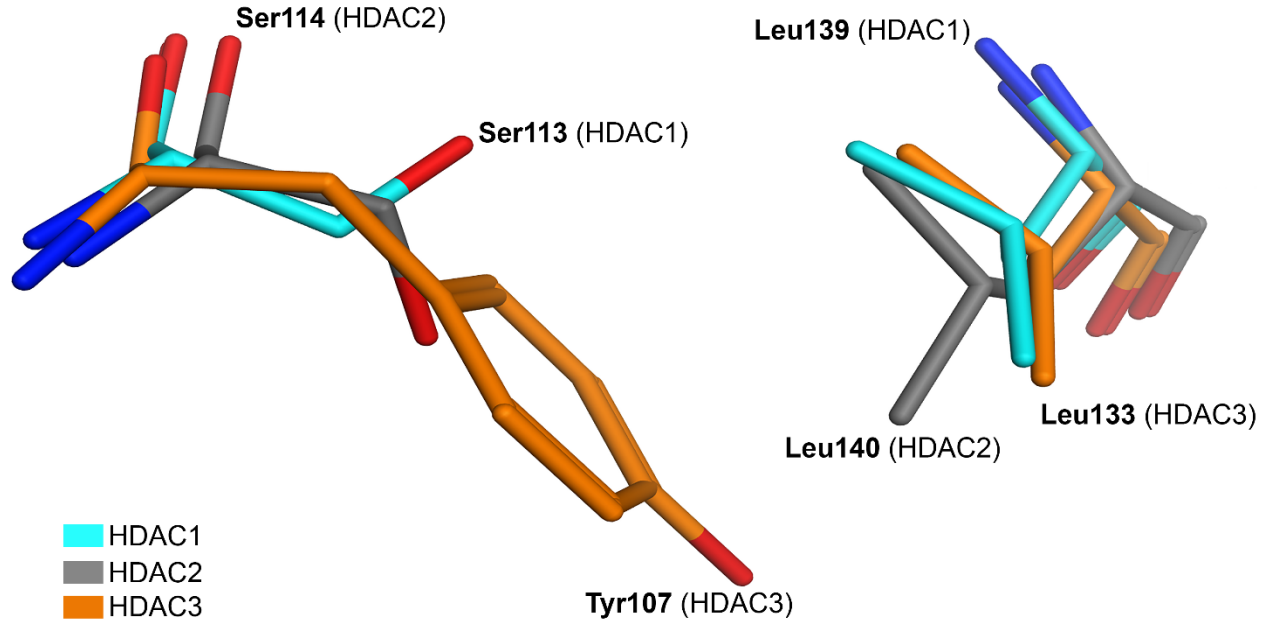
Traditionally, developing selective HDAC3 inhibitors has led to very limited success. With the development of entinostat, PD-106, and T326 being the most notable.¹⁸³ This is largely in part due to the high level of homology showcased between HDACs 1-3 (**Figure 1.4**). In this study, we

have shown that by maintaining the trans-pentene geometry of the crotonyl-based PTMs and introducing fluorines around the *ortho*-aminoanilide ring (**Figure 3.8** and **Figure 3.9**), a highly potent and selective HDAC3 inhibitor can be achieved. This inhibitor defines a chemotype that promotes selective HDAC3 inhibition. Interestingly, **2a** also showed selective slow-on/slow-off kinetics for HDAC3 but not HDAC 1 (**Figure 3.9**). This is in contrast to previous findings that described benzamide-containing HDAC inhibitors to possess time-dependent binding kinetics vs class I HDACs.¹⁵⁸ It is interesting to note that a previous study presented rationale behind why fluorination in certain positions around the benzamide ring may lead to HDAC3 selectivity, postulating that the intramolecular constraints of a pocket dwelling Leucine was different in HDAC3 compared to HDAC2.¹⁶⁵ This difference allowed the authors to develop an inhibitor that was selective for HDAC3. However, their explanation does not adequately cover the striking similarities between this conserved Leucine when comparing HDAC3 with HDAC1 (**Figure 5.1**). While it is undoubted that fluorination plays a key part in both their inhibitors' design as well as ours, there is still much to be studied. Further, the discovery of potent HDAC inhibitors possessing internal metal chelation groups, the potential to develop even more potent and selective inhibitors could become more realized.^{141, 184}

The effects on NF- κ B, NO production, and HMGB-1 secretion in activated macrophages by inhibitor **2a** indicate that HDAC3 activity plays a key role in pro-inflammatory signaling. HDAC3 itself has been implicated in the regulation of inflammatory gene transcription in macrophages.¹⁸⁵ However, based on our results, HDAC3 activity also plays other roles; such as regulating its own cellular localization and the duration of NF- κ B p65 nuclear localization (**Figure 3.10d**). Our findings are consistent with previous observations⁴² which suggest that HDAC3

controls NF- κ B p65 Lys122/123 acetylation status, its cellular localization, and rate of recovery to its latent state complex in the cytosol. Additionally, NO production is closely linked to NF- κ B

Figure 5.1. Crystal structure overlay of key pocket residues in HDACs 1-3.



Crystal structure overlay of HDACs 1-3. Leu133 of HDAC3 and Leu139 of HDAC1 possess a very similar conformation and intramolecular assembly. HDAC2, however, does demonstrate different geometry as previously reported. PDB files: 5ICN, 3MAX, and 4A69 for HDACs 1-3 respectively.

activation in macrophages¹⁸⁶⁻¹⁸⁸, thus it is not surprising that NO production is attenuated by **2a**.

Our findings also demonstrate the ability of HDAC3 to control the acetylation of Lys382 of p53.

There are several reports of the effects of inhibitors demonstrating different effects on this Lysine. Further study controlling for cell type, concentrations of inhibitors, and length of treatment is undoubtedly needed.

HMGB-1 contains multiple PTMs, including acetylation and formylation of lysine.¹⁷⁰ Upon stimulation, acetylated HMGB-1 translocates from the nucleus to the cytosol primed for secretion¹⁷⁰ and sequential activation of inflammasomes is required for HMGB-1 secretion.¹⁸⁹⁻¹⁹¹

Selective HDAC3 inhibition prevents HMGB-1 secretion similar to the pan-HDAC inhibition of

vorinostat (**Figure 3.10c**). A similar result was observed for IL-1B secretion in macrophages, which also requires a two-step process for its secretion.¹⁹² Since acetylated HMGB-1 accumulates in the cytosol and HDAC3 activity is required for its secretions, this suggests HDAC3 likely plays a role in inflammasome activation during the second phase of secretion. Since HDAC3 has both deacetylase and select deacylase activity, it is likely that the presented anti-inflammatory effects are due to an increase in lysine acetylation or certain acyl-PTMs of specific lysine substrates.

5.2. Conclusions and Perspectives: Development of Allosteric Hydrazide-Containing Class I Histone Deacetylase Inhibitors for Use in Acute Myeloid Leukemia.

To date, all FDA approved HDAC inhibitors or those in clinical trials contain promiscuous metal-chelating groups. The hydroxamic acid was the first metal-chelating group to be introduced, and to this day remains the most common, but others such as the disulfide bond of romidepsin, or the *ortho*-aminoanilide of entinostat have also been used. These groups are all generally acidic in nature, and have been shown to be subject to glucuronidation. This addition of steric bulk and charge neutralization removes the ability of these inhibitors to get into the narrow active site and ionically bind to the positively charged zinc that is paramount to HDAC deacylase activity. In this study we demonstrated that very potent and selective inhibition of class I HDACs is possible with the novel utilization of the metal chelating group, hydrazide. Further, we demonstrated that these compounds likely work through an allosteric mode of inhibition. This possibly indicates the presence of a non-catalytic metal-center target of these hydrazide compounds. Thus far, discoveries of allosteric, small molecule inhibitors of class I HDACs have not been well established in the literature. Inhibitors that lack a known metal-chelating group

that have been shown to inhibit HDACs were shown to display canonical competitive Michaelis-Menten enzyme kinetics when further interrogated.¹⁹³

The results in this manuscript suggest our compounds are also highly resistant to glucuronidation, indicating they possess little anionic charge, and display mixed/non-competitive inhibition, giving further credibility to the possibility that they may bind to a non-catalytic site on HDACs irrespective of whether substrate is bound. Further, this allosteric site is present *ex vivo*, as their recombinant enzyme inhibition prowess translated directly to cellular efficacy as well. Discovery of a potential allosteric binding site benefits more than just medicinal chemistry surrounding HDAC inhibitors. By having a combination of agents that work both at the active site, and allosterically on HDACs, the possibility of dual mechanism therapies for acute myeloid leukemia arises.

Lastly, while this paper established a >60 fold improvement in potency over the initial lead inhibitor generated by Wang and colleagues, our most potent of which breaching the picomolar range for recombinant human HDAC3 inhibition, further refinement of these inhibitors is also possible. Further alterations surrounding N-benzylbenzamide group that provided so much of these molecules' potencies would be the first place to start. Stepwise methylation at key sites, or the introduction of electron donating or withdrawing groups around either of the phenyl rings could provide additional potency.

Our lead inhibitors **11i**, **12d**, and **13b**, were used ubiquitously throughout the manuscript. All of these agents display higher levels of *ex vivo* potency than vorinostat or entinostat. The most potent, **13b**, contains a Michael-acceptor group in the form of an α, β -unsaturated ketone. While once a forbidden group in medicinal chemistry, recently approved effective therapies such as

dimethyl fumarate demonstrate that not all Michael-acceptors are detrimental to patient health, even in long term use. However, when comparing **13b**'s potency to that of **12d**, we see an approximate 2.5 fold decrease in EC₅₀ in MV4-11 cells at the cost of a 10 fold increase in PBMC based toxicity. Further, this was the only one of our compounds tested in human liver microsomes to demonstrate a metabolite, being reduced about its unsaturated bond. This was surprising, as no external reducing substrates such as NADH or NADPH were added to the reaction vessel. This indicates that even the residual concentrations of these reducing agents leftover from extraction were enough to metabolize this compound. As such, the superior metabolic stability, and better toxicity profiles of **12d** make it a more beneficial candidate worth pursuing.

5.3. Conclusions and Perspectives: In vivo testing and mechanistic determination of Hydrazone-Containing Class I Histone Deacetylase Inhibitors.

The stability of our lead inhibitors, determined via liver microsomes, stomach acid environments, intestinal environments, and human serum all demonstrated no appreciable glucuronidation or degradation as far out as 24 hours. These results were also seen with in vivo Pk/Pd studies in mice. Compounds **13b** and **14a** both demonstrated appreciably long half-lives (3.2 and 8 hours respectively) highly indicative of daily or less frequent dosing in humans. With efficacy studies on-going in vivo, it's difficult to definitively draw conclusions regarding the degree to which these compounds are likely to show effect in higher order animals including humans. An interesting question raised by the results of the Pk/Pd study is that of dosing frequency and intensity. That is, AML cells respond to high dose, infrequent therapy, or lower dose constant therapy. A similar phenomena is seen in bacteria. Antimicrobials are notoriously

dosed based on C_{max} or time above minimal inhibitor concentration. A follow-up to the ongoing efficacy study would be to determine if it's better to treat daily, biweekly, or weekly at appropriate and safe doses for each regimen. Maximal tolerated doses for each frequency would have to be established before this could be done.

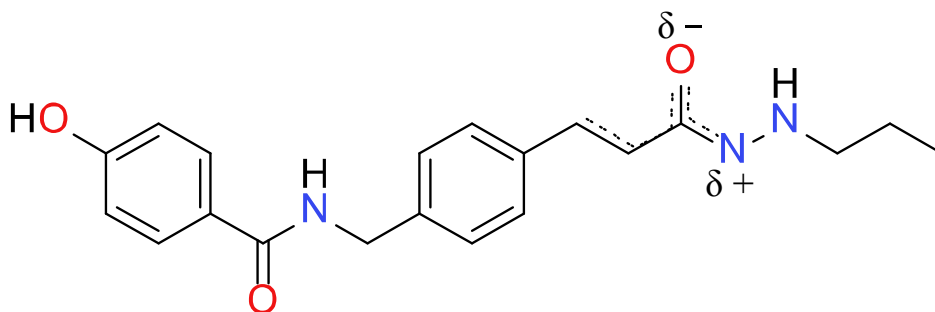
Transitioning to the inquiry of mechanism, the lack of effect of ZVAD-FMK and chloroquine on the efficacy of the hydrazide-based inhibitors in the Acute Myeloid Leukemia cell line is certainly interesting. It implies that a non-caspase, non-autophagy mediated pathway is responsible for the potent and selective killing seen in these cells. Neither **12d**, **13b**, or **14a** were affected by the presence of these inhibitors. An alternative explanation may lie with p53, however, further analysis is needed. The results of the large scale NIH cell panel screen will quickly give more validity to this hypothesis or render it flawed.

Lastly, it's interesting to note a structural difference between panobinostat and other transcinamic acids with hydroxamates. It uses a slightly modified tryptophan that seemingly has little bearing on its efficacy. Instead, I believe this group was added to improve Pk/Pd profiles, particularly to improve drug penetrance into cells and its half-life in vivo. A similar scenario was seen with a compound valacyclovir. This compound, differing from acyclovir only by addition of a valine group increased the drug's half-life 5 fold, turning it from a 5 times per day dose (acyclovir) to the once daily dose (valacyclovir). This is due to the amino acid receptors in the kidney recognizing the valine and recycling it, preventing excretion. It is interesting to note that panobinostat, possessing a different amino acid mimetic in the way of tryptophan has a 27 hour half-life in humans. As such, I believe addition of a para-position hydroxyl group to the benzamide on the "left" side of **12d** or **13b** may produce a mimetic tyrosine that possesses similar effects to

panobinostat and valacyclovir in terms of kidney recycling in vivo. This simple change may yield very large dividends on druggability with minimal effect on efficacy.

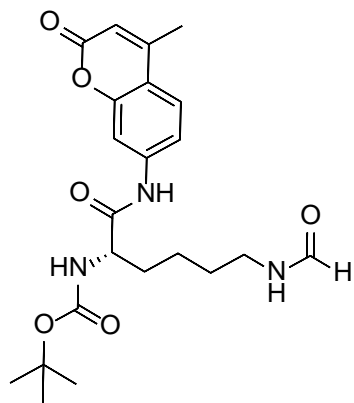
Individuals familiar with isoniazid may have associated the presence of its hydrazide motif and liver toxicity to our hydrazide motif. Lesser known compounds containing this moiety also include: benmoxin, iproclozide, iproniazid, isocarboxazid, nialamide, pivhydrazine. Nearly all of these compounds, excluding isocarboxazid, have been shown to induce hepatitis or acute liver damage. Interestingly, many of them have been associated with Monoamine oxidase inhibition as well. The hepatotoxicity seems to stem from cleavage about the nitrogen-carbonyl bond yielding an aldehyde and primary amine. The primary amine can be acetylated forming acetylhydrazide, a rather hepatotoxic compound. Secondary acetylation to the remaining primary nitrogen, however, nullifies this toxicity. In an effort to prevent this cleavage, I propose the acrylamide group present in **13b** be repositioned to generate the following molecule. This molecule retains the propylhydrazide structure but possibly thwarts cleavage of the nitrogen-carbonyl bond of hydrazide by way of inductive resonance stabilizing the bond (**Figure 5.2**).

Figure 5.2. Proposed Hydrazide Derivative with transcinamic acid and tyrosine mimetic.



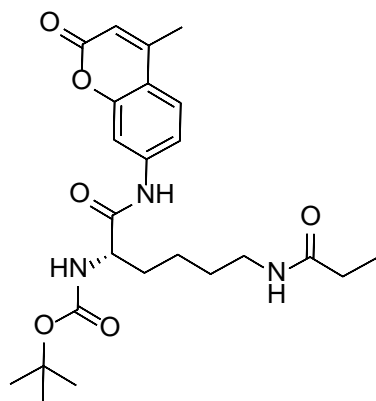
6.1. Detailed Synthetic Procedures.

Acylated substrates synthesis:



Formyl-substrate. $N\alpha$ -(tert-Butoxycarbonyl)-L-Lysine-7-amido-4-methylcoumarin (100mg, 0.25 mmole) was dissolved in Dimethylformamide with catalytic amount of DIPEA. **Formyl-substrate** was generated by adding 2,2,2-Trifluoroethyl Formate (128 mg, 1 mmole 4 equiv) and reacted for 12 hours. The reaction mixture was injected directly into Combiflash instrument in HPLC

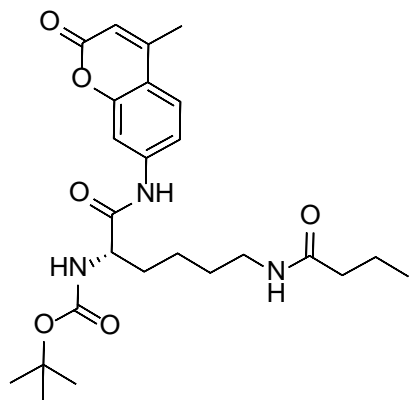
format to obtain the desired product. ^1H NMR (400 MHz, DMSO): δ 10.43 (s, 1H), 7.99 (s, 2H), 7.78 (d, 1H, $J = 2$ Hz), 7.73 (d, 1H, $J = 8$ Hz), 7.50 (d, 1H, $J = 8$ Hz), 7.13 (d, 1H, $J = 8$ Hz), 6.27 (s, 1H), 4.06 (m, 1H), 3.07 (m, 2H), 2.41 (s, 3H), 1.66-1.60 (m, 2H), 1.42-1.39 (m, 11H), 1.30-1.27 (m, 2H); ^{13}C HSQC (400MHz, 100MHz, DMSO): δ 126.4, 115.7, 112.7, 106.1, 55.7, 37.4, 31.7, 29.3, 28.7, 28.6, 18.5. $[(m+H^+)/z = 432.1]$



Propionyl-substrate. $N\alpha$ -(tert-Butoxycarbonyl)-L-Lysine-7-amido-4-methylcoumarin (100mg, 0.25mmole) was dissolved in Dimethylformamide with catalytic amount of DIPEA. **Propionyl-substrate** was generated by adding propionyl chloride (92mg, 1mmole 4equiv) and reacted for 12 hours. The reaction mixture was injected directly into Combiflash instrument in HPLC format

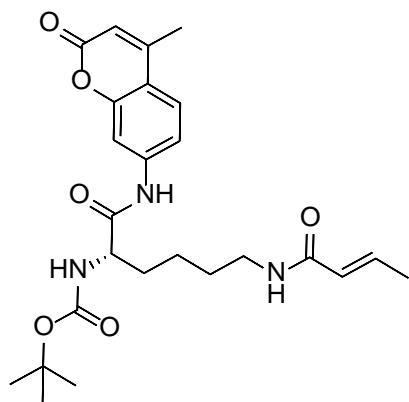
to obtain the desired product. 41% yield. ^1H NMR (400 MHz, DMSO): δ 10.42 (s, 1H), 7.79 (d, 1H, $J = 2$ Hz), 7.75-7.71 (m, 2H), 7.72 (d, 1H, $J = 8$ Hz), 7.11 (d, 1H, $J = 8$ Hz), 6.28 (s, 1H), 4.08-4.03 (m, 1H), 3.05-3.00 (m, 2H), 2.41 (s, 3H), 2.07-2.01 (q, 2H, $J = 8$ Hz), 1.69-1.60 (m, 2H), 1.42-1.37 (m,

11H), 1.32-1.28 (m, 2H), 0.97 (t, 3H, J = 8 Hz); ¹³C HSQC (400MHz, 100MHz, DMSO): δ 126.4, 115.7, 112.7, 106.1, 55.7, 38.6, 31.7, 29.0, 28.7, 28.6, 23.5, 18.5, 10.5. LC/MS: [(m+H⁺)/z = 460.2]



Butyryl-substrate. Nα-(tert-Butoxycarbonyl)-L-Lysine-7-amido-4-methylcoumarin (100mg, 0.25 mmole) was dissolved in Dimethylformamide with catalytic amount of DIPEA. **Butyryl-substrate** was generated by adding butyryl chloride (107mg, 1 mmole 4 equiv) and reacted for 12 hours. The reaction mixture was injected directly into Combiflash instrument in HPLC

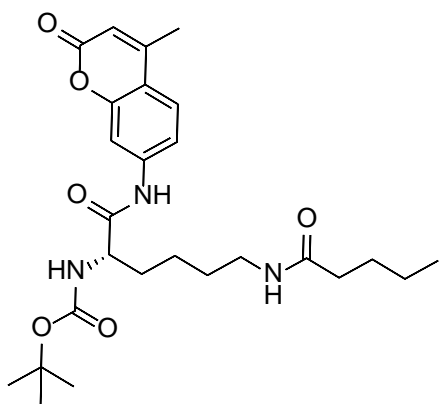
format to obtain the desired product. ¹H NMR (400 MHz, DMSO): δ 10.42 (s, 1H), 7.79 (s, 1H), 7.75-7.73 (m, 2H), 7.50 (d, 1H, J = 8 Hz), 7.11 (d, 1H, J = 8 Hz), 6.28 (s, 1H), 4.07-4.04 (m, 1H), 3.05-3.01 (m, 2H), 2.41 (s, 3H), 2.00 (t, 2H, J = 7 Hz), 1.69-1.55 (m, 2H), 1.53-1.45 (m, 2H), 1.44-1.40 (m, 11), 1.31-1.28 (m, 2H), 0.82 (t, 3H, J = 8 Hz); ¹³C HSQC (400MHz, 100MHz, DMSO): δ 126.4, 115.7, 112.7, 106.1, 55.7, 38.5, 37.9, 31.7, 28.7, 28.6, 23.5, 19.2, 18.5, 14.2. LC/MS: [(m+H⁺)/z = 474.1]



Crotonyl-substrate. Nα-(tert-Butoxycarbonyl)-L-Lysine-7-amido-4-methylcoumarin (100mg, 0.25 mmole) was dissolved in Dimethylformamide with catalytic amount of DIPEA. **Crotonyl-substrate** was generated by adding crotonyl anhydride (105mg, 1 mmole 4 equiv) and reacted for 12 hours. The reaction mixture was injected directly into Combiflash

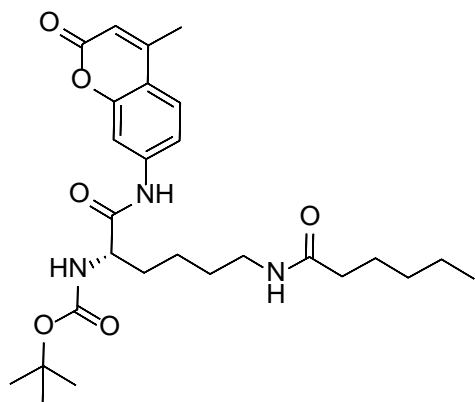
instrument in HPLC format to obtain the desired product. ¹H NMR (400 MHz, DMSO): δ 10.42 (s,

1H), 7.86 (t, 1H, J = 6 Hz), 7.78 (s, 1H), 7.73 (d, 1H, J = 8 Hz), 7.50 (d, 1H, J = 8 Hz), 7.12 (d, 1H, J = 8 Hz), 6.61-6.55 (m, 1H), 6.27 (s, 1H), 5.87 (d, 1H, J = 11 Hz), 4.07-4.04 (m, 1H), 3.12-3.07 (m, 2H), 2.41 (s, 3H), 1.77 (d, 3H, J = 7 Hz), 1.67-1.60 (m, 2H), 1.45-1.39 (m, 11H), 1.32-1.29 (m, 2H); ¹³C HSQC (400MHz, 100MHz, DMSO): δ 137.8, 126.5, 126.4, 115.7, 112.7, 106.1, 55.8, 31.7, 29.4, 28.7, 28.6, 23.5, 18.5, 17.8. [(m+H⁺)/z = 572.3]



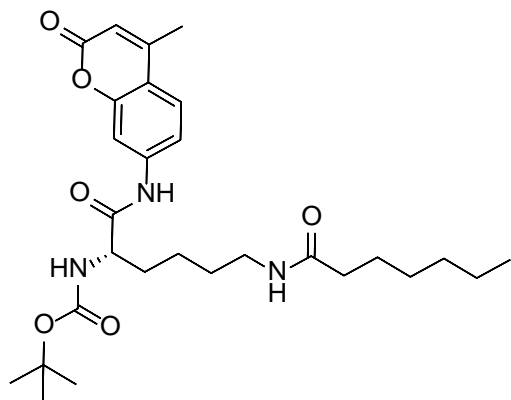
Valeryl-substrate. Nα-(tert-Butoxycarbonyl)-L-Lysine-7-amido-4-methylcoumarin (100mg, 0.25 mmole) was dissolved in Dimethylformamide with catalytic amount of DIPEA. **Valeryl-substrate** was generated by adding valeryl chloride (121mg, 1 mmole 4 equiv) and reacted for 12 hours.

The reaction mixture was injected directly into Combiflash instrument in HPLC format to obtain the desired product. ¹H NMR (400 MHz, DMSO): δ 10.43 (s, 1H), 7.79 (d, 1H, J = 2 Hz), 7.74-7.73 (m, 2H), 7.51 (d, 1H, J = 9 Hz), 7.11 (d, 1H, J = 8 Hz), 6.28 (s, 1H), 4.08-4.03 (m, 1H), 3.04-3.00 (m, 2H), 2.41 (s, 3H), 2.02 (t, 2H, J = 8 Hz), 1.65-1.62 (m, 2H), 1.47-1.40 (m, 13H), 1.29-1.22 (m, 4H), 0.84 (t, 3H, J = 8 Hz); ¹³C HSQC (400MHz, 100MHz, DMSO): δ 126.4, 115.7, 112.7, 106.1, 55.7, 38.6, 35.6, 31.7, 27.9, 28.8, 28.7, 23.5, 22.3, 18.5, 14.2. [(m+H⁺)/z = 488.3]



Hexanoyl-substrate. N α -(tert-Butoxycarbonyl)-L-Lysine-7-amido-4-methylcoumarin (100mg, 0.25 mmole) was dissolved in Dimethylformamide with catalytic amount of DIPEA. **Hexanoyl-substrate** was generated by adding hexanoyl chloride (135mg, 1 mmole 4 equiv) and reacted for 12 hours. The reaction mixture was injected directly

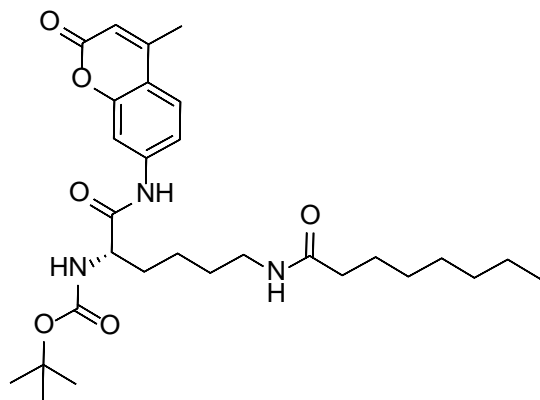
into Combiflash instrument in HPLC format to obtain the desired product. ¹H NMR (400 MHz, DMSO): δ 10.42 (s, 1H), 7.79 (d, 1H, J = 1 Hz), 7.75-7.73 (m, 2H), 7.50 (d, 1H, J = 9 Hz), 7.11 (d, 1H, J = 8 Hz), 6.28 (s, 1H), 4.07-4.04 (m, 1H), 3.04-3.00 (m, 2H), 2.41 (s, 3H), 2.01 (t, 2H, J = 8 Hz), 1.67-1.60 (m, 2H), 1.45-1.39 (m, 13H), 1.29-1.18 (m, 6H), 0.84 (t, 3H, J = 7 Hz); ¹³C HSQC (400MHz, 100MHz, DMSO): δ 126.4, 115.7, 112.7, 106.0, 55.7, 38.5, 35.9, 31.7, 31.4, 28.7, 28.5, 23.5, 22.3, 18.5, 14.3. [(m+H⁺)/z = 502.2]



Heptanoyl-substrate. N α -(tert-Butoxycarbonyl)-L-Lysine-7-amido-4-methylcoumarin (100mg, 0.25 mmole) was dissolved in Dimethylformamide with catalytic amount of DIPEA. **Heptanoyl-substrate** was generated by adding Heptanoyl Chloride (149mg, 1 mmole 4 equiv) and reacted for 12 hours. The reaction

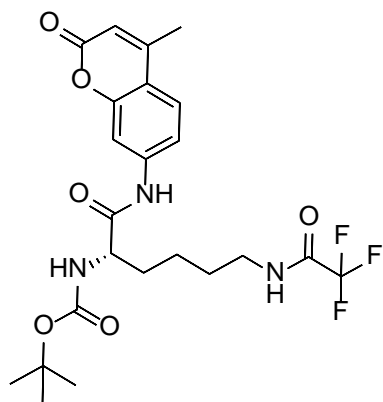
mixture was injected directly into Combiflash instrument in HPLC format to obtain the desired product. ¹H NMR (400 MHz, DMSO): δ 10.42 (s, 1H), 7.79 (d, 1H, J = 2 Hz), 7.75-7.73 (m, 2H), 7.50 (d, 1H, J = 8 Hz), 7.10 (d, 1H, J = 8 Hz), 6.28 (s, 1H), 4.08-4.03 (m, 1H), 3.04-3.00 (m, 2H), 2.41 (s, 3H), 2.01 (t, 2H, J = 8 Hz), 1.69-1.61 (m, 2H), 1.44-1.39 (m, 13H), 1.29-1.20 (m, 8H), 0.85 (t, 3H, J

= 7 Hz); ¹³C HSQC (400MHz, 100MHz, DMSO): δ 126.4, 115.8, 112.8, 106.1, 55.7, 38.5, 35.9, 31.7, 31.4, 28.8, 28.7, 28.5, 25.7, 23.4, 22.5, 18.5, 14.4. [(m+H⁺)/z = 516.4]



Octanoyl-substrate. Nα-(tert-Butoxycarbonyl)-L-Lysine-7-amido-4-methylcoumarin (100mg, 0.25 mmole) was dissolved in Dimethylformamide with catalytic amount of DIPEA. **Octanoyl-substrate** was generated by adding Octanoyl Chloride (163mg, 1 mmole 4 equiv) and reacted for 12 hours. The

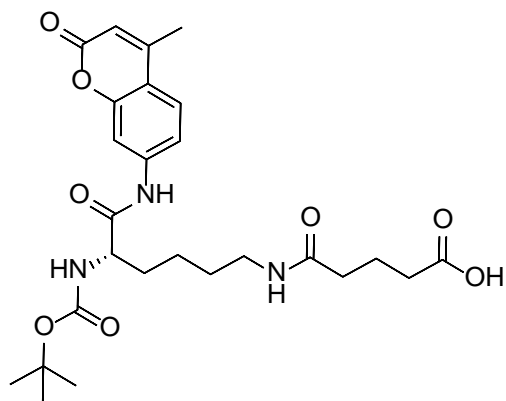
reaction mixture was injected directly into Combiflash instrument in HPLC format to obtain the desired product. ¹H NMR (400 MHz, DMSO): δ 10.42 (s, 1H), 7.79 (d, 1H, J = 2 Hz), 7.75-7.73 (m, 2H), 7.50 (d, 1H, J = 8 Hz), 7.10 (d, 1H, J = 8 Hz), 6.28 (s, 1H), 4.07-4.03 (m, 1H), 3.04-3.00 (m, 2H), 2.41 (s, 3H), 2.01 (t, 2H, J = 8 Hz), 1.64-1.60 (m, 2H), 1.46-1.39 (m, 13H), 1.29-1.21 (m, 10H), 0.87-0.83 (m, 3H); ¹³C HSQC (400MHz, 100MHz, DMSO): δ 126.3, 115.7, 112.7, 106.1, 55.7, 38.6, 35.9, 31.7, 31.6, 29.4, 28.9, 28.7, 28.5, 25.8, 23.4, 22.5, 18.5, 14.4. [(m+H⁺)/z = 530.2]



TFA-substrate. Nα-(tert-Butoxycarbonyl)-L-Lysine-7-amido-4-methylcoumarin (100mg, 0.25 mmole) was dissolved in Dimethylformamide with catalytic amount of DIPEA. **TFA-substrate** was generated by adding trifluoroacetic anhydride (210mg, 1 mmole 4 equiv) and reacted for 12 hours. The reaction mixture was injected directly into Combiflash instrument in HPLC

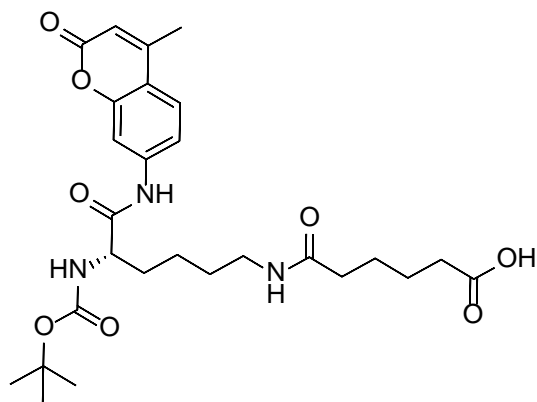
format to obtain the desired product. ¹H NMR (400 MHz, DMSO): δ 10.46 (s, 1H), 9.42 (t, 1H, J =

2 Hz), 7.78 (d, 1H, J = 2 Hz), 7.74 (d, 1H, J = 9 Hz), 7.50 (d, 1H, J = 9 Hz), 7.14 (d, 1H, J = 8 Hz), 6.28 (s, 1H), 4.09-4.05 (m, 1H), 3.20-3.16 (m, 2H), 2.41 (s, 3H), 1.69-1.60 (m, 2H), 1.55-1.46 (m, 2H), 1.39 (s, 9H), 1.34-1.25 (m, 2H); ¹³C HSQC (400MHz, 100MHz, DMSO): δ 126.5, 115.7, 112.8, 106.1, 55.6, 39.5, 31.6, 28.7, 28.5, 28.4, 18.5. [(m+H⁺)/z = 500.2]



Glutaryl-substrate. N α -(tert-Butoxycarbonyl)-L-Lysine-7-amido-4-methylcoumarin (100mg, 0.25 mmole) was dissolved in Dimethylformamide with catalytic amount of DIPEA. **Glutaryl-substrate** was generated by adding glutaric anhydride (114mg, 1 mmole 4 equiv) and reacted for 12 hours. The reaction mixture was injected

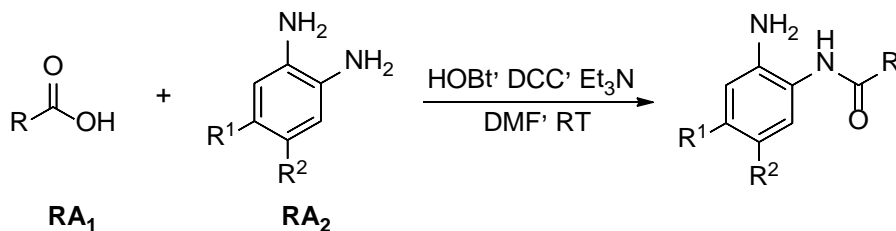
directly into Combiflash instrument in HPLC format to obtain the desired product. ¹H NMR (400 MHz, DMSO): δ 10.43 (s, 1H), 7.81-7.78 (m, 2H), 7.73 (d, 1H, J = 9 Hz), 7.50 (d, 1H, J = 9 Hz), 7.11 (d, 1H, J = 8 Hz), 6.27 (s, 1H), 4.08-4.03 (m, 1H), 3.34-3.01 (m, 2H), 2.41 (s, 3H), 2.18 (t, 2H, J = 8 Hz), 2.07 (t, 2H, J = 8 Hz), 1.73-1.60 (m, 4H), 1.45-1.38 (m, 13H); ¹³C HSQC (400MHz, 100MHz, DMSO): δ 126.4, 115.7, 112.7, 106.1, 55.7, 38.6, 35.0, 33.6, 31.7, 29.4, 28.7, 28.6, 21.2, 18.5. [(m+H⁺)/z = 518.2]



Adipoyl-substrate, N α -(tert-Butoxycarbonyl)-L-Lysine-7-amido-4-methylcoumarin (100mg, 0.25mmole) was dissolved in Dimethylformamide (DMF), 2-(1H-benzotriazol-1-yl)-1,1,3,3-tetramethyluronium hexafluorophosphate (HBTU),

Hydroxybenzotriazole (HOBT), and adipic acid (1:1:1 equiv.) with catalytic amount of DIPEA were dissolved in DMF. **Adipoyl-substrate** was generated by dripping Boc-Lys-AMC solution slowly into the activated adipic acid solution (four equiv.) and reacted for 2 hours. The reaction mixture was stopped by adding water into the reaction and injected directly into Combiflash instrument in HPLC format to obtain the desired product. ¹H NMR (400 MHz, DMSO): δ 10.46 (s, 1H), 7.79-7.77 (m, 2H), 7.74 (d, 1H, J = 9 Hz), 7.51 (d, 1H, J = 9 Hz), 7.11 (d, 1H, J = 6 Hz), 6.28 (s, 1H), 4.06-4.04 (m, 1H), 3.04-3.01 (m, 2H), 2.41 (s, 3H), 2.18 (t, 2H, J = 7Hz), 2.03 (t, 2H, J = 7 Hz), 1.69-1.59 (m, 2H), 1.41-1.45 (m, 4H), 1.39 (s, 9H), 1.30-1.28 (m, 4H); ¹³C HSQC (400MHz, 100MHz, DMSO): δ 126.4, 115.7, 112.7, 106.1, 55.8, 38.6, 35.6, 34.0, 31.7, 29.4, 28.7, 28.6, 24.8, 23.6, 18.5. [(m+H⁺)/z = 532.2]

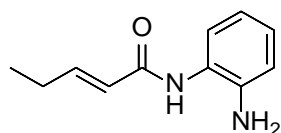
Inhibitor synthesis (Families 1 and 2)



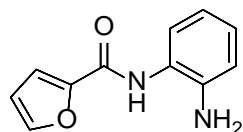
Carboxylic acid **RA₁** (2 mmol, 1 equiv), HOBT (4 mmol, 2 equiv), and DCC (4 mmol, 2 equiv) were dissolved in 50 mL DMF, to which was added Et₃N (4mmol, 2 equiv), and the resulting solution was stirred at room temperature for 30 mins. *o*-Phenylenediamine **RA₂**(2 mmol, 1 equiv) was then added to the solution, and the mixture was stirred overnight. Pour the mixture into 100 mL water, and extract it with 250 mL ethyl acetate. The organic phase was washed with saturated NaHCO₃ and brine successively, and it was then dried over MgSO₄ and filtered. The filtrates were

concentrated under vacuum, and the residue was purified by Combiflash instrument to obtain the desired product.

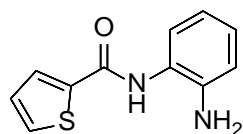
HDAC3 Inhibitor Characterization



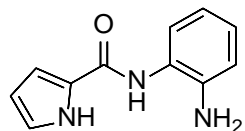
Compound **1**, (E)-N-(2-aminophenyl)pent-2-enamide, white solid, 28% yield. ^1H NMR (400 MHz, DMSO): δ 9.23 (s, 1H), 7.24-7.22 (d, J = 7.6 Hz, 1H), 6.92-6.78 (m, 2H), 6.73 (dd, J_1 = 8.0 Hz, J_2 = 0.8 Hz, 1H), 6.55 (td, J_1 = 7.2 Hz, J_2 = 1.6 Hz, 1H), 6.15 (d, J = 15.2 Hz, 1H), 4.85 (br, 1H), 2.23-2.17 (m, 2H), 1.03 (t, J = 7.2 Hz, 3H); ^{13}C NMR (100 MHz, DMSO) δ 172.2, 164.1, 145.9, 142.2, 126.2, 125.4, 123.8, 116.8, 116.5, 25.0, 12.9. LC/MS: [(m+H⁺)/z = 191.25].



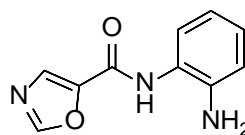
Compound **1a**, N-(2-aminophenyl)furan-2-carboxamide, white solid, 70% yield. ^1H NMR (400 MHz, CDCl₃): δ 8.20 (br, 1H), 7.45-7.44 (m, 1H), 7.34 (d, J = 8.0 Hz, 1H), 7.18 (d, J = 3.2 Hz, 1H), 7.04-7.01 (m, 1H), 6.80-6.76 (m, 2H), 6.52-6.51 (m, 1H), 3.91 (br, 2H); ^{13}C NMR (100 MHz, CDCl₃) δ 156.6, 147.6, 144.5, 140.8, 127.2, 125.3, 123.6, 119.5, 118.1, 115.3, 112.4. LC/MS: [(m+H⁺)/z = 203.33].



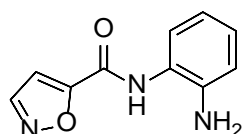
Compound **1b**, N-(2-aminophenyl)thiophene-2-carboxamide, white solid, 62% yield. ^1H NMR (400 MHz, DMSO): δ 9.74 (s, 1H), 7.98-7.97 (m, 1H), 7.79 (dd, J_1 = 4.8 Hz, J_2 = 1.2 Hz, 1H), 7.21-7.19 (m, 1H), 7.13-7.11 (m, 1H), 7.01-6.97 (m, 1H), 6.78 (dd, J_1 = 8.0 Hz, J_2 = 0.8 Hz, 1H), 6.63-6.59 (m, 1H), 5.50-3.50 (br, 2H); ^{13}C NMR (100 MHz, DMSO) δ 160.5, 143.6, 140.3, 131.8, 129.6, 128.5, 127.4, 127.3, 123.2, 117.0, 116.7. LC/MS: [(m+H⁺)/z = 219.19].



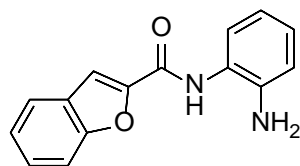
Compound **1c**, N-(2-aminophenyl)-1H-pyrrole-2-carboxamide, white solid, 31% yield. ^1H NMR (400 MHz, DMSO): δ 11.6 (s, 1H), 9.32 (s, 1H), 7.17-7.14 (m, 1H), 7.02-6.93 (m, 4H), 6.80-6.78 (m, 1H), 6.63-6.59 (m, 2H), 6.19-6.17 (m, 1H), 4.86 (br, 2H). ^{13}C NMR (100 MHz, DMSO) δ 159.8, 143.4, 126.9, 126.6, 126.4, 123.9, 122.5, 117.0, 116.7, 111.7, 109.3. LC/MS: [(m+H⁺)/z = 202.23].



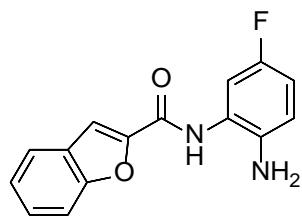
Compound **1d**, N-(2-aminophenyl)oxazole-5-carboxamide, white solid, 44% yield. ^1H NMR (400 MHz, DMSO): δ 9.80 (s, 1H), 8.59 (s, 1H), 7.93 (s, 1H), 7.12-7.10 (m, 1H), 7.01-6.97 (m, 1H), 6.78-6.76 (m, 1H), 6.61 (m, 1H), 4.94 (br, 2H). ^{13}C NMR (100 MHz, DMSO) δ 155.7, 154.0, 145.8, 143.8, 130.1, 127.5, 127.4, 122.0, 116.7, 116.5. LC/MS: [(m+H⁺)/z = 204.19].



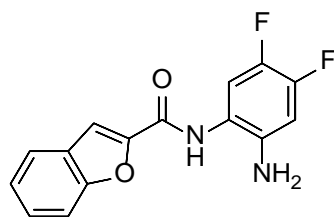
Compound **1e**, N-(2-aminophenyl)isoxazole-5-carboxamide, white solid, 22% yield. ^1H NMR (400 MHz, DMSO): δ 10.08 (s, 1H), 8.77 (d, J = 1.6 Hz, 1H), 7.20 (d, J = 1.6 Hz, 1H), 7.13-7.10 (m, 1H), 7.02-6.98 (m, 1H), 6.79-6.76 (m, 1H), 6.61-6.57 (m, 1H), 4.99 (br, 2H). ^{13}C NMR (100 MHz, DMSO) δ 163.2, 154.9, 152.1, 144.0, 127.8, 127.5, 121.7, 116.6, 116.5, 106.9. LC/MS: [(m+H⁺)/z = 204.17].



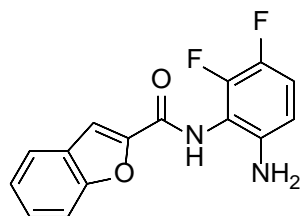
Compound **1f**, N-(2-aminophenyl)benzofuran-2-carboxamide, white solid, 75% yield. ^1H NMR (400 MHz, DMSO): δ 9.94 (s, 1H), 7.81 (d, J = 8.0 Hz, 1H), 7.73-7.69 (m, 2H), 7.51-7.47 (m, 1H), 7.37-7.33 (m, 1H), 7.23-7.21 (m, 1H), 7.03-6.99 (m, 1H), 6.84-6.81 (m, 1H), 6.65 (m, 1H), 4.98 (br, 2H). ^{13}C NMR (100 MHz, DMSO) δ 157.4, 154.8, 149.4, 143.6, 127.6, 127.4(127.4), 127.2, 124.2, 123.3, 122.7, 116.9, 116.7, 112.3, 110.7. LC/MS: [(m+H⁺)/z = 253.23].



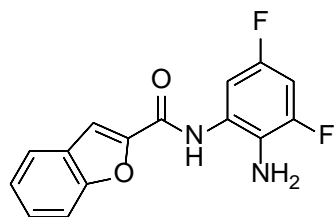
Compound **2**, N-(2-amino-5-fluorophenyl)benzofuran-2-carboxamide, white solid, 80% yield. ^1H NMR (400 MHz, DMSO): δ 9.88 (s, 1H), 7.83-7.81 (m, 1H), 7.74-7.70 (m, 2H), 7.52-7.48 (m, 1H), 7.39-7.35 (m, 1H), 7.20-7.16 (m, 1H), 6.62-6.58 (m, 1H), 6.42-6.38 (m, 1H), 5.35 (s, 2H). ^{13}C NMR (100 MHz, DMSO) δ 161.8 (d, $J = 239$ Hz), 157.7, 154.8, 149.5, 146.1 (d, $J = 13.3$ Hz), 129.2 (d, $J = 11.7$ Hz), 127.6, 127.4, 124.2, 123.3, 118.6, 112.3, 110.6, 102.6 (d, $J = 23.4$ Hz), 102.0 (d, $J = 25.1$ Hz). ^{19}F NMR (400 MHz, DMSO): δ -115.9. LC/MS: [(m+H⁺)/z = 271.17].



Compound **2a**, N-(2-amino-4,5-difluorophenyl)benzofuran-2-carboxamide, white solid, 78% yield. ^1H NMR (400 MHz, DMSO): δ 9.89 (br, 1H), 7.83-7.81 (m, 1H), 7.73-7.70 (m, 2H), 7.52-7.48 (m, 1H), 7.38-7.28 (m, 2H), 6.77-6.72 (m, 1H), 5.19 (s, 2H). ^{13}C NMR (100 MHz, DMSO) δ 157.6, 154.8, 149.2, 141.4, 141.3, 127.6, 127.5, 124.3, 123.3, 118.1, 116.0, 115.8, 112.3, 111.0, 103.6, 103.4. ^{19}F NMR (400 MHz, DMSO): δ -140.9, -153.8. LC/MS: [(m+H⁺)/z = 289.08]



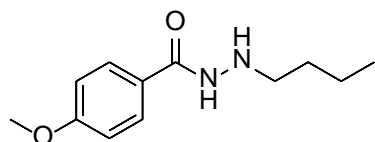
Compound **2b**, N-(6-amino-2,3-difluorophenyl)benzofuran-2-carboxamide, white solid, 66% yield. ^1H NMR (400 MHz, DMSO): δ 10.0 (s, 1H), 7.83 (d, $J = 3.86$ Hz, 1H), 7.2 (d, $J = 5.40$ Hz, 2H), 7.51 (t, $J = 2.74$ Hz, 1H), 7.37 (t, $J = 2.75$ Hz, 1H), 7.02-6.98 (m, 1H), 6.58 (q, $J = 6.85$ Hz, 1H), 5.41 (s, 2H). ^{13}C NMR (100 MHz, DMSO): δ 157.8, 154.8, 149.3, 140.5, 138.2, 135.0, 127.6, 127.5, 124.2, 123.3, 119.9, 112.3, 110.8, 102.7, 102.5. ^{19}F NMR (400 MHz, DMSO): δ -141.5, -158.2. LC/MS [(m+H⁺)/z = 289.08].



Compound **2c**, N-(2-amino-3,5-difluorophenyl)benzofuran-2-carboxamide, light orange solid, 54% yield. ^1H NMR (400 MHz, DMSO): δ 9.72 (s, 1H), 7.82 (d, $J = 3.72$ Hz, 1H), 7.72-7.70 (m, 2H), 7.50 (t, $J = 5.66$ Hz, 1H), 7.37 (t, $J = 5.66$ Hz, 1H), 6.39-6.33 (m, 2H), 5.73 (s, 1H). ^{13}C NMR (100 MHz, DMSO): δ 163.0, 160.8, 158.1, 154.8, 149.2, 127.6, 127.5, 124.2, 123.3, 112.3, 110.8, 106.0, 105.8, 96.8, 90.9. ^{19}F NMR (400 MHz, DMSO): δ -112.7, -117.2. LC/MS [($m+\text{H}^+$)/ $z = 289.08$].

Synthesis of butylhydrazide derivatives (**11a-11l**).

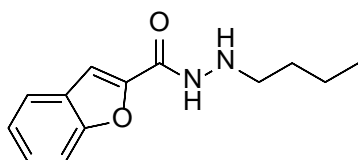
Series 11 General Procedure. Once the corresponding hydrazide was generated, 1.1 equivalents of butaldehyde and 10 equivalents of magnesium sulfate were stirred in 10 mL of ethanol with the hydrazide. The reaction was stirred at room temperature and monitored via TLC. After disappearance of starting material, the excess magnesium sulfate was removed via vacuum filtration, and the collected solution condensed under vacuum. The intermediate was resuspended in 4 mL of methanol followed by addition of 1.2 equivalents of sodium cyanoborohydride and a pinch of methyl orange. Argon was bubbled through the resulting yellow solution for 5 minutes. At this time a solution of concentrated HCl in methanol (1:1 v/v) was added dropwise until the solution turned and stayed red. The mixture was allowed to stir overnight under argon. Volatiles were removed under vacuum and purified on C18 reverse phase columns eluted with acetonitrile and water to yield the desired product.



N'-butyl-4-methoxybenzohydrazide (**11a**). 498.54 mg (3 mmol) of 4-methoxybenzohydrazide was reacted as described in **Series 11**

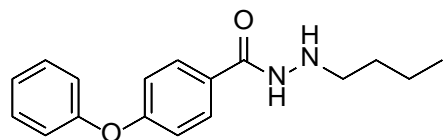
General Procedure to yield 317.9 mg of dry product (48% yield). ^1H NMR (400 MHz, DMSO): δ

9.89 (s, 1H), 7.82 (d, $J = 8.8$ Hz, 2H), 6.99 (d, $J = 8.8$ Hz, 2H), 4.99 (s, 1H), 3.81 (s, 3H), 2.79-2.76 (m, 2H), 1.48-1.40 (m, 2H), 1.38-1.32 (m, 2H), 0.89 (t, $J = 7.2$ Hz, 3H). ^{13}C NMR (100 MHz, DMSO): δ 165.4, 162.0, 129.3, 125.9, 114.0, 55.8, 51.5, 30.3, 20.3, 14.3. $[(m+H^+)/z = 223.25]$. (λ_{254}) purity 95.4%, t_R 9.28 mins.



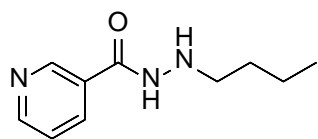
N'-butylbenzofuran-2-carbohydrazide (**11b**). 324.0 mg (2 mmol) of benzofuran-2-carboxylic acid was suspended in 5 mL of methylene chloride. The flask was flushed with argon for 10 minutes before

injection of 0.4 mL (4 mmol) oxalyl chloride. Two drops of dimethylformamide were injected and furious bubbling began. The sealed vessel was continuously flushed with argon and vented for 2 hours at room temperature. 10 mL of sieve dried ethanol was slowly injected and allowed to stir for an additional hour. Volatiles were removed under vacuum and the crude intermediate was resuspended in 5 mL ethanol. To this solution was added 250 mg (5 mmol) of hydrazine water salt. The reaction was refluxed for 3 hours to give the corresponding hydrazide. Volatiles were removed under vacuum and the product suspended in 10 mL of ethanol. From here the reaction proceeded as described in **Series 11 General Procedure** to yield 369.1 mg of dry product (72% yield). ^1H NMR (400 MHz, DMSO): δ 10.26 (d, $J = 6.0$ Hz, 1H), 7.78 (d, $J = 8.0$ Hz, 1H), 7.66 (d, $J = 8.4$ Hz, 1H), 7.54 (s, 1H), 7.49-7.45 (m, 1H), 7.36-7.32 (m, 1H), 5.16-5.13 (m, 1H), 2.84-2.79 (m, 2H), 1.48-1.41 (m, 2H), 1.39-1.33 (m, 2H), 0.90 (t, $J = 7.2$ Hz, 3H); ^{13}C NMR (100 MHz, DMSO): δ 157.7, 154.7, 148.7, 127.5, 127.2, 124.2, 123.1, 112.2, 109.6, 51.2, 30.2, 20.3, 14.4. $[(m+H^+)/z = 233.25]$. (λ_{254}) purity 98.8%, t_R 11.53 mins.



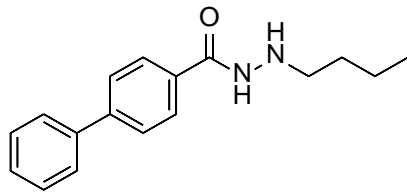
N'-butyl-4-phenoxybenzohydrazide (**11c**). 685 mg (3 mmol) of 4-phenoxybenzohydrazide was suspended in 10 mL of

ethanol. From here the reaction proceeded as described in **Series 11 General Procedure** to yield 596.7 mg of dry product (70% yield). ^1H NMR (400 MHz, DMSO): δ 9.99 (s, 1H), 7.88 (d, $J = 8.8$ Hz, 2H), 7.46-7.42 (m, 2H), 7.23-7.20 (m, 1H), 7.09 (d, $J = 8.0$ Hz, 2H), 7.03 (d, $J = 8.8$ Hz, 2H), 5.07 (s, 1H), 2.81-2.77 (m, 2H), 1.47-1.41 (m, 2H), 1.38-1.32 (m, 2H), 0.89 (t, $J = 7.2$ Hz, 3H); ^{13}C NMR (100 MHz, DMSO): δ 165.1, 159.9, 156.1, 130.7, 129.7, 128.4, 124.7, 119.9, 117.9, 51.4, 30.3, 20.3, 14.4. [(m+H⁺)/z = 285.25]. (λ_{254}) purity 98.2%, t_{R} 12.60 mins.



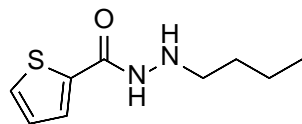
N'-butylnicotinohydrazide (**11d**). 1068 mg (6 mmol) of nicotinoyl chloride was suspended in 20 mL of methanol. To this solution was

added 1.7 mL (12 mmol) of triethylamine. The reaction was stirred at room temperature for 1 hour. 750 mg (15 mmol) hydrazine water salt was added and the solution was refluxed for 3 hours yielding the corresponding hydrazide. Volatiles were removed under vacuum and the intermediate was resuspended in 30 mL of methanol. From here the reaction proceeded as described in **Series 11 General Procedure** to yield 721.7 mg of dry product (62% yield). ^1H NMR (400 MHz, DMSO): δ 10.21 (s, 1H), 8.99 (s, 1H), 8.72-8.70 (m, 1H), 8.19-8.10 (m, 1H), 7.52-7.49 (m, 1H), 5.15 (s, 1H), 2.83-2.79 (m, 2H), 1.48-1.42 (m, 2H), 1.38-1.32 (m, 2H), 0.89 (t, $J = 7.2$ Hz, 3H); ^{13}C NMR (100 MHz, DMSO): δ 164.2, 152.3, 148.6, 135.2, 129.3, 124.0, 51.3, 30.2, 20.3, 14.4. [(m+H⁺)/z = 194.25]. (λ_{254}) purity 95.6%, t_{R} 6.17 mins.



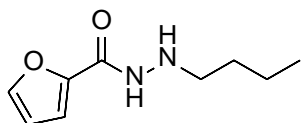
N'-butyl-[1,1'-biphenyl]-4-carbohydrazide (**11e**). 890 mg (3.8 mmol) of methyl [1,1'-biphenyl-4-carboxylate was suspended in 20 mL of methanol. To this solution, 945 mg (18.9 mmol) of

hydrazine water salt was added. The solution was brought to reflux and reacted for 3 hours. The solution was cooled and volatiles evaporated under vacuum. From here the reaction proceeded as described in **Series 11 General Procedure** to yield 555.1 mg of dry product (54% yield). ¹H NMR (400 MHz, DMSO): δ 10.08 (d, *J* = 6 Hz, 1H), 7.94-7.92 (m, 2H), 7.78-7.73 (m, 4H), 7.52-7.48 (m, 2H), 7.44-7.40 (m, 1H), 5.13-5.09 (m, 1H), 2.84-2.79 (m, 2H), 1.49-1.42 (m, 2H), 1.40-1.35 (m, 2H), 0.91 (t, *J* = 7.2 Hz, 3H); ¹³C NMR (100 MHz, DMSO): δ 165.4, 143.2, 139.6, 132.5, 129.5, 128.5, 128.2, 127.3, 127.0, 51.4, 30.3, 20.3, 14.4. [(*m*+*H*⁺)/*z* = 269.25]. (λ₂₅₄) purity 96.7%, *t*_R 12.82 mins.



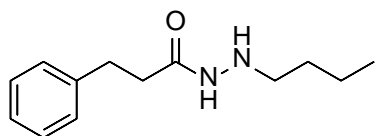
N'-butylthiophene-2-carbohydrazide (**11f**). 1500 mg (10 mmol) of thiophene-2-carbonyl chloride was injected into 10 mL of sieve dried

methanol and bubbled with argon for 10 minutes. To this mixture was injected two drops of dimethylformamide. The reaction proceeded at room temperature for 1 hour before addition of 600 mg (12 mmol) hydrazine water salt. The solution was refluxed for 3 hours before being cooled and condensed in vacuo. The reaction then proceeded as described in **Series 11 General Procedure** to yield 1235 mg of dry product (62% yield). ¹H NMR (400 MHz, DMSO): δ 10.02 (s, 1H), 7.76-7.74 (m, 2H), 7.15-7.13 (m, 1H), 5.03 (s, 1H), 2.80-2.77 (m, 2H), 1.45-1.40 (m, 2H), 1.37-1.32 (m, 2H), 0.89 (m, *J* = 7.2 Hz, 3H); ¹³C NMR (100 MHz, DMSO): δ 161.0, 138.8, 131.0, 128.4, 128.2, 51.3, 30.3, 20.3, 14.4. [(*m*+*H*⁺)/*z* = 199.17]. (λ₂₅₄) purity 97.5%, *t*_R 8.47 mins.



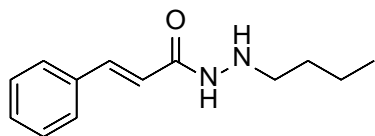
N'-butylfuran-2-carbohydrazide (**11g**). 1100 mg (8.4 mmol) of furan-2-carbonyl chloride was injected into 10 mL of sieve dried methanol

that was bubbled with argon for 10 minutes prior to addition. To this mixture was injected 1780 mg (17.6 mmol) of triethylamine. After 60 minutes, 1000 mg (20 mmol) of hydrazine water salt was added, and heated to reflux for 3 hours. The reaction was cooled and condensed under vacuum. From here the reaction proceeded as described in **Series 11 General Procedure** to yield 861 mg of dry product (56% yield). ^1H NMR (400 MHz, DMSO): δ 9.90 (s, 1H), 7.83-7.82 (m, 1), 7.11-7.10 (m, 1H), 6.62-6.60 (m, 1H), 5.00 (s, 1H), 2.79-2.74 (m, 2H), 1.44-1.40 (m, 2H), 1.38-1.30 (m, 2H), 0.88 (t, $J = 7.2$ Hz, 3H); ^{13}C NMR (100 MHz, DMSO): δ 157.6, 147.3, 145.4, 113.6, 112.1, 51.3, 30.2, 20.3, 14.4. [(m+H⁺)/z = 183.17]. (λ_{254}) purity 98.4%, t_R 7.43 mins.



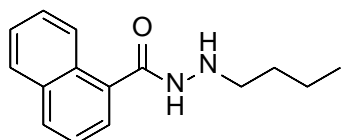
N'-butyl-3-phenylpropanehydrazide (**11h**). 1012 mg (6 mmol) of 3-phenylpropanoyl chloride was injected into 10 mL of argon

bubbled, sieve dried methanol. The reaction was allowed to stir for 1 hour before addition of 900 mg (18 mmol) hydrazine water salt. The mixture was brought to reflux for 3 hours before being cooled to room temperature and condensed under vacuum. From here the reaction proceeded as described in **Series 11 General Procedure** to yield 911 mg of dry product (68% yield). ^1H NMR (400 MHz, DMSO): δ 9.25 (s, 1H), 7.29-7.25 (m, 2H), 7.21-7.26 (m, 3H), 4.77 (s, 1H), 2.82 (t, $J = 7.6$ Hz, 2H), 2.63-2.59 (m, 2H), 2.33 (t, $J = 7.6$ Hz, 2H), 1.31-1.25 (m, 4H), 0.85 (t, $J = 7.2$ Hz, 3H); ^{13}C NMR (100 MHz, DMSO): δ 170.5, 141.5, 128.7 (d), 126.3, 51.2, 35.6, 31.5, 30.1, 20.2, 14.4. [(m+H⁺)/z = 221.25]. (λ_{254}) purity 98.9%, t_R 8.56 mins.



N'-butylcinnamohydrazide (**11i**). 1480 mg (10 mmol) of trans-cinnamic acid was suspended in 50 mL of acetonitrile. To this

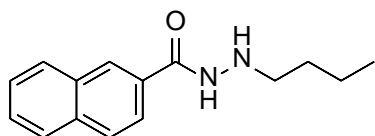
solution was added 1620 mg (12 mmol) of 1-hydroxybenzotriazole and 2478 mg (12 mmol) N, N'-dicyclohexylcarbodiimide. The solution stirred overnight at room temperature before addition of 600 mg (12 mmol) hydrazine water salt, which was refluxed for 3 hours. The solution was brought to room temperature and condensed under vacuum. From here the reaction proceeded as described in **Series 11 General Procedure** to yield 885 mg of dry product (40% yield). ^1H NMR (400 MHz, DMSO): δ 9.62 (s, 1H), 7.58-7.56 (m, 2H), 7.45-7.38 (m, 4H), 6.57 (d, $J = 16.0$ Hz, 1H), 5.05 (s, 1H), 2.76-2.72 (m, 2H), 1.44-1.28 (m, 4H), 0.89 (t, $J = 7.2$ Hz, 3H); ^{13}C NMR (100 MHz, DMSO): δ 164.3, 139.0, 135.4, 129.9, 129.4, 127.9, 120.8, 51.4, 30.2, 20.2, 14.4. $[(m+H^+)/z = 219.25]$. (λ_{254}) purity 97.5%, t_R 10.95 mins.



N'-butyl-1-naphthohydrazide (**11j**). 1033 mg (6 mmol) of 1-naphthoic acid was suspended in 20 mL of argon flushed methylene chloride.

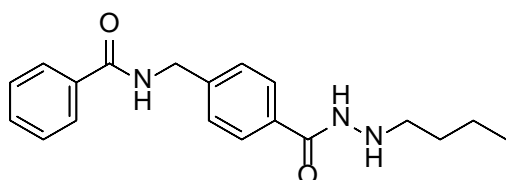
To this solution was injected 1143 mg (9 mmol) of oxalyl chloride followed by injection of 2 drops of dimethylformamide. Furious bubbling was seen, with gas being exhausted and argon flushing continually throughout the room temperature reaction. After one hour, 20 mL of sieve dried methanol was injected slowly. After reacting for an additional hour at room temperature, the solution was condensed under vacuum and resuspended in 30 mL of methanol. To this was added 1500 mg (30 mmol) of hydrazine water salt. The reaction was brought to reflux for 3 hours before being cooled and condensed under vacuum. From here the reaction proceeded as described in **Series 11 General Procedure** to yield 1050 mg of dry product (72% yield). ^1H NMR (400 MHz, DMSO): δ 9.97 (s, 1H), 8.22-8.19 (m, 1H), 8.04-7.98 (m, 2H), 7.61-7.53 (m, 4H), 5.23 (s,

1H), 2.92-2.87 (m, 2H), 1.53-1.42 (m, 2H), 1.40-1.38 (m, 2H), 0.93 (t, $J = 7.2$ Hz, 3H); ^{13}C NMR (100 MHz, DMSO): δ 167.8, 133.7, 133.6, 130.4, 130.4, 128.7, 127.2, 126.7, 125.8, 125.7, 125.5, 51.3, 30.3, 20.3, 14.4. $[(m+H^+)/z = 243.25]$. (λ_{254}) purity >99%, t_R 11.00 mins.



N'-butyl-2-naphthohydrazide (**11k**). 1120 mg (6 mmol) of 2-naphthohydrazide was reacted as described in **Series 11 General**

Procedure to yield 1016 mg of dry product (70% yield). ^1H NMR (400 MHz, DMSO): δ 10.2 (s, 1H), 8.46 (s, 1H), 8.04 -7.93 (m, 4H), 7.64-7.58 (m, 2H), 5.17 (s, 1H), 2.87-2.83 (m, 2H), 1.51-1.46 (m, 2H), 1.41-1.35 (m, 2H), 0.91 (t, $J = 7.2$ Hz, 3H); ^{13}C NMR (100 MHz, DMSO): δ 165.8, 134.6, 132.6, 131.1, 129.3, 128.4, 128.1, 128.0, 127.8, 127.2, 124.4, 51.4, 30.3, 20.3, 14.4. $[(m+H^+)/z = 243.25]$. (λ_{254}) purity >99%, t_R 11.42 mins.



N-(4-(2-butylhydrazine-1-carbonyl)benzyl)benzamide (**11l**). To a mixture of sieve dried methylene chloride, was added 711 mg (4 mmol) of methyl 4-

(aminoethyl)benzoate. This vessel was flushed with argon for 30 minutes before injection of 560 mg (4 mmol) of benzoyl chloride and 607 mg (6 mmol) of trimethylamine. The reaction was stirred at room temperature for 2 hours before being condensed under vacuum. The crude intermediate was resuspended in 30 mL of methanol and 1000 mg (20 mmol) of hydrazine water salt was added as one portion. The solution was refluxed for 3 hours before being cooled and condensed under vacuum. From here the reaction proceeded as described in **Series 11 General Procedure** to yield 601 mg of dry product (46% yield). ^1H NMR (400 MHz, DMSO): δ 9.99 (s, 1H), 9.13-9.10 (t, $J = 6.0$ Hz, 1H), 7.93-7.91 (m, 2H), 7.81-7.79 (m, 2H), 7.57-7.47 (m, 3H), 7.41-7.39 (m,

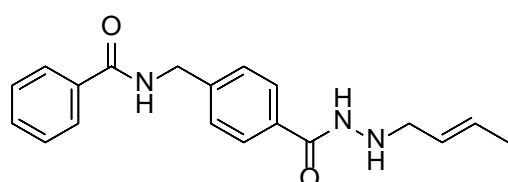
2H), 5.07 (s, 1H), 4.54 (d, $J = 6.0$ Hz, 2H); ^{13}C NMR (100 MHz, DMSO): δ 166.7, 165.6, 143.5, 134.7, 132.2, 131.8, 128.8, 12.7, 127.6, 127.5, 51.4, 42.9, 30.3, 20.3, 14.4. HRMS-ESI $[(m+H^+)/z]$ calculated for $\text{C}_{19}\text{H}_{23}\text{N}_3\text{O}_2$: 326.18697; found, 326.18622. (λ_{254}) purity 96.3%, t_R 11.92 mins.

Synthesis of N-(4-(hydrazide)benzyl)benzamide derivatives (12a-12m).

Intermediate formation. 6050 mg (40 mmol) of 4-(aminomethyl)benzoic acid was dissolved in 200 mL of methanol, to which was added 6 mL of concentrated HCl in one portion. The mixture was refluxed overnight and the volatiles condensed under vacuum. The resulting white solid was suspended in ethyl ether and separated via vacuum filtration to yield the benzoate HCl salt. This compound was dissolved in a 1:2 mixture of ethyl acetate and water and chilled to 0°C to which 11040 mg (80 mmol) was added followed by addition of 5623 mg benzoyl chloride (40 mmol). The vessel was warmed to room temperature and stirred for 2 additional hours. The mixture was separated via acid/base extraction, washing the water phase twice with ethyl acetate. All organic phases were combined and condensed under vacuum to yield a white solid. This was suspended in 200 mL of methanol and 10000 mg (200 mmol) of hydrazine water salt was added. The solution was refluxed for 48 hours, cooled to room temperature, and volatiles were removed under vacuum. This intermediate (**12sm**) was used as the starting material for all further reactions for this family.

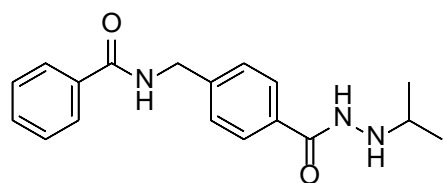
Series 12 General Procedure. The mixture of **12sm** and aldehyde of interest were stirred at room temperature overnight; vacuum filtration afforded the desired intermediate, which was dissolved in 30 mL of methanol. To this solution was added a pinch of methyl orange, and the solution's color turned yellow. The solution was bubbled under argon for 5 minutes, and 2.2

mmol of sodium cyanoborohydride was then added to it. A 1:1 mixture of methanol and concentrated HCl was added dropwise until the solution turned red. After addition, the mixture was stirred at room temperature for 6 hours. The reaction was quenched with sodium hydroxide, and organic solvents were removed under vacuum. The residues were extracted twice with ethyl acetate, and organic phases were combined and dried over magnesium sulfate. After filtration, organic solvents were removed and the residues were purified by flash chromatography.



(E)-N-(4-(2-(but-2-en-1-yl)hydrazine-1-carbonyl)benzyl)benzamide (**12a**). 2 mmol of **12sm** was dissolved in 100 mL ethanol with ultra-sonication aid.

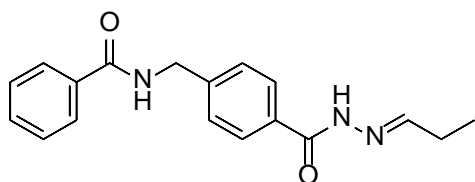
To this solution was added 40 mmol of magnesium sulfate and 2 mmol of (E)-but-2-enal. From here the reaction proceeded as described in **Series 12 General Procedure** to yield 208 mg (32% yield). ^1H NMR (400 MHz, DMSO): δ 9.97 (d, J = 5.6 Hz, 1H), 9.12 (t, J = 6.0 Hz, 1H), 7.93-7.91 (m, 2H), 7.81-7.78 (m, 2H), 7.58-7.48 (m, 3H), 7.41-7.39 (m, 2H), 5.63-5.50 (m, 2H), 5.11-5.07 (m, 1H), 4.54 (d, J = 6.0 Hz, 2H), 3.37-3.35 (m, 2H), 1.65 (d, J = 5.6 Hz, 3H); ^{13}C NMR (100 MHz, DMSO): δ 166.8, 165.7, 143.5, 134.7, 132.2, 131.8, 128.8, 128.4, 128.2, 127.7, 127.6, 127.5, 53.6, 42.9, 18.2. [(m+H⁺)/z = 324.17]. (λ_{254}) purity >99%, t_R 10.00 mins.



N-(4-(2-isopropylhydrazine-1-carbonyl)benzyl)benzamide (**12b**). 2 mmol of **12sm** was dissolved in 100 mL ethanol with ultra-sonication aid. To this solution was added 40 mmol of

magnesium sulfate and 2 mmol of isopropanol. From here the reaction proceeded as described in **Series 12 General Procedure** to yield yielded 324 mg (52% yield). ^1H NMR (400 MHz, DMSO):

δ 9.95 (d, $J = 6.8$ Hz, 1H), 9.11 (t, $J = 6.0$ Hz, 1H), 7.92-7.90 (m, 2H), 7.82-7.80 (m, 2H), 7.58-7.48 (m, 3H), 7.41-7.39 (m, 2H), 4.95-4.92 (m, 1H), 4.53 (d, $J = 6.0$ Hz, 2H), 3.11-3.03 (m, 1H), 1.02 (d, $J = 10.4$ Hz, 6H); ^{13}C NMR (100 MHz, DMSO): δ 166.8, 166.0, 143.5, 134.7, 132.2, 131.8, 128.8, 127.7, 127.6, 127.4, 50.8, 42.9, 21.4. [(m+H⁺)/z = 312.25]. (λ_{254}) purity 98.8%, t_R 8.68 mins.



(E)-N-(4-(2-propylidenehydrazine-1-

carbonyl)benzyl)benzamide (**12c**). 2 mmol of **12sm** was

dissolved in 100 mL ethanol with ultra-sonication aid. To

this solution was added 40 mmol of magnesium sulfate and 2 mmol of propanal. From here the

reaction proceeded as described in **Series 12 General Procedure** to yield 347 mg (56% yield). ^1H

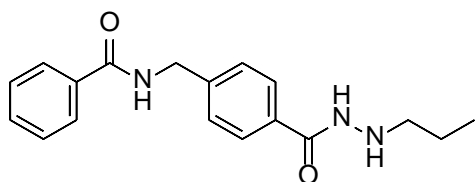
NMR (400 MHz, DMSO): δ 11.39 (s, 1H), 9.13 (t, $J = 6.0$ Hz, 1H), 7.93-7.90 (m, 2H), 7.84-7.75 (m,

3H), 7.58-7.38 (m, 5H), 4.56-4.53 (m, 2H), 2.30-2.25 (m, 2H), 1.06 (t, $J = 7.2$ Hz, 3H); ^{13}C NMR (100

MHz, DMSO): δ 166.8, 163.1, 153.5, 143.9, 134.7, 131.8, 128.8, 128.1, 127.7, 127.5(d), 42.9, 25.9,

11.1. HRMS-ESI [(m+H⁺)/z] calculated for C₁₈H₁₉N₃O₂: 310.15567; found, 310.15529. (λ_{254}) purity

97.5%, t_R 11.60 mins.



N-(4-(2-propylhydrazine-1-carbonyl)benzyl)benzamide

(**12d**). 2 mmol of **12sm** was dissolved in 100 mL ethanol

with ultra-sonication aid. To this solution was added 40

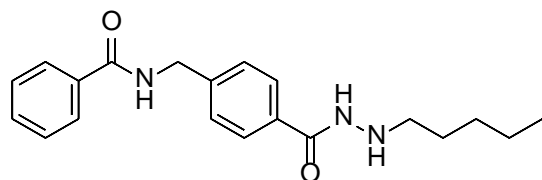
mmol of magnesium sulfate and 2 mmol of propanal. From here the reaction proceeded as

described in **Series 12 General Procedure** to yield 318 mg (51% yield). ^1H NMR (400 MHz, DMSO):

δ 9.98 (d, $J = 6.0$ Hz, 1H), 9.11 (t, $J = 6.0$ Hz, 1H), 7.92-7.91 (m, 2H), 7.81-7.79 (m, 2H), 7.56-7.48

(m, 3H), 7.41-7.39 (m, 2H), 5.11-5.07 (m, 1H), 4.53 (d, $J = 6.0$ Hz, 2H), 2.78-2.73 (m, 2H), 1.49-1.44

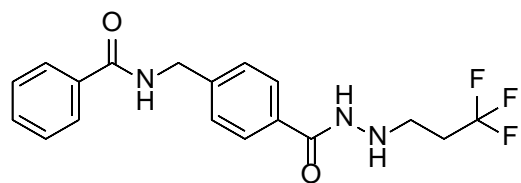
(m, 2H), 0.92 (t, $J = 7.6$ Hz, 3H); ^{13}C NMR (100 MHz, DMSO): δ 166.7, 165.6, 143.5, 134.7, 132.2, 131.8, 128.8, 127.7, 127.6, 127.4, 53.6, 42.9, 21.3, 12.1. HRMS-ESI $[(m+H^+)/z]$ calculated for $\text{C}_{18}\text{H}_{21}\text{N}_3\text{O}_2$: 312.17132; found, 312.17127. (λ_{254}) purity >99%, t_R 12.28 mins.



N-(4-(2-pentylhydrazine-1-

carbonyl)benzyl)benzamide (**12e**). 2 mmol of **12sm** was dissolved in 100 mL ethanol with ultra-

sonication aid. To this solution was added 40 mmol of magnesium sulfate and 2 mmol of pentanal. From here the reaction proceeded as described in **Series 12 General Procedure** to yield 312 mg (46% yield). ^1H NMR (400 MHz, DMSO): δ 9.99 (s, 1H), 9.11 (t, $J = 6.0$ Hz, 1H), 7.93-7.91 (m, 2H), 7.81-7.79 (m, 2H), 7.57-7.47 (m, 3H), 7.41-7.39 (m, 2H), 5.07 (s, 1H), 4.53 (d, $J = 6.0$ Hz, 2H), 2.78 (s, 2H), 1.48-1.44 (m, 2H), 1.33-1.29 (m, 4H), 0.88 (t, $J = 6.8$ Hz, 3H); ^{13}C NMR (100 MHz, DMSO): δ 166.8, 165.6, 143.5, 134.7, 132.2, 131.8, 128.8, 127.7, 127.6, 127.5, 51.7, 42.9, 29.4, 27.8, 22.5, 14.4. $[(m+H^+)/z = 340.25]$. (λ_{254}) purity >99%, t_R 11.30 mins.

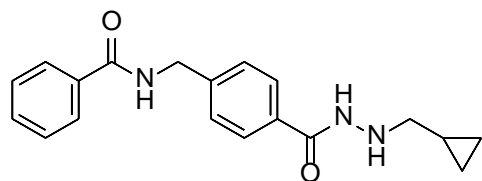


N-(4-(2-(3,3,3-trifluoropropyl)hydrazine-1-

carbonyl)benzyl)benzamide (**12f**). 2 mmol of **12sm** was dissolved in 100 mL ethanol with ultra-sonication

aid. To this solution was added 40 mmol of magnesium sulfate and 2 mmol of 3,3,3-trifluoropropanal. From here the reaction proceeded as described in **Series 12 General Procedure** to yield 445 mg (61% yield). ^1H NMR (400 MHz, DMSO): δ 10.03 (d, $J = 6.0$ Hz, 1H), 9.11 (t, $J = 6.0$ Hz, 1H), 7.92-7.90 (m, 2H), 7.82-7.80 (m, 2H), 7.58-7.48 (m, 3H), 7.42-7.40 (m, 2H), 5.43-5.39 (m, 1H), 4.54 (d, $J = 6.0$ Hz, 2H), 3.05-3.00 (m, 2H), 2.54-2.44 (m, 2H); ^{13}C -HSQC

(100MHz, 400 MHz, DMSO) δ 131.8, 128.8, 127.7, 127.6, 127.5, 44.55, 42.8, 32.1. $[(m+H^+)/z = 366.25]$. (λ_{254}) purity 97.7%, t_R 10.85 mins.

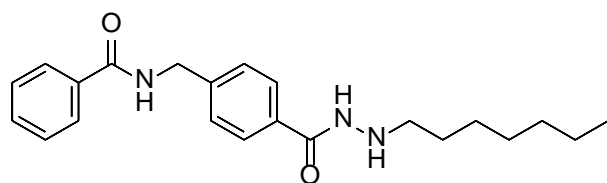


N-(4-(2-(cyclopropylmethyl)hydrazine-1-

carbonyl)benzyl)benzamide (**12g**). 2 mmol of **12sm** was dissolved in 100 mL ethanol with ultra-sonication aid. To

this solution was added 40 mmol of magnesium sulfate and 2 mmol of cyclopropanecarbaldehyde. From here the reaction proceeded as described in **Series 12 General**

Procedure to yield 415 mg (64% yield). 1H NMR (400 MHz, DMSO): δ 10.06 (s, 1H), 9.13 (s, 1H), 7.93-7.92 (m, 2H), 7.85-7.80 (m, 2H), 7.57-7.47 (m, 3H), 7.41-7.39 (m, 2H), 5.12 (s, 1H), 4.55 (s, 2H), 2.66 (s, 2H), 0.93-0.91 (m, 1H), 0.46-0.44 (m, 2H), 0.16-0.15 (m, 2H); ^{13}C NMR (100 MHz, DMSO): δ 166.8, 165.5, 143.5, 134.7, 132.2, 131.8, 128.8, 127.7, 127.6, 127.5, 56.6, 42.9, 9.95, 3.61. $[(m+H^+)/z = 324.17]$. (λ_{254}) purity 97.4%, t_R 9.27 mins.

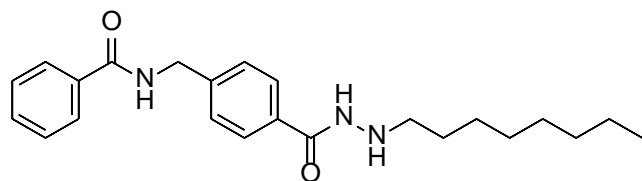


N-(4-(2-heptylhydrazine-1-

carbonyl)benzyl)benzamide (**12h**). 2 mmol of **12sm** was dissolved in 100 mL ethanol with

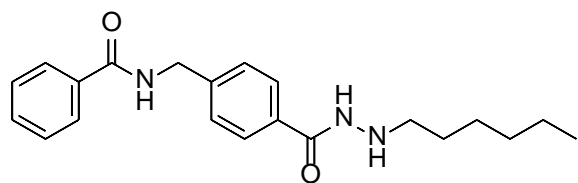
ultra-sonication aid. To this solution was added 40 mmol of magnesium sulfate and 2 mmol of heptanal. From here the reaction proceeded as described in **Series 12 General Procedure** to yield 345 mg (47% yield). 1H NMR (400 MHz, DMSO): δ 10.00 (s, 1H), 9.12 (t, $J = 6.0$ Hz, 1H), 7.93-7.91 (m, 2H), 7.82-7.80 (m, 2H), 7.57-7.47 (m, 3H), 7.41-7.39 (m, 2H), 5.08-5.05 (m, 1H), 4.54 (d, $J = 6.0$ Hz, 2H), 2.81-2.76 (m, 2H), 1.48-1.44 (m, 2H), 1.34-1.26 (m, 8H), 0.86 (t, $J = 6.4$ Hz, 3H); ^{13}C

NMR (100 MHz, DMSO): δ 166.7, 165.6, 143.5, 134.7, 132.2, 131.8, 128.8, 127.7, 127.6, 127.4, 51.7, 42.9, 31.8, 29.1, 28.1, 27.1, 22.6, 14.4. [(m+H⁺)/z = 368.33]. (λ_{254}) purity >99%, t_R 13.25 mins.



N-(4-(2-octylhydrazine-1-carbonyl)benzyl)benzamide (**12i**). 2 mmol of **12sm** was dissolved in 100 mL ethanol with

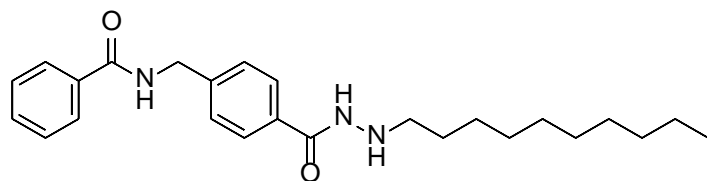
ultra-sonication aid. To this solution was added 40 mmol of magnesium sulfate and 2 mmol of octanal. From here the reaction proceeded as described in **Series 12 General Procedure** to yield 305 mg (40% yield). ¹H NMR (400 MHz, DMSO): δ 10.00 (s, 1H), 9.12 (t, J = 6.0 Hz, 1H), 7.93-7.91 (m, 2H), 7.82-7.80 (m, 2H), 7.55-7.46 (m, 3H), 7.41-7.39 (m, 2H), 5.07-5.06 (m, 1H), 4.54 (d, J = 5.6 Hz, 2H), 2.80-2.76 (m, 2H), 1.47-1.42 (m, 2H), 1.34-1.25 (m, 10H), 0.86 (t, J = 6.4 Hz, 3H); ¹³C NMR (100 MHz, DMSO): δ 166.7, 165.6, 143.5, 134.7, 132.2, 131.8, 128.8, 127.7, 127.6, 127.4, 51.7, 42.9, 31.7, 29.4, 29.2, 28.1, 27.2, 22.6, 14.4. [(m+H⁺)/z = 382.33]. (λ_{254}) purity 95.8%, t_R 13.97 mins.



N-(4-(2-hexylhydrazine-1-carbonyl)benzyl)benzamide (**12j**). 2 mmol of **12sm** was dissolved in 100 mL ethanol with ultra-

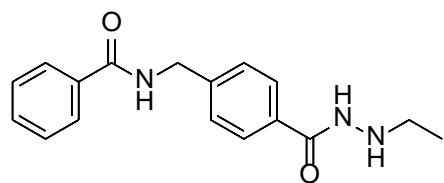
sonication aid. To this solution was added 40 mmol of magnesium sulfate and 2 mmol of hexanal. From here the reaction proceeded as described in **Series 12 General Procedure** to yield 367 mg (52% yield). ¹H NMR (400 MHz, DMSO): δ 9.99 (s, 1H), 9.12 (t, J = 6.0 Hz, 1H), 7.93-7.91 (m, 2H), 7.81-7.79 (m, 2H), 7.58-7.47 (m, 3H), 7.41-7.39 (m, 2H), 5.08-5.05 (m, 1H), 4.54 (d, J = 6.0 Hz, 2H), 2.81-2.76 (m, 2H), 1.49-1.42 (m, 2H), 1.37-1.26 (m, 6H), 0.87 (t, J = 6.4 Hz, 3H); ¹³C NMR (100

MHz, DMSO): δ 166.7, 165.6, 143.5, 134.7, 132.2, 131.8, 128.8, 127.7, 127.6, 127.4, 51.7, 42.9, 31.7, 28.1, 26.8, 22.6, 14.4. [(m+H⁺)/z = 354.33]. (λ_{254}) purity 98.8%, t_R 12.45 mins.



N-(4-(2-decylhydrazine-1-carbonyl)benzyl)benzamide (**12k**). 2 mmol of **12sm** was dissolved in 100 mL

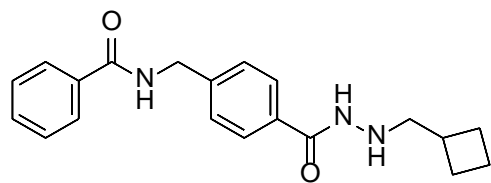
ethanol with ultra-sonication aid. To this solution was added 40 mmol of magnesium sulfate and 2 mmol of decanal. From here the reaction proceeded as described in **Series 12 General Procedure** to yield 295 mg (36% yield). ¹H NMR (400 MHz, DMSO): δ 9.99 (s, 1H), 9.12 (t, J = 6.0 Hz, 1H), 7.93-7.91 (m, 2H), 7.81-7.79 (m, 2H), 7.57-7.54 (m, 3H), 7.41-7.39 (m, 2H), 5.07-5.05 (m, 1H), 4.54 (d, J = 6.0 Hz, 2H), 2.80-2.75 (m, 2H), 1.48-1.42 (m, 2H), 1.33-1.25 (m, 14H), 0.86 (t, J = 6.8 Hz, 3H); ¹³C NMR (100 MHz, DMSO): δ 166.7, 165.6, 143.5, 134.7, 132.2, 131.8, 128.8, 127.7, 127.5, 127.4, 51.7, 42.9, 31.8, 29.5(d), 29.2, 28.1, 27.2, 22.6, 14.4. [(m+H⁺)/z = 410.33]. (λ_{254}) purity 98.2%, t_R 15.01 mins.



N-(4-(2-ethylhydrazine-1-carbonyl)benzyl)benzamide (**12l**). 2 mmol of **12sm** was dissolved in 100 mL ethanol with ultra-sonication aid. To this solution was added 40 mmol of

magnesium sulfate and 2 mmol of acetaldehyde. From here the reaction proceeded as described in **Series 12 General Procedure** to yield 404 mg (68% yield). ¹H NMR (400 MHz, DMSO): δ 10.00 (s, 1H), 9.13-9.11 (m, 1H), 7.93-7.90 (m, 2H), 7.81-7.89 (m, 2H), 7.56-7.47 (m, 3H), 7.42-7.39 (m, 2H), 5.07 (s, 1H), 4.54 (s, 2H), 2.83-2.80 (m, 2H), 1.06-1.02 (m, 3H); ¹³C NMR (100 MHz, DMSO): δ

166.8, 165.7, 143.5, 134.7, 132.2, 131.8, 128.8, 127.7, 127.6, 127.5, 46.0, 42.9, 13.6. [(m+H⁺)/z = 298.25]. (λ_{254}) purity 95.6%, t_R 7.71 mins.



N-(4-(2-(cyclobutylmethyl)hydrazine-1-

carbonyl)benzyl)benzamide (**12m**). 2 mmol of **12sm** was dissolved in 100 mL ethanol with ultra-sonication aid. To

this solution was added 40 mmol of magnesium sulfate and 2 mmol of cyclobutanecarbaldehyde.

From here the reaction proceeded as described in **Series 12 General Procedure** to yield 438 mg

(65% yield). ¹H NMR (400 MHz, DMSO): δ 9.97 (s, 1H), 9.14-9.10 (m, 1H), 7.93-7.91 (m, 2H), 7.80-

7.78 (m, 2H), 7.58-7.48 (m, 3H), 7.40-7.38 (m, 2H), 5.06 (s, 1H), 4.53 (d, J = 6.0 Hz, 2H), 2.83 (d, J

= 7.2 Hz, 2H), 2.49-2.43 (m, 1H), 2.05-2.03 (m, 2H), 1.89-1.78 (m, 2H), 1.74-1.65 (m, 2H); ¹³C NMR

(100 MHz, DMSO): δ 166.7, 165.6, 143.5, 134.7, 132.2, 131.8, 128.8, 127.7, 127.5, 127.4, 57.5,

42.9, 34.2, 26.5, 18.8. [(m+H⁺)/z = 338.17]. (λ_{254}) purity 96.7%, t_R 10.55 mins.

Synthesis of N-(4-(hydrazide)benzyl)cinnamamide Derivatives (**13a-13e**).

Intermediate formation. Transcinnamic acid (40 mmol) was dissolved in 500 mL of methylene

chloride. The apparatus was purged with argon and bubbled through the solution. To this

solution was injected 60 mmol of oxalyl chloride and 10 drops of dimethylformamide. The

mixture was stirred at room temperature for 3 hours under constant argon flush. The solution

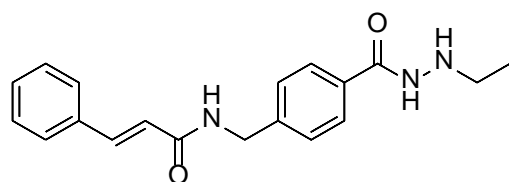
was condensed under vacuum and brought to 0°C. A pre-chilled 1:2 mixture of ethyl acetate and

water was slowly added followed by addition of potassium carbonate (80 mmol) and methyl 4-

(aminomethyl)benzoate HCl (40 mmol). The reaction was brought to room temperature slowly

and allowed to stir for 2 additional hours. The water and organic phases were separated, and

the water phase washed twice with ethyl acetate. The organic phases were combined and dried under vacuum. A white solid was obtained and used in the next step without further purification. The product was resuspended in a 2:2:1 solution of methanol, tetrahydrofuran, and water at 0°C. To this solution was cautiously added 48 lithium hydroxide (48 mmol). The solution was allowed to warm to room temperature and stir overnight. Volatiles were removed under vacuum and the residue was acidified with 1 M HCl before extraction with ethyl acetate; volatiles were once again removed under vacuum and lyophilized. The resulting white crystalline powder was used in the next step without further purification. The 4-(cinnamamidomethyl)benzoic acid generated in the above steps was suspended in 400 mL of dimethylformamide, to which was added Hydroxybenzotriazole (80 mmol) and N-N'-Dicyclohexylcarbodiimide (80 mmol). This solution was stirred for 6 hours at RT before addition of hydrazine water salt (48 mmol) at 0°C in one portion. The mixture was allowed to warm to room temperature and stir overnight before being extracted with 1200 mL of water. The water phase was extracted with ethyl acetate twice, and the organic layers were combined and condensed under vacuum. The product (**13sm**) was purified via flash chromatography to yield the corresponding hydrazide that will be used as a starting material for all further reactions for this family (**13a-13e**).

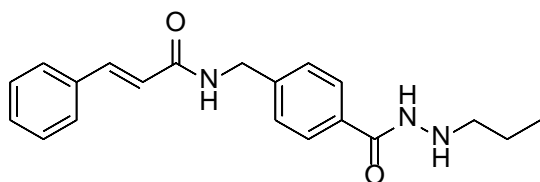


N-(4-(2-ethylhydrazine-1-carbonyl)benzyl)cinnamamide (**13a**). 2 mmol of **13sm** was dissolved in 100 mL ethanol with ultra-sonication

aid. To this solution was added 40 mmol of magnesium sulfate and 2 mmol of ethanal. From here the reaction proceeded as described in **Series 12 General Procedure** to yield 454 mg (70% yield).

¹H NMR (400 MHz, DMSO): δ 10.0 (s, 1H), 8.70 (t, *J* = 5.9 Hz, 1H), 7.80 (d, *J* = 8.2 Hz, 2H), 7.58 (d,

$J = 6.8$ Hz, 2H), 7.49 (d, $J = 15.8$ Hz, 1H), 7.43-7.36 (m, 5H), 6.72 (d, $J = 15.8$ Hz, 1H), 5.06 (s, 1H), 4.46 (d, $J = 6.0$ Hz, 2H), 2.85-2.79 (m, 2H), 2.51 (t, $J = 1.7$ Hz, 2H), 1.04 (t, $J = 7.2$ Hz, 3H); ^{13}C NMR (100MHz, DMSO): δ 165.6, 165.5, 143.2, 139.6, 135.3, 132.3, 130.0, 129.4, 128.0, 127.6, 122.4, 46.0, 42.5, 13.6. $[(m+H^+)/z = 324.25]$. (λ_{254}) purity 97.5%, t_R 10.38 mins.

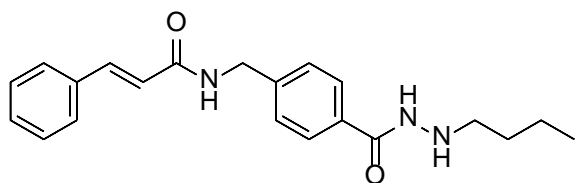


N-(4-(2-propylhydrazine-1-

carbonyl)benzyl)cinnamamide (**13b**). 2 mmol of

13sm was dissolved in 100 mL ethanol with ultra-

sonication aid. To this solution was added 40 mmol of magnesium sulfate and 2 mmol of propanal. From here the reaction proceeded as described in **Series 12 General Procedure** to yield 546 mg (81% yield). ^1H NMR (400 MHz, DMSO): δ 10.00 (s, 1H), 8.70 (t, $J = 6.0$ Hz, 1H), 7.82-7.80 (m, 2H), 7.60-7.58 (m, 2H), 7.50 (d, $J = 16$ Hz, 1H), 7.45-7.37 (m, 5H), 6.72 (d, $J = 15.6$, 1H), 5.11-5.08 (m, 1H), 4.47 (d, $J = 5.6$ Hz, 2H), 2.78-2.74 (m, 2H), 1.51-1.45 (m, 2H), 0.92 (t, $J = 7.2$ Hz, 3H); ^{13}C NMR (100 MHz, DMSO): δ 165.6, 165.5, 143.2, 139.6, 135.3, 132.3, 130.0, 129.4, 128.0, 127.6 (d), 122.4, 53.6, 42.5, 21.3, 12.1. HRMS-ESI $[(m+H^+)/z]$ calculated for $\text{C}_{20}\text{H}_{23}\text{N}_3\text{O}_2$: 338.18697; found, 338.18726. (λ_{254}) purity 98.4%, t_R 12.42 mins.



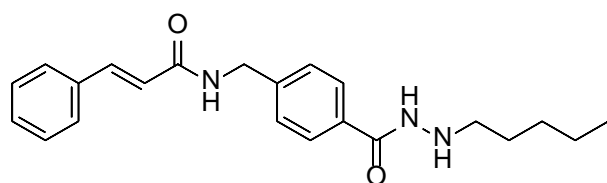
N-(4-(2-butylhydrazine-1-

carbonyl)benzyl)cinnamamide (**13c**). 2 mmol of

13sm was dissolved in 100 mL ethanol with ultra-

sonication aid. To this solution was added 40 mmol of magnesium sulfate and 2 mmol of butanal. From here the reaction proceeded as described in **Series 12 General Procedure** to yield 576 mg (82% yield). ^1H NMR (400 MHz, DMSO): δ 10.0 (s, 1H), 8.7 (t, $J = 6.0$ Hz, 1H), 7.8 (d, $J = 8.3$ Hz, 2H),

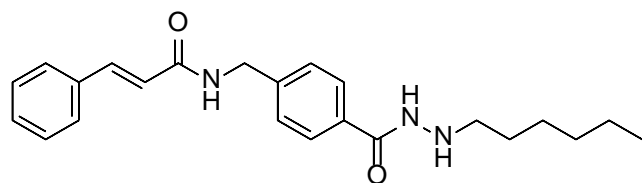
7.58 (d, $J = 6.8$ Hz, 2H), 7.49 (d, $J = 15.8$ Hz, 1H), 7.43-7.36 (m, 5H), 6.71 (d, $J = 15.8$ Hz, 1H), 5.06 (s, 1H), 4.45 (d, $J = 6.0$ Hz, 2H), 2.80-2.76 (m, 2H), 2.51 (t, $J = 1.8$ Hz, 2H), 1.48-1.41 (m, 2H), 1.40-1.30 (m, 2H), 0.89 (t, $J = 7.2$ Hz, 3H); ^{13}C NMR (100MHz, DMSO): δ 165.5, 165.5, 143.2, 139.6, 135.3, 132.3, 130.0, 129.4, 128.0, 127.6, 122.4, 51.4, 42.5, 30.3, 20.3, 14.4. $[(m+H^+)/z = 352.25]$. (λ_{254}) purity 98.9%, t_R 12.67 mins.



N-(4-(2-pentylhydrazine-1-

carbonyl)benzyl)cinnamamide (**13d**). 2 mmol of **13sm** was dissolved in 100 mL ethanol with

ultra-sonication aid. To this solution was added 40 mmol of magnesium sulfate and 2 mmol of pentanal. From here the reaction proceeded as described in **Series 12 General Procedure** to yield 584 mg (80% yield). ^1H NMR (400 MHz, DMSO): δ 10.0 (s, 1H), 8.7 (t, $J = 6.0$ Hz, 1H), 7.8 (d, $J = 8.3$ Hz, 2H), 7.58 (d, $J = 6.8$ Hz, 2H), 7.49 (d, $J = 15.8$ Hz, 1H), 7.45-7.35 (m, 5H), 6.71 (d, $J = 15.8$ Hz, 1H), 5.06 (s, 1H), 4.45 (d, $J = 6.0$ Hz, 2H), 2.80-2.75 (m, 2H), 2.51 (t, $J = 1.8$ Hz, 2H), 1.47-1.44 (m, 2H), 1.33-1.29 (m, 4H), 0.88 (t, $J = 7.2$ Hz, 3H); ^{13}C NMR (100MHz, DMSO): δ 165.5, 165.5, 143.2, 139.6, 135.3, 132.3, 130.0, 129.4, 128.0, 127.6, 122.4, 51.7, 42.5, 29.3, 27.8, 22.5, 14.4. $[(m+H^+)/z = 366.25]$. (λ_{254}) purity 97.5%, t_R 13.34 mins.

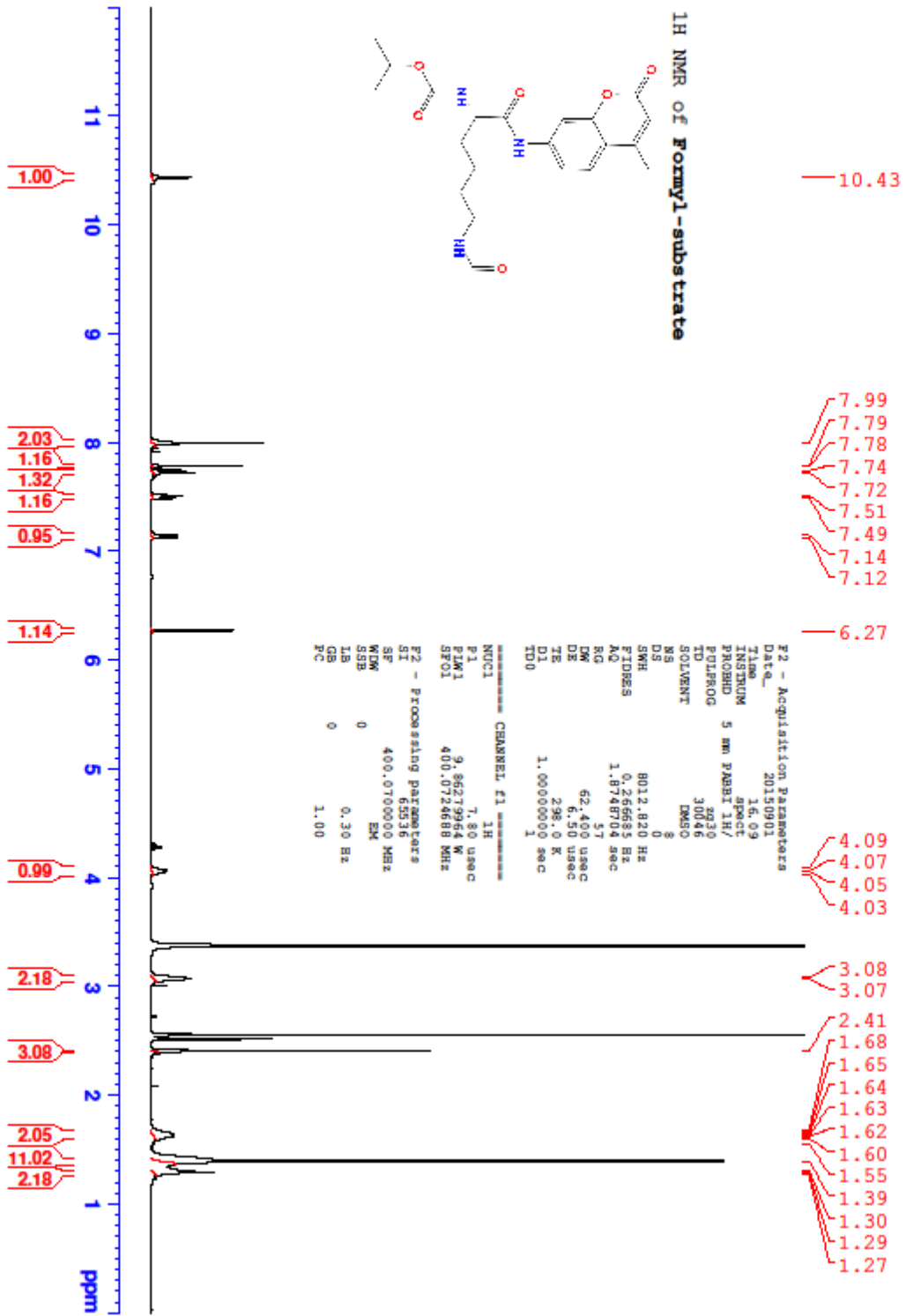


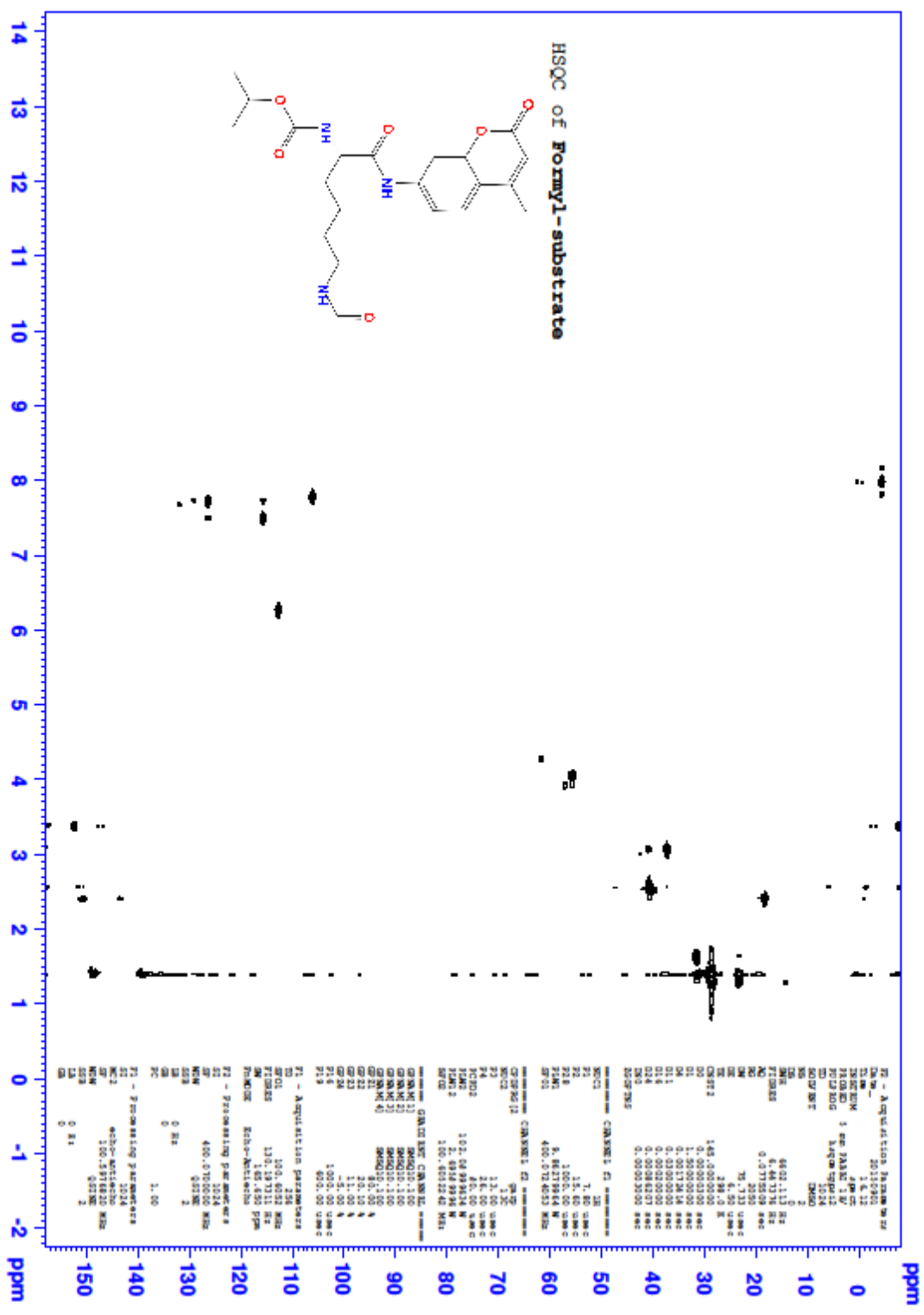
N-(4-(2-hexylhydrazine-1-

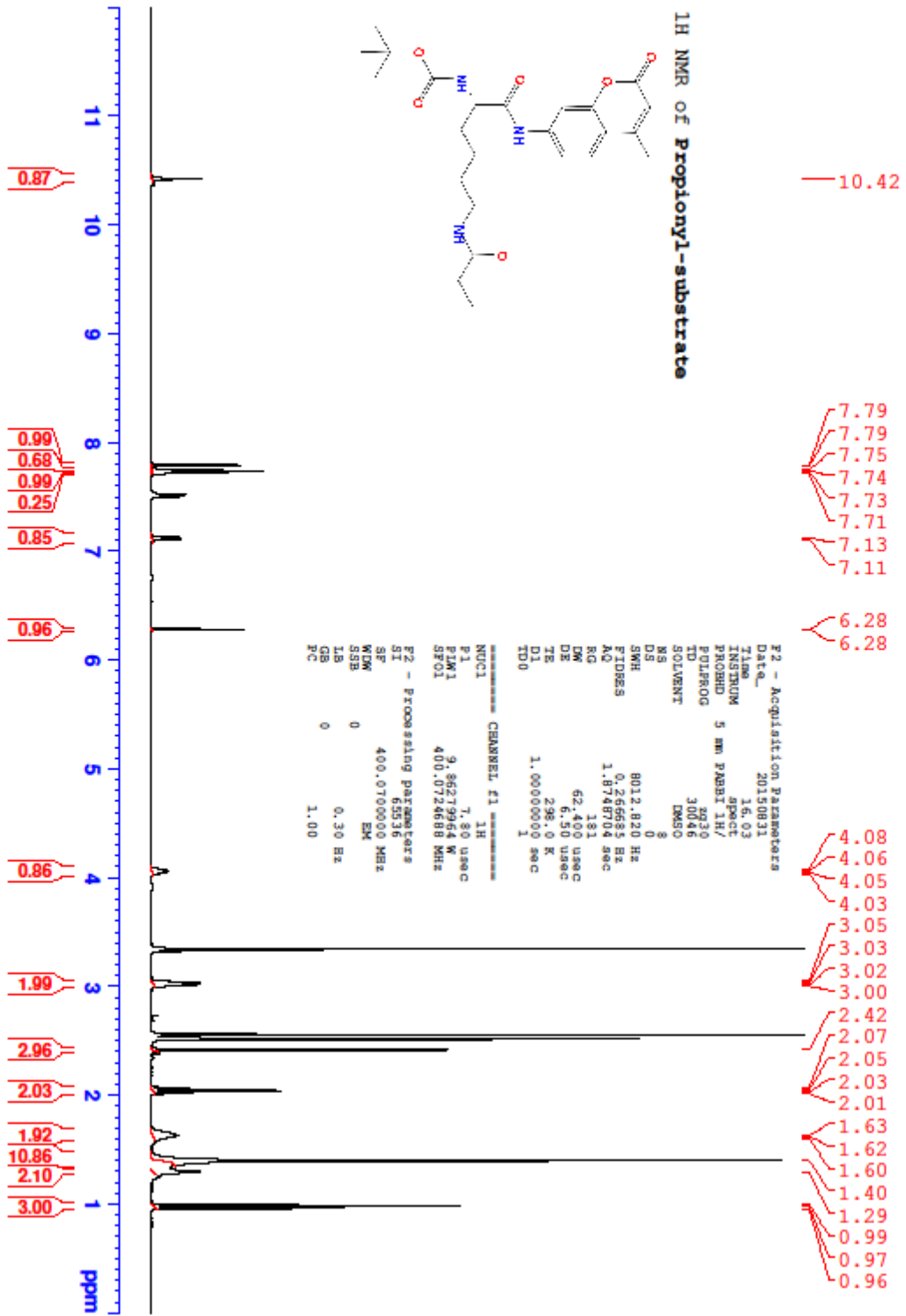
carbonyl)benzyl)cinnamamide (**13e**). 2 mmol of **13sm** was dissolved in 100 mL ethanol with

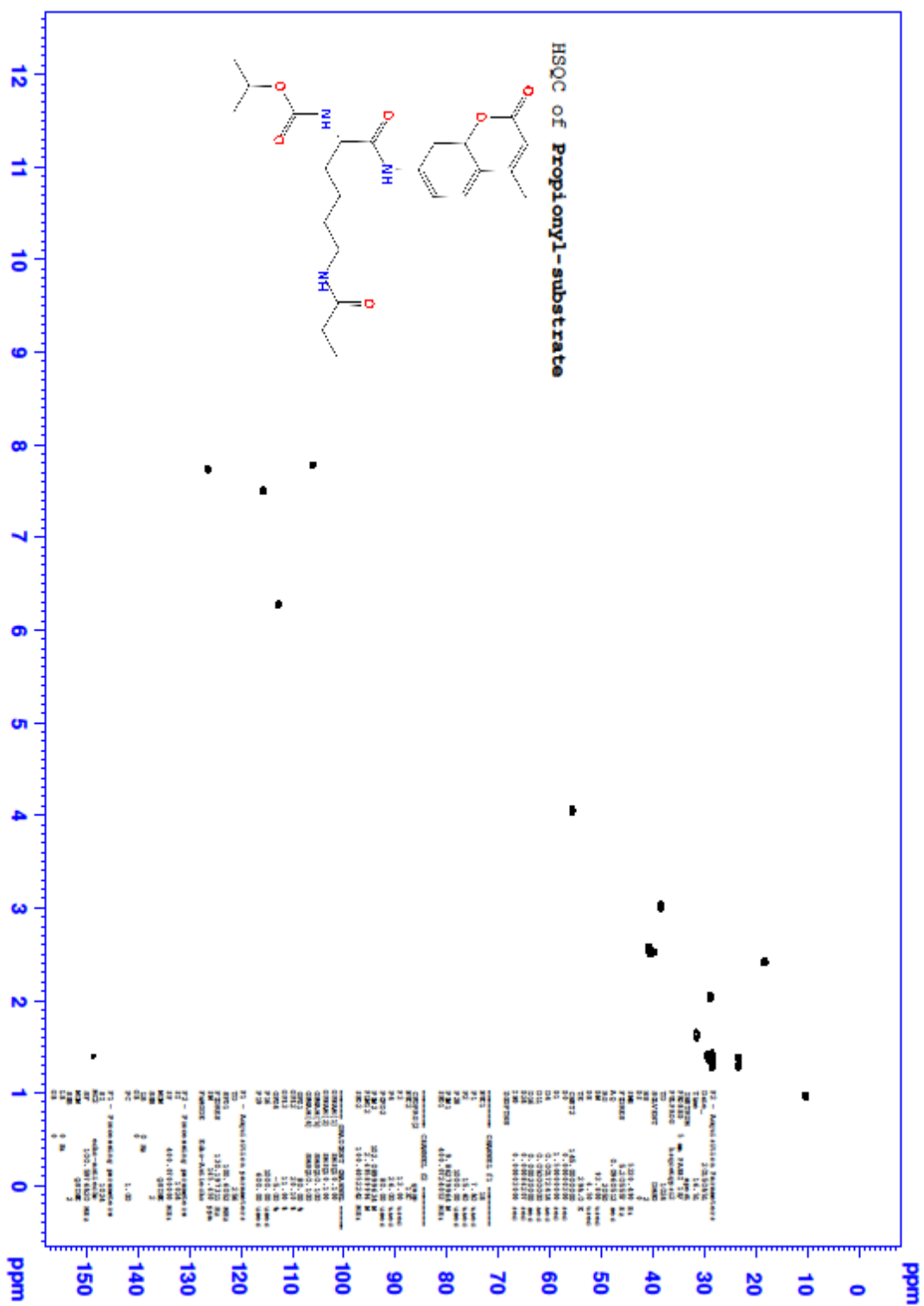
ultra-sonication aid. To this solution was added 40 mmol of magnesium sulfate and 2 mmol of hexanal. From here the reaction proceeded as described in **Series 12 General Procedure** to yield

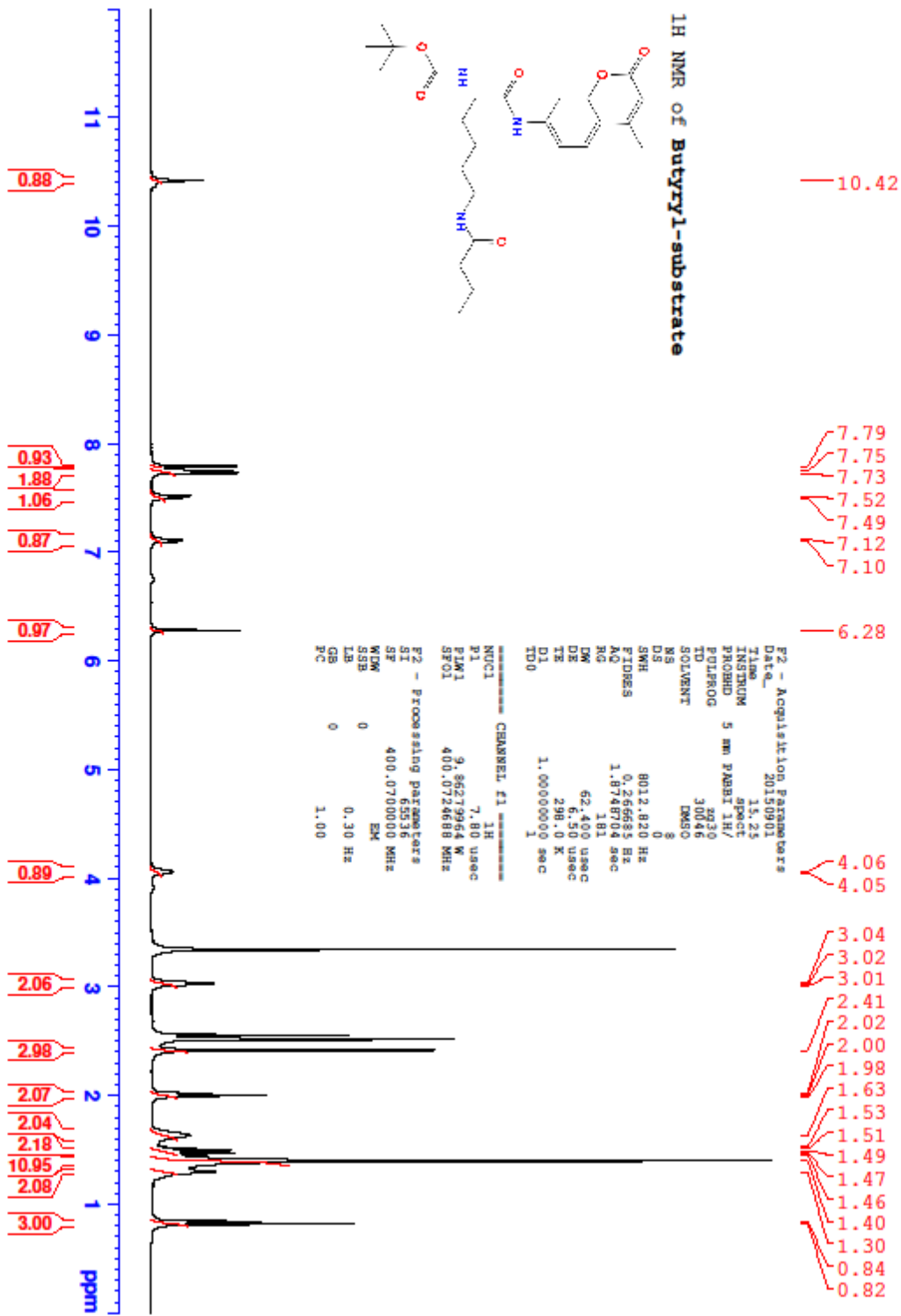
616 mg (81% yield). ^1H NMR (400 MHz, DMSO): δ 10.00 (s, 1H), 8.71 (t, $J = 6.0$ Hz, 1H), 7.82-7.82 (m, 2H), 7.60-7.58 (m, 2H), 7.55 (d, $J = 16$ Hz, 1H), 7.45-7.36 (m, 5H), 6.73 (d, $J = 15.6$ Hz, 1H), 5.07 (s, 1H), 4.47 (d, $J = 6.0$ Hz, 2H), 2.81-2.76 (m, 2H), 1.49-1.41 (m, 2H), 1.37-1.27 (m, 6H), 0.86 (t, $J = 6.8$ Hz, 3H); ^{13}C NMR (100 MHz, DMSO): δ 165.6, 165.5, 143.2, 139.6, 135.3, 132.3, 130.0, 129.4, 128.0, 127.6 (d), 122.4, 51.7, 42.5, 31.7, 28.1, 26.8, 22.6, 14.4. $[(\text{m}+\text{H}^+)/z = 380.33]$. (λ_{254}) purity 95.5%, t_{R} 13.62 mins.

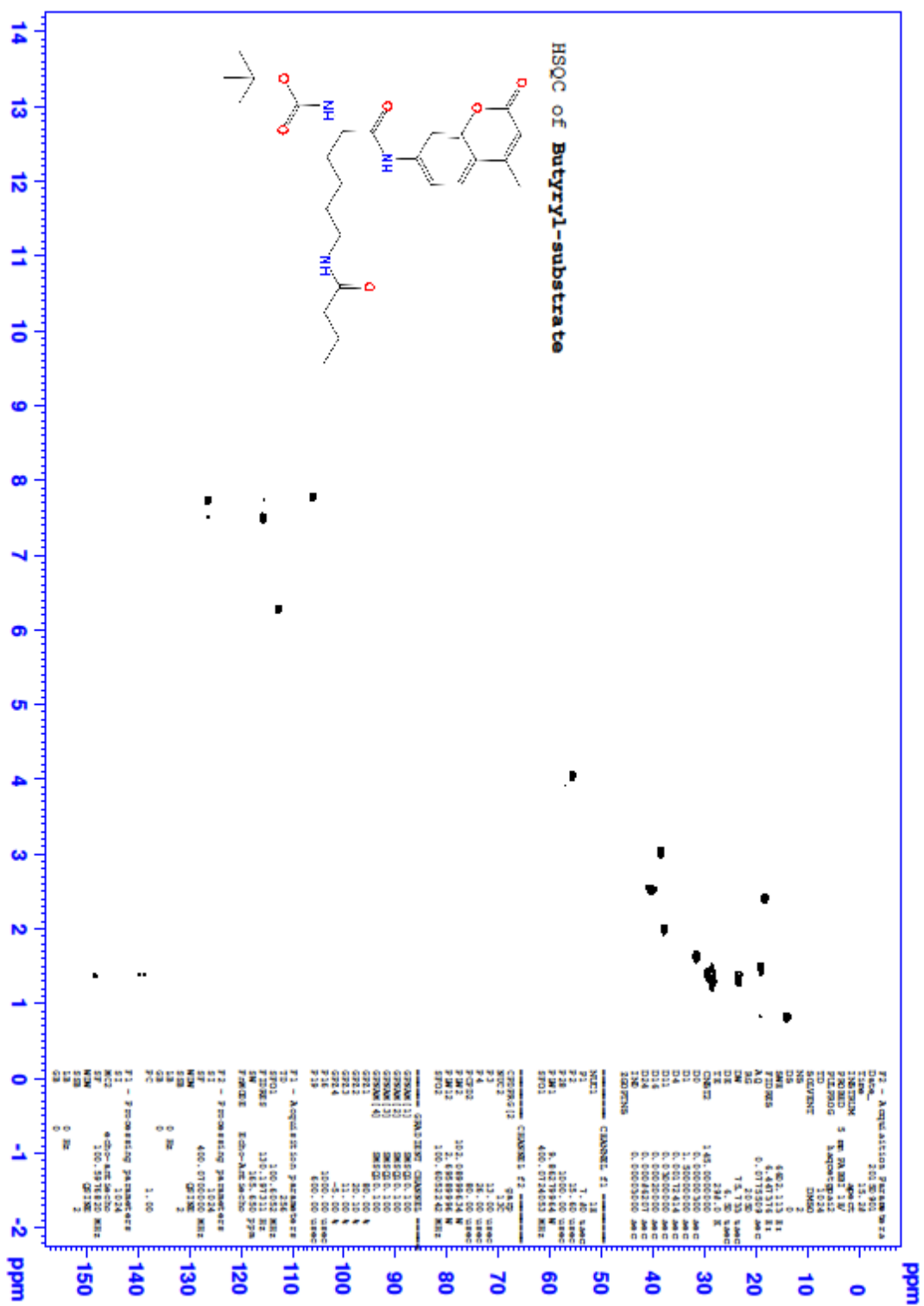


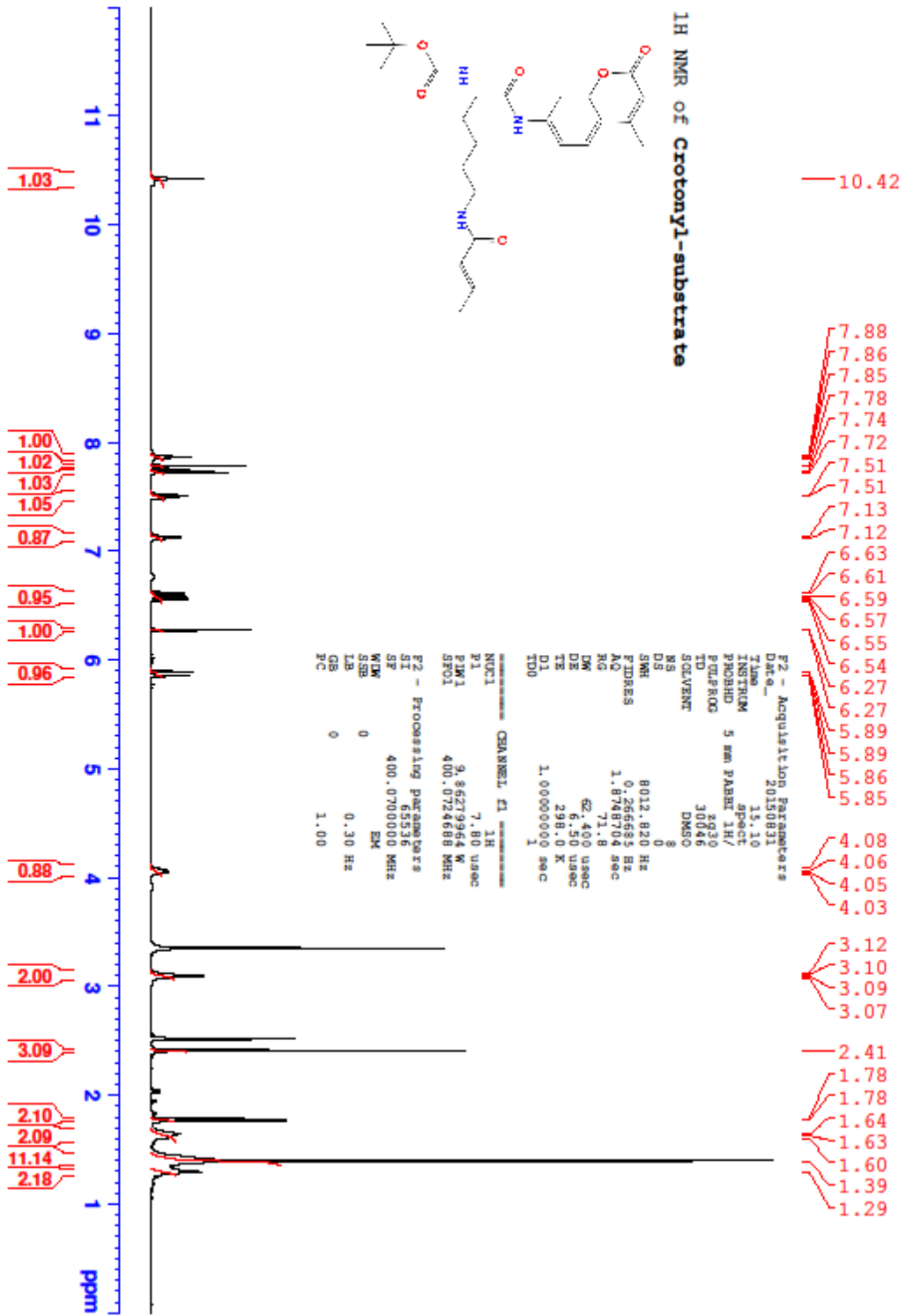


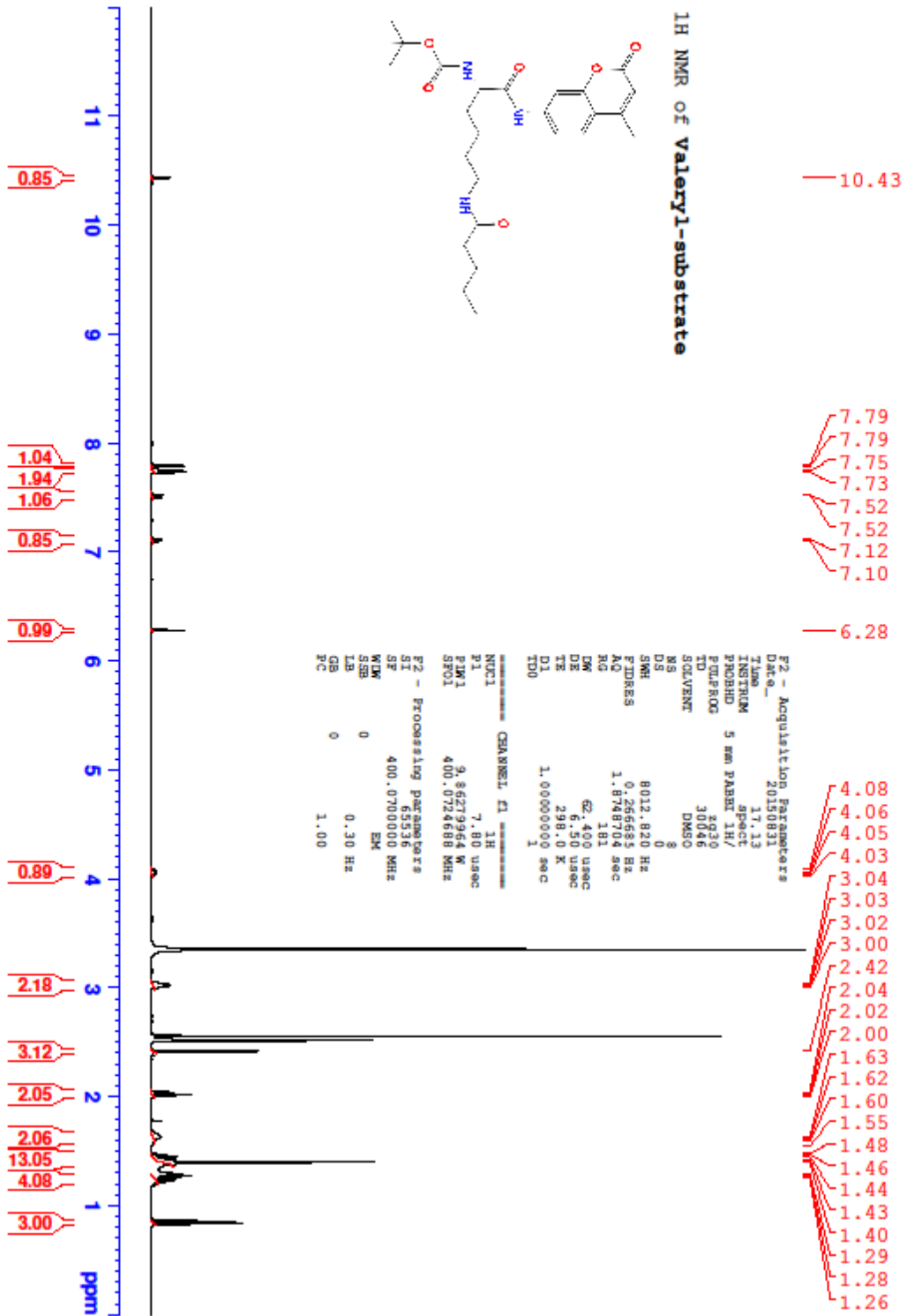


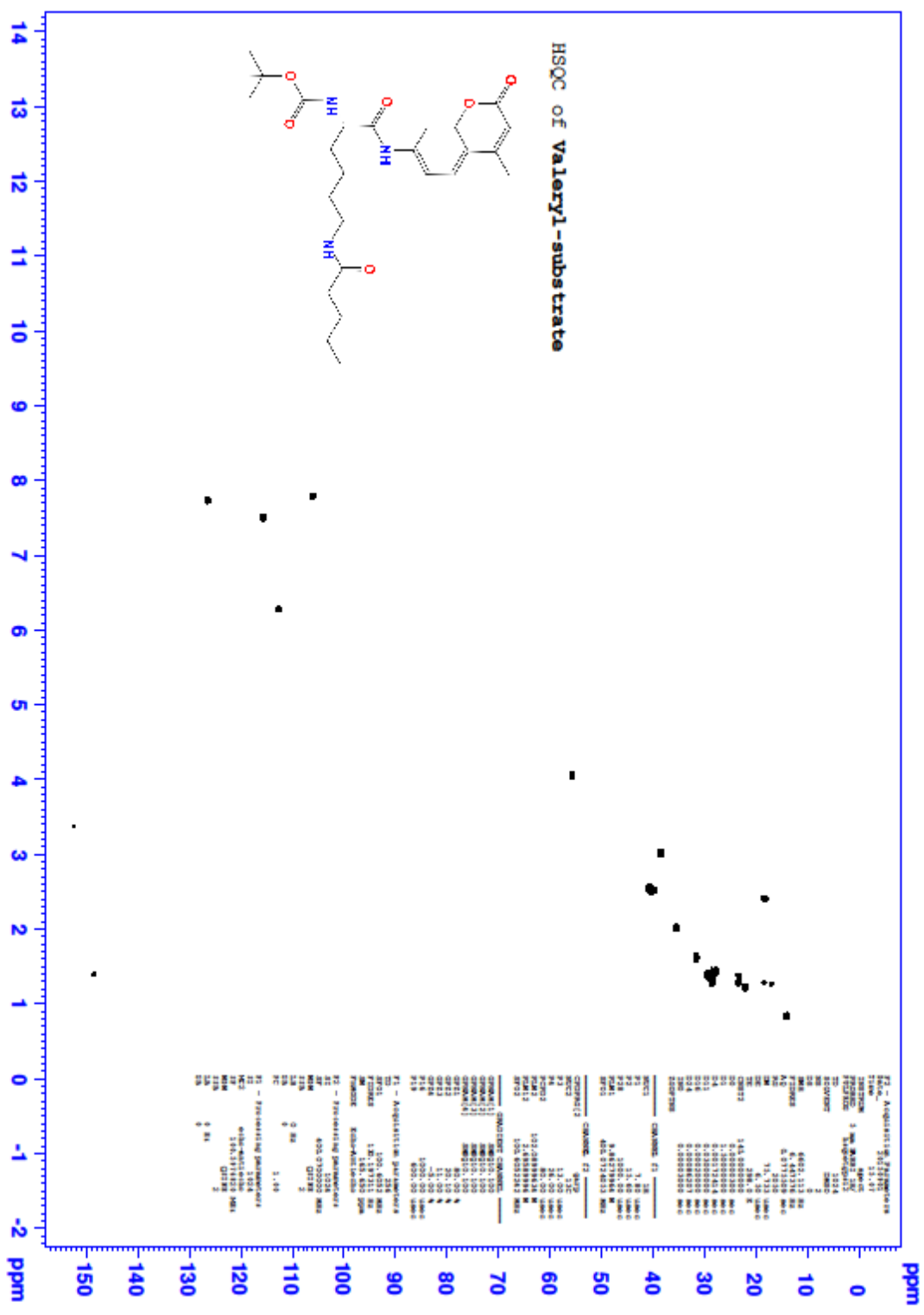


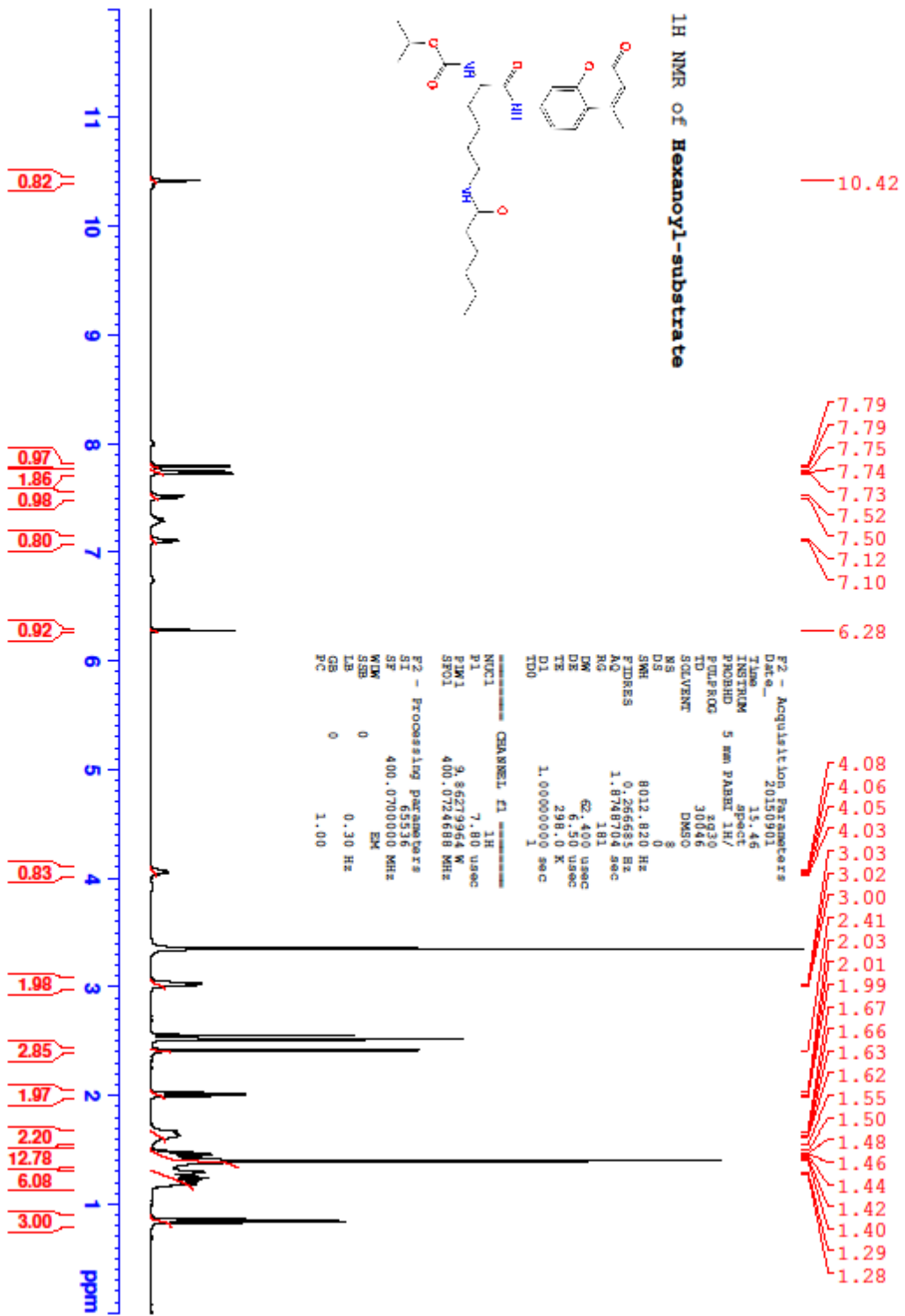


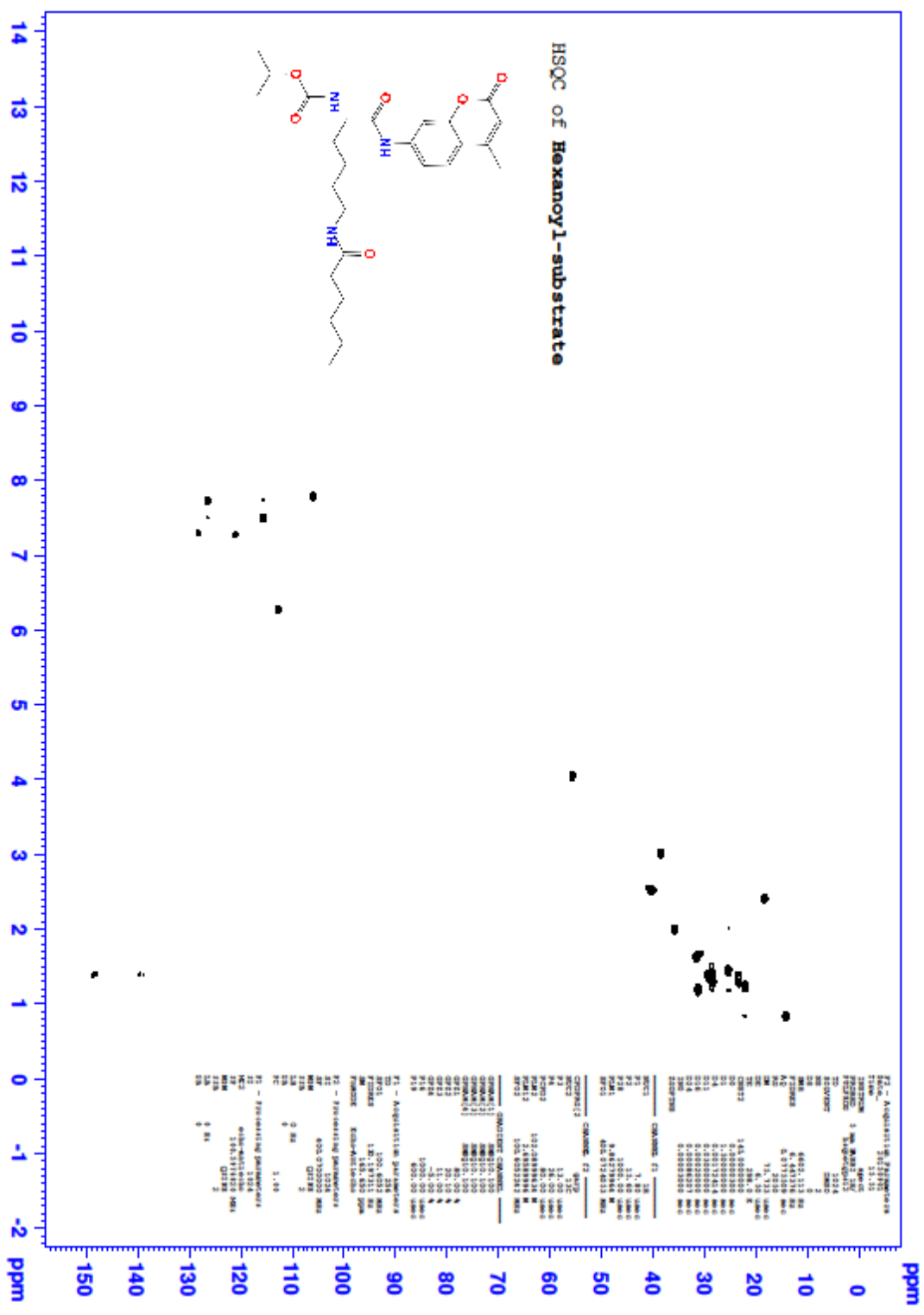


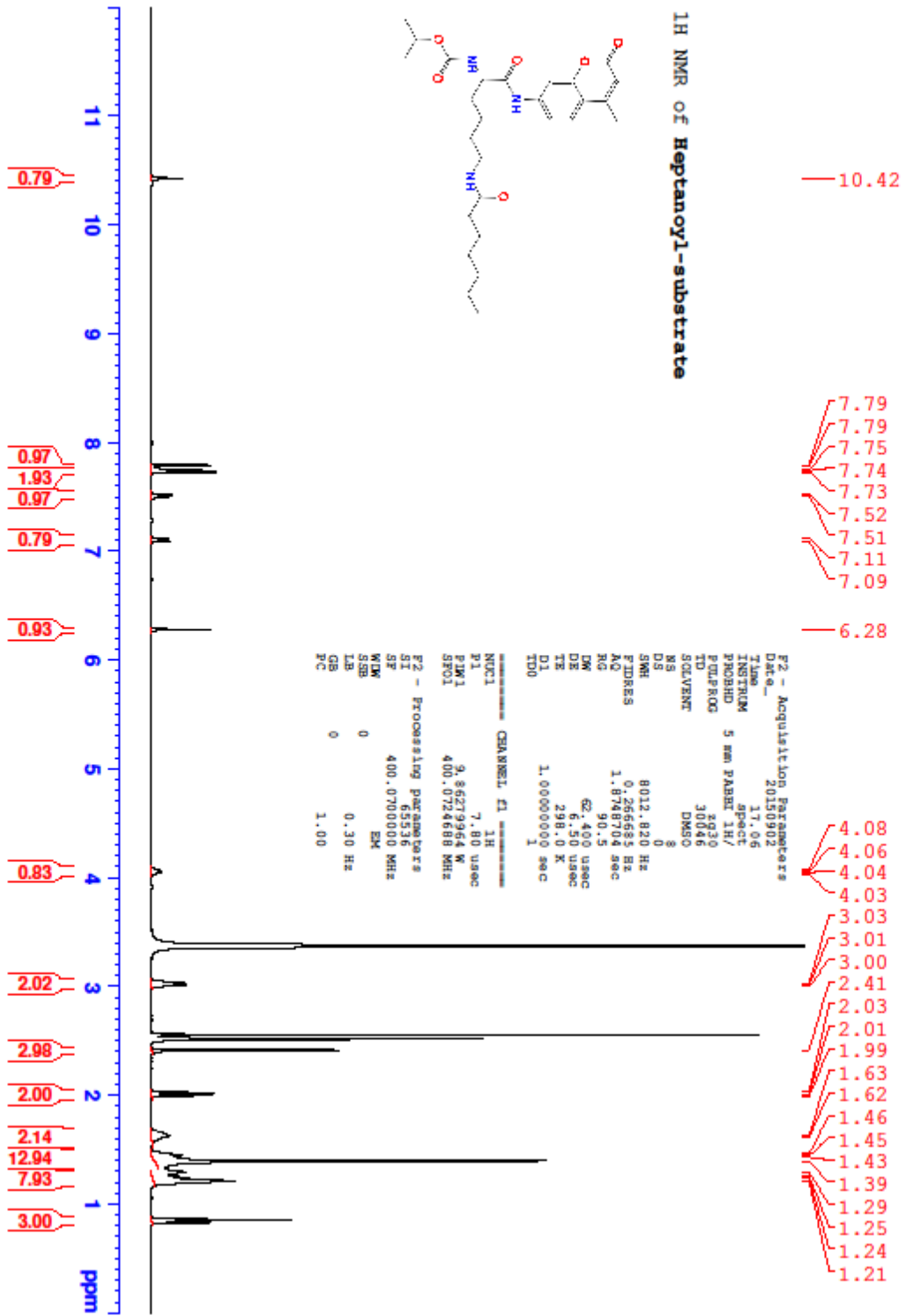


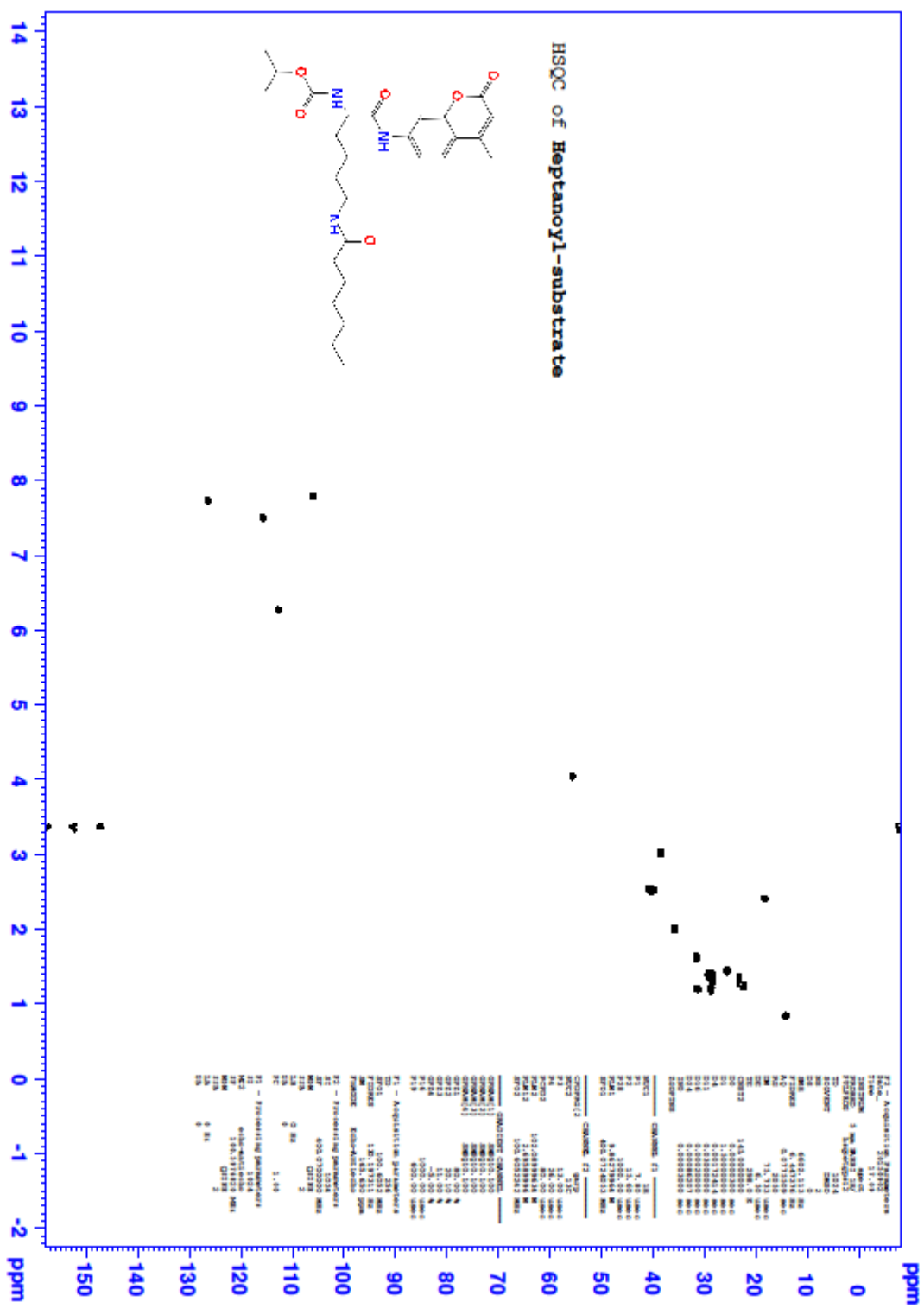




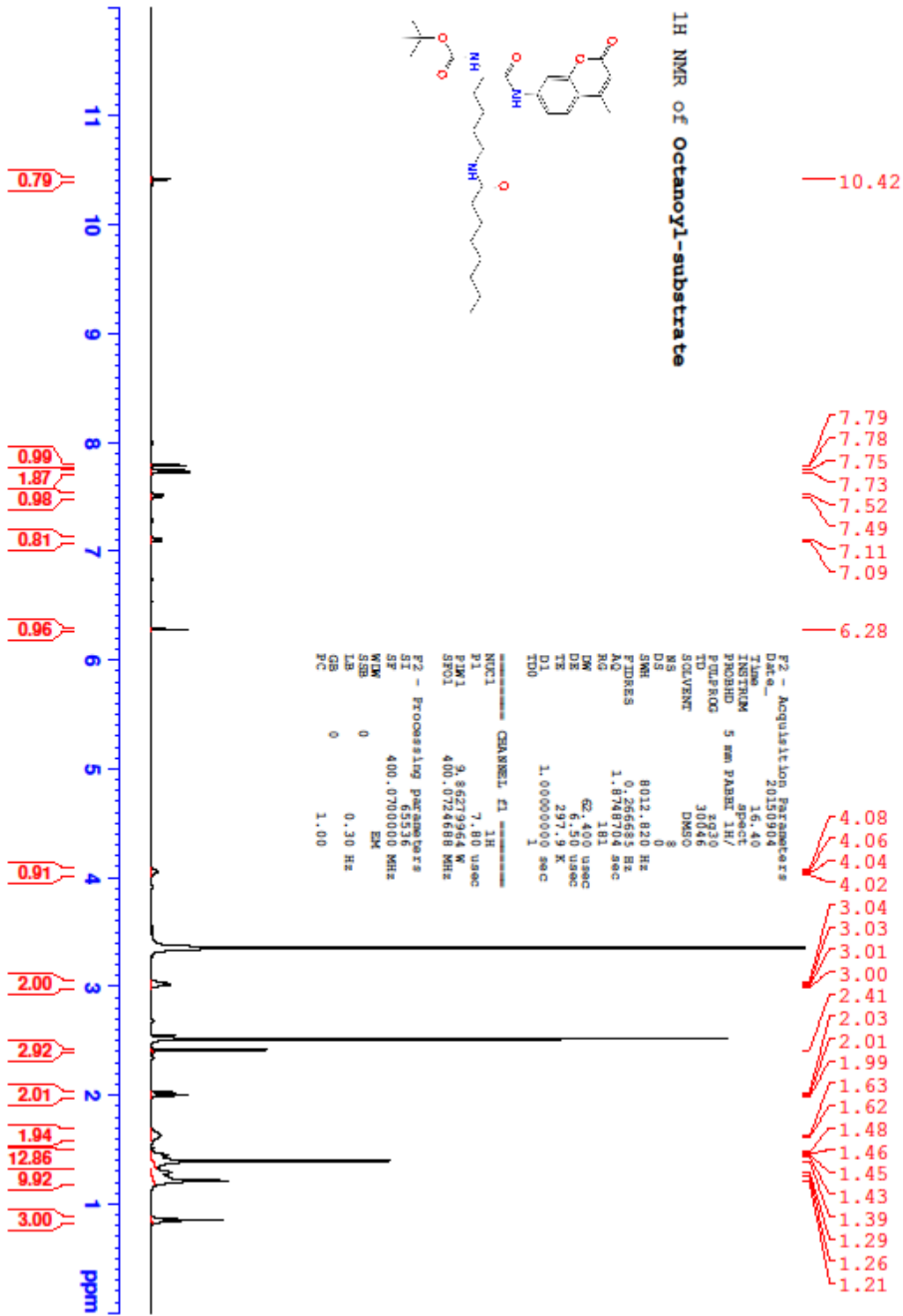
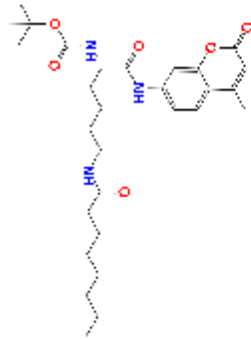




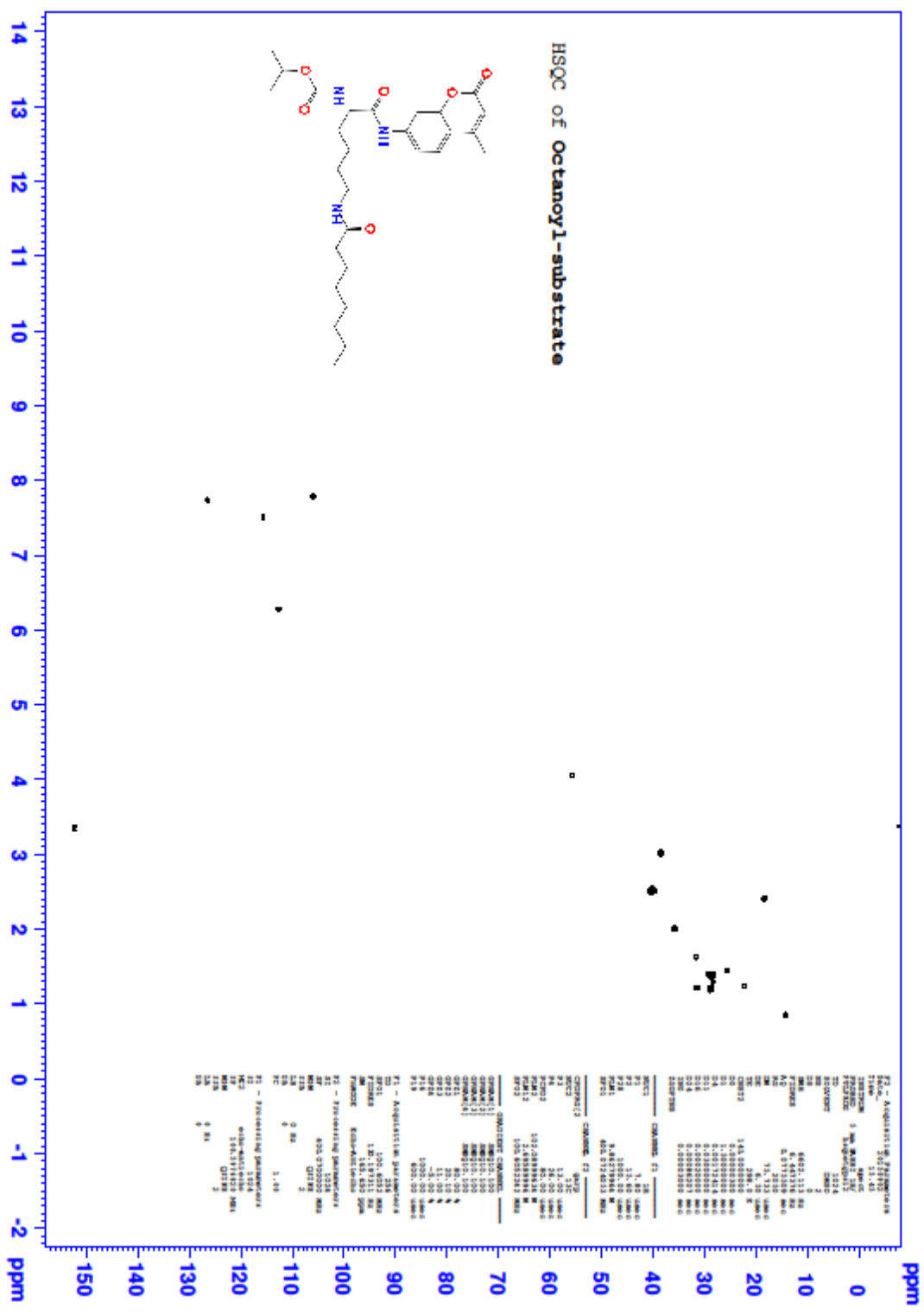


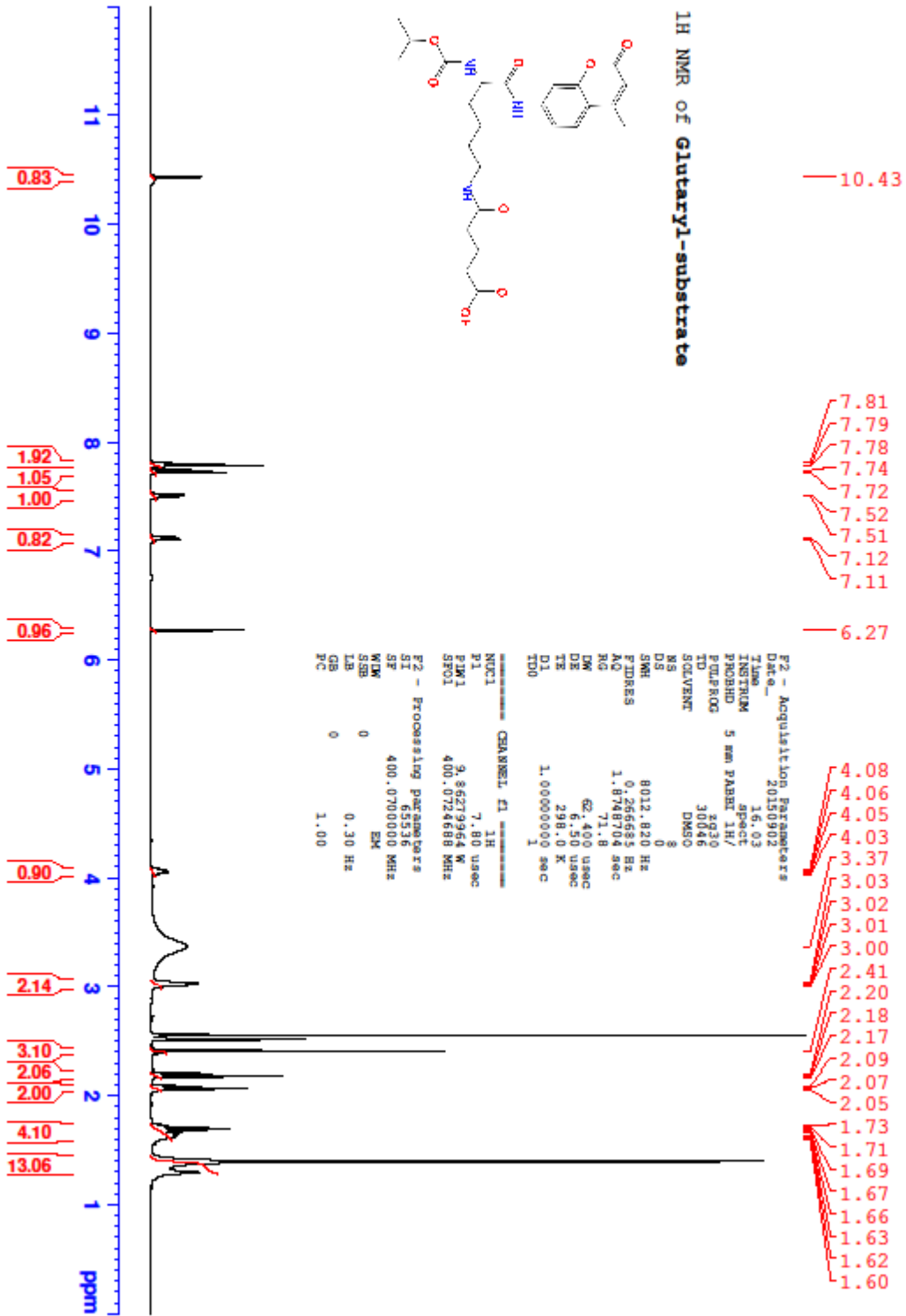


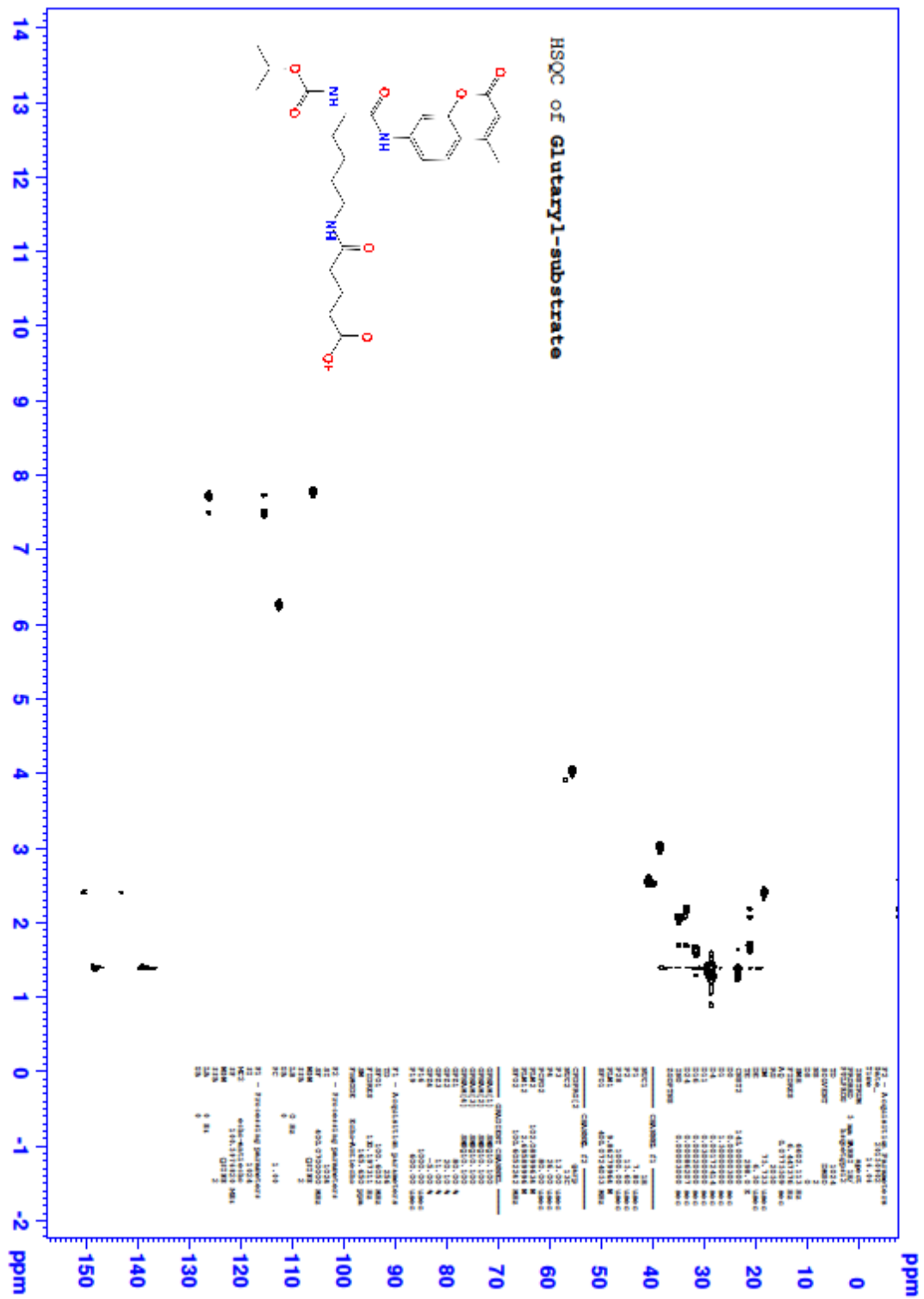
¹H NMR of Octanoyl-substrate

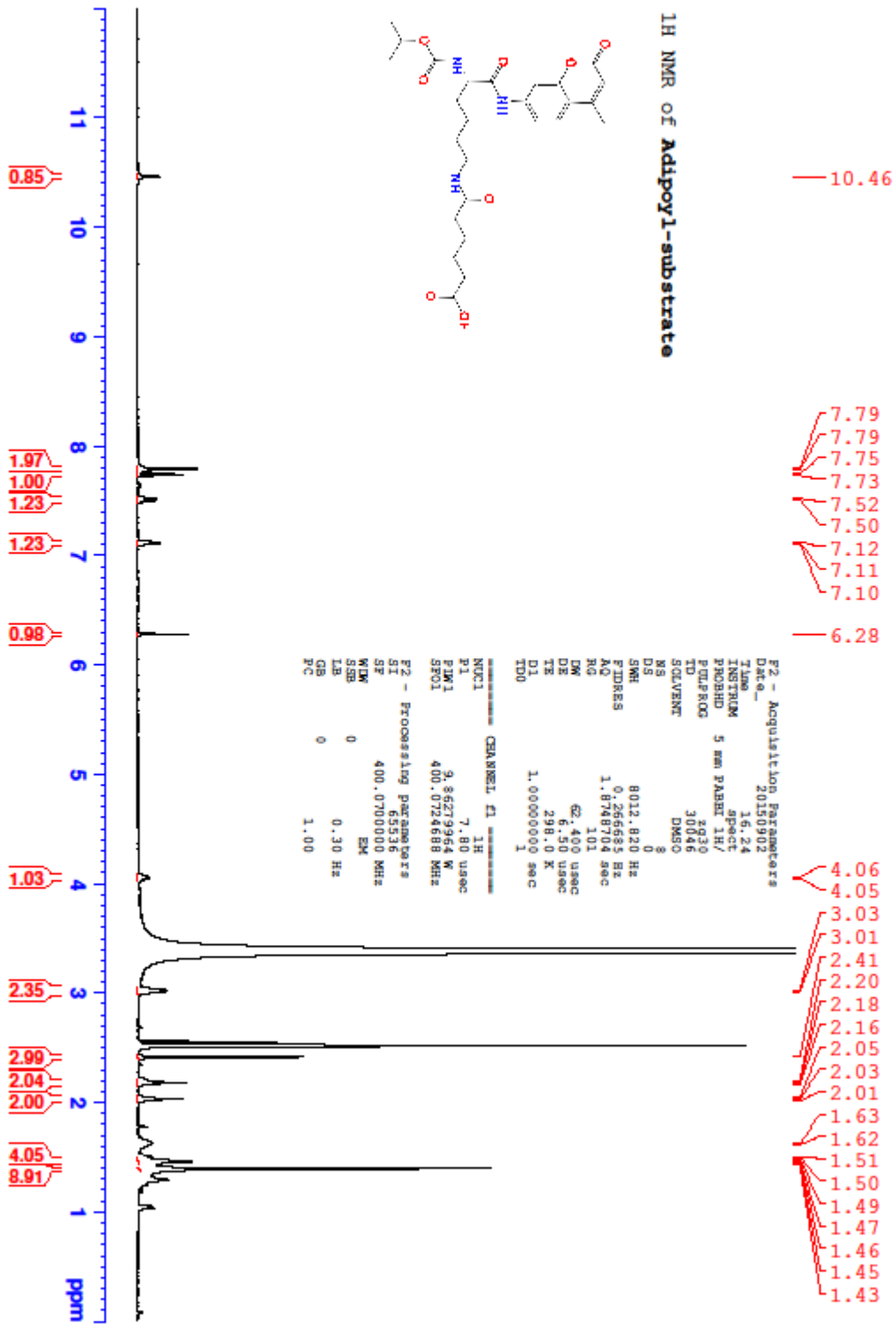


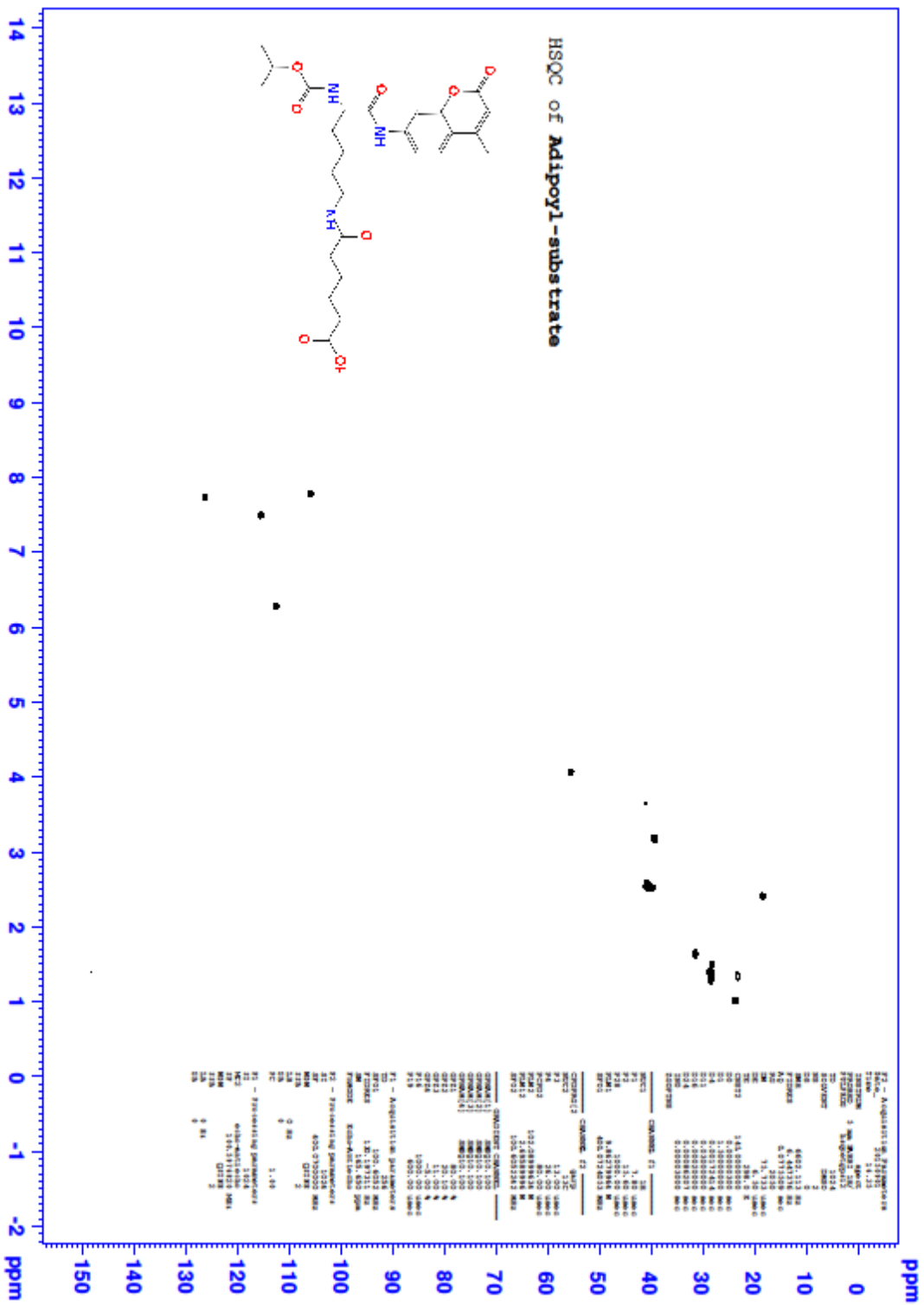
F2 - Acquisition Parameters
 Date_ 20150904
 Time 15.40
 INSTRUM spect
 PROBRD 5 mm PABBI 1H/
 PULPROG zg30
 ID 30046
 SOLVENT DMSO
 NS 8
 DS 0
 SWH 8012.820 Hz
 FIDRES 0.266685 Hz
 AQ 1.8748704 sec
 RG 181
 DE 62.400 usec
 TE 297.9 K
 D1 1.00000000 sec
 TD 1
 CHANNEL1 CHAN01 F1
 NUC1 1H
 P1 7.80 usec
 PL1 9.8627964 W
 SFO1 400.0724688 MHz
 F2 - Processing parameters
 SI 65516
 SF 400.0700000 MHz
 WIDW EM
 SSB 0
 LB 0.30 Hz
 GB 0
 PC 1.00

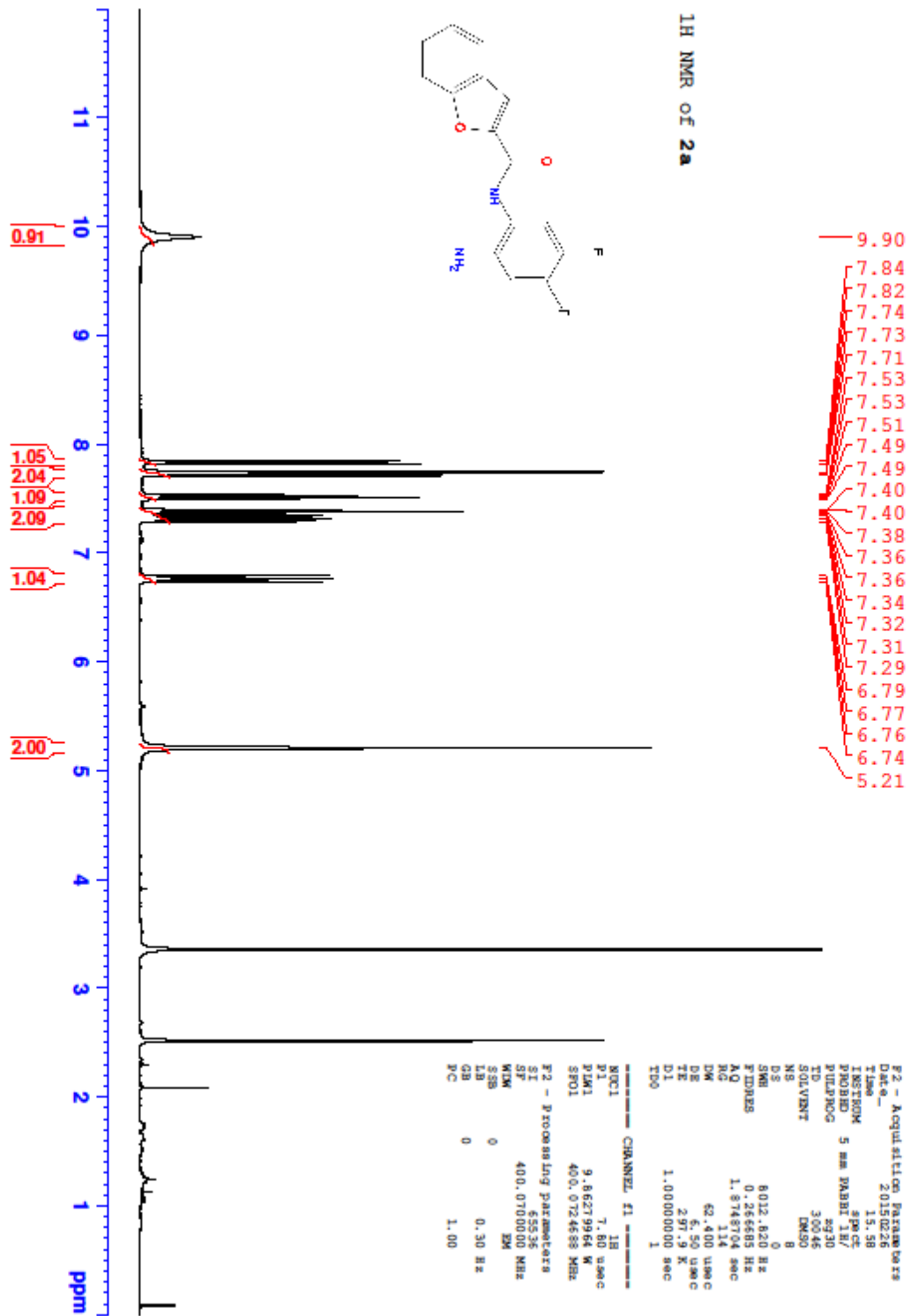






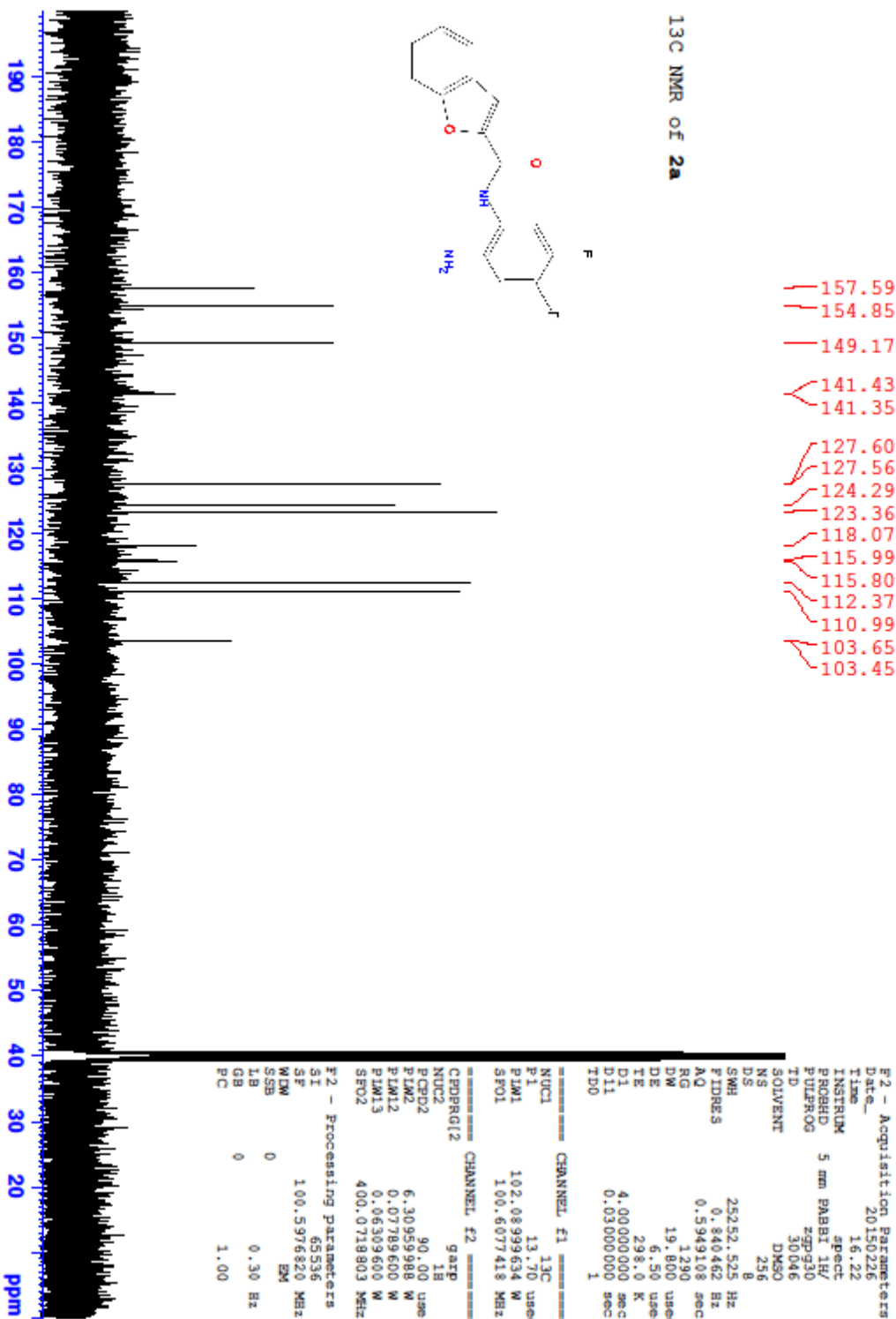
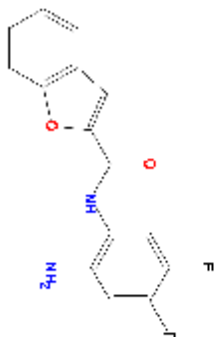


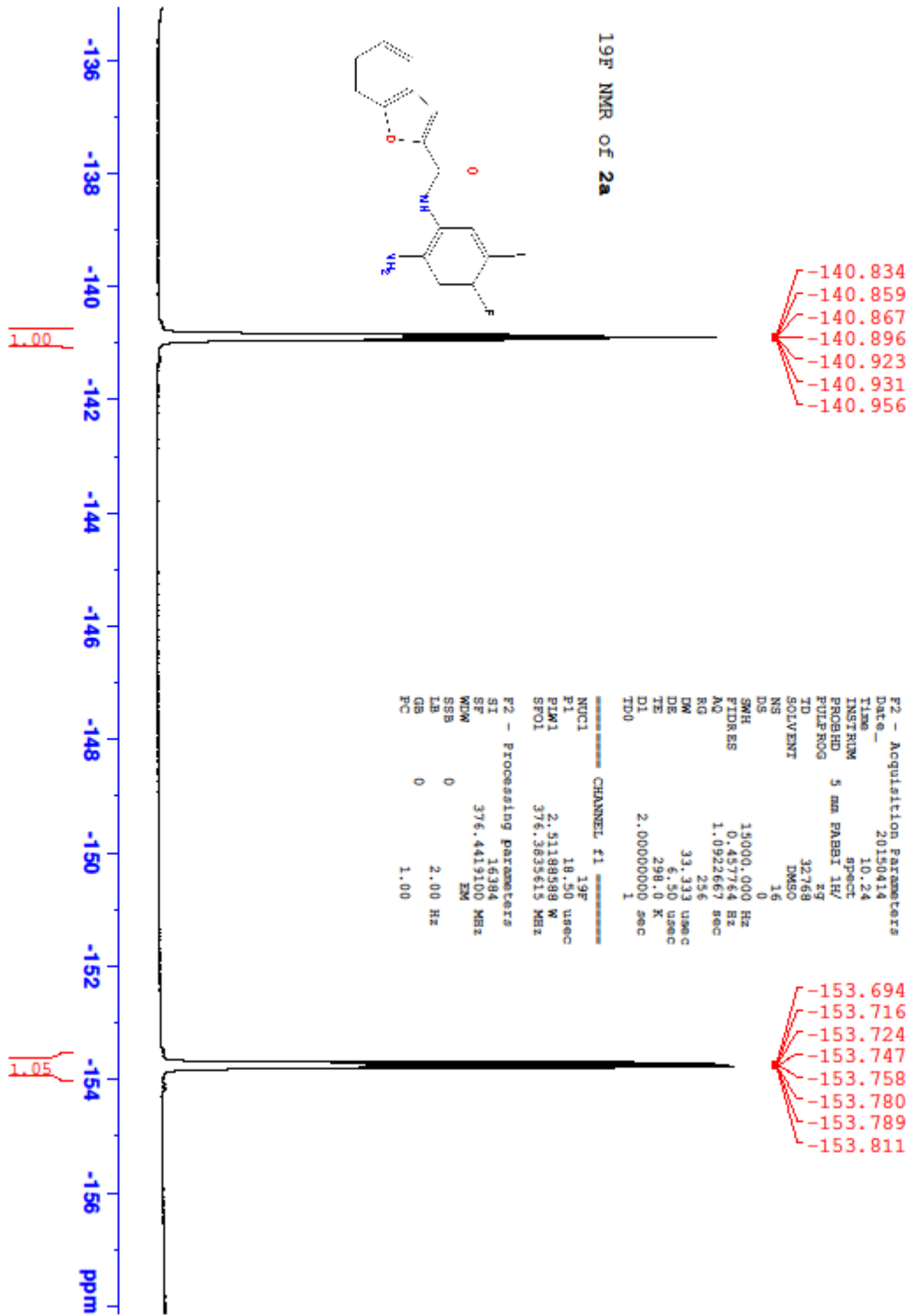




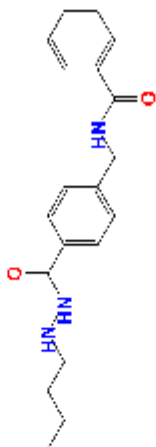
- 157.59
- 154.85
- 149.17
- 141.43
- 141.35
- 127.60
- 127.56
- 124.29
- 123.36
- 118.07
- 115.99
- 115.80
- 112.37
- 110.99
- 103.65
- 103.45

¹³C NMR of 2a





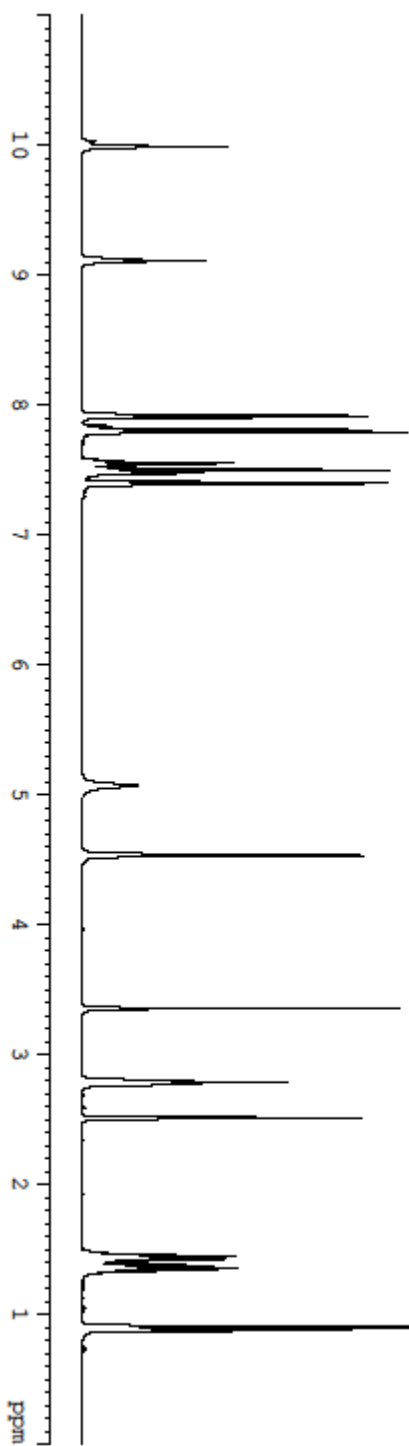
2015-11-05_111



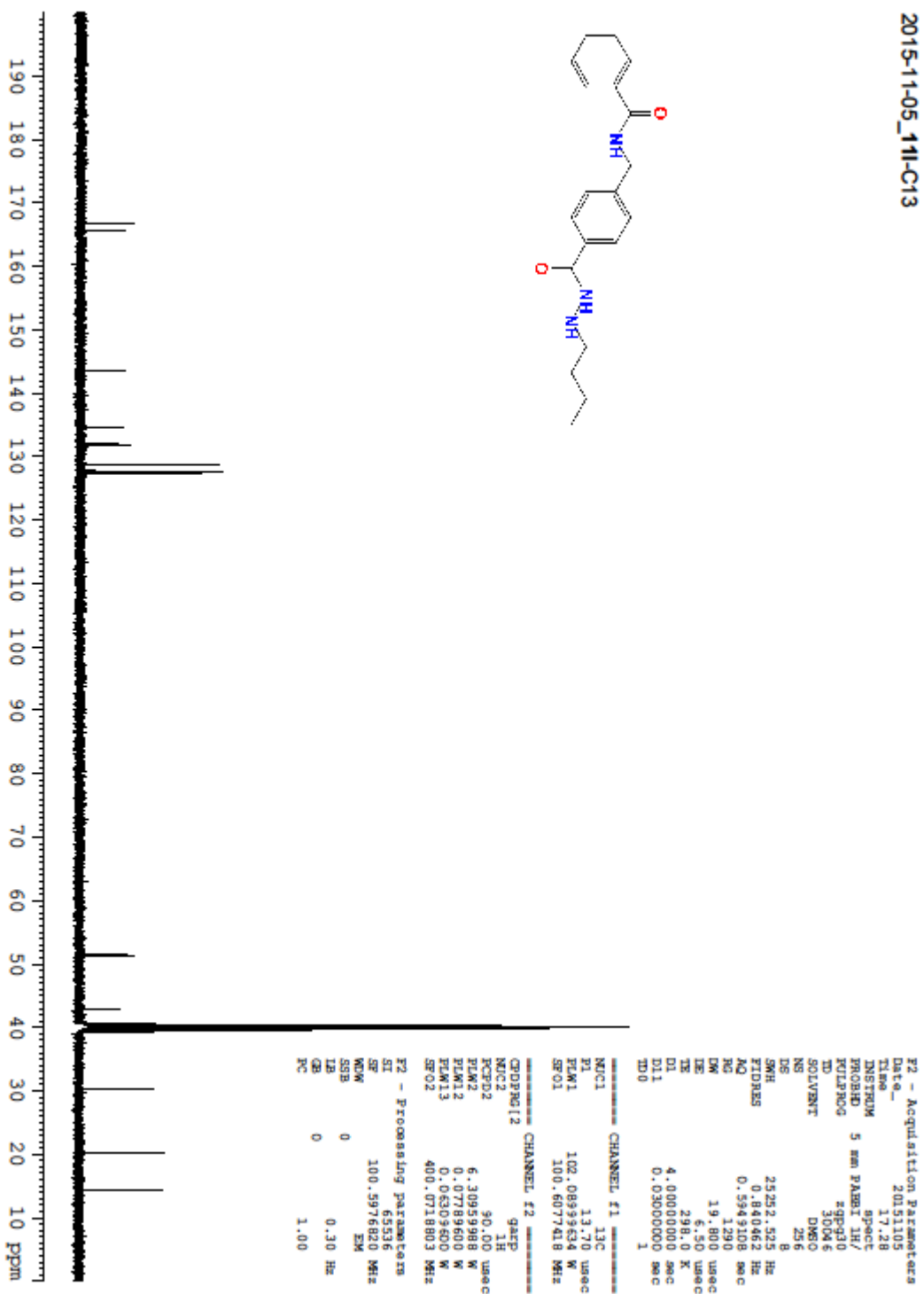
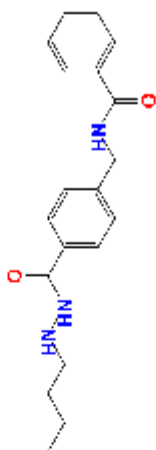
F2 - Acquisition Parameters
Date_ 20151105
Time 17.04
INSTRUM spect
PROBHD 5 mm PABBT 1B/
PULPROG zg30
TD 32046
SOLVENT DMSO
NS 8
DS 0
SWE 8012.820 Bz
FIDRES 0.26688 Bz
AQ 1.8748704 sec
RG 50.8
DW 62.400 usec
DE 6.50 usec
TE 298.0 K
D1 1.00000000 sec
TDO 1

===== CHANNEL f1 =====
NUC1 13C
P1 9.86279664 usec
PLW1 400.0724688 MHz
SFO1 400.0724688 MHz

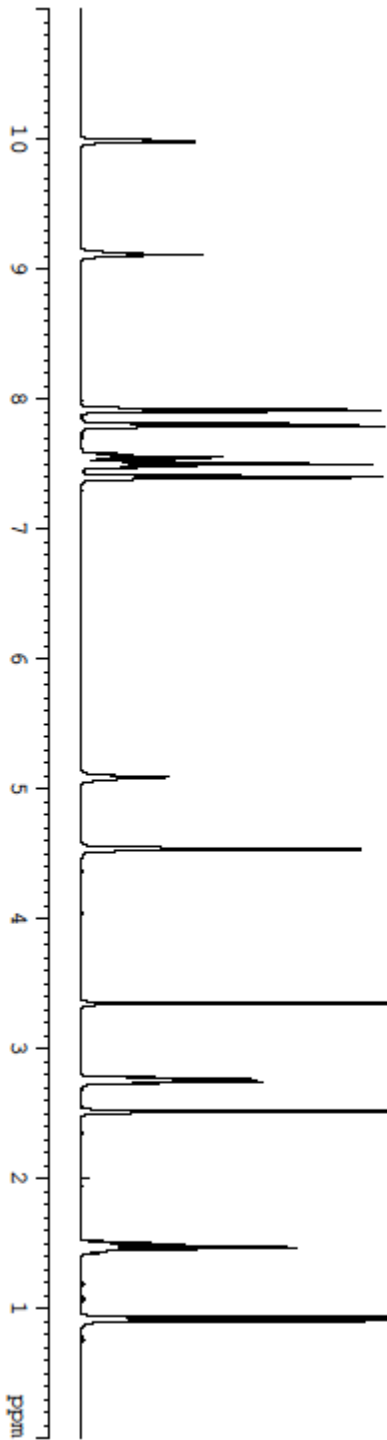
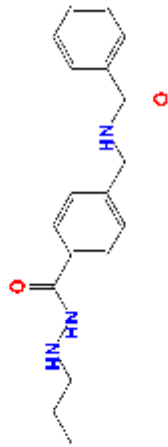
F2 - Processing parameters
SI 65536
SF 400.0700000 MHz
WDW EM
SSB 0
LB 0
GB 0
PC 1.00



2015-11-05_11I-C13



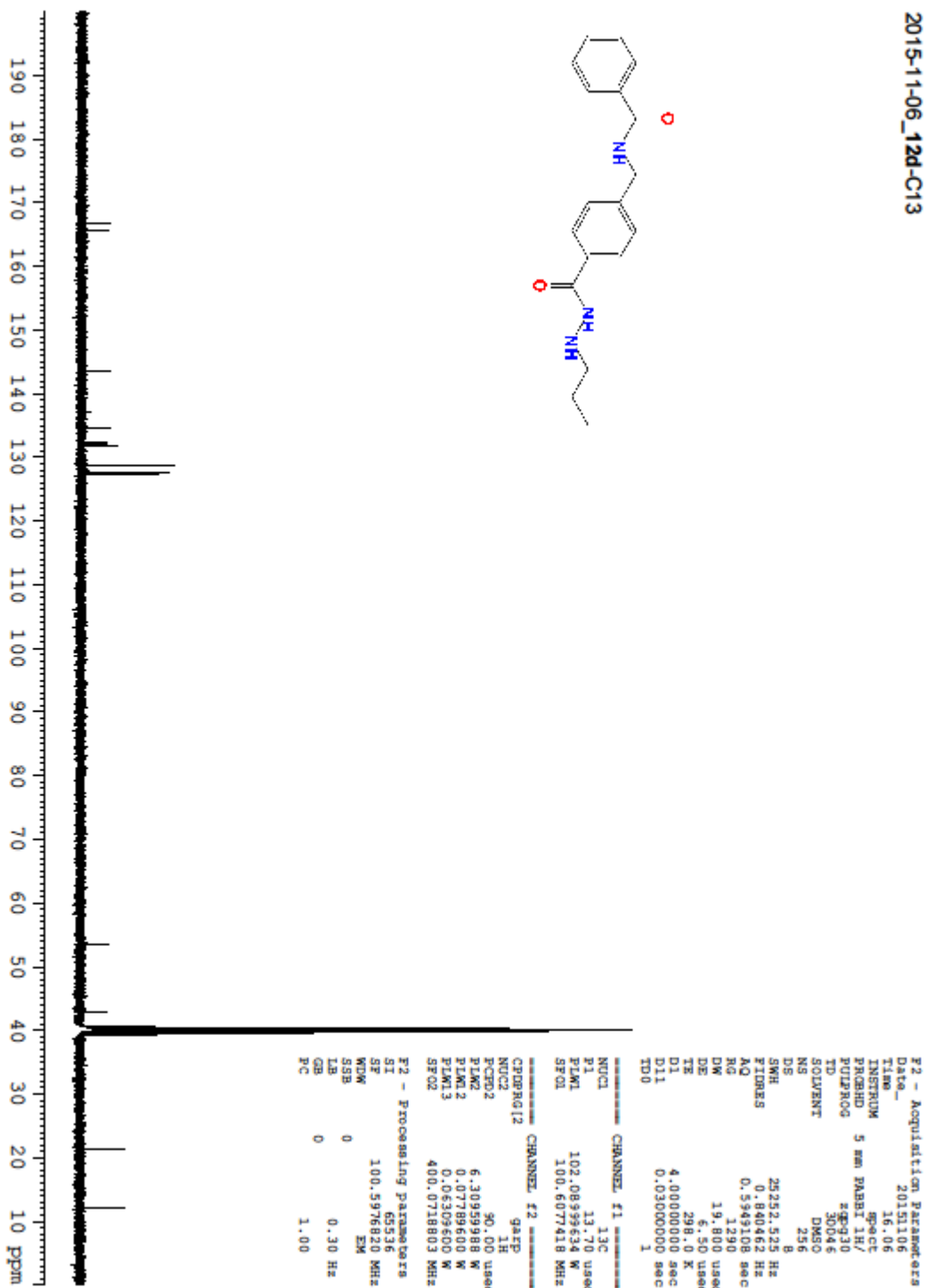
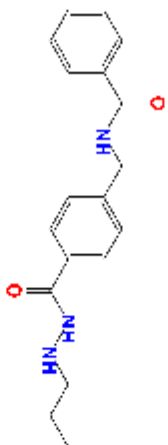
2015-11-05_12d



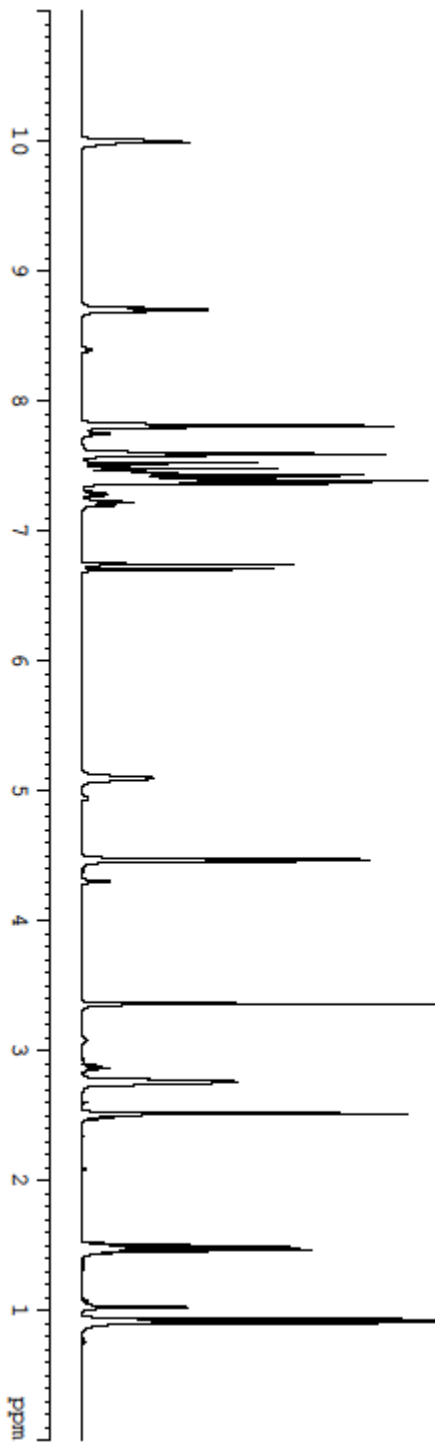
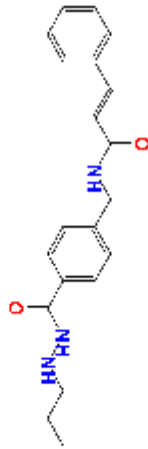
F2 - Acquisition Parameters
Date_ 20151105
Time 15:42
INSTRUM spect
PROBHD 5 mm PABBI 1H/
PULPROG zg30
TD 30646
SOLVENT DMSO
NS 8
DS 0
SWH 8012.520 Hz
FIDRES 0.266655 Hz
AQ 1.8748704 sec
RG 90.5
RW 62.400 uHz
DE 6.50 uHz
TE 298.0 K
D1 1.00000000 sec
ZD0 1

NAME: CEMNMR1.F1
NOX1 1H
P1 7.80 uHz
P1W1 9.86279664 W
SFO1 400.0724688 MHz
F2 - Processing parameters
SI 65536
SF 400.0700000 MHz
WDW EM
SSB 0
LB 0.30 Hz
GB 0
PC 1.00

2015-11-06_12d-C13



2015-11-10_13b

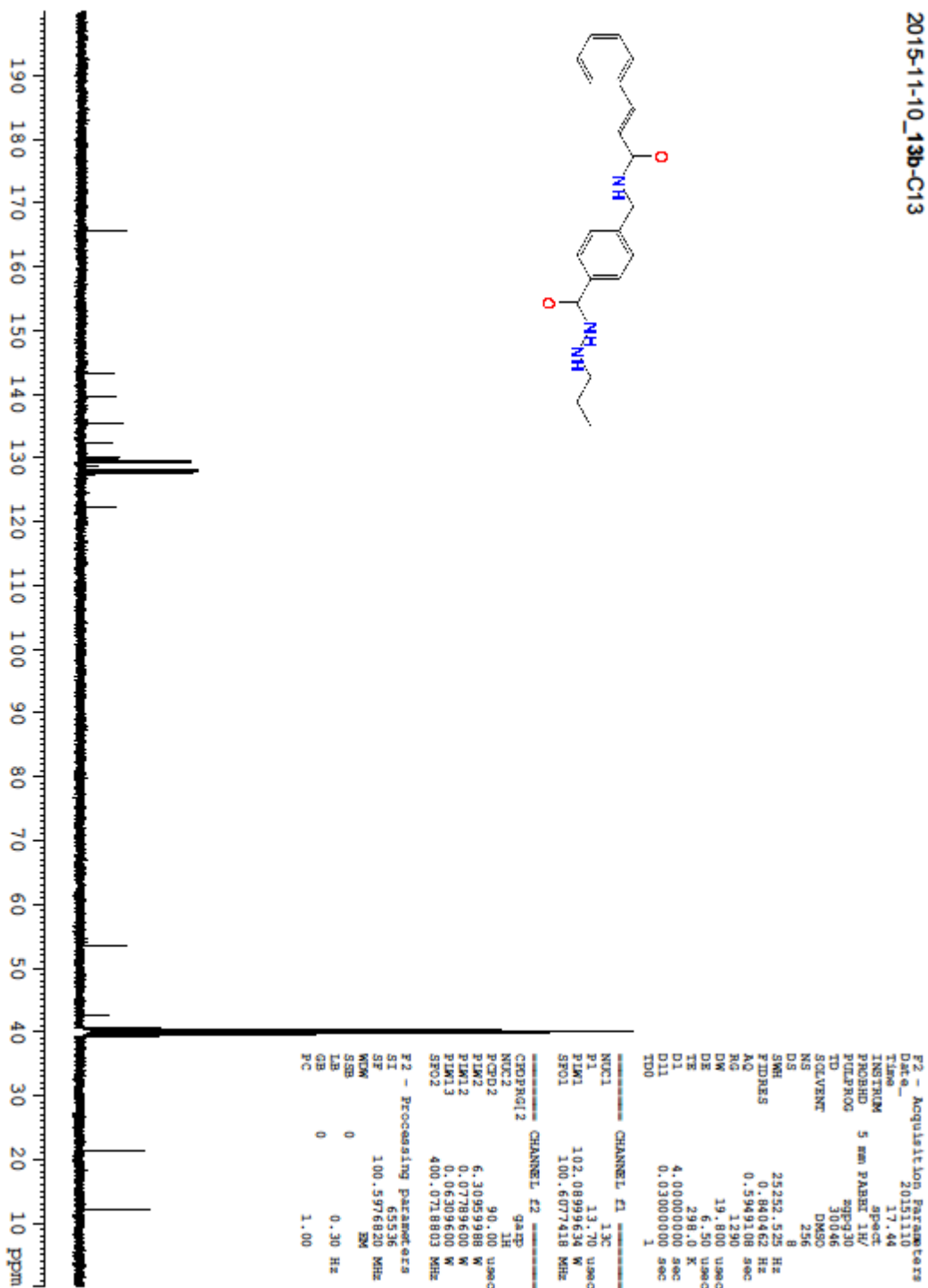
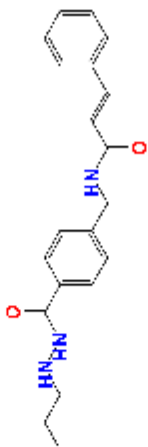


F2 - Acquisition Parameters
Date_ 20151110
Time 17.19
INSTRUM spect
PROBHD 5 mm PABBI 1H/
PULPROG zg30
TD 30046
SOLVENT DMSO
NS 8
DS 0
SWH 8012.820 Hz
FIDRES 0.26668 Hz
AQ 1.8748704 sec
RG 80.6
DW 62.400 usec
DE 6.50 usec
TE 298.1 K
D1 1.00000000 sec
TD0 1

CHANNEL F1
NUC1 1H
P1 7.80 usec
PLM1 9.8627964 W
SFO1 400.0724688 MHz

F2 - Processing parameters
SI 5535
SF 400.0700000 MHz
WDW EM
SSB 0
LA 0.30 Hz
GB 0
PC 1.00

2015-11-10_13b-C13



1. Inoue, A.; Fujimoto, D., Histone deacetylase from calf thymus. *Biochimica et biophysica acta* **1970**, *220* (2), 307-16.
2. Gallwitz, D.; Sekeris, C. E., The acetylation of histones of rat liver nuclei in vitro by acetyl-CoA. *Hoppe-Seyler's Zeitschrift fur physiologische Chemie* **1969**, *350* (2), 150-4.
3. Wagner, G. R.; Hirschey, M. D., Non-enzymatic protein acylation as a carbon stress regulated by sirtuin deacylases. *Molecular cell* **2014**, *54* (1), 5-16.
4. James, A. M.; Hoogewijs, K.; Logan, A.; Hall, A. R.; Ding, S.; Fearnley, I. M.; Murphy, M. P., Non-enzymatic N-acetylation of Lysine Residues by AcetylCoA Often Occurs via a Proximal S-acetylated Thiol Intermediate Sensitive to Glyoxalase II. *Cell Reports* **2017**, *18* (9), 2105-2112.
5. Ollia, A. S.; Barker, K.; McCullough, C. E.; Tang, H.-Y.; Speicher, D. W.; Qiu, J.; LaBaer, J.; Marmorstein, R., Non-enzymatic protein acetylation detected by NAPPA protein arrays(*). *ACS chemical biology* **2015**, *10* (9), 2034-2047.
6. Yang, X. J.; Seto, E., The Rpd3/Hda1 family of lysine deacetylases: from bacteria and yeast to mice and men. *Nature reviews. Molecular cell biology* **2008**, *9* (3), 206-18.
7. Ramakrishnan, V., Histone structure and the organization of the nucleosome. *Annual review of biophysics and biomolecular structure* **1997**, *26*, 83-112.
8. Ropero, S.; Esteller, M., The role of histone deacetylases (HDACs) in human cancer. *Molecular Oncology* **2007**, *1* (1), 19-25.
9. Barneda-Zahonero, B.; Parra, M., Histone deacetylases and cancer. *Molecular Oncology* **2012**, *6* (6), 579-589.
10. Bolden, J. E.; Peart, M. J.; Johnstone, R. W., Anticancer activities of histone deacetylase inhibitors. *Nat Rev Drug Discov* **2006**, *5* (9), 769-84.
11. Marks, P. A., The clinical development of histone deacetylase inhibitors as targeted anticancer drugs. *Expert opinion on investigational drugs* **2010**, *19* (9), 1049-1066.
12. Gregoret, I. V.; Lee, Y. M.; Goodson, H. V., Molecular evolution of the histone deacetylase family: functional implications of phylogenetic analysis. *Journal of molecular biology* **2004**, *338* (1), 17-31.
13. Jones, P.; Altamura, S.; De Francesco, R.; Gallinari, P.; Lahm, A.; Neddermann, P.; Rowley, M.; Serafini, S.; Steinkuhler, C., Probing the elusive catalytic activity of vertebrate class IIa histone deacetylases. *Bioorganic & medicinal chemistry letters* **2008**, *18* (6), 1814-9.
14. Riester, D.; Wegener, D.; Hildmann, C.; Schwienhorst, A., Members of the histone deacetylase superfamily differ in substrate specificity towards small synthetic substrates. *Biochemical and Biophysical Research Communications* **2004**, *324* (3), 1116-1123.
15. Lahm, A.; Paolini, C.; Pallaoro, M.; Nardi, M. C.; Jones, P.; Neddermann, P.; Sambucini, S.; Bottomley, M. J.; Lo Surdo, P.; Carfi, A.; Koch, U.; De Francesco, R.; Steinkühler, C.; Gallinari, P., Unraveling the hidden catalytic activity of vertebrate class IIa histone deacetylases. *Proceedings of the National Academy of Sciences* **2007**, *104* (44), 17335-17340.
16. Martin, M.; Kettmann, R.; Dequiedt, F., Class IIa histone deacetylases: regulating the regulators. *Oncogene* **2007**, *26* (37), 5450-5467.
17. Kelly, R. D.; Cowley, S. M., The physiological roles of histone deacetylase (HDAC) 1 and 2: complex co-stars with multiple leading parts. *Biochemical Society transactions* **2013**, *41* (3), 741-9.
18. Muoio, D. M., HDAC3 sets the timer on muscle fuel switching. *Nature medicine* **2017**, *23* (2), 148-150.

19. Remsberg, J. R.; Ediger, B. N.; Ho, W. Y.; Damle, M.; Li, Z.; Teng, C.; Lanzillotta, C.; Stoffers, D. A.; Lazar, M. A., Deletion of histone deacetylase 3 in adult beta cells improves glucose tolerance via increased insulin secretion. *Molecular metabolism* **2017**, *6* (1), 30-37.
20. Mehdipour, P.; Santoro, F.; Botrugno, O. A.; Romanenghi, M.; Pagliuca, C.; Matthews, G. M.; Johnstone, R. W.; Minucci, S., HDAC3 activity is required for initiation of leukemogenesis in acute promyelocytic leukemia. *Leukemia* **2017**, *31* (4), 995-997.
21. Walsh, M. E.; Van Remmen, H., Emerging roles for histone deacetylases in age-related muscle atrophy. *Nutrition and healthy aging* **2016**, *4* (1), 17-30.
22. Tanimoto, A.; Takeuchi, S.; Arai, S.; Fukuda, K.; Yamada, T.; Roca, X.; Ong, S. T.; Yano, S., Histone Deacetylase 3 Inhibition Overcomes BIM Deletion Polymorphism-Mediated Osimertinib Resistance in EGFR-Mutant Lung Cancer. *Clinical cancer research : an official journal of the American Association for Cancer Research* **2016**.
23. Yang, X.; Wu, Q.; Zhang, L.; Feng, L., Inhibition of Histone Deacetylase 3 (HDAC3) Mediates Ischemic Preconditioning and Protects Cortical Neurons against Ischemia in Rats. *Frontiers in molecular neuroscience* **2016**, *9*, 131.
24. Angiolilli, C.; Kabala, P. A.; Grabiec, A. M.; Van Baarsen, I. M.; Ferguson, B. S.; Garcia, S.; Malvar Fernandez, B.; McKinsey, T. A.; Tak, P. P.; Fossati, G.; Mascagni, P.; Baeten, D. L.; Reedquist, K. A., Histone deacetylase 3 regulates the inflammatory gene expression programme of rheumatoid arthritis fibroblast-like synoviocytes. *Annals of the rheumatic diseases* **2017**, *76* (1), 277-285.
25. Chhabra, S., Novel Proteasome Inhibitors and Histone Deacetylase Inhibitors: Progress in Myeloma Therapeutics. *Pharmaceuticals (Basel, Switzerland)* **2017**, *10* (2).
26. Zhang, X.; Yang, J.; Wang, H.; Guo, R.; Yin, Y.; Zhang, D.; Zhang, Q.; Wang, H.; Zhou, Z.; Chen, L.; Zhou, J.; Liu, L., Overexpression of Hdac6 extends reproductive lifespan in mice. *Protein & cell* **2017**.
27. Perry, S.; Kiragasi, B.; Dickman, D.; Ray, A., The Role of Histone Deacetylase 6 in Synaptic Plasticity and Memory. *Cell Rep* **2017**, *18* (6), 1337-1345.
28. Ryu, H. W.; Shin, D. H.; Lee, D. H.; Choi, J.; Han, G.; Lee, K. Y.; Kwon, S. H., HDAC6 deacetylates p53 at lysines 381/382 and differentially coordinates p53-induced apoptosis. *Cancer Lett* **2017**, *391*, 162-171.
29. Li, Z. Y.; Zhang, C.; Zhang, Y.; Chen, L.; Chen, B. D.; Li, Q. Z.; Zhang, X. J.; Li, W. P., A novel HDAC6 inhibitor Tubastatin A: Controls HDAC6-p97/VCP-mediated ubiquitination-autophagy turnover and reverses Temozolomide-induced ER stress-tolerance in GBM cells. *Cancer Lett* **2017**, *391*, 89-99.
30. Millard, C. J.; Watson, P. J.; Celardo, I.; Gordiyenko, Y.; Cowley, S. M.; Robinson, C. V.; Fairall, L.; Schwabe, J. W., Class I HDACs share a common mechanism of regulation by inositol phosphates. *Mol Cell* **2013**, *51* (1), 57-67.
31. Watson, P. J.; Millard, C. J.; Riley, A. M.; Robertson, N. S.; Wright, L. C.; Godage, H. Y.; Cowley, S. M.; Jamieson, A. G.; Potter, B. V. L.; Schwabe, J. W. R., Insights into the activation mechanism of class I HDAC complexes by inositol phosphates. *Nature Communications* **2016**, *7*, 11262.
32. Watson, P. J.; Fairall, L.; Santos, G. M.; Schwabe, J. W. R., Structure of HDAC3 bound to co-repressor and inositol tetrakisphosphate. *Nature* **2012**, *481* (7381), 335-340.
33. Gilmore, T. D., Introduction to NF- κ B: players, pathways, perspectives. *Oncogene* **2006**, *25* (51), 6680-6684.

34. Hoesel, B.; Schmid, J. A., The complexity of NF- κ B signaling in inflammation and cancer. *Molecular Cancer* **2013**, *12*, 86-86.
35. Spange, S.; Wagner, T.; Heinzl, T.; Kramer, O. H., Acetylation of non-histone proteins modulates cellular signalling at multiple levels. *The international journal of biochemistry & cell biology* **2009**, *41* (1), 185-98.
36. Ito, K., Impact of post-translational modifications of proteins on the inflammatory process. *Biochemical Society transactions* **2007**, *35* (Pt 2), 281-3.
37. Chen, L.; Fischle, W.; Verdin, E.; Greene, W. C., Duration of nuclear NF-kappaB action regulated by reversible acetylation. *Science (New York, N.Y.)* **2001**, *293* (5535), 1653-7.
38. Chen, L. F.; Mu, Y.; Greene, W. C., Acetylation of RelA at discrete sites regulates distinct nuclear functions of NF-kappaB. *Embo j* **2002**, *21* (23), 6539-48.
39. Huang, B.; Yang, X. D.; Lamb, A.; Chen, L. F., Posttranslational modifications of NF-kappaB: another layer of regulation for NF-kappaB signaling pathway. *Cellular signalling* **2010**, *22* (9), 1282-90.
40. Buerki, C.; Rothgiesser, K. M.; Valovka, T.; Owen, H. R.; Rehrauer, H.; Fey, M.; Lane, W. S.; Hottiger, M. O., Functional relevance of novel p300-mediated lysine 314 and 315 acetylation of RelA/p65. *Nucleic acids research* **2008**, *36* (5), 1665-80.
41. Ziesche, E.; Kettner-Buhrow, D.; Weber, A.; Wittwer, T.; Jurida, L.; Soelch, J.; Muller, H.; Newel, D.; Kronich, P.; Schneider, H.; Dittrich-Breiholz, O.; Bhaskara, S.; Hiebert, S. W.; Hottiger, M. O.; Li, H.; Burstein, E.; Schmitz, M. L.; Kracht, M., The coactivator role of histone deacetylase 3 in IL-1-signaling involves deacetylation of p65 NF-kappaB. *Nucleic acids research* **2013**, *41* (1), 90-109.
42. Kiernan, R.; Brès, V.; Ng, R. W. M.; Coudart, M.-P.; El Messaoudi, S.; Sardet, C.; Jin, D.-Y.; Emiliani, S.; Benkirane, M., Post-activation Turn-off of NF- κ B-dependent Transcription Is Regulated by Acetylation of p65. *Journal of Biological Chemistry* **2003**, *278* (4), 2758-2766.
43. Leus, N. G.; van der Wouden, P. E.; van den Bosch, T.; Hooghiemstra, W. T.; Ourailidou, M. E.; Kistemaker, L. E.; Bischoff, R.; Gosens, R.; Haisma, H. J.; Dekker, F. J., HDAC 3-selective inhibitor RGFP966 demonstrates anti-inflammatory properties in RAW 264.7 macrophages and mouse precision-cut lung slices by attenuating NF-kappaB p65 transcriptional activity. *Biochemical pharmacology* **2016**, *108*, 58-74.
44. Malvaez, M.; McQuown, S. C.; Rogge, G. A.; Astarabadi, M.; Jacques, V.; Carreiro, S.; Rusche, J. R.; Wood, M. A., HDAC3-selective inhibitor enhances extinction of cocaine-seeking behavior in a persistent manner. *Proceedings of the National Academy of Sciences of the United States of America* **2013**, *110* (7), 2647-52.
45. Baylin, S. B.; Ohm, J. E., Epigenetic gene silencing in cancer - a mechanism for early oncogenic pathway addiction? *Nature reviews. Cancer* **2006**, *6* (2), 107-16.
46. Pandolfi, P. P., Histone deacetylases and transcriptional therapy with their inhibitors. *Cancer chemotherapy and pharmacology* **2001**, *48 Suppl 1*, S17-9.
47. Marks, P. A.; Jiang, X., Histone deacetylase inhibitors in programmed cell death and cancer therapy. *Cell cycle (Georgetown, Tex.)* **2005**, *4* (4), 549-51.
48. West, A. C.; Johnstone, R. W., New and emerging HDAC inhibitors for cancer treatment. *The Journal of clinical investigation* **2014**, *124* (1), 30-9.
49. Yang, X.-J.; Seto, E., The Rpd3/Hda1 family of lysine deacetylases: from bacteria and yeast to mice and men. *Nature reviews. Molecular cell biology* **2008**, *9* (3), 206-218.
50. Lin, H.; Su, X.; He, B., Protein Lysine Acylation and Cysteine Succination by Intermediates of Energy Metabolism. *ACS Chemical Biology* **2012**, *7* (6), 947-960.

51. Cote, S.; Rosenauer, A.; Bianchini, A.; Seiter, K.; Vandewiele, J.; Nervi, C.; Miller, W. H., Jr., Response to histone deacetylase inhibition of novel PML/RARalpha mutants detected in retinoic acid-resistant APL cells. *Blood* **2002**, *100* (7), 2586-96.
52. He, L. Z.; Tolentino, T.; Grayson, P.; Zhong, S.; Warrell, R. P., Jr.; Rifkind, R. A.; Marks, P. A.; Richon, V. M.; Pandolfi, P. P., Histone deacetylase inhibitors induce remission in transgenic models of therapy-resistant acute promyelocytic leukemia. *The Journal of clinical investigation* **2001**, *108* (9), 1321-30.
53. Halkidou, K.; Gaughan, L.; Cook, S.; Leung, H. Y.; Neal, D. E.; Robson, C. N., Upregulation and nuclear recruitment of HDAC1 in hormone refractory prostate cancer. *The Prostate* **2004**, *59* (2), 177-89.
54. Choi, J. H.; Kwon, H. J.; Yoon, B. I.; Kim, J. H.; Han, S. U.; Joo, H. J.; Kim, D. Y., Expression profile of histone deacetylase 1 in gastric cancer tissues. *Japanese journal of cancer research : Gann* **2001**, *92* (12), 1300-4.
55. Wilson, A. J.; Byun, D. S.; Popova, N.; Murray, L. B.; L'Italien, K.; Sowa, Y.; Arango, D.; Velcich, A.; Augenlicht, L. H.; Mariadason, J. M., Histone deacetylase 3 (HDAC3) and other class I HDACs regulate colon cell maturation and p21 expression and are deregulated in human colon cancer. *The Journal of biological chemistry* **2006**, *281* (19), 13548-58.
56. Zhang, Z.; Yamashita, H.; Toyama, T.; Sugiura, H.; Ando, Y.; Mita, K.; Hamaguchi, M.; Hara, Y.; Kobayashi, S.; Iwase, H., Quantitation of HDAC1 mRNA expression in invasive carcinoma of the breast*. *Breast cancer research and treatment* **2005**, *94* (1), 11-6.
57. Zhu, P.; Martin, E.; Mengwasser, J.; Schlag, P.; Janssen, K. P.; Gottlicher, M., Induction of HDAC2 expression upon loss of APC in colorectal tumorigenesis. *Cancer cell* **2004**, *5* (5), 455-63.
58. Song, J.; Noh, J. H.; Lee, J. H.; Eun, J. W.; Ahn, Y. M.; Kim, S. Y.; Lee, S. H.; Park, W. S.; Yoo, N. J.; Lee, J. Y.; Nam, S. W., Increased expression of histone deacetylase 2 is found in human gastric cancer. *APMIS : acta pathologica, microbiologica, et immunologica Scandinavica* **2005**, *113* (4), 264-8.
59. Koenke, E.; Witt, O.; Oehme, I., HDAC Family Members Intertwined in the Regulation of Autophagy: A Druggable Vulnerability in Aggressive Tumor Entities. *Cells* **2015**, *4* (2), 135.
60. Zhi, X.; Zhong, Q., Autophagy in cancer. *F1000prime reports* **2015**, *7*, 18.
61. Auberger, P.; Puissant, A., Autophagy, a key mechanism of oncogenesis and resistance in leukemia. *Blood* **2017**, *129* (5), 547-552.
62. Evangelisti, C.; Evangelisti, C.; Chiarini, F.; Lonetti, A.; Buontempo, F.; Neri, L. M.; McCubrey, J. A.; Martelli, A. M., Autophagy in acute leukemias: A double-edged sword with important therapeutic implications. *Biochimica et Biophysica Acta (BBA) - Molecular Cell Research* **2015**, *1853* (1), 14-26.
63. Boyault, C.; Zhang, Y.; Fritah, S.; Caron, C.; Gilquin, B.; Kwon, S. H.; Garrido, C.; Yao, T.-P.; Vourc'h, C.; Matthias, P.; Khochbin, S., HDAC6 controls major cell response pathways to cytotoxic accumulation of protein aggregates. *Genes & Development* **2007**, *21* (17), 2172-2181.
64. Boyault, C.; Gilquin, B.; Zhang, Y.; Rybin, V.; Garman, E.; Meyer-Klaucke, W.; Matthias, P.; Müller, C. W.; Khochbin, S., HDAC6-p97/VCP controlled polyubiquitin chain turnover. *The EMBO Journal* **2006**, *25* (14), 3357-3366.
65. Moresi, V.; Carrer, M.; Grueter, C. E.; Rifki, O. F.; Shelton, J. M.; Richardson, J. A.; Bassel-Duby, R.; Olson, E. N., Histone deacetylases 1 and 2 regulate autophagy flux and skeletal muscle homeostasis in mice. *Proceedings of the National Academy of Sciences of the United States of America* **2012**, *109* (5), 1649-54.

66. Xie, H. J.; Noh, J. H.; Kim, J. K.; Jung, K. H.; Eun, J. W.; Bae, H. J.; Kim, M. G.; Chang, Y. G.; Lee, J. Y.; Park, H.; Nam, S. W., HDAC1 inactivation induces mitotic defect and caspase-independent autophagic cell death in liver cancer. *PLoS one* **2012**, *7* (4), e34265.
67. Chun, P., Histone deacetylase inhibitors in hematological malignancies and solid tumors. *Archives of Pharmacal Research* **2015**, *38* (6), 933-949.
68. Yamaguchi, T.; Cubizolles, F.; Zhang, Y.; Reichert, N.; Kohler, H.; Seiser, C.; Matthias, P., Histone deacetylases 1 and 2 act in concert to promote the G1-to-S progression. *Genes & Development* **2010**, *24* (5), 455-469.
69. Zupkovitz, G.; Grausenburger, R.; Brunmeir, R.; Senese, S.; Tischler, J.; Jurkin, J.; Rembold, M.; Meunier, D.; Egger, G.; Lagger, S.; Chiocca, S.; Propst, F.; Weitzer, G.; Seiser, C., The Cyclin-Dependent Kinase Inhibitor p21 Is a Crucial Target for Histone Deacetylase 1 as a Regulator of Cellular Proliferation. *Molecular and Cellular Biology* **2010**, *30* (5), 1171-1181.
70. Xiao, W.; Chen, X.; Liu, X.; Luo, L.; Ye, S.; Liu, Y., Trichostatin A, a histone deacetylase inhibitor, suppresses proliferation and epithelial-mesenchymal transition in retinal pigment epithelium cells. *Journal of Cellular and Molecular Medicine* **2014**, *18* (4), 646-655.
71. Park, J.-H.; Jong, H.-S.; Kim, S. G.; Jung, Y.; Lee, K.-W.; Lee, J.-H.; Kim, D.-K.; Bang, Y.-J.; Kim, T.-Y., Inhibitors of histone deacetylases induce tumor-selective cytotoxicity through modulating Aurora-A kinase. *Journal of Molecular Medicine* **2008**, *86* (1), 117-128.
72. Wang, C.; Chen, J.; Cao, W.; Sun, L.; Sun, H.; Liu, Y., Aurora-B and HDAC synergistically regulate survival and proliferation of lymphoma cell via AKT, mTOR and Notch pathways. *European journal of pharmacology* **2016**, *779*, 1-7.
73. Zhang, J.; Zhong, Q., Histone deacetylase inhibitors and cell death. *Cellular and Molecular Life Sciences* **2014**, *71* (20), 3885-3901.
74. Johnstone, R. W., Histone-deacetylase inhibitors: novel drugs for the treatment of cancer. *Nat Rev Drug Discov* **2002**, *1* (4), 287-299.
75. Minucci, S.; Pelicci, P. G., Histone deacetylase inhibitors and the promise of epigenetic (and more) treatments for cancer. *Nature reviews. Cancer* **2006**, *6* (1), 38-51.
76. Insinga, A.; Monestiroli, S.; Ronzoni, S.; Gelmetti, V.; Marchesi, F.; Viale, A.; Altucci, L.; Nervi, C.; Minucci, S.; Pelicci, P. G., Inhibitors of histone deacetylases induce tumor-selective apoptosis through activation of the death receptor pathway. *Nature medicine* **2005**, *11* (1), 71-76.
77. Bangert, A.; Cristofanon, S.; Eckhardt, I.; Abhari, B. A.; Kolodziej, S.; Hacker, S.; Vellanki, S. H. K.; Lausen, J.; Debatin, K. M.; Fulda, S., Histone deacetylase inhibitors sensitize glioblastoma cells to TRAIL-induced apoptosis by c-myc-mediated downregulation of cFLIP. *Oncogene* **2012**, *31* (44), 4677-4688.
78. Riley, J. S.; Hutchinson, R.; McArt, D. G.; Crawford, N.; Holohan, C.; Paul, I.; Van Schaeybroeck, S.; Salto-Tellez, M.; Johnston, P. G.; Fennell, D. A.; Gately, K.; O'Byrne, K.; Cummins, R.; Kay, E.; Hamilton, P.; Stasik, I.; Longley, D. B., Prognostic and therapeutic relevance of FLIP and procaspase-8 overexpression in non-small cell lung cancer. *Cell Death Dis* **2013**, *4*, e951.
79. Juan, L.-J.; Shia, W.-J.; Chen, M.-H.; Yang, W.-M.; Seto, E.; Lin, Y.-S.; Wu, C.-W., Histone Deacetylases Specifically Down-regulate p53-dependent Gene Activation. *Journal of Biological Chemistry* **2000**, *275* (27), 20436-20443.
80. Luo, J.; Su, F.; Chen, D.; Shiloh, A.; Gu, W., Deacetylation of p53 modulates its effect on cell growth and apoptosis. *Nature* **2000**, *408* (6810), 377-381.

81. Ito, A.; Kawaguchi, Y.; Lai, C. H.; Kovacs, J. J.; Higashimoto, Y.; Appella, E.; Yao, T. P., MDM2–HDAC1-mediated deacetylation of p53 is required for its degradation. *The EMBO Journal* **2002**, *21* (22), 6236-6245.
82. Prives, C.; Manley, J. L., Why Is p53 Acetylated? *Cell* **2001**, *107* (7), 815-818.
83. Tang, Y.; Zhao, W.; Chen, Y.; Zhao, Y.; Gu, W., Acetylation Is Indispensable for p53 Activation. *Cell* **2008**, *133* (4), 612-626.
84. Vogelstein, B.; Lane, D.; Levine, A. J., Surfing the p53 network. *Nature* **2000**, *408* (6810), 307-310.
85. Prives, C.; Hall, P. A., The p53 pathway. *The Journal of pathology* **1999**, *187* (1), 112-26.
86. Stolzel, F.; Pfirrmann, M.; Aulitzky, W. E.; Kaufmann, M.; Bodenstern, H.; Bornhauser, M.; Rollig, C.; Kramer, M.; Mohr, B.; Oelschlagel, U.; Schmitz, N.; Soucek, S.; Thiede, C.; Ehninger, G.; Schaich, M., Risk stratification using a new prognostic score for patients with secondary acute myeloid leukemia: results of the prospective AML96 trial. *Leukemia* **2011**, *25* (3), 420-428.
87. Seifert, H.; Mohr, B.; Thiede, C.; Oelschlagel, U.; Schakel, U.; Illmer, T.; Soucek, S.; Ehninger, G.; Schaich, M., The prognostic impact of 17p (p53) deletion in 2272 adults with acute myeloid leukemia. *Leukemia* **2009**, *23* (4), 656-663.
88. Network, T. C. G. A. R., Genomic and Epigenomic Landscapes of Adult De Novo Acute Myeloid Leukemia. *New England Journal of Medicine* **2013**, *368* (22), 2059-2074.
89. Brosh, R.; Rotter, V., When mutants gain new powers: news from the mutant p53 field. *Nature reviews. Cancer* **2009**, *9* (10), 701-713.
90. Cleven, A. H.; Nardi, V.; Ok, C. Y.; Goswami, M.; Dal Cin, P.; Zheng, Z.; Iafrate, A. J.; Abdul Hamid, M. A.; Wang, S. A.; Hasserjian, R. P., High p53 protein expression in therapy-related myeloid neoplasms is associated with adverse karyotype and poor outcome. *Modern pathology : an official journal of the United States and Canadian Academy of Pathology, Inc* **2015**, *28* (4), 552-63.
91. Quintas-Cardama, A.; Santos, F. P. S.; Garcia-Manero, G., Histone deacetylase inhibitors for the treatment of myelodysplastic syndrome and acute myeloid leukemia. *Leukemia* **2011**, *25* (2), 226-235.
92. Friend, C.; Scher, W.; Holland, J. G.; Sato, T., Hemoglobin synthesis in murine virus-induced leukemic cells in vitro: stimulation of erythroid differentiation by dimethyl sulfoxide. *Proceedings of the National Academy of Sciences of the United States of America* **1971**, *68* (2), 378-82.
93. Marks, P. A.; Breslow, R., Dimethyl sulfoxide to vorinostat: development of this histone deacetylase inhibitor as an anticancer drug. *Nat Biotech* **2007**, *25* (1), 84-90.
94. Bradner, J. E.; West, N.; Grachan, M. L.; Greenberg, E. F.; Haggarty, S. J.; Warnow, T.; Mazitschek, R., Chemical phylogenetics of histone deacetylases. *Nat Chem Biol* **2010**, *6* (3), 238-243.
95. Butler, K. V.; Kalin, J.; Brochier, C.; Vistoli, G.; Langley, B.; Kozikowski, A. P., Rational Design and Simple Chemistry Yield a Superior, Neuroprotective HDAC6 Inhibitor, Tubastatin A. *Journal of the American Chemical Society* **2010**, *132* (31), 10842-10846.
96. Jaganathan, S.; Malek, E.; Vallabhapurapu, S.; Vallabhapurapu, S.; Driscoll, J. J., Bortezomib induces AMPK-dependent autophagosome formation uncoupled from apoptosis in drug resistant cells. *Oncotarget* **2014**, *5* (23), 12358-12370.
97. Vogl, D. T.; Raje, N.; Jagannath, S.; Richardson, P.; Hari, P.; Orłowski, R.; Supko, J. G.; Tamang, D.; Yang, M.; Jones, S. S.; Wheeler, C.; Markelewicz, R. J.; Lonial, S., Ricolinostat, the

- First Selective Histone Deacetylase 6 Inhibitor, in Combination with Bortezomib and Dexamethasone for Relapsed or Refractory Multiple Myeloma. *Clinical Cancer Research* **2017**.
98. Wade, P. A.; Jones, P. L.; Vermaak, D.; Wolffe, A. P., A multiple subunit Mi-2 histone deacetylase from *Xenopus laevis* cofractionates with an associated Snf2 superfamily ATPase. *Current Biology* **1998**, *8* (14), 843-846.
99. Zhang, Y.; LeRoy, G.; Seelig, H. P.; Lane, W. S.; Reinberg, D., The dermatomyositis-specific autoantigen Mi2 is a component of a complex containing histone deacetylase and nucleosome remodeling activities. *Cell* **1998**, *95* (2), 279-289.
100. Hassig, C. A.; Fleischer, T. C.; Billin, A. N.; Schreiber, S. L.; Ayer, D. E., Histone deacetylase activity is required for full transcriptional repression by mSin3A. *Cell* **1997**, *89* (3), 341-347.
101. Laherty, C. D.; Yang, W. M.; Jian-Min, S.; Davie, J. R.; Seto, E.; Eisenman, R. N., Histone deacetylases associated with the mSin3 corepressor mediate Mad transcriptional repression. *Cell* **1997**, *89* (3), 349-356.
102. Bantscheff, M., Chemoproteomics profiling of HDAC. *Nat Biotechnol* **2011**, *29*, 255-265.
103. Itoh, T.; Fairall, L.; Muskett, F. W.; Milano, C. P.; Watson, P. J.; Arnaudo, N.; Saleh, A.; Millard, C. J.; El-Mezgueldi, M.; Martino, F.; Schwabe, J. W. R., Structural and functional characterization of a cell cycle associated HDAC1/2 complex reveals the structural basis for complex assembly and nucleosome targeting. *Nucleic acids research* **2015**, *43* (4), 2033-2044.
104. Reynolds, N.; Latos, P.; Hynes-Allen, A.; Loos, R.; Leaford, D.; O'Shaughnessy, A.; Mosaku, O.; Signolet, J.; Brennecke, P.; Kalkan, T.; Costello, I.; Humphreys, P.; Mansfield, W.; Nakagawa, K.; Strouboulis, J.; Behrens, A.; Bertone, P.; Hendrich, B., NuRD suppresses pluripotency gene expression to promote transcriptional heterogeneity and lineage commitment. *Cell Stem Cell* **2012**, *10* (5), 583-594.
105. Lai, A. Y.; Wade, P. A., Cancer biology and NuRD: A multifaceted chromatin remodelling complex. *Nature Reviews Cancer* **2011**, *11* (8), 588-596.
106. Ramirez, J.; Hagman, J., The Mi-2/NuRD complex: a critical epigenetic regulator of hematopoietic development, differentiation and cancer. *Epigenetics* **2009**, *4* (8), 532-6.
107. Yoshida, T.; Hazan, I.; Zhang, J.; Ng, S. Y.; Naito, T.; Snippert, H. J.; Heller, E. J.; Qi, X.; Lawton, L. N.; Williams, C. J.; Georgopoulos, K., The role of the chromatin remodeler Mi-2beta in hematopoietic stem cell self-renewal and multilineage differentiation. *Genes Dev* **2008**, *22* (9), 1174-89.
108. Gao, H.; Lukin, K.; Ramirez, J.; Fields, S.; Lopez, D.; Hagman, J., Opposing effects of SWI/SNF and Mi-2/NuRD chromatin remodeling complexes on epigenetic reprogramming by EBF and Pax5. *Proceedings of the National Academy of Sciences of the United States of America* **2009**, *106* (27), 11258-63.
109. Williams, C. J.; Naito, T.; Arco, P. G.; Seavitt, J. R.; Cashman, S. M.; De Souza, B.; Qi, X.; Keables, P.; Von Andrian, U. H.; Georgopoulos, K., The chromatin remodeler Mi-2beta is required for CD4 expression and T cell development. *Immunity* **2004**, *20* (6), 719-33.
110. Naito, T.; Gomez-Del Arco, P.; Williams, C. J.; Georgopoulos, K., Antagonistic interactions between Ikaros and the chromatin remodeler Mi-2beta determine silencer activity and Cd4 gene expression. *Immunity* **2007**, *27* (5), 723-34.
111. Andres, M. E.; Burger, C.; Peral-Rubio, M. J.; Battaglioli, E.; Anderson, M. E.; Grimes, J.; Dallman, J.; Ballas, N.; Mandel, G., CoREST: A functional corepressor required for regulation of neural-specific gene expression. *Proceedings of the National Academy of Sciences of the United States of America* **1999**, *96* (17), 9873-9878.

112. Yang, M.; Gocke, C. B.; Luo, X.; Borek, D.; Tomchick, D. R.; Machius, M.; Otwinowski, Z.; Yu, H., Structural Basis for CoREST-Dependent Demethylation of Nucleosomes by the Human LSD1 Histone Demethylase. *Molecular Cell* **2006**, *23* (3), 377-387.
113. Kim, S. A.; Chatterjee, N.; Jennings, M. J.; Bartholomew, B.; Tan, S., Extranucleosomal DNA enhances the activity of the LSD1/CoREST histone demethylase complex. *Nucleic acids research* **2015**, *43* (10), 4868-4880.
114. Pagliuca, F.; Collins, M.; Lichawska, A.; Zegerman, P.; Choudhary, J.; Pines, J., Quantitative Proteomics Reveals the Basis for the Biochemical Specificity of the Cell-Cycle Machinery. *Molecular Cell* **2011**, *43* (3), 406-417.
115. Bantscheff, M.; Hopf, C.; Savitski, M. M.; Dittmann, A.; Grandi, P.; Michon, A. M.; Schlegl, J.; Abraham, Y.; Becher, I.; Bergamini, G.; Boesche, M.; Delling, M.; Dumpelfeld, B.; Eberhard, D.; Huthmacher, C.; Mathieson, T.; Poeckel, D.; Reader, V.; Strunk, K.; Sweetman, G.; Kruse, U.; Neubauer, G.; Ramsden, N. G.; Drewes, G., Chemoproteomics profiling of HDAC inhibitors reveals selective targeting of HDAC complexes. *Nat Biotechnol* **2011**, *29* (3), 255-65.
116. Cowley, S. M.; Iritani, B. M.; Mendrysa, S. M.; Xu, T.; Cheng, P. F.; Yada, J.; Liggitt, H. D.; Eisenman, R. N., The mSin3A chromatin-modifying complex is essential for embryogenesis and T-cell development. *Molecular and Cellular Biology* **2005**, *25* (16), 6990-7004.
117. Clark, M. D.; Marcum, R.; Graveline, R.; Chan, C. W.; Xie, T.; Chen, Z.; Ding, Y.; Zhang, Y.; Mondragón, A.; David, G.; Radhakrishnan, I., Structural insights into the assembly of the histone deacetylase-associated Sin3L/Rpd3L corepressor complex. *Proceedings of the National Academy of Sciences of the United States of America* **2015**, *112* (28), E3669-E3678.
118. Hudson, G. M.; Watson, P. J.; Fairall, L.; Jamieson, A. G.; Schwabe, J. W. R., Insights into the recruitment of class IIa histone deacetylases (HDACs) to the SMRT/NCoR transcriptional repression complex. *Journal of Biological Chemistry* **2015**, *290* (29), 18237-18244.
119. Shen, S.; Kozikowski, A. P., Why Hydroxamates May Not Be the Best Histone Deacetylase Inhibitors--What Some May Have Forgotten or Would Rather Forget? *ChemMedChem* **2016**, *11* (1), 15-21.
120. Patnaik, A.; Rowinsky, E. K.; Villalona, M. A.; Hammond, L. A.; Britten, C. D.; Siu, L. L.; Goetz, A.; Felton, S. A.; Burton, S.; Valone, F. H.; Eckhardt, S. G., A phase I study of pivaloyloxymethyl butyrate, a prodrug of the differentiating agent butyric acid, in patients with advanced solid malignancies. *Clinical cancer research : an official journal of the American Association for Cancer Research* **2002**, *8* (7), 2142-8.
121. Gojo, I.; Jiemjit, A.; Trepel, J. B.; Sparreboom, A.; Figg, W. D.; Rollins, S.; Tidwell, M. L.; Greer, J.; Chung, E. J.; Lee, M. J.; Gore, S. D.; Sausville, E. A.; Zwiebel, J.; Karp, J. E., Phase I and pharmacologic study of MS-275, a histone deacetylase inhibitor, in adults with refractory and relapsed acute leukemias. *Blood* **2007**, *109* (7), 2781-90.
122. Kummar, S.; Gutierrez, M.; Gardner, E. R.; Donovan, E.; Hwang, K.; Chung, E. J.; Lee, M. J.; Maynard, K.; Kalnitskiy, M.; Chen, A.; Melillo, G.; Ryan, Q. C.; Conley, B.; Figg, W. D.; Trepel, J. B.; Zwiebel, J.; Doroshow, J. H.; Murgo, A. J., Phase I trial of MS-275, a histone deacetylase inhibitor, administered weekly in refractory solid tumors and lymphoid malignancies. *Clinical cancer research : an official journal of the American Association for Cancer Research* **2007**, *13* (18 Pt 1), 5411-7.
123. Garcia-Manero, G.; Assouline, S.; Cortes, J.; Estrov, Z.; Kantarjian, H.; Yang, H.; Newsome, W. M.; Miller, W. H., Jr.; Rousseau, C.; Kalita, A.; Bonfils, C.; Dubay, M.; Patterson, T. A.; Li, Z.; Besterman, J. M.; Reid, G.; Laille, E.; Martell, R. E.; Minden, M., Phase 1 study of

the oral isotype specific histone deacetylase inhibitor MGCD0103 in leukemia. *Blood* **2008**, *112* (4), 981-9.

124. Siu, L. L.; Pili, R.; Duran, I.; Messersmith, W. A.; Chen, E. X.; Sullivan, R.; MacLean, M.; King, S.; Brown, S.; Reid, G. K.; Li, Z.; Kalita, A. M.; Laille, E. J.; Besterman, J. M.; Martell, R. E.; Carducci, M. A., Phase I study of MGCD0103 given as a three-times-per-week oral dose in patients with advanced solid tumors. *Journal of clinical oncology : official journal of the American Society of Clinical Oncology* **2008**, *26* (12), 1940-7.

125. Reid, T.; Valone, F.; Lipera, W.; Irwin, D.; Paroly, W.; Natale, R.; Sreedharan, S.; Keer, H.; Lum, B.; Scappaticci, F.; Bhatnagar, A., Phase II trial of the histone deacetylase inhibitor pivaloyloxymethyl butyrate (Pivanex, AN-9) in advanced non-small cell lung cancer. *Lung cancer (Amsterdam, Netherlands)* **2004**, *45* (3), 381-6.

126. Ramalingam, S. S.; Belani, C. P.; Ruel, C.; Frankel, P.; Gitlitz, B.; Koczywas, M.; Espinoza-Delgado, I.; Gandara, D., Phase II study of belinostat (PXD101), a histone deacetylase inhibitor, for second line therapy of advanced malignant pleural mesothelioma. *Journal of thoracic oncology : official publication of the International Association for the Study of Lung Cancer* **2009**, *4* (1), 97-101.

127. Duvic, M.; Talpur, R.; Ni, X.; Zhang, C.; Hazarika, P.; Kelly, C.; Chiao, J. H.; Reilly, J. F.; Ricker, J. L.; Richon, V. M.; Frankel, S. R., Phase 2 trial of oral vorinostat (suberoylanilide hydroxamic acid, SAHA) for refractory cutaneous T-cell lymphoma (CTCL). *Blood* **2007**, *109* (1), 31-9.

128. Olsen, E. A.; Kim, Y. H.; Kuzel, T. M.; Pacheco, T. R.; Foss, F. M.; Parker, S.; Frankel, S. R.; Chen, C.; Ricker, J. L.; Arduino, J. M.; Duvic, M., Phase IIb multicenter trial of vorinostat in patients with persistent, progressive, or treatment refractory cutaneous T-cell lymphoma. *Journal of clinical oncology : official journal of the American Society of Clinical Oncology* **2007**, *25* (21), 3109-15.

129. Choudhary, C.; Kumar, C.; Gnad, F.; Nielsen, M. L.; Rehman, M.; Walther, T. C.; Olsen, J. V.; Mann, M., Lysine acetylation targets protein complexes and co-regulates major cellular functions. *Science (New York, N.Y.)* **2009**, *325* (5942), 834-40.

130. Crump, M.; Coiffier, B.; Jacobsen, E. D.; Sun, L.; Ricker, J. L.; Xie, H.; Frankel, S. R.; Randolph, S. S.; Cheson, B. D., Phase II trial of oral vorinostat (suberoylanilide hydroxamic acid) in relapsed diffuse large-B-cell lymphoma. *Annals of oncology : official journal of the European Society for Medical Oncology / ESMO* **2008**, *19* (5), 964-9.

131. Vansteenkiste, J.; Van Cutsem, E.; Dumez, H.; Chen, C.; Ricker, J. L.; Randolph, S. S.; Schoffski, P., Early phase II trial of oral vorinostat in relapsed or refractory breast, colorectal, or non-small cell lung cancer. *Investigational new drugs* **2008**, *26* (5), 483-8.

132. Woyach, J. A.; Kloos, R. T.; Ringel, M. D.; Arbogast, D.; Collamore, M.; Zwiebel, J. A.; Grever, M.; Villalona-Calero, M.; Shah, M. H., Lack of therapeutic effect of the histone deacetylase inhibitor vorinostat in patients with metastatic radioiodine-refractory thyroid carcinoma. *The Journal of clinical endocrinology and metabolism* **2009**, *94* (1), 164-70.

133. Shah, M. H.; Binkley, P.; Chan, K.; Xiao, J.; Arbogast, D.; Collamore, M.; Farra, Y.; Young, D.; Grever, M., Cardiotoxicity of histone deacetylase inhibitor depsipeptide in patients with metastatic neuroendocrine tumors. *Clinical cancer research : an official journal of the American Association for Cancer Research* **2006**, *12* (13), 3997-4003.

134. Stadler, W. M.; Margolin, K.; Ferber, S.; McCulloch, W.; Thompson, J. A., A phase II study of depsipeptide in refractory metastatic renal cell cancer. *Clinical genitourinary cancer* **2006**, *5* (1), 57-60.

135. Odenike, O. M.; Alkan, S.; Sher, D.; Godwin, J. E.; Huo, D.; Brandt, S. J.; Green, M.; Xie, J.; Zhang, Y.; Vesole, D. H.; Stiff, P.; Wright, J.; Larson, R. A.; Stock, W., Histone deacetylase inhibitor romidepsin has differential activity in core binding factor acute myeloid leukemia. *Clinical cancer research : an official journal of the American Association for Cancer Research* **2008**, *14* (21), 7095-101.
136. Du, J.; Zhou, Y.; Su, X.; Yu, J. J.; Khan, S.; Jiang, H.; Kim, J.; Woo, J.; Kim, J. H.; Choi, B. H.; He, B.; Chen, W.; Zhang, S.; Cerione, R. A.; Auwerx, J.; Hao, Q.; Lin, H., Sirt5 Is an NAD-Dependent Protein Lysine Demalonylase and Desuccinylase(). *Science (New York, N.Y.)* **2011**, *334* (6057), 806-809.
137. Wong, N. S.; Seah, E.; Wang, L. Z.; Yeo, W. L.; Yap, H. L.; Chuah, B.; Lim, Y. W.; Ang, P. C.; Tai, B. C.; Lim, R.; Goh, B. C.; Lee, S. C., Impact of UDP-gluconoryltransferase 2B17 genotype on vorinostat metabolism and clinical outcomes in Asian women with breast cancer. *Pharmacogenetics and genomics* **2011**, *21* (11), 760-8.
138. Wang, L. Z.; Ramirez, J.; Yeo, W.; Chan, M. Y.; Thuya, W. L.; Lau, J. Y.; Wan, S. C.; Wong, A. L.; Zee, Y. K.; Lim, R.; Lee, S. C.; Ho, P. C.; Lee, H. S.; Chan, A.; Ansher, S.; Ratain, M. J.; Goh, B. C., Glucuronidation by UGT1A1 is the dominant pathway of the metabolic disposition of belinostat in liver cancer patients. *PloS one* **2013**, *8* (1), e54522.
139. Mulder, G. J.; Meerman, J. H., Sulfation and glucuronidation as competing pathways in the metabolism of hydroxamic acids: the role of N,O-sulfonation in chemical carcinogenesis of aromatic amines. *Environmental Health Perspectives* **1983**, *49*, 27-32.
140. Zhang, Q.; Wu, H.; Wen, C.; Sun, F.; Yang, X.; Hu, L., Metabolic changes in rats after intragastric administration of MGCD0103 (Mocetinostat), a HDAC class I inhibitor. *International Journal of Clinical and Experimental Pathology* **2015**, *8* (8), 9320-9325.
141. Wang, Y.; Stowe, R. L.; Pinello, C. E.; Tian, G.; Madoux, F.; Li, D.; Zhao, L. Y.; Li, J. L.; Wang, Y.; Wang, Y.; Ma, H.; Hodder, P.; Roush, W. R.; Liao, D., Identification of histone deacetylase inhibitors with benzoylhydrazide scaffold that selectively inhibit class I histone deacetylases. *Chemistry & biology* **2015**, *22* (2), 273-84.
142. Zencheck, W. D.; Xiao, H.; Weiss, L. M., Lysine post-translational modifications and the cytoskeleton. *Essays in biochemistry* **2012**, *52*, 135-45.
143. Lin, Y.-y.; Kiihl, S.; Suhail, Y.; Liu, S.-Y.; Chou, Y.-h.; Kuang, Z.; Lu, J.-y.; Ni Khor, C.; Lin, C.-L.; Bader, J. S.; Irizarry, R.; Boeke, J. D., Functional dissection of lysine deacetylases reveals that HDAC1 and p300 regulate AMPK. *Nature* **2012**, *482* (7384), 251-255.
144. Jiang, T.; Zhou, X.; Taghizadeh, K.; Dong, M.; Dedon, P. C., N-formylation of lysine in histone proteins as a secondary modification arising from oxidative DNA damage. *Proceedings of the National Academy of Sciences of the United States of America* **2007**, *104* (1), 60-5.
145. Wisniewski, J. R.; Zougman, A.; Mann, M., Nepsilon-formylation of lysine is a widespread post-translational modification of nuclear proteins occurring at residues involved in regulation of chromatin function. *Nucleic acids research* **2008**, *36* (2), 570-7.
146. Chen, Y.; Sprung, R.; Tang, Y.; Ball, H.; Sangras, B.; Kim, S. C.; Falck, J. R.; Peng, J.; Gu, W.; Zhao, Y., Lysine propionylation and butyrylation are novel post-translational modifications in histones. *Molecular & cellular proteomics : MCP* **2007**, *6* (5), 812-9.
147. Zhang, K.; Chen, Y.; Zhang, Z.; Zhao, Y., Identification and verification of lysine propionylation and butyrylation in yeast core histones using PTMap software. *Journal of proteome research* **2009**, *8* (2), 900-6.
148. Tan, M.; Luo, H.; Lee, S.; Jin, F.; Yang, J. S.; Montellier, E.; Buchou, T.; Cheng, Z.; Rousseaux, S.; Rajagopal, N.; Lu, Z.; Ye, Z.; Zhu, Q.; Wysocka, J.; Ye, Y.; Khochbin, S.; Ren,

- B.; Zhao, Y., Identification of 67 histone marks and histone lysine crotonylation as a new type of histone modification. *Cell* **2011**, *146* (6), 1016-28.
149. Peng, C.; Lu, Z.; Xie, Z.; Cheng, Z.; Chen, Y.; Tan, M.; Luo, H.; Zhang, Y.; He, W.; Yang, K.; Zwaans, B. M.; Tishkoff, D.; Ho, L.; Lombard, D.; He, T. C.; Dai, J.; Verdin, E.; Ye, Y.; Zhao, Y., The first identification of lysine malonylation substrates and its regulatory enzyme. *Molecular & cellular proteomics : MCP* **2011**, *10* (12), M111.012658.
150. Xie, Z.; Dai, J.; Dai, L.; Tan, M.; Cheng, Z.; Wu, Y.; Boeke, J. D.; Zhao, Y., Lysine succinylation and lysine malonylation in histones. *Molecular & cellular proteomics : MCP* **2012**, *11* (5), 100-7.
151. Jiang, H.; Khan, S.; Wang, Y.; Charron, G.; He, B.; Sebastian, C.; Du, J.; Kim, R.; Ge, E.; Mostoslavsky, R.; Hang, H. C.; Hao, Q.; Lin, H., SIRT6 regulates TNF-alpha secretion through hydrolysis of long-chain fatty acyl lysine. *Nature* **2013**, *496* (7443), 110-3.
152. Yang, Y.-Y.; Ascano, J. M.; Hang, H. C., Bioorthogonal Chemical Reporters for Monitoring Protein Acetylation. *Journal of the American Chemical Society* **2010**, *132* (11), 3640-3641.
153. Tan, M.; Peng, C.; Anderson, K. A.; Chhoy, P.; Xie, Z.; Dai, L.; Park, J.; Chen, Y.; Huang, H.; Zhang, Y.; Ro, J.; Wagner, G. R.; Green, M. F.; Madsen, A. S.; Schmiesing, J.; Peterson, B. S.; Xu, G.; Ilkayeva, O. R.; Muehlbauer, M. J.; Braulke, T.; Muhlhausen, C.; Backos, D. S.; Olsen, C. A.; McGuire, P. J.; Pletcher, S. D.; Lombard, D. B.; Hirschey, M. D.; Zhao, Y., Lysine glutarylation is a protein posttranslational modification regulated by SIRT5. *Cell metabolism* **2014**, *19* (4), 605-17.
154. Bürlü, R. W.; Luckhurst, C. A.; Aziz, O.; Matthews, K. L.; Yates, D.; Lyons, K. A.; Beconi, M.; McAllister, G.; Breccia, P.; Stott, A. J.; Penrose, S. D.; Wall, M.; Lamers, M.; Leonard, P.; Müller, I.; Richardson, C. M.; Jarvis, R.; Stones, L.; Hughes, S.; Wishart, G.; Haughan, A. F.; O'Connell, C.; Mead, T.; McNeil, H.; Vann, J.; Mangette, J.; Maillard, M.; Beaumont, V.; Munoz-Sanjuan, I.; Dominguez, C., Design, Synthesis, and Biological Evaluation of Potent and Selective Class IIa Histone Deacetylase (HDAC) Inhibitors as a Potential Therapy for Huntington's Disease. *Journal of Medicinal Chemistry* **2013**, *56* (24), 9934-9954.
155. Tessier, P.; Smil, D. V.; Wahhab, A.; Leit, S.; Rahil, J.; Li, Z.; Deziel, R.; Besterman, J. M., Diphenylmethylenedihydroxamic acids as selective class IIa histone deacetylase inhibitors. *Bioorganic & medicinal chemistry letters* **2009**, *19* (19), 5684-8.
156. Inks, E. S.; Josey, B. J.; Jesinkey, S. R.; Chou, C. J., A Novel Class of Small Molecule Inhibitors of HDAC6. *ACS Chemical Biology* **2012**, *7* (2), 331-339.
157. Madsen, A. S.; Olsen, C. A., Profiling of substrates for zinc-dependent lysine deacetylase enzymes: HDAC3 exhibits decrotonylase activity in vitro. *Angewandte Chemie (International ed. in English)* **2012**, *51* (36), 9083-7.
158. Chou, C. J.; Herman, D.; Gottesfeld, J. M., Pimelic diphenylamide 106 is a slow, tight-binding inhibitor of class I histone deacetylases. *The Journal of biological chemistry* **2008**, *283* (51), 35402-9.
159. Haggarty, S. J.; Koeller, K. M.; Wong, J. C.; Grozinger, C. M.; Schreiber, S. L., Domain-selective small-molecule inhibitor of histone deacetylase 6 (HDAC6)-mediated tubulin deacetylation. *Proceedings of the National Academy of Sciences of the United States of America* **2003**, *100* (8), 4389-94.
160. El-Ansary, A. K.; Ben Bacha, A. G.; Al- Ayahdi, L. Y., Plasma fatty acids as diagnostic markers in autistic patients from Saudi Arabia. *Lipids in Health and Disease* **2011**, *10*, 62-62.

161. Maria E. Cardona, E. C., Susanne Stern, Bo Tjellstrom, Elisabeth Norin, Tore Midtvét, Correlation between faecal iso-butyric and iso-valeric acids in different species. *Microbial Ecology in Health and Disease* **2005**, *17*, 177-182.
162. Saito, A.; Yamashita, T.; Mariko, Y.; Nosaka, Y.; Tsuchiya, K.; Ando, T.; Suzuki, T.; Tsuruo, T.; Nakanishi, O., A synthetic inhibitor of histone deacetylase, MS-27-275, with marked in vivo antitumor activity against human tumors. *Proceedings of the National Academy of Sciences of the United States of America* **1999**, *96* (8), 4592-7.
163. Jayne, S.; Zwartjes, C. G.; van Schaik, F. M.; Timmers, H. T., Involvement of the SMRT/NCOR-HDAC3 complex in transcriptional repression by the CNOT2 subunit of the human Ccr4-Not complex. *Biochem J* **2006**, *398* (3), 461-7.
164. Richon, V. M.; Emiliani, S.; Verdin, E.; Webb, Y.; Breslow, R.; Rifkind, R. A.; Marks, P. A., A class of hybrid polar inducers of transformed cell differentiation inhibits histone deacetylases. *Proceedings of the National Academy of Sciences of the United States of America* **1998**, *95* (6), 3003-7.
165. Wagner, F. F.; Lundh, M.; Kaya, T.; McCarren, P.; Zhang, Y.-L.; Chattopadhyay, S.; Gale, J. P.; Galbo, T.; Fisher, S. L.; Meier, B. C.; Vetere, A.; Richardson, S.; Morgan, N. G.; Christensen, D. P.; Gilbert, T. J.; Hooker, J. M.; Leroy, M.; Walpita, D.; Mandrup-Poulsen, T.; Wagner, B. K.; Holson, E. B., An Isochemogenic Set of Inhibitors To Define the Therapeutic Potential of Histone Deacetylases in β -Cell Protection. *ACS Chemical Biology* **2016**, *11* (2), 363-374.
166. Gao, Z.; He, Q.; Peng, B.; Chiao, P. J.; Ye, J., Regulation of nuclear translocation of HDAC3 by IkappaBalpha is required for tumor necrosis factor inhibition of peroxisome proliferator-activated receptor gamma function. *J Biol Chem* **2006**, *281* (7), 4540-7.
167. Zhao, Y.; Lu, S.; Wu, L.; Chai, G.; Wang, H.; Chen, Y.; Sun, J.; Yu, Y.; Zhou, W.; Zheng, Q.; Wu, M.; Otterson, G. A.; Zhu, W.-G., Acetylation of p53 at Lysine 373/382 by the Histone Deacetylase Inhibitor Depsipeptide Induces Expression of p21Waf1/Cip1. *Molecular and Cellular Biology* **2006**, *26* (7), 2782-2790.
168. Tang, D.; Shi, Y.; Jang, L.; Wang, K.; Xiao, W.; Xiao, X., Heat shock response inhibits release of high mobility group box 1 protein induced by endotoxin in murine macrophages. *Shock (Augusta, Ga.)* **2005**, *23* (5), 434-40.
169. Wang, H.; Yang, H.; Czura, C. J.; Sama, A. E.; Tracey, K. J., HMGB1 as a late mediator of lethal systemic inflammation. *American journal of respiratory and critical care medicine* **2001**, *164* (10 Pt 1), 1768-73.
170. Bonaldi, T.; Talamo, F.; Scaffidi, P.; Ferrera, D.; Porto, A.; Bachi, A.; Rubartelli, A.; Agresti, A.; Bianchi, M. E., Monocytic cells hyperacetylate chromatin protein HMGB1 to redirect it towards secretion. *The EMBO Journal* **2003**, *22* (20), 5551-5560.
171. Walsky, R. L.; Bauman, J. N.; Bourcier, K.; Giddens, G.; Lapham, K.; Negahban, A.; Ryder, T. F.; Obach, R. S.; Hyland, R.; Goosen, T. C., Optimized assays for human UDP-glucuronosyltransferase (UGT) activities: altered alamethicin concentration and utility to screen for UGT inhibitors. *Drug metabolism and disposition: the biological fate of chemicals* **2012**, *40* (5), 1051-65.
172. Parise, R. A.; Holleran, J. L.; Beumer, J. H.; Ramalingam, S.; Egorin, M. J., A liquid chromatography–electrospray ionization tandem mass spectrometric assay for quantitation of the histone deacetylase inhibitor, vorinostat (suberoylanilide hydroxamic acid, SAHA), and its metabolites in human serum. *Journal of Chromatography B* **2006**, *840* (2), 108-115.

173. Richon, V. M., Cancer biology: mechanism of antitumour action of vorinostat (suberoylanilide hydroxamic acid), a novel histone deacetylase inhibitor. *British Journal of Cancer* **2006**, 95 (Suppl 1), S2-S6.
174. Matsuo, Y.; MacLeod, R. A.; Uphoff, C. C.; Drexler, H. G.; Nishizaki, C.; Katayama, Y.; Kimura, G.; Fujii, N.; Omoto, E.; Harada, M.; Orita, K., Two acute monocytic leukemia (AML-M5a) cell lines (MOLM-13 and MOLM-14) with interclonal phenotypic heterogeneity showing MLL-AF9 fusion resulting from an occult chromosome insertion, ins(11;9)(q23;p22p23). *Leukemia* **1997**, 11 (9), 1469-77.
175. Birnie, G. D., The HL60 cell line: a model system for studying human myeloid cell differentiation. *The British Journal of Cancer. Supplement* **1988**, 9, 41-45.
176. Stong, R. C.; Korsmeyer, S. J.; Parkin, J. L.; Arthur, D. C.; Kersey, J. H., Human acute leukemia cell line with the t(4;11) chromosomal rearrangement exhibits B lineage and monocytic characteristics. *Blood* **1985**, 65 (1), 21-31.
177. Andersson, L. C.; Nilsson, K.; Gahmberg, C. G., K562--a human erythroleukemic cell line. *International journal of cancer* **1979**, 23 (2), 143-7.
178. Quentmeier, H.; Reinhardt, J.; Zaborski, M.; Drexler, H. G., FLT3 mutations in acute myeloid leukemia cell lines. *Leukemia* **2003**, 17 (1), 120-4.
179. Grofova, M.; Popovic, M.; Ogura, H.; Matoska, J.; Lizonova, A.; Nilsson, K.; Kuzela, S., The retrovirus particles in human myeloma cells RPMI8226: morphological, biochemical, immunological and infective transmission studies. *Neoplasma* **1978**, 25 (4), 423-37.
180. Hubbert, C.; Guardiola, A.; Shao, R.; Kawaguchi, Y.; Ito, A.; Nixon, A.; Yoshida, M.; Wang, X. F.; Yao, T. P., HDAC6 is a microtubule-associated deacetylase. *Nature* **2002**, 417 (6887), 455-8.
181. Edrissi, B.; Taghizadeh, K.; Dedon, P. C., Quantitative analysis of histone modifications: formaldehyde is a source of pathological n(6)-formyllysine that is refractory to histone deacetylases. *PLoS genetics* **2013**, 9 (2), e1003328.
182. Palijan, A.; Fernandes, I.; Bastien, Y.; Tang, L.; Verway, M.; Kourelis, M.; Tavera-Mendoza, L. E.; Li, Z.; Bourdeau, V.; Mader, S.; Yang, X. J.; White, J. H., Function of Histone Deacetylase 6 as a Cofactor of Nuclear Receptor Coregulator LCoR. *Journal of Biological Chemistry* **2009**, 284 (44), 30264-30274.
183. Suzuki, T.; Kasuya, Y.; Itoh, Y.; Ota, Y.; Zhan, P.; Asamitsu, K.; Nakagawa, H.; Okamoto, T.; Miyata, N., Identification of Highly Selective and Potent Histone Deacetylase 3 Inhibitors Using Click Chemistry-Based Combinatorial Fragment Assembly. *PloS one* **2013**, 8 (7), e68669.
184. McClure, J. J.; Zhang, C.; Inks, E. S.; Peterson, Y. K.; Li, J.; Chou, C. J., Development of Allosteric Hydrazide-Containing Class I Histone Deacetylase Inhibitors for Use in Acute Myeloid Leukemia. *J Med Chem* **2016**, 59 (21), 9942-9959.
185. Chen, X.; Barozzi, I.; Termanini, A.; Prosperini, E.; Recchiuti, A.; Dalli, J.; Mietton, F.; Matteoli, G.; Hiebert, S.; Natoli, G., Requirement for the histone deacetylase Hdac3 for the inflammatory gene expression program in macrophages. *Proceedings of the National Academy of Sciences of the United States of America* **2012**, 109 (42), E2865-74.
186. Hatano, E.; Bennett, B. L.; Manning, A. M.; Qian, T.; Lemasters, J. J.; Brenner, D. A., NF-kappaB stimulates inducible nitric oxide synthase to protect mouse hepatocytes from TNF-alpha and Fas-mediated apoptosis. *Gastroenterology* **2001**, 120 (5), 1251-62.
187. Griscavage, J. M.; Wilk, S.; Ignarro, L. J., Inhibitors of the proteasome pathway interfere with induction of nitric oxide synthase in macrophages by blocking activation of transcription

factor NF-kappa B. *Proceedings of the National Academy of Sciences of the United States of America* **1996**, *93* (8), 3308-3312.

188. Jones, E.; Adcock, I. M.; Ahmed, B. Y.; Punctard, N. A., Modulation of LPS stimulated NF-kappaB mediated Nitric Oxide production by PKC ϵ and JAK2 in RAW macrophages. *Journal of Inflammation (London, England)* **2007**, *4*, 23-23.

189. Lu, B.; Wang, H.; Andersson, U.; Tracey, K. J., Regulation of HMGB1 release by inflammasomes. *Protein & cell* **2013**, *4* (3), 163-7.

190. Lu, B.; Nakamura, T.; Inouye, K.; Li, J.; Tang, Y.; Lundback, P.; Valdes-Ferrer, S. I.; Olofsson, P. S.; Kalb, T.; Roth, J.; Zou, Y.; Erlandsson-Harris, H.; Yang, H.; Ting, J. P. Y.; Wang, H.; Andersson, U.; Antoine, D. J.; Chavan, S. S.; Hotamisligil, G. S.; Tracey, K. J., Novel role of PKR in inflammasome activation and HMGB1 release. *Nature* **2012**, *488* (7413), 670-674.

191. Willingham, S. B.; Allen, I. C.; Bergstralh, D. T.; Brickey, W. J.; Huang, M. T.; Taxman, D. J.; Duncan, J. A.; Ting, J. P., NLRP3 (NALP3, Cryopyrin) facilitates in vivo caspase-1 activation, necrosis, and HMGB1 release via inflammasome-dependent and -independent pathways. *Journal of immunology (Baltimore, Md. : 1950)* **2009**, *183* (3), 2008-15.

192. Stammler, D.; Eigenbrod, T.; Menz, S.; Frick, J. S.; Sweet, M. J.; Shakespear, M. R.; Jantsch, J.; Siegert, I.; Wolfle, S.; Langer, J. D.; Oehme, I.; Schaefer, L.; Fischer, A.; Knievel, J.; Heeg, K.; Dalpke, A. H.; Bode, K. A., Inhibition of Histone Deacetylases Permits Lipopolysaccharide-Mediated Secretion of Bioactive IL-1beta via a Caspase-1-Independent Mechanism. *Journal of immunology (Baltimore, Md. : 1950)* **2015**, *195* (11), 5421-31.

193. Vickers, C. J.; Olsen, C. A.; Leman, L. J.; Ghadiri, M. R., Discovery of HDAC Inhibitors That Lack an Active Site Zn(2+)-Binding Functional Group. *ACS Medicinal Chemistry Letters* **2012**, *3* (6), 505-508.